

MOLECULAR MANAGEMENT FOR REFINING OPERATIONS

A thesis submitted to The University of Manchester for the degree of
Doctor of Philosophy
in the Faculty of Engineering and Physical Sciences

2010

Yongwen Wu

**Centre for Process Integration
School of Chemical Engineering and Analytical Science**

Table of Contents

List of Figures	8
List of Tables	12
Abstract	16
Declaration	18
Copyright Statement	19
Acknowledgements	21
Chapter 1 Introduction	22
1.1 Introduction	23
1.2 A Refinery Scheme	23
1.3 Current Status of Refining Industry	24
1.3.1 Product Specifications.....	24
1.3.2 Changing Market Demands and Supply	27
1.3.3 Refining Margin and Refinery Optimisation	28
1.4 Molecular Management	30
1.5 Present Research	30
1.6 Structure of Thesis	31
Chapter 2 Molecular Characterisation of Petroleum Fractions	33
2.1 Introduction.....	34
2.2 Complexity Nature of Petroleum Fractions	34
2.3 Review of Previous Methods	35
2.3.1 Traditional Methods.....	35
2.3.2 Modern Analytical Laboratory Methods.....	36
2.3.3 Computer-aided Molecular Explicit Methods.....	38
2.3.3.1 Challenges of Molecular Characterisation Methods.....	38
2.3.3.2 Stochastic Methods	39
2.3.3.3 Deterministic Methods.....	41
2.3.4 Existing MTHS Methods	43
2.3.5 Limitations of Existing MTHS Methods	44
2.3.5.1 Limitation of Representation Matrix.....	44

2.3.5.2	Limitation of the Transformation Method	45
2.3.6	A Brief Case Showing the Shortcomings of the Existing Methods	45
2.4	A Modified MTHS Framework	48
2.5	Improved MTHS Matrix Representation Model.....	49
2.5.1	Improved MTHS Matrix Representation Model for Light Petroleum Fractions.....	49
2.5.2	Improved MTHS Matrix Representation Model for Middle Petroleum Fractions.....	50
2.6	Transformation Methodology	55
2.6.1	Assumptions.....	55
2.6.1.1	Statistical Distribution Assumption	55
2.6.1.2	Property Estimation Assumption	57
2.6.2	Mathematical Model	60
2.6.2.1	Objective Function	61
2.6.2.2	Constraints	62
2.7	Optimisation Engines	65
2.8	Case Studies	67
2.8.1	FCC Gasoline Stream Case.....	67
2.8.2	SRGO Feed	70
2.8.3	LCO Feed	75
2.9	Summary	77
Chapter 3	Molecular Modelling of Gasoline Blending	78
3.1	Introduction.....	79
3.2	Gasoline Blending.....	79
3.2.1	A Brief Introduction of Gasoline Blending.....	79
3.2.1.1	Blending Process.....	80
3.2.1.2	Blending Type.....	80
3.2.1.3	Gasoline Blending Stocks	81
3.2.1.4	Gasoline Specifications.....	82
3.2.2	Motivation of this Research on Gasoline Blending	85
3.3	A New Molecular Model for Property Prediction	86
3.3.1	Review of Previous Methodologies for ON.....	87
3.3.2	A New Methodology Correlating ON with Bulk Properties.....	87

3.3.2.1	Assumptions.....	87
3.3.2.2	Methodology	91
3.3.3	Case Study.....	96
3.3.3.1	Result of the Regression Phase	97
3.3.3.2	Result of the Prediction Phase	100
3.4	Gasoline Blending Model	101
3.4.1	Review of Gasoline Blending Models	101
3.4.2	Existing Blending Models for ON and RVP Properties	102
3.4.2.1	Octane Number	102
3.4.2.2	Reid Vapour Pressure.....	105
3.4.3	A New Molecular Gasoline Blending Methodology	106
3.4.3.1	Diagram.....	106
3.4.3.2	Mathematical Model	107
3.4.4	Gasoline Blending Optimisation Model	108
3.4.5	Case Study.....	109
3.4.5.1	Traditional Method	110
3.4.5.2	Molecular Blending Model	111
3.5	Summary	112
3.6	Nomenclature	112
Chapter 4	Molecular Modelling of Semiregenerative Catalytic Reforming	114
4.1	Introduction.....	116
4.1.1	Catalytic Reforming Process.....	117
4.1.2	Feed Characteristics	119
4.1.3	Operating Conditions	120
4.1.4	Product	122
4.1.5	Review of Previous Work.....	123
4.1.6	Motivation of Molecular Modelling of Catalytic Reforming	126
4.2	Chemical Reactions Network and Kinetics	127
4.2.1	Dehydrogenation of Naphthenes to Aromatics.....	128
4.2.2	Isomerisation of Paraffins and Naphthenes	129
4.2.3	Dehydrocyclisation of Paraffins.....	129
4.2.4	Hydrocracking and Dealkylation	130

4.2.5	Kinetics	131
4.3	Process Model	131
4.4	Case Study.....	134
4.4.1	Simulation of the Process.....	135
4.4.2	Sensitivity Analysis of Operating Conditions.....	139
4.5	Catalyst Deactivation	142
4.5.1	Mathematical Model of Catalyst Deactivation	142
4.5.2	Multi-period Process Model.....	144
4.6	Catalytic Reforming Process Optimisation.....	146
4.6.1	Mathematical Model	147
4.6.2	Optimisation Approach	148
4.7	Case Study – Multi-period Process Simulation and Optimisation.....	148
4.7.1	Multi-period Process Simulation	148
4.7.2	Sensitivity Analysis of Operating Temperatures	150
4.7.3	Process Optimisation.....	151
4.8	Summary	153
4.9	Nomenclature	154
Chapter 5	Molecular Modelling of Diesel Hydrotreater	156
5.1	Introduction.....	157
5.1.1	Diesel Hydrotreating Process.....	157
5.1.2	Feed Characteristics	159
5.1.3	Operating Conditions	159
5.1.4	Product Specification	161
5.1.5	Motivation of a Molecular Model for Diesel Hydrotreater.....	162
5.2	Reactions Network and Kinetics.....	163
5.2.1	Hydrodesulphurisation (HDS)	164
5.2.1.1	Sulphur Compounds.....	164
5.2.1.2	Reactions Network and Kinetics.....	166
5.2.1.3	Obtaining Kinetic Parameters – Structure Contribution Approach	168
5.2.2	Hydrodearomatisation (HDA).....	171
5.2.2.1	Aromatic Compounds	171
5.2.2.2	Reactions Network and Kinetics.....	171

5.2.2.3	Obtaining Kinetic Parameters	173
5.3	Modelling of a Trickle – bed Reactor	174
5.3.1	Mathematical Equations.....	175
5.3.2	Estimation of Physical Properties	177
5.3.3	Mathematical Methodology and Solving Procedure.....	179
5.4	Case Study – Modelling of Diesel Hydrotreater.....	181
5.4.1	Simulation of a Diesel Hydrotreater	181
5.4.2	Sensitivity Analysis of Operating Conditions.....	183
5.5	Catalyst Deactivation	186
5.5.1	Mathematical Model of Catalyst Deactivation	186
5.5.2	Multi-period Model of Catalyst Deactivation.....	188
5.6	Diesel Hydrotreater Optimisation.....	189
5.6.1	Mathematical Model	190
5.7	Case Study – Optimisation of Diesel Hydrotreater.....	191
5.8	Summary	192
5.9	Nomenclature	193
Chapter 6	Integrated Site and Process Optimisation with Molecular Modelling	195
6.1	Introduction.....	196
6.1.1	Challenges of Refinery Optimisation.....	196
6.1.2	Decomposition Strategy for Refinery Optimisation (Zhang, 2000)	198
6.2	Incorporating Molecular Management into Refinery Optimisation	199
6.3	Application I: Exploitation of Interaction between Refinery Material Processing Network and Processes	199
6.3.1	Introduction.....	199
6.3.2	Site Level Model.....	200
6.3.3	Site Optimisation with Process Simulation.....	202
6.3.4	Integrated Site and Process Optimisation	204
6.3.5	Case Study.....	205
6.3.5.1	Problem Definition.....	205
6.3.5.2	Modelling of Refining Streams and Processes	207
6.3.5.3	Strategy of Case Study	208
6.3.5.4	Optimisation Results.....	209

6.4	Application II: Exploitation of Interactions between Hydrogen Network and Hydroprocesses	215
6.4.1	Introduction	215
6.4.1.1	Hydrogen Network in Refinery.....	215
6.4.1.2	Hydrogen Network Management.....	216
6.4.2	Integrating Hydrogen Network and Hydroprocesses.....	220
6.4.3	Site Level Model.....	220
6.4.4	Site Optimisation with Process Simulation.....	226
6.4.5	Integrated Site and Process Optimisation	227
6.4.6	Case Study.....	228
6.5	Summary	232
6.6	Nomenclature	233
6.6.1	Application I	233
6.6.2	Application II	233
Chapter 7	Conclusions and Future Work.....	236
7.1	Conclusions.....	237
7.2	Future Work	239
References	241	
Appendix A	Joback Group Contribution.....	258
Appendix B	Parameters of Kinetic Model of Catalytic Reformer.....	259
Appendix C	Parameters of Group Contribution Approach.....	261
Appendix D	Physical Properties Calculation.....	264
Appendix E	Boundary Value Problem.....	271
Appendix F	RFCC Model.....	275

List of Figures

Figure 1.1 Flowsheet of a refinery (Gary and Handwerk, 1994).....	24
Figure 1.2 Oil demand growth by product, in North America, Europe, Asia and Middle East, 2008-2014 (Oil Market Report, 2009).....	27
Figure 2.1 Complexity of typical petroleum hydrocarbon type analysis (www.epa.gov).....	35
Figure 2.2 Chemical complexity of higher boiling products (Read, 1976)	35
Figure 2.3 Flow diagram of stochastic modelling of molecular structures and compositions of a complex feedstock (Campbell, 1998).....	40
Figure 2.4 Schematic representation of the methodology (Aye, 2003)	43
Figure 2.5 Research octane number of isooctane isomers (Ghosh, 2006).....	45
Figure 2.6 Predicted molecular composition with 40 sample matrices	47
Figure 2.7 Predicted molecular composition with 80 sample matrices	47
Figure 2.8 New MTHS framework for the characterisation of refining streams....	48
Figure 2.9 MTHS Matrix representation of diesel fractions (Peng, 1999)	50
Figure 2.10 C ₁₅ H ₁₂ isomer corresponding to Table 2.5 generated by SMOG	52
Figure 2.11 (C ₁₇ , A) isomers distribution with boiling point.....	53
Figure 2.12 Gamma distribution fitted fractions within PONA homologous series of a FCC gasoline stream (Chen, 1995).....	56
Figure 2.13 Gamma distribution fitted fractions within homologous series of a middle distillate (Fafet, 1995).....	56
Figure 2.14 Calculation procedure based on the second assumption	57
Figure 2.15 Simulated annealing algorithm (Kirkpatrick, 1983).....	66
Figure 2.16 Comparison of the detailed PIONA volume fraction between the measured and those based on the existing and proposed methodologies.....	69
Figure 2.17 Distillation profiles of the SRGO from the measured and the predicted	74
Figure 3.1 Simplified petroleum refinery flowsheet (Gupta, 2008)	80
Figure 3.2 Research Octane Number of different families of hydrocarbons (Riazi, 2005)	86
Figure 3.3 Nonlinear interactions between two molecules belonging to different homologous series (Ghosh, 2006).....	88
Figure 3.4 Simplified diagram for predicting ON of blending streams	89

Figure 3.5 Diagram for the methodology of predicting ON of gasoline streams from one of refining process	91
Figure 3.6 Series of procedures for achieving the optimal coefficients for predicting ONs of PIONA lumps.....	93
Figure 3.7 Normalised distributions of the related properties for the proposed methodology (Each dot stands for a different sample)	96
Figure 3.8 Comparison of PIONA volume fractions between the measured and predicted in regression phase	97
Figure 3.9 Comparison of RON between the measured and predicted in regression phase.....	98
Figure 3.10 Comparison of MON between the measured and predicted in regression phase	98
Figure 3.11 Comparison of RVP between the measured and predicted in regression phase.....	99
Figure 3.12 Proposed molecular gasoline blending methodology.....	106
Figure 4.1 Simplified semiregenerative process of catalytic reforming (Gary and Handwerk, 2001).....	118
Figure 4.2 Pressure influence (Robert, 2003)	121
Figure 4.3 Generalised reaction network	127
Figure 4.4 Diagram of the simulation of catalytic reforming	134
Figure 4.5 Reactors configuration and operating conditions	135
Figure 4.6 Distillate profiles of feedstock and product from the measured and the predicted.....	136
Figure 4.7 Comparison of the product molecular composition	137
Figure 4.8 Profiles of composition through the reactors.....	138
Figure 4.9 Composition profiles under the adiabatic operating mode.....	138
Figure 4.10 Temperature and pressure profile under the adiabatic operating mode	139
Figure 4.11 Influence of temperature on quality of reformate and yield (Pressure of 150 psi).....	140
Figure 4.12 Influence of temperature on product yields (Pressure of 150 psi).....	140
Figure 4.13 Influence of pressure on reformate yield and quality (T: 783.15K)..	141
Figure 4.14 Influence of pressure on product distribution and yield (T: 783.15K)	141

Figure 4.15 Influence of WHSV on reformat yield and quality.....	142
Figure 4.16 Influence of WHSV on product distribution	142
Figure 4.17 Simulation procedure of the proposed multi-period process model..	145
Figure 4.18 Profit and reformat ON through running cycle.....	149
Figure 4.19 Product distributions through running cycle	149
Figure 4.20 Catalyst activities of three reactors through running cycle	150
Figure 4.21 Influence of temperature on overall profit and RON	150
Figure 4.22 Influence of temperature on the overall hydrogen and reformat yields	151
Figure 4.23 Optimal operating temperature through the running periods targeting the maximal profit.....	152
Figure 4.24 Product distribution through the running periods targeting the maximal profit.....	153
Figure 5.1 A simplified diesel hydrotreating process flowsheet (Gary, 2001).....	158
Figure 5.2 Difficulties of desulphurisation of different sulphur compounds (Froment, 2007)	164
Figure 5.3 Reaction Network for the HDS of DBT	166
Figure 5.4 HDA reactions in diesel hydrotreater (Neurock, 1990).....	171
Figure 5.5 Solving procedure for a diesel hydrotreater tickle-bed reactor	179
Figure 5.6 simulated process integrated with H ₂ S scrubber and flash	180
Figure 5.7 Axial profiles of the sulphur compound content and the partial pressure of H ₂ S (625 K).....	182
Figure 5.8 Axial concentration of hydrogen in the liquid phase and partial pressure of hydrogen in the vapour phase (625 K)	183
Figure 5.9 Influence of temperature on the product compositions	184
Figure 5.10 Influence of the LHSV on the product compositions	184
Figure 5.11 Influence of the pressure on the product composition.....	185
Figure 5.12 Influence of the H ₂ /oil ratio on the product composition	185
Figure 5.13 Influence of catalyst activity on the sulphur removal.....	186
Figure 5.14 Multi-period of run length on the catalyst activity basis division	189
Figure 6.1 A general connection	200
Figure 6.2 Site level optimisation with process simulation	203
Figure 6.3 Integration of site level optimisation and process optimisation	204
Figure 6.4 Flowsheet of a refinery	205

Figure 6.5 Composition of gasoline90 in different modes.....	212
Figure 6.6 Composition of gasoline93 in different modes.....	213
Figure 6.7 Composition of gasoline95 in different modes.....	213
Figure 6.8 Composition of gasoline97 in different modes.....	213
Figure 6.9 Composition of diesel in different modes.....	214
Figure 6.10 A typical hydrogen network	216
Figure 6.11 Simplified diagram of a hydrogen consumer (Alves, 1999)	217
Figure 6.12 Composite curves (Liu, 2002)	218
Figure 6.13 A hydrogen surplus diagram (Liu, 2002)	218
Figure 6.14 Balanced hydrogen surplus cascade diagram (Liu, 2002).....	218
Figure 6.15 Representation change of a process for new method	221
Figure 6.16 Modified diagram of a hydrogen consuming process	221
Figure 6.17 Site optimisation with process simulation/optimisation.....	227
Figure 6.18 Integration of hydrogen network and hydroprocesses.....	228
Figure 6.19 The hydrogen network of the case (Sun, 2004).....	229
Figure 6.20 Hydrogen surplus diagram.....	230
Figure 6.21 Hydrogen surplus diagrams of periods	231

List of Tables

Table 1.1 European Union diesel specification (Official Journal of the European Communities, 2009).....	25
Table 1.2 European Union petrol specification	26
Table 2.1 Typical Measured Isomer Distribution (wt %) for <i>i</i> -Octane (Ghosh, 2006)	44
Table 2.2 Distillation profile of a FCC stream.....	46
Table 2.3 Comparisons of properties between measured and two groups of estimated	46
Table 2.4 New MTHS representation matrix for light petroleum fractions.....	49
Table 2.5 One of C ₁₅ H ₁₂ isomers output from SMOG.....	52
Table 2.6 Isomers generation of each homologous series (* represent the property of the entry is calculated by extrapolation or interpolation)	54
Table 2.7 Properties estimation methodology for pure compounds and mixtures, mixing rules.....	58
Table 2.8 Properties comparison of a gasoline stream based on both correlations and mixing rules	60
Table 2.9 Measured molecular composition of a FCC stream (vol %)......	67
Table 2.10 Generated matrix for the FCC stream by the proposed methodology ..	68
Table 2.11 Comparison of properties.....	68
Table 2.12 Comparison of distillation profile between the measured and the predicted from the developed method.....	70
Table 2.13 Properties of SRGO Feed (Marafi, 2007).....	71
Table 2.14 MTHS matrix (wt %) generated for GO-LF SRGO by simulated annealing algorithm.....	72
Table 2.15 Parameters of homologous series predicted for the gamma distribution and the distribution.....	73
Table 2.16 Comparison of the SRGO properties between the measured and the predicted.....	74
Table 2.17 Properties verification between calculated based on mixing rule and correlations.....	75
Table 2.18 Measured properties of LCO	76
Table 2.19 Comparison of LCO properties between the predicted and measured ..	76

Table 3.1 Clean Air Act and CARB specifications (USA) (Aye, 2003)	82
Table 3.2 California (USA) Phase 2 specifications for gasoline (Simon, 2007)	84
Table 3.3 Coefficients of Equation 3.20 (Riazi, 2006)	94
Table 3.4 Model performance in regression phase	99
Table 3.5 Model performance of the direct correlated model (see section 3.3.3.1)	99
Table 3.6 Model performance of interpolation prediction in the prediction phase	100
Table 3.7 Result of an example of extrapolation prediction	100
Table 3.8 Coefficients in ethyl octane blending equations (Healy et al., 1959) ...	104
Table 3.9 Available feedstock properties and information about blending components	109
Table 3.10 Product specifications for two grades of gasolines	109
Table 3.11 Detailed product distribution (the conventional approach)	110
Table 3.12 Blended product properties (the conventional approach)	110
Table 3.13 Detailed product distribution (molecular modelling)	111
Table 3.14 Blended product properties (molecular modelling)	111
Table 4.1 Compositions of two typical feeds (Gary, 2001)	119
Table 4.2 Typical product distribution from paraffinic feed at 15 bar with RON of 98 (George, 2004)	122
Table 4.3 Typical composition (wt %) of reformates with low operating pressure (George, 2004)	123
Table 4.4 Molecular composition of feedstock (mol %) (Ancheyta, 2000)	135
Table 4.5 Comparison of the properties between the measured and predicted for feedstock and product	136
Table 4.6 Product distribution based on 100 mol feedstock	137
Table 4.7 Objectives of base case	152
Table 5.1 Typical characteristics of feed to diesel hydrotreaters (Heinrich et al, 2001)	159
Table 5.2 EN 590 diesel fuel requirements – date introduced: 1/1/2005	161
Table 5.3 Sulphur distribution in various LCO fractions (Depauw, 1997; Carciá, 2002; Nylén, 2004)	165
Table 5.4 kinetic parameters number needed for the kinetic model of HDS with molecules represented by the MTHS matrix	169
Table 5.5 Physical property of the model	178

Table 5.6 Properties estimation methods	178
Table 5.7 Configuration of the reactor and operating conditions	181
Table 5.8 Composition and properties of the product of the measured and predicted	182
Table 5.9 Monoaromatics content and sulphur content of the products with three different reactor temperatures	182
Table 5.10 Activity division of catalyst for three stages.....	191
Table 5.11 Constraints of the optimisation case	192
Table 5.12 Optimal operating conditions and results	192
Table 6.1 Unit capacity	205
Table 6.2 Properties of two crudes.....	206
Table 6.3 Availability of crudes.....	206
Table 6.4 Major market conditions of refining products	207
Table 6.5 Investigation modes of case study	208
Table 6.6 Gasoline specification	208
Table 6.7 Diesel specification	208
Table 6.8 Total profit of the refinery in the different modes	209
Table 6.9 Crude oil selection in the different modes	210
Table 6.10 Process utilisation in the different modes	210
Table 6.11 Main product distribution in different modes	211
Table 6.12 Gasoline90 product properties in different modes.....	211
Table 6.13 Gasoline97 product properties in different modes.....	212
Table 6.14 Diesel product properties in different modes.....	212
Table 6.15 Operating conditions of processes in different modes.....	214
Table 6.16 Calibrated data of hydrogen sinks (Sun, 2004).....	229
Table 6.17 Calibrated data of hydrogen sources (Sun, 2004).....	229
Table 6.18 Operating conditions of DHT for base case.....	230
Table 6.19 Constraints of operating conditions for DHT	231
Table 6.20 Optimal operating conditions of diesel hydrotreater in each period...	231
Table A.1 Joback group contribution for boiling point and Gibbs energy	258
Table B.1 Factors for pressure effect (Ancheyta, 1994).....	259
Table B.2 Activation energies for each reforming reaction (Henningsen, 1970).259	
Table B.3 Kinetic constants of the model (Ancheyta, 2000)	260

Table C.1 Numerical values for the structural contributions for (s)DBT at 573K (Froment, 2004)	261
Table C.2 Rate and adsorption parameters related to HDS of DBT (Froment, 2008)	262
Table D.1 Constants for the simple and heavy reference fluid.....	266
Table D.2 Constants used for the generalised viscosity correlation	267
Table D.3 Constants used for the generalised correlation for thermal conductivity	268

Abstract

Molecular management targets the right molecules to be at the right place, at the right time and at the right price. It consists of molecular characterisation of refining streams, molecular modelling and optimisation of refining processes, as well as overall refinery optimisation integrating material processing system and utility system on the molecular level. The need to increase modelling details to a molecular level is not just a result of political regulations, which force refiners to managing the molecule properly, but also seems to be a very promising to increase the refining margin. In this work, four aspects of molecular management are investigated respectively.

Molecular Type Homologous Series (MTHS) matrix framework is enhanced on both representation construction and transformation methodology. To improve the accuracy and adequacy of the representation model, different strategies are formulated separately to consider isomers for light and middle distillates. By introducing statistical distribution, which takes the composition distribution of molecules into account, the transformation approach is revolutionised to increase the usability, and tackle the challenge of possibly achieving significantly different compositions from the same bulk properties by the existing approaches. The methodology is also enhanced by applying extensive bulk properties. Case studies demonstrate the effectiveness and accuracy of the methodology.

Based on the proposed characterisation method, refining processes are modelled on a molecular level, and then process level optimisation is preformed to have an insight view of economic performance. Three different processes, including gasoline blending, catalytic reforming, and diesel hydrotreating, are investigated respectively. Regarding gasoline blending, the property prediction of blending components, and the blending nonlinearity are discussed. To tightly control on the property giveaway, a molecular model of gasoline blending is developed, and then integrated into the recipe optimisation. As for the conversion processes, catalytic reforming and diesel hydrotreating, reactions and reactors are modelled separately, and then followed by the consideration of catalyst deactivation. A homogeneous rigorous molecular model of a semiregenerative catalytic reforming process,

considering pressure drop, has been developed. In addition, a multi-period process optimisation model has been formulated. Regarding diesel hydrotreating, a molecular model of reactions with a three-phase trickle-bed reactor has been developed. The concept of reaction family is successfully applied. A structural contribution approach is used to obtain kinetics and adsorption parameters. A series of procedures are developed to solve the complex problem. Thereafter, a process optimisation model has been developed with the consideration of catalyst deactivation, with a new strategy on the division of catalyst life.

Finally, a two-level decomposition optimisation method is extended to incorporate molecular modelling into the overall refinery optimisation, and then applied in two aspects. Firstly, with the integration of the process and the site-level models, a better perspective is obtained with regard to a material processing system. By molecular modelling of refining streams and processes, the integrated approach not only controls the molecules in products properly, but also increases the overall performance. In the second application, a framework integrating a hydrogen network with hydroprocesses is developed to target the maximum profit, rather than saving hydrogen. It allocates hydrogen on the hydrogen network level and utilise hydrogen efficiently on the process level by optimising operating conditions. Consequently, the extent of achieving the maximum profit could be fully exploited with optimal hydrogen utilisation.

Declaration

No portion of the work referred to in this thesis has been submitted in support of an application for another degree or qualification of this or any other university or other institution of learning.

Yongwen Wu

Copyright Statement

- [i] The author of this thesis (including any appendices and/or schedules to this thesis) owns any copyright in it (the “Copyright”) and he has given The University of Manchester the right to use such Copyright for any administrative, promotional, educational and/or teaching purposes.
- [ii] Copies of this thesis, either in full or in extracts, may be made only in accordance with the regulations of the John Rylands University Library of Manchester. Details of these regulations may be obtained from the Librarian. This page must form part of any such copies made.
- [iii] The ownership of any patents, designs, trade marks and any and all other intellectual property rights except for the Copyright (the “Intellectual Property Rights”) and any reproductions of copyright works, for example graphs and tables (“Reproductions”), which may be described in this thesis, may not be owned by the author and may be owned by third parties. Such Intellectual Property Rights and Reproductions cannot and must not be made available for use without the prior written permission of the owner(s) of the relevant Intellectual Property Rights and/or Reproductions.
- [iv] Further information on the conditions under which disclosure, publication and exploitation of this thesis, the Copyright and any Intellectual Property Rights and/or Reproductions described in it may take place is available from the Head of School of Chemical Engineering & Analytical Science.

To
My parents, Ximu Wu and Jumei Bao
&
Wife, Lu Chen

Acknowledgements

I would like to show my sincere gratitude towards my supervisor, Dr. Nan Zhang, for his continuous source of guidance, support and advice throughout the period of my research. I very much appreciate his encouraged independent research style while providing feedback on both the theoretical and practical aspects of my work, which enhances my independent work capability. Also, thanks to his zealous guidance of badminton techniques.

Many thanks to the Centre of Process Integration, the School of Chemical Engineering and Analytical Science, and the Overseas Research Scholarship Scheme. Without their financial support, this research would never have been started or completed.

Special thanks to all staffs of Centre for Process Integration for their direct and indirect helps during my PhD study. I would like to express my special thanks to Professor Robin Smith and Dr. Qiying Scarlet Yin for providing opportunities during my application.

I have great pleasure in expressing my appreciations to all students of CPI for providing a stimulating and friendly environment. Thanks to Imran, Nan Jia, Xuesong, Yuhang, Yu Rong, Zixin, Yufei, Kok Siew, Muneeb, Ankur, Bostjan, Sourabh, Sonia for their kind help and sharing experience of life in Manchester.

Last but not least, I would like to express my deepest gratitude towards my family. Without the continuous unconditional support and love from my parents throughout my life, I would not become who I am today. My warmest gratitude goes to my wife, Lu, for her priceless love, support and understanding.

Chapter 1 Introduction

1.1	Introduction	23
1.2	A Typical Refinery Scheme	23
1.3	Current Status of Refining Industry	24
1.3.1	Product Specifications.....	24
1.3.2	Changing Market Demands and Supply	26
1.3.3	Refining Margin and Refinery Optimisation	28
1.4	Molecular Management	30
1.5	Present Research	30
1.6	Structure of Thesis	31

1.1 Introduction

The refining industry has been experiencing tremendous changes, especially in the past decades due to the ever volatising margins, tightening governmental regulations and arrival of new and competitive fuels such as biofuels. On the other hand, the significant amount of oil consumption, also rapidly increased, leads to the great importance of refining economy. Refiners are running out of conventional options to comply with higher product quality specifications and more stringent environmental regulations as it targets molecular species, which hits the very heart of the traditional refinery configurations. Therefore, a new refining strategy to help satisfy the molecular specifications, and simultaneously maintain/improve the profit margins is of importance for refiners to survive.

Molecular management is a promising technology to satisfy the restriction of the contents of specific components or component classes in fuels. More importantly, it helps refiners to yield significant economic benefits considering refining optimisation of both individual processes and refinerywide models (Zhang, 2005; Katzer, 2000; Briesen, 2004). In this chapter, a typical refinery scheme is introduced firstly, followed by a brief review of challenges facing the refinery industry. Then the strategy of molecular management is concluded to be very necessary to a refinery, which leads to the objective of present research. Finally, the structure of thesis is presented with a brief overview of each chapter.

1.2 A Refinery Scheme

Nowadays, oil refining is a joint production system with a very complex technical structure and a vast number of outputs that are strongly correlated. A general refinery consists of crude oil operations, conversion units, and product blending among which involves many different and complicated connections as Figure 1.1 illustrates.

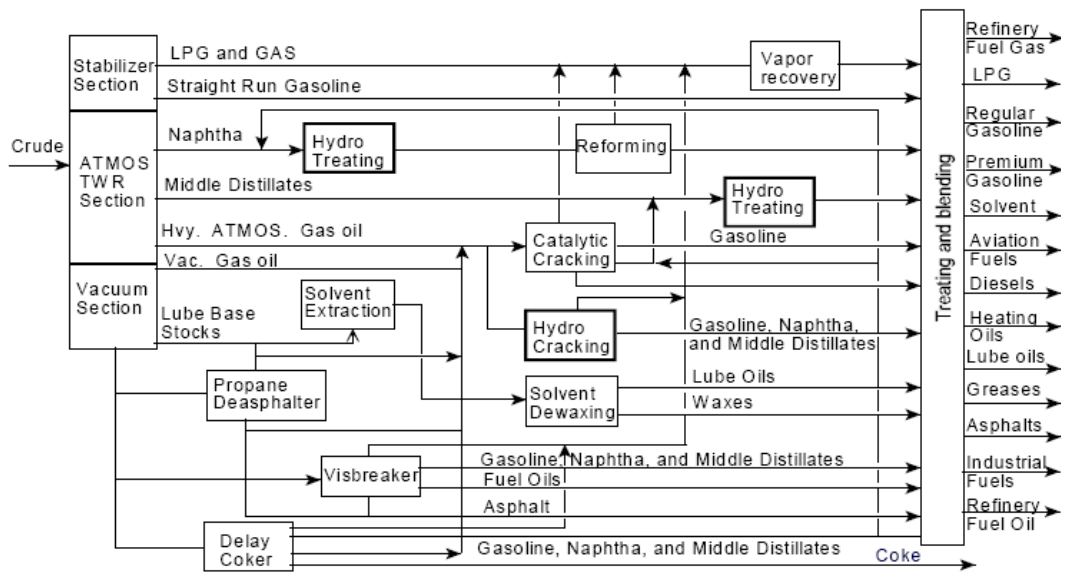


Figure 1.1 Flowsheet of a refinery (Gary and Handwerk, 1994)

Refining starts from Atmosphere Distillation Unit (ADU) which is fed with crude oil to obtain gas, light/heavy naphtha, kerosene, and diesel. To remain competitive, the bottom of ADU would be vacuum distilled to retrieve gas oil for upgrading to lighter products, and even heavy end processes such as Delayed Coker, Visbreaking and Residue Fluid Catalytic Cracking (RFCC) are adopted to handle the residue from Vacuum Distillation Unit (VDU). Blend stocks of gasoline are mainly from the products of Catalytic Reforming Unit (CCRU) and Fluid Catalytic Cracking Unit (FCCU). CCRU fed by heavy naphtha is as octane number improver while FCCU converts gas oil into more profitable gasoline. Straight run diesel and streams from hydrocracker and FCCU compose of the major composition of diesel products. To comply with the environmental regulations on products and improve the performance of some particular processes, hydroprocessing helps to eliminate and reduce sulphur and nitrogen contents. The schematic layout only depicts one of hundreds of different refining configurations.

1.3 Current Status of Refining Industry

1.3.1 Product Specifications

The refining industry today has to comply with higher product quality specifications and more stringent environmental regulations, with more emphasis on the molecular composition of refining products. Composition concerns such as

benzene, total aromatics, total olefin and oxygenates are being phased in since 1992, in addition to the traditional qualities, and gradually tightened to a critical level. For instance, in 1995, the U.S. Environmental Protection Agency fixed the average benzene content has to be less than 1 volume percent in gasoline for Federal Phase I, and retains the benzene limit for Phase II in 2000, followed by the maximum level of benzene reduced to 0.8 volume percent for Phase III in 2004, and even an annual average maximum benzene content of 0.62 liquid volume percent becoming effective from 2011 (Bacon, 2009). Obviously, the increases in the environmental awareness and concerns are demanding refining fuels to be cleaner.

Table 1.1 European Union diesel specification (Official Journal of the European Communities, 2009)

	EN 590	Directive 98/70	Directive 98/70	Directive 98/70
Entry to force	1993/1996	2000	2005	2009
Polycyclic aromatic hydrocarbons [% v/v] max	-	11	11	6
Sulphur [ppm] max	2000/500	350	50	10
Cetane number, min	46 - 49	51	51	51
Density at 15 °C [kg/m ³], max	860	845	845	845
Distillation T95 [°C] max	360	360	360	360
Fatty Acid Methyl Ester (FAME) content [% v/v] max	-	-	-	7

Table 1.1 and Table 1.2 list European Union fuel specifications including gasoline and diesel respectively. These specifications might be well above the restriction imposed in many other countries but it is reasonable to postulate that these could be adopted in more countries around the world. These tightening specifications challenge the conventional refining technologies. For instance, sulphur contents in both gasoline and diesel fuels see a dramatic reduction, from 500 ppm to 10 ppm, almost free, which demands that refiners should have a clear understanding about different sulphur compounds present in refining streams because different sulphur compounds have very different kinetic properties, and then require quite different

operating conditions to eliminate. To implement it, a molecular level understanding about refining streams and processes should be achieved.

Table 1.2 European Union petrol specification

	EN 228	Directive 98/70	Directive 98/70	Directive 98/70
Entry to force	1993/1995	2000	2005	2009
Vehicle emission Standard equivalent	Euro II	Euro III	Euro IV	Euro V
Sulphur [ppm] max	500	150	50	10
Ried Vapour Pressure (RVP) [kPa] summer	35 - 100	60/70	60/70	60/70
Distillation [% v/v] min				
E100 (°C)	-	46	46	46
E150 (°C)	-	75	75	75
Hydrocarbon analysis:				
Olefins [% v/v] max	-	18	18	18
Aromatics [% v/v] max	-	42	35	35
Benzene [% v/v] max	5.0	1.0	1.0	1.0
Oxygen [% m/m] max	-	2.7	2.7	2.7
Oxygenates [% v/v] max				
Methanol	-	3	3	3
Ethanol	-	5	5	10
Iso-propyl alcohol	-	10	10	12
Tert-butyl alcohol	-	7	7	15
Iso-butyl alcohol	-	10	10	15
Ethers containing 5 or more carbon atoms	-	15	15	22
Other oxygenates	-	10	10	15
Use of additives				(MMT banned from 2010)

MMT: Methylcyclopentadienyl Manganese Tricarbonyl

1.3.2 Changing Market Demands and Supply

Basically, the oil consumption is expected to increase due to the rapidly growing economy of the world, especially in China and India. In 2030, the world is expected to consume nearly 27% more oil than in 2006, increased from 4029 Mtoe to 5109 Mtoe (World Energy Outlook, 2009). As the price of crude oil increases, the heavy fuel oil, as the feed for generating electricity, becomes less economic attractive. At the same time, it is forecasted that the fastest growing petroleum products will be distillate (including diesel, jet fuel, and kerosene), liquefied petroleum gas (LPG), and gasoline as illustrated in Figure 1.2 (Oil Market Report, 2009).

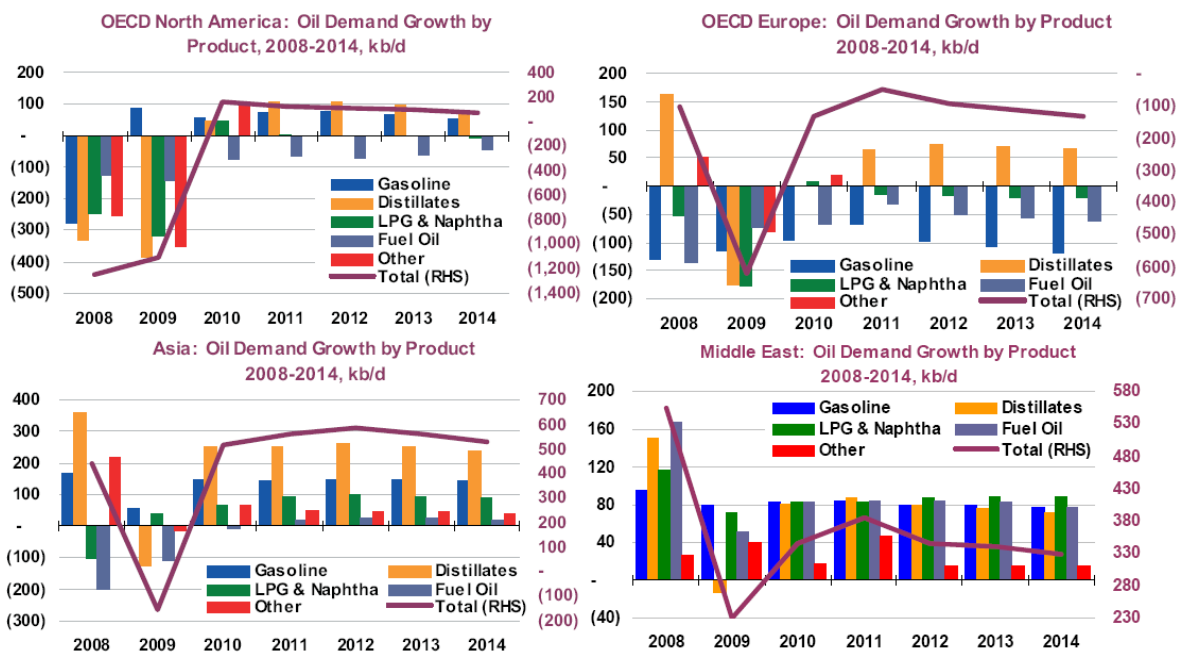


Figure 1.2 Oil demand growth by product, in North America, Europe, Asia and Middle East, 2008-2014 (Oil Market Report, 2009)

Many European countries have seen a rapid growth on the demand of diesel used by private cars due to its high driving characteristics, and commercial diesel use is also growing strongly in the Mediterranean and Eastern Europe. Much of the current refining capacity in Europe was commissioned at a time when the demand for diesel was relatively small and gasoline production was the key aim of refiners. While the overall refining capacity is roughly in line with current demand, there is a considerable imbalance in supply and demand between gasoline and diesel.

Since the late 1980s, crude oil slates have become heavier and sourer (Swain, 1998). Usually heavy crude oil would consume more utilities and capacities on the thermal and/or catalytic conversion processes. Moreover, the more heteroatom such as S, N, O, etc, contained in the heavy crude oil brings problems associated with pollution, catalyst poisoning, etc. This has led to an economic incentive to minimise invaluable heavier products and to maximise production of the more valuable light products.

The ability and extent of a refiner to achieve swinging products from gasoline to diesel and changing the selection of crude oil will largely depend on individual refining configurations. For example, a simple refinery with no upgrading facilities can only really influence product yields by processing alternative crudes. While there is an opportunity to target crudes with high middle distillate content, these are currently trading at a significant cost premium over heavier, more sour crudes. In addition, it is unlikely that there will be significant spare capacity in the downstream hydrotreater, which is essential to meet the current diesel sulphur specifications. Therefore, the changing market demand and supply restrains the achievable profit from the refinery.

1.3.3 Refining Margin and Refinery Optimisation

Refiners face difficulties in practically meeting the tight specifications with existing blend stocks and limiting the cut range of blend stocks, and current market demand. Hence, the product yield and the profit are reduced due to the increment in the production of lower value products. Much of the profit comes from processing a high throughput of crude oil in a refinery although it sees periods of high profitability in recent years.

Low refining margin has been promoting extensive work on process modelling and refinery optimisation, with the aim of pushing the operation of a refinery to give optimal performance and hence, maximum profit. Considerable research effort has been put into refinery optimisation since early 1950s, when linear programming technology started to produce industrial applications, mainly for planning purpose. Since 1970s, along with the rapid development of computer technology, more interests have been attracted to nonlinear programming and its application to

rigorous process simulation and optimisation. It is, however, apparent that models relating to process operations of different refinery units are highly non-linear. This then led to further research on how to handle the non-linearities related to the kinetics, thermodynamics, etc. of each process through non-linear programming technologies. The challenge then was to develop a rigorous approach that can account for both highly non-linear process models (containing detailed descriptions of operating conditions e.g. temperatures, pressures, etc.) and at the same time optimise the overall refinery performance.

On the other hand, as the basis of refinery optimisation, the industrial widely used conventional modelling methodology based on bulk property characterisation of feedstock has the inherent disadvantages. First of all, the specifications of molecular requirement on the refining products are not easily targeted since the conventional simulation model could not provide molecule information of products. On the other hand, the developed process models are not practical any more since the characteristics of feed stock and operating conditions are different. For example, with the less demand on fuel oils in the market, the heavy oils and residua may require deep processing in FCC. Thus modern FCC units are often required to process multiple feed streams from various sources such as a vacuum distillation column, delayed coker, hydrocracker, etc. In this case, bulk property characterisation cannot properly describe the composition of feedstocks with different processing history any more, because feedstocks with similar bulk properties could have significantly different molecular compositions. Various studies have indicated that reaction patterns differ between different molecule structures, therefore possibly leading to quite different product distribution for those different feed stocks. Therefore, the refiners are forced to deal with molecules rather than boiling ranges to manage its molecules to ensure survival.

Molecules are the common foundation for feedstock composition, property calculation, process chemistry, and reaction kinetics and thermodynamics. Molecule-based models can incorporate multilevel information from the surface and quantum chemical calculations to the process issues and can serve a common fundamental form for both process and chemistry research and development. Although detailed feed characterisation and chemistry insights on molecule level

are highly desirable in the refining processes modelling, it was unlikely to distinguish petroleum mixtures in the level of individual molecules due to the enormous complexities of petroleum fractions in the past few decades. Two technological advancements have helped modelling at the molecular level becomes achievable. One is recent developments in analytical chemistry that now permit the direct, or at least indirect, measurement of molecules in complex feedstocks and products. The other is advancements in information technology, especially the explosion of computational power, provide the possibility to track molecules during both reaction and separation processes. Collectively, these two enabling advancements motivate the development of refinery optimisation on a molecular level to help refineries conquer these external and internal challenges.

1.4 Molecular Management

Molecular management targets the right molecules to be at the right place, at the right time and at the right price (Aye and Zhang, 2005). It consists of molecular characterisation of refining streams, molecular modelling of refining processes, process level optimisation, and overall refinery optimisation integrating material processing system and utility system on the molecular level. As seen, the need to increase modelling details is not just a result of political regulations. The increase in the details of composition by means of molecular information also seems to be a very promising. In a long-sighted article on the future development of refining, Katzer et al. (2000) stated: “We believe the refinery will change more in the next 20–30 years than it has in the last 70 years.” One of the key issues they raised is how to increase the level of composition detail. This will bring a paradigm shift toward considering refinery processes “more and more like today’s chemical plants.” With such a molecular level of modelling detail, it should be possible to track the path of each individual molecule as it is processed. This should allow us to get the most value out of any molecular species.

1.5 Present Research

It is obvious that molecular management is of importance to ensure refiners’ survival, but achieving it is facing lots of challenges, which will be addressed separately in different chapters in terms of different aspects of molecular

management. In this work, four aspects relating to molecular management, including molecular characterisation of refining streams, molecular modeling of refining processes, process level optimisation on a molecular level, and overall refinery optimisation considering utility system, will be explored related to two most profitable products, which are gasoline and diesel.

1.6 Structure of Thesis

This thesis consists of seven chapters. A brief overview of each chapter is as follows.

Chapter 2 Molecular characterisation of petroleum fractions

The complexity nature of petroleum fractions is introduced firstly, followed by a brief review of existing methods including traditional methods, laboratory analytical methods, as well as computer-aided molecularly explicit characterisation methods which is the focus of this research. By illustrating the limitations of the existing methods, finally a novel methodology is proposed to overcome these disadvantages.

Chapter 3 Molecular modelling of gasoline blending

This chapter consists of three distinct aspects. Firstly, a brief introduction about gasoline blending operation including blending streams, the type of blending, as well as the gasoline specifications, is described. In the second section, a series of procedures are developed to predict the properties and compositions of blending feedstocks based on the easily obtained information with a high accuracy by employing the molecular modelling technique. The last part will introduce a molecular blending model to achieve an optimal recipe of gasoline blending with the tighter control on the property giveaway for the maximum profit.

Chapter 4 Molecular modelling of catalytic reforming

This chapter, first, briefly introduces catalytic reforming process, along with a short review of previous work on modelling of catalytic reforming. To build up a molecular model of a catalytic reformer, chemical reactions and modelling of the reactor are described respectively. Another important issue of catalyst deactivation,

which has a serious impact on the economic performance of a catalytic reforming, is also considered in a reasonable way. Finally, a multi-period process level optimisation model is developed with the consideration of catalyst deactivation.

Chapter 5 Molecular modelling of diesel hydrotreating

In the chapter, a detailed kinetic model for hydrotreating process with a three-phase reactor based on feedstocks and products in terms of the MTHS matrix representation is developed. Beyond the molecular modelling of a diesel hydrotreater, a multi-period model of run cycle is proposed to take the catalyst deactivation into account, and a process optimisation model is developed to help the refiners increase margins as well.

Chapter 6 Integrated site and process optimisation with molecular modelling

This chapter, first, introduces the challenges of refinery optimisation, followed by a brief review of optimisation techniques. Then, a decomposed strategy is incorporated with molecular management. The integrated framework is applied in an overall refinery optimisation, including site and process level optimisation based on molecular management. Secondly, an exploitation of interactions between hydroprocesses, with rigorous process models based on molecular information, and a hydrogen network is investigated by applying the proposed methodology.

Chapter 7 Conclusions and future work

Conclusions are drawn from this research, and some suggestions are made for future work.

Chapter 2 Molecular Characterisation of Petroleum Fractions

2.1	Introduction	34
2.2	Complexity Nature of Petroleum Fractions	34
2.3	Review of Previous Methods	35
2.3.1	Traditional Methods	35
2.3.2	Modern Analytical Laboratory Methods.....	36
2.3.3	Computer-aided Molecular Explicit Methods.....	38
2.3.4	Existing MTHS Methods	43
2.3.5	Limitations of Existing MTHS Methods.....	44
2.3.6	A Brief Case Showing the Shortcomings of the Existing Methods	45
2.4	A Modified MTHS Framework	48
2.5	Improved MTHS Matrix Representation Model.....	49
2.5.1	Improved MTHS Matrix Representation Model for Light Petroleum Fractions	49
2.5.2	Improved MTHS Matrix Representation Model for Middle Petroleum Fractions	50
2.6	Transformation Methodology	55
2.6.1	Assumptions.....	55
2.6.2	Mathematical Model	60
2.7	Optimisation Engines	65
2.8	Case Studies	67
2.8.1	FCC Gasoline Stream Case.....	67
2.8.2	SRGO Feed	70
2.8.3	LCO Feed	75
2.9	Summary	77

2.1 Introduction

The characterisation of petroleum fractions has received significant attention in recent decades because the understanding of refining feedstock and products is the very fundamental step to the design and operation of almost every refining process, which consequently has a significant impact on economic performance in refining industry. Most of traditional characterisation methods are based on physical bulk properties such as boiling point, specific gravity, etc., mostly due to the limitations in the analytical chemistry and computer hardware and software capabilities. Along with the state-of-art chemistry analytical technological advancements, and the explosive growth of information technology, molecularly explicit characterisation methods have been developed intensively to comply with higher product quality specifications and more stringent environmental regulations, with more emphasis on the molecular composition of refining products.

In this chapter, the complexity nature of petroleum fractions is introduced firstly, followed by a brief review of existing methods including the traditional methods, laboratory analytical methods, as well as computer-aided molecularly explicit characterisation methods. By illustrating the limitations of the existing methods, finally a novel methodology is proposed to overcome these disadvantages, which is demonstrated in case studies.

2.2 Complexity Nature of Petroleum Fractions

Refining streams or petroleum fractions are the products or intermediate products of crude oil through three major different refining processes of separation, conversion and finishing, and each of them is a unique mixture of thousands of different molecules. These molecules mainly fall into two categories: hydrocarbon composing of hydrogen and carbon atoms only, and hydrocarbon with heteroatoms such as sulphur, nitrogen, oxygen, etc. Crude oil composition schematic (Environmental Protection Agency, USA) in Figure 2.1 shows the complexity of typical petroleum hydrocarbon type analysis for Arabian heavy crude. In addition, Figure 2.2 shows the numbers of isomers become literally astronomical in heavy petroleum fractions. Besides dealing with the numerous isomers, the heteroatoms

such as sulphur, nitrogen and oxygen, etc. that involve a variety of functional groups at various possible locations within a molecule impose further difficulties in carrying out exact compositional analysis. Although such molecule by molecule analysis might not be essential, but to comply with the environmental regulations and further understand the nature of streams, molecular analysis to a certain extent is necessary.

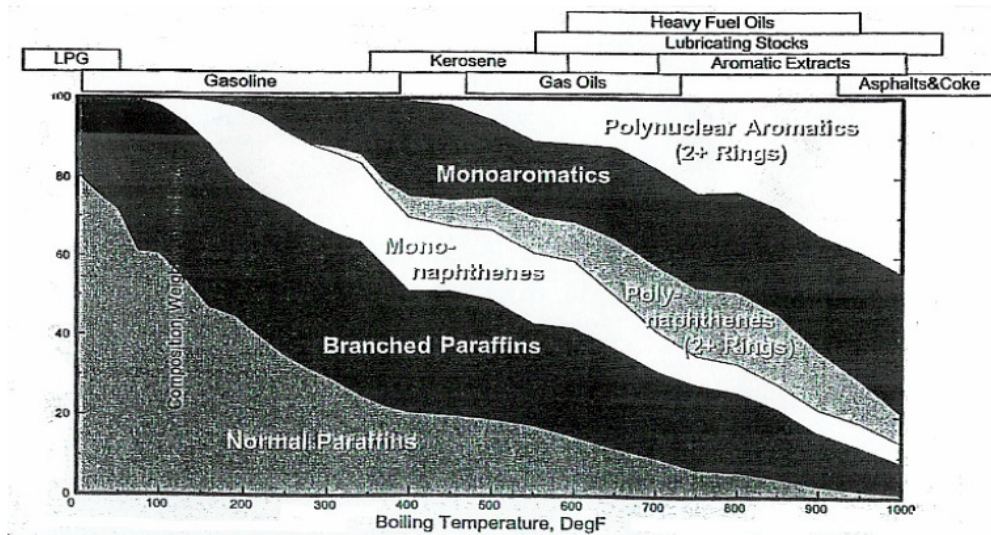


Figure 2.1 Complexity of typical petroleum hydrocarbon type analysis (www.epa.gov)

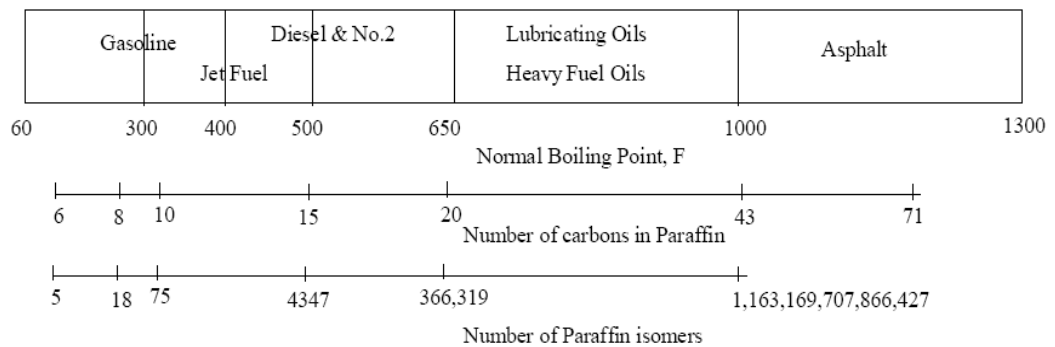


Figure 2.2 Chemical complexity of higher boiling products (Read, 1976)

2.3 Review of Previous Methods

2.3.1 Traditional Methods

Most traditional process models and even the current widely used commercial software tools group the molecules mainly according to its bulk properties. Three characterisation methods with the non-molecule basis are pseudocomponent

characterisation, compound class characterisation, and average structure parameters characterisation.

The pseudocomponent concept (Katz and Brown, 1933) is to transpose ASTM (American Society for Testing and Materials) curves into a representative set of components. A petroleum fraction or crude oil TBP (True Boiling Point) curve is divided into close-cut fractions, which are then handled as pure components. Design procedures for crude oil distillation based on pseudocomponents have been proposed and have found widespread industrial acceptance. Compound class characterisation is based on chromatographic separation and describes oil mixtures, in terms of operationally defined fractions. As the compound classes are defined by their solubility characteristics, their molecular nature is not well defined. Average structural parameter methods describe a petroleum mixture using structural parameters, such as the number of aromatic rings, the carbon/hydrogen ratio, etc., from results obtained from laboratory methods such as nuclear magnetic resonance spectrometry and elemental analysis. The pitfall of these methods is that the functional groups fail to provide information about the actual components.

One of common disadvantages on the traditional characterisation methodology is that they fail to represent detailed molecule information, which both increasing technical and environmental concerns have focused on.

2.3.2 Modern Analytical Laboratory Methods

Along with the state-of-art chemistry analytical technological advancements, laboratory methodology such as gas chromatography (GC), high performance liquid chromatography (HPLC), mass spectroscopy (MS), nuclear magnetic resonance spectroscopy (NMR) and many other newly developed methods could identify and quantify most of several hundred molecules present in the petroleum fractions. The basic principles and the typical applications of these analytical methods would be briefly interpreted in the following sections since they are fundamental to the molecularly explicit characterisation models.

Basically GC, mainly used in the analysis of light and middle distillates due to its high resolution, separates molecules according to their boiling points. It is invented by Martin and Synge, who suggested its possibility in a paper on liquid

chromatography published in 1941 (Martin and Synge, 1941). Johansen et al. (1985) developed a gas chromatography method to analyse the hydrocarbons by structural group type in gasoline and distillates. Matisová et al. (1985) claimed that high resolution capillary gas chromatography (HRCGC) could provide complete component analysis of refining streams and hence offer petrochemical engineers with the information and knowledge required to convert crude petroleum into profitable products. Teng (1994) developed a gas chromatography – mass spectrometric (GC-MS) method equipped with special software and included the analysis of oxygenated compounds in a single run. It is one of the few techniques capable of distinguishing between paraffins and naphthenes, thus providing a true PIONA (Paraffins, Isoparaffins, Olefins, Naphthenes, and Aromatics) analysis, which is often required in the control of gasoline production.

HPLC utilises a column that holds chromatographic packing material (stationary phase), a pump that moves the mobile phase(s) through the column, and a detector that shows the retention times of the molecules. The mechanism of adsorption, desorption and partition of those components between packing and solvent is used in HPLC to separate components. It is widely used in the analysis of heavier petroleum fractions. Separation of aromatic compounds based on the number of aromatic rings is one of the features of HPLC analysis.

NMR is based on the principle that proton and ^{13}C nuclei in different chemical groups have different electronic environments and hence different resonance conditions. They can measure directly aromatic and aliphatic carbons; hydrogen distributions and the concentration of various structural groups can be determined when combined with elemental analysis. ^1H and ^{13}C are responsible for revealing the complicated structures of petroleum fractions.

MS by far provides the most detailed information on the compositions of petroleum fractions. It analyses compounds according to their molecular weight and chemical formula $\text{C}_n\text{H}_{2n+Z}\text{X}$, where C is Carbon, H is hydrogen while X refers to heteroatoms while n is the number of carbon and Z is the hydrogen deficiency. Although it could provide important information about the molecular structure, its application is limited to light petroleum fractions such as gasoline.

Compared with the traditional characterisation approaches, modern laboratory analytical technology to some certain extent shows its advantage of retrieving the detailed molecule information directly or indirectly. On the other hand, it is these capabilities of chemistry analysis that enhances the possibility of bringing the brand new characterisation methodology for refining streams. However, the main two disadvantages of time and cost consumption preclude its wide use in the refining industry, especially for the refinery online/offline optimisation. More importantly, then analytical approach has reached its limitations due to the complexity nature of heavy stream as reviewed in the previous section.

2.3.3 Computer-aided Molecular Explicit Methods

With the development of information technology, computer-aided molecular explicit methods have seen a more rapid growth. Most endeavors on this contain two basic problems. One is a representation model - what can be used to represent petroleum streams with the astronomical number of hydrocarbons and hydrocarbons with heteroatoms. The other is a transformation methodology - how molecular information is obtained since streams with similar bulk properties could have significantly different molecular compositions. To solve these problems, several challenges need to be tackled properly.

2.3.3.1 Challenges of Molecular Characterisation Methods

As mentioned before, the complexity nature of petroleum fractions precludes determining the complete molecular composition. Therefore, how to select the representative molecules, as well as how to consider isomers in a reasonable way is the first challenge to molecular characterisation of petroleum fractions.

Even the representative molecules have been determined, a large amount of properties of the representative molecules are not easily obtained. Properties of a mixture depend on the properties of its constituents. Generally, properties include physical properties, thermodynamic properties, and transport properties. Physical properties have density, boiling point, molecular weight, and refractive index, etc., and thermodynamic properties include enthalpy, heat capacity, heat of vaporization, equilibrium ratios, and fugacity, etc. Transport properties include viscosity, thermal conductivity, diffusion coefficient, and surface tension, etc.

There are also some properties which reflect the quality of fuels, such as cetane number for diesel, octane number for gasoline, etc. Although not all of these properties are necessary for the molecular characterisation, it would enhance the accuracy of predicting the molecular composition if applying more properties, because different characteristics of molecules could be captured.

Most of properties do not blend linearly, which means different mixing rules should be built up to calculate the properties of the mixture based on the properties of pure compounds. Sometimes, established mixing rules could only be applied in a certain narrow range. Therefore, they should be used properly.

The common practice to characterise petroleum fractions on a molecular level is transforming bulk properties into molecular composition by minimising the difference of the bulk properties between the calculated and measured. However, lots of different molecules could have similar properties, which make this method hard to distinguish molecules with different structures but similar properties, while the molecules with different structures have quite different reaction patterns.

Regarding to representation model for characterisation, two kinds of methods have been developed: stochastic and deterministic methodology. The main difference between these two methods is the way to decide the representative molecules.

2.3.3.2 Stochastic Methods

The idea behind the stochastic methodology is that any molecule in a petroleum stream can be viewed as a collection of molecular attributes (number of aromatic rings, number of naphthenic rings, number of side chains, length of side chains, etc.), each of which is represented by a PDF (probability density function). The PDF is a function that provides the probability of finding the value or less of a given attribute. By sampling the attribute PDFs, the values of the structural attributes for an individual molecule can be determined, which in turn specifies the molecule.

Neurock et al. (1990, 1994) developed a Monte Carlo construction technique whereby petroleum molecules are stochastically constructed by random sampling of PDFs, one for each molecular attribute. Monte Carlo sampling of the set of

PDFs provides a large ensemble of “computer” molecules whose properties can be compared to experimentally measured values. Campbell (1998) developed the overall steps to transform indirect analytical information about the molecules in a feedstock into a molecular representation. Both the identities and weight fractions of the molecules are sought (see Figure 2.3). Recent work on the stochastic method was done by Hudebine and his colleagues (2002, 2004).

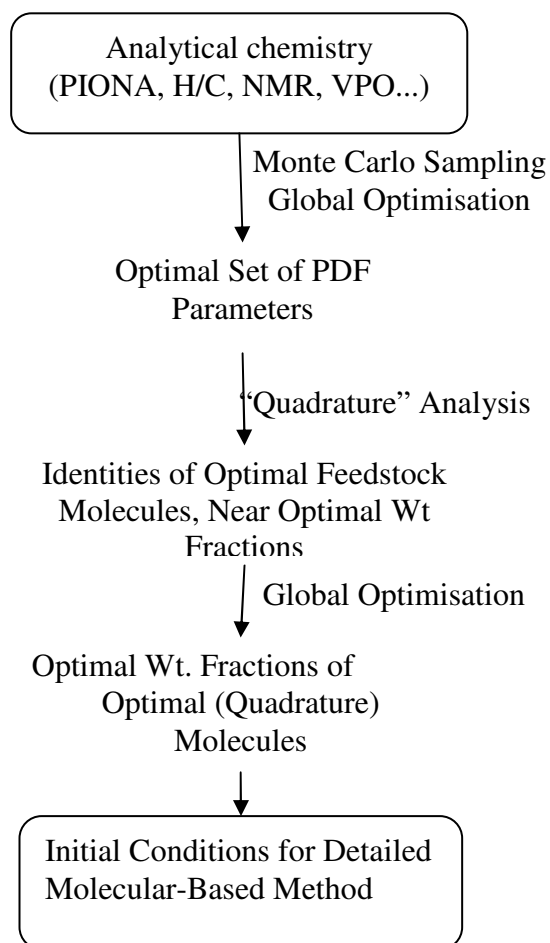


Figure 2.3 Flow diagram of stochastic modelling of molecular structures and compositions of a complex feedstock (Campbell, 1998)

It is worthy to note that the concept of using PDFs to describe complex mixtures has existed for a long time. Flory (1936) developed a modified gamma distribution to describe the molecular size distribution of condensation polymers. Libanati (1992) studied the thermal degradation of an infinite polymer and indicated that the molecular weights of the products followed a log-normal distribution. The application of probability distribution functions was extended to petroleum fractions when it was hypothesized and later confirmed that kerogen, which breaks

down to form oil, could be modelled as an infinite polymer, and thus, the molecular weight distribution of oil should be similar to that of polymer products. Shibata et al. (1987) used mixed distributions to enhance phase equilibrium calculations for a petroleum reservoir. Whitson (1990) used a gamma distribution to fit the molar and weight distribution of the C₇₊ fraction of crude oil, further supporting the notion of representing crude oil components with PDFs. Riazi et al. (1997) developed a versatile correlation based on an extensive analysis of more than 100 mixtures. In addition, direct experimental evidences also provide the same pattern. Pederson et al. (1992) showed that an exponential distribution could be used to accurately predict the quantities of heavier components.

Although the stochastic method was fairly accurate in representing the composition in heavy oil, the method is impractical for use in detailed kinetic modelling with the computational power available today, especially for the refinery optimisation.

2.3.3.3 Deterministic Methods

The main reason of the time-consuming characteristic for the stochastic method is that a new library of possible molecules is generated for each new simulation. A deterministic methodology is significantly faster than stochastic methods by predefining a molecular library which makes it more attractive for commercial packages. Thus the predefined library is extremely important for the accuracy to represent the petroleum fractions since if an important component is not included in the library, the obtained composition can never be representative for the mixture. The ways for constructing a molecular library range from experimental methods (Wahl et al., 2002) to group contribution methods (Hudebine et al., 2002).

Jabr et al. (1992) attempted to characterise petroleum naphtha by dividing it into five cuts with unified boiling ranges, the physical properties of which are calculated using correlations from the literature. For each cut, representative chemical components are assumed, the compositions of which are determined by solving a system of linear equations to arrive at the properties of the blend. However, the assumption that only five components or less can be used within each cut, since only five independent properties were considered, led the authors to

use 9 true components and 16 pseudocomponents in a 25-component feed when testing the method on a debutanizer feed.

Albahri (2005) recognised that a boiling point curve provides an infinite number of experimental data which can be used to estimate the composition of any number of pure components as desired. However, the number of components chosen to represent a petroleum fraction, the key factor to determine the representation accuracy, is hard to decide. Van et al. (2007) developed a methodology based on Shannon's entropy criterion and allows generating a molecular composition of a naphtha fraction that meets all the boundary conditions set by the industrially available commercial indices. It is attractively fast due to the transformation of a nonlinear equation in the N mole fractions ($N \sim 102$) into a nonlinear equation in with maximal 14 parameters. Similarly, the candidate feedstock molecules as the crucial element for the success of representing petroleum fractions is not easy to decide, as the paper showed that the simulation results from a library with 173 components is observed worse than that with the reduced library containing 37 molecules. As the author pointed out that the main reason for this behaviour is that the entropy method is too insensitive to predict mole fractions of non-important components accurately, because it differentiates between components based on the difference in physical properties of these components.

García et al (2010) developed a method to characterise gas oil, and thereafter, the achieved molecular composition is successfully applied in hydrotreating. By representing composition of gas oil by 28 chemical families and 30 carbon numbers (from 1 to 30), the method applies two standard distributions for the families with and without polycyclic core for the length of the alkyl side chains to calculate the distribution of molecules within each family, and the overall fraction of each family is calculated based on three chemical analyses.

As reviewed above, one key to the accuracy of representing a petroleum streams is a proper representative molecule model. Molecule Type Homologous Series (MTHS) matrix representation, firstly presented by Peng (1999) followed by continuous development, brings the possibility to overcome this problem.

2.3.4 Existing MTHS Methods

In an attempt to extend the molecular modelling into the refinery optimisation framework, Peng (1999) introduced the concept where MTHS characterisation of a petroleum mixture is visualised as a matrix where the rows represent carbon number and the column representing the homologous series.

Molecules that belong to a homologous series have the same base structure with varying carbon numbers. In the matrix, molecules belonging to a homologous series with the same carbon number are lumped into a single entry. Apart from the hydrocarbon molecules, different sulphur and nitrogen compounds are also present in the matrix. The different base structures of each series are captured by difference in molecular types such as benzene ring, naphthene. The element defined in the matrix represents molar/weight percent of either a single molecule or a lump of all possible molecular isomers.

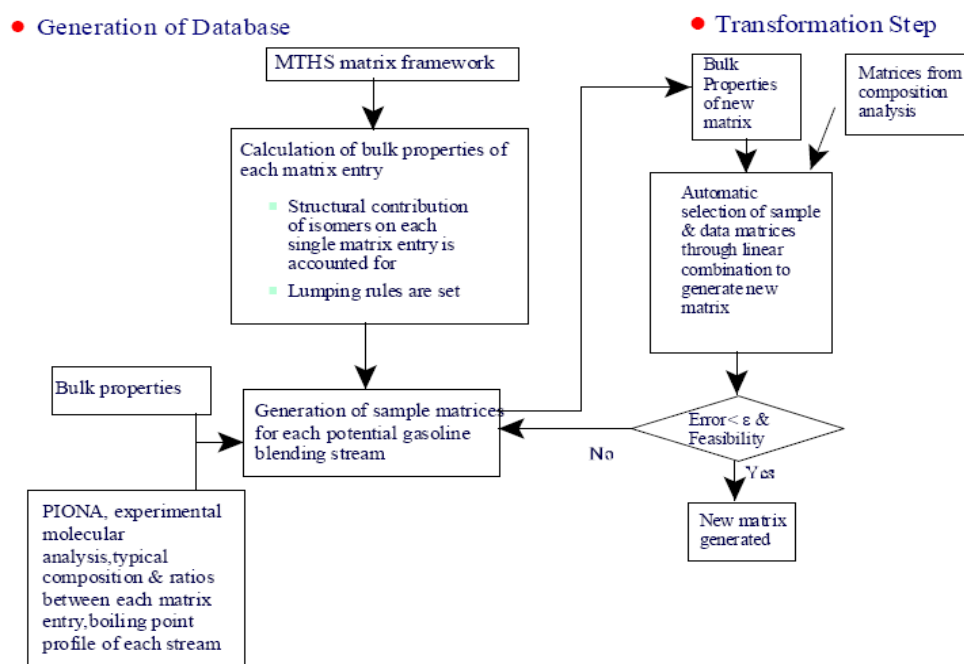


Figure 2.4 Schematic representation of the methodology (Aye, 2003)

Based on MTHS matrix, Zhang (1999) developed an approach to transfer bulk properties into molecular composition. Aye (2003) extended MTHS framework to consider isomers, and enhanced the transformation method by generating sample streams database to consider the processing history as shown in Figure 2.4.

2.3.5 Limitations of Existing MTHS Methods

The existing MTHS methodology to some extent improves the performance of characterisation of light fractions. However, its inherent limitation prevents the wide application. The limitations of the existing MTHS methodology would be analysed on both representative model and transformation method.

2.3.5.1 Limitation of Representation Matrix

The representation MTHS matrix is different for light and middle petroleum fractions because that molecular species existing in middle fractions are more complex than those in the light fractions. So the limitations of representation matrix of existing method will be discussed for two types of fractions separately.

Table 2.1 Typical Measured Isomer Distribution (wt %) for *i*-Octane (Ghosh, 2006)

Stream Type	Monomethyls	Dimethyls	Trimethyls
Alkylates	0	18.5	81.5
Reformats	68.9	31.1	0

For light fractions, the assumption of the fixed internal distribution between isomers for all refinery processes in the exiting MTHS matrix is not accurately applicable in practice. The methodology assumes that the isomers are in thermodynamic equilibrium then lumping isomers into one entry of matrix. This assumption is true for some processes, but not for all processes. Table 2.1 shows that the distribution of isooctane in reformates is inconsistent with that in alkylates.

Lumping all isomers together neglects the significant difference on both physical and chemistry properties. The analysis results from the American Petroleum Institute Research Project 45 demonstrate that the structural contributions lead to dramatic changes of research octane number between isomers, well illustrated by Figure 2.5. Similar difference could be observed in other properties such as Reid Vapour Pressure (RVP), viscosity, etc. Meanwhile, chemistry patterns would differ significantly for different isomers (Lappas, 1999).

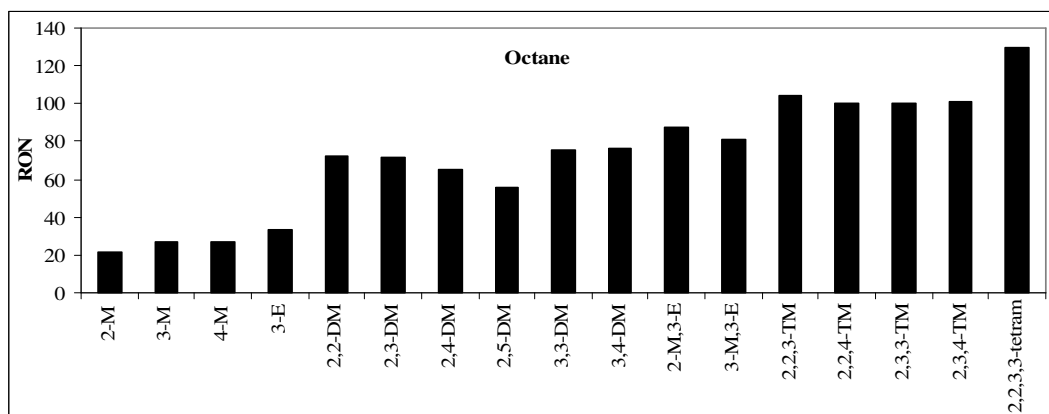


Figure 2.5 Research octane number of isooctane isomers (Ghosh, 2006)

Regarding to the representation matrix for middle petroleum fractions, isomers of each entry have not been taken into consideration, in which currently just straight chain alkyl substitute is used as a representative for each entry.

2.3.5.2 Limitation of the Transformation Method

In terms of the transformation methodology, there exist several shortcomings. First of all, the existing approach demands a large amount of sample matrices in the database, which is extremely difficult, especially for heavy fractions. Secondly, if the properties of sample streams do not cover the properties of the predicted streams, molecular composition cannot be predicted accurately because it assumes that the predicted stream is a blend of several well-characterised sample streams. Thirdly, the problem that the fractions with similar properties could have significantly different molecular compositions is not tackled at all. Last but not least, from mathematical perspectives, the problem of existing lots of local optimums, which present different molecular compositions, has not been considered.

2.3.6 A Brief Case Showing the Shortcomings of the Existing Methods

To illustrate the shortcomings of the existing approach, a simple case is studied. The stream is the gasoline product of a FCC process, with the distillation profile in Table 2.2 and the measured properties.

Table 2.2 Distillation profile of a FCC stream

Cumulative (vol%)	Temperature (°F)
5	74.85
10	87.71
30	149.58
50	204.91
70	281.51
90	328.09
95	347.15

Two groups of results were presented by applying two different sample matrix numbers from a sample database containing 250 samples (Desai, 2008). Seed40 is with 40 samples, while seed80 has 80. Table 2.3 compares the result of measured properties between measured and two groups of estimated properties respectively.

Table 2.3 Comparisons of properties between measured and two groups of estimated

Properties Comparison					
	Msd	Seed40	Diff (%)	Seed80	Diff (%)
MW	97.49	97.49	0.00	97.49	0.00
SG	0.75	0.75	0.00	0.75	0.00
RVP(psi)	6.17	6.17	0.00	6.17	0.00
RON	90.89	91.68	0.86	92.07	1.29
MON	78.06	77.73	-0.43	78.20	0.18
P(vol%)	4.22	4.22	0.00	4.22	0.00
I	24.80	24.80	0.00	24.80	0.00
O	32.99	32.99	0.00	32.99	0.00
N	8.97	8.97	0.00	8.97	0.00
A	29.02	29.02	0.00	29.02	0.00

Msd: the Measured

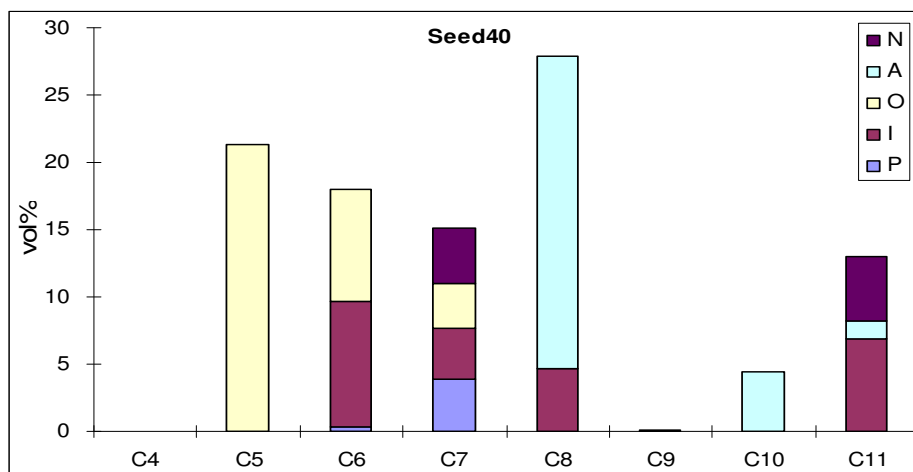


Figure 2.6 Predicted molecular composition with 40 sample matrices

Illustrated as Table 2.3, the existing MTHS method has an excellent performance on minimising the difference between the measured and the estimated. Regarding to molecular composition for the FCC gasoline, two totally different results are observed as Figure 2.6 and Figure 2.7. The predicted molecular composition with 40 sample matrices has a small C₉ concentration of 0.11%, olefin fully occupied by C₅, and high aromatics of C₈ etc., which obviously fits badly with reality.

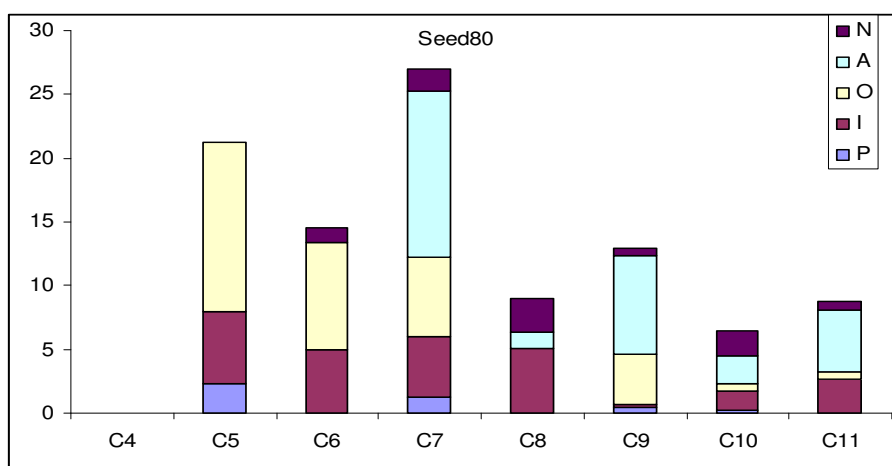


Figure 2.7 Predicted molecular composition with 80 sample matrices

Another issue related to molecular characterisation of petroleum fractions is also presented in this case, which is that streams with different molecular compositions could have similar bulk properties as seen from the results with seed40 and seed80.

To summarise, the existing approach is needed to improve, and some aspects even have not been considered at all. In this work, an improved MTHS framework is developed in order to address the shortcomings of the existing approach.

2.4 A Modified MTHS Framework

The proposed modified MTHS framework as Figure 2.8 consists of two separated steps, namely database setup and transformation step. The database setup starts with collecting pure component properties from the property databanks of API-TDB, AIChE-DIPPR, PGL and others, and estimating the properties using correlations for those which are not available. The second step in database setup is to calculate properties of each entry of the proposed MTHS representation matrix introduced in section 2.5 by proper mixing rules.

Regarding to the transformation step, the emphasis of this step is the transformation of bulk properties into molecular composition by integrating the assumptions detailed in section 2.6.1. The first step is the laboratory analysis of petroleum fractions, comprising the measurement of fundamental properties such as distillation profile, specific gravity, etc. The other properties, if not available, could be estimated by correlations. The second step in this scheme comprises using an optimisation program that calculates the optimal molecular composition for the predicted fraction. The mathematical model is discussed in section 2.6.2.

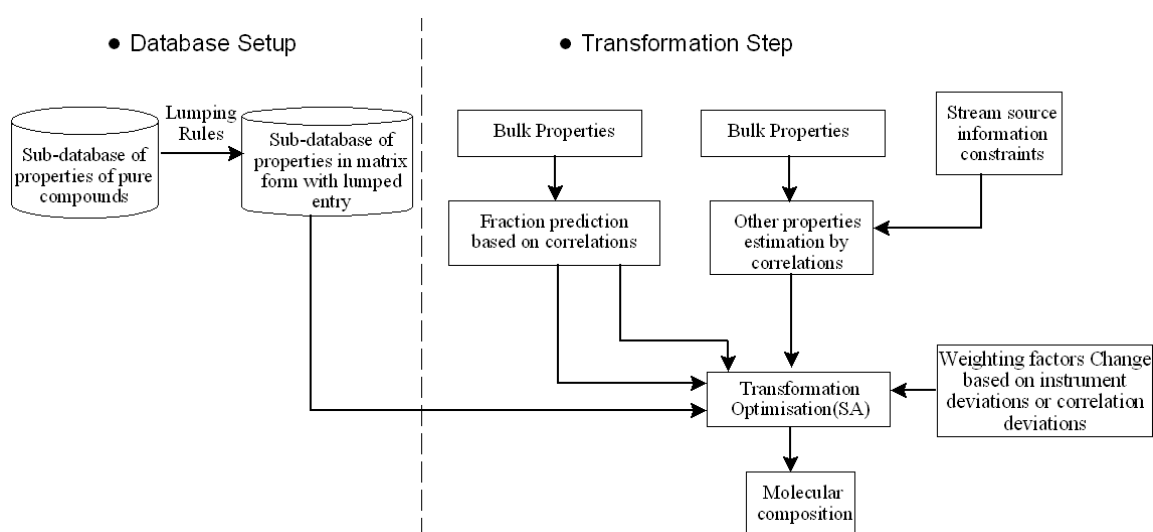


Figure 2.8 New MTHS framework for the characterisation of refining streams

2.5 Improved MTHS Matrix Representation Model

2.5.1 Improved MTHS Matrix Representation Model for Light Petroleum Fractions

Table 2.4 New MTHS representation matrix for light petroleum fractions

Sulphur Content (wt %) = Nitrogen Content (wt %) = Oxygenates content (wt %) =								
	NP	MP	DP	TP	NO	BO	N	A
C4								
C5								
C6								
C7								
C8								
C9								
C10								
C11								
C12								

Table 2.4 illustrates the new MTHS representation matrix for light petroleum fractions, where the rows stand for carbon numbers and the columns for homologous series, with sulphur, nitrogen and oxygenate contents. The molecules with the same homologous series and carbon number are lumped into one entry of the matrix as they have similar properties. The elements defined in the matrix represent the molar/weight/volume percent of either a single molecule or a lump of all possible structural molecular isomers.

The limitations of the analytical techniques and the knowledge on refinery process chemistry determine which molecular types and homologous series are incorporated in the matrix. Aye (2005) tried to catch the structural contribution on properties by assuming thermodynamic equilibrium for calculating the internal distribution between isomers. Instead of lumping all isomers into one entry, the new MTHS matrix lumps isoparaffins into three homologous series: monomethyls (MP), dimethyls (DP), and trimethyls (TP) isoparaffins, and lumps olefins into two series: normal (NO) and branched olefins (BO). The main reason for constructing

the new homologous series is based on the observations that the two key properties of gasoline streams – ON and RVP (Reid Vapour Pressure) are similar for isomers within each new homologous series, and molecules belonging to MP, DP and TP take the majority of the isoparaffins concentration. Although the physical properties for olefin isomers do not differ significantly, chemistry patterns are different (Lappas, 1999). Regarding naphthenes and aromatics, there are small variations in the physical properties of isomers and the detailed information on isomers might not be available. In summary, each entry is a lump of isomers with the same homologous series and carbon number.

2.5.2 Improved MTHS Matrix Representation Model for Middle Petroleum Fractions

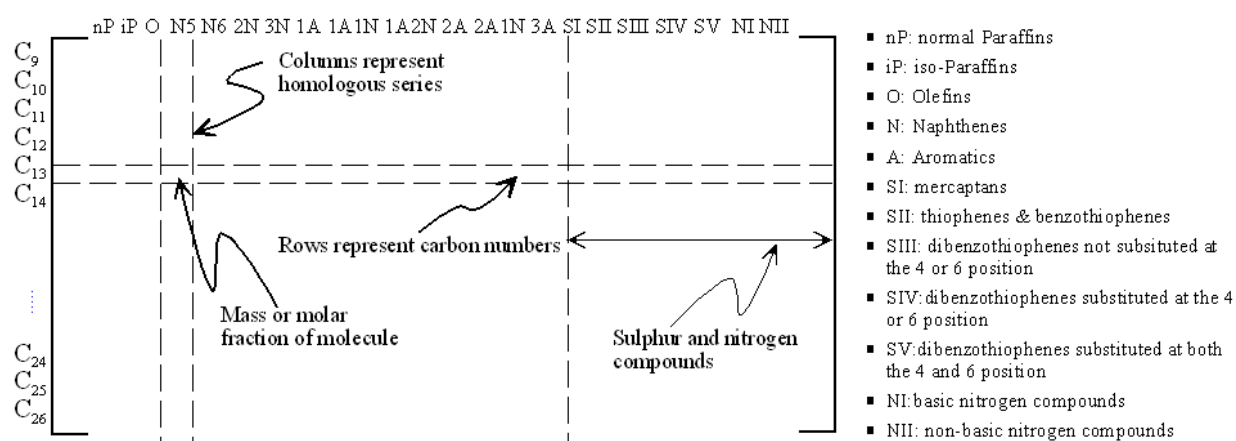


Figure 2.9 MTHS Matrix representation of diesel fractions (Peng, 1999)

Figure 2.9 shows the MTHS representation matrix for diesel streams, which is different from the matrix for gasoline stream. Generally, gasoline streams cover C₄ to C₁₂, and diesel streams cover C₉ to C₂₆. Due to astronomical number of isomers for heavier hydrocarbons, isoparaffins are lumped into one homologous series rather than three as for gasoline. More homologous series are incorporated into the matrix for diesel streams. Hydrocarbons are divided into 13 homologous series: nP, iP for normal and iso-paraffins, O for olefins, 1N, 2N, 3N for naphthenic compounds, 1A, 2A, 3A for one-ring to three-ring aromatic compounds, 1A1N, 2A1N, 1A2N for compounds containing both naphthenic and aromatic rings. Regarding hydrocarbons with heteroatoms, sulphur compounds are lumped into five homologous series, SI, SII, SIII, SIV and SV, according to different kinetic

characteristics, which is critical to the refining processes modelling, especially hydroprocessing. The same strategy is applied for nitrogen compounds, as lumping it into NI and NII.

One of the most challenging problems for petroleum fraction analysis is the rapid growing number of isomers with increasing boiling point of petroleum fractions, especially in middle and heavy petroleum fractions. Read (1976) demonstrated that the number of paraffin isomers reaches the order of 10^7 or 10^8 when the carbon number comes to 25. To consider isomers for middle petroleum fractions properly, a set of rules is set up.

- Enumerating isomers of each entry in the MTHS matrix using the software (SMOG, Institute of Organic Chemistry, Russian Academy of Sciences), up to a carbon number as high as possible;
- For those entries for which not all isomers can be enumerated, parts of molecules with a certain characteristics (low Gibbs Energy) are enumerated;
- Apply the group contribution method (Prausnitz, 2001) to calculate the properties of each isomer;
- Assume that isomers are in the thermodynamic equilibrium, and calculate the internal distribution of isomers;
- These isomers are lumped into each entry, and the properties of each entry are calculated based on mixing rules.

Structural Molecular Generation (SMOG) is a program for exhaustive, irredundant, and efficient generation of chemical isomers by their gross formula and a set of structural constraints (Institute of Organic Chemistry, Russian Academy of Sciences). In our case, the structural constraint is the basic structure of each homologous series. The output of SMOG is a matrix, which represents the connection between elements as Table 2.5 and Figure 2.10 show.

The entry which connects carbon and carbon in the matrix represents the bond number, such as C2 and C3 connected by double bonds. The entry connecting carbon and hydrogen represents hydrogen number. The matrices from SMOG are transformed to basic structures that the Joback group contribution method needs.

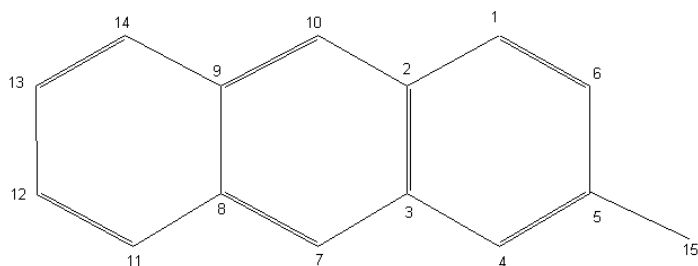


Figure 2.10 $C_{15}H_{12}$ isomer corresponding to Table 2.5 generated by SMOG

Table 2.5 One of $C_{15}H_{12}$ isomers output from SMOG

	C1	C2	C3	C4	C5	C6	C7	C8	C9	C10	C11	C12	C13	C14	C15
C1	-														
C2	1	-													
C3	0	2	-												
C4	0	0	1	-											
C5	0	0	0	2	-										
C6	2	0	0	0	1	-									
C7	0	0	1	0	0	0	-								
C8	0	0	0	0	0	0	2	-							
C9	0	0	0	0	0	0	0	1	-						
C10	0	1	0	0	0	0	0	0	2	-					
C11	0	0	0	0	0	0	0	1	0	0	-				
C12	0	0	0	0	0	0	0	0	0	0	2	-			
C13	0	0	0	0	0	0	0	0	0	0	0	1	-		
C14	0	0	0	0	0	0	1	0	0	0	0	0	2	-	
C15	0	0	0	0	1	0	0	0	0	0	0	0	0	0	-
H	1	0	0	1	0	1	0	0	1	1	1	1	1	1	3

To set up and simplify isomers generation rules, some entries of each homologous series are investigated to get the property of boiling point and distribution between isomers based on the assumption that isomers are in the state of thermodynamic equilibrium. Figure 2.11 shows the result of molecules (C_{17} , A).

Some observations for the entry of (C_{17} , A) are outlined as follows:

- The entry of (C_{17} , A) has 26071 isomers;

- Joback group contribution method can distinguish 56 different isomers without the capability to consider the position of basic structures;
- Boiling points of isomers have a big difference between each other, which can be as high as 605 – 640 K;
- The majority of the isomer composition is occupied by a small part of isomers, which have branches on an aromatics ring as many as possible.

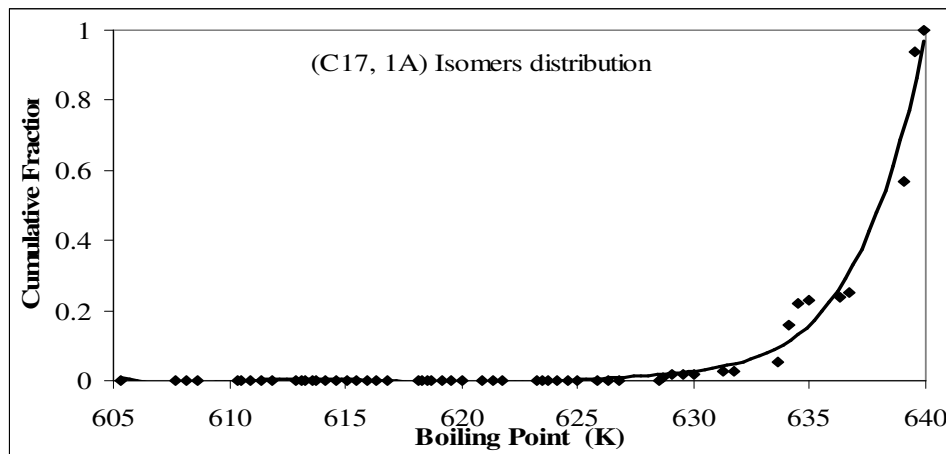


Figure 2.11 (C₁₇, A) isomers distribution with boiling point

The analysis is carried out on some entries to find out the particular characteristics for each homologous series. Based on these observations and characteristics analysis, a structure fragments list is generated to reduce isomer generation for those entries with an astronomical number of isomers. The molecules constructed by those fragments would have lower Gibbs energy, which then take the majority of the isomer composition. Table 2.6 gives the isomer number of each entry from SMOG.

Group contribution methods are based on the principle that the properties of a compound are the function of the atoms and structural groups combining to form the compound. Group contribution methods estimate the physical properties of a species by using the contributions that have been assigned to different atoms and atomic groups for each type of physical constant (Prausnitz et al., 2001). The method of Joback and Reid (1987) is adapted in this work as it covers a broad range of compounds and functional groups and is simple in application.

Table 2.6 Isomers generation of each homologous series (* represent the property of the entry is calculated by extrapolation or interpolation)

	IP	IO	1N	2N	3N	1A	1A1N	1A2N	2A	2A1N	3A
9	34	153	12			11					
10	74	377	40	1		32	1		1		
11	158	914	106	3		79	4		2		
12	354	2281	317	20		218	22		12		
13	801	5690	868	81		555	80		32		
14	1857	14397	2462	349	1	1471	290	1	110	1	1
15	4346	36564	6778	1292	4	3812	936	6	310	5	5
16	10358	93650	18801	4660	35	9998	2952	45	920	32	30
17	24893	240916	51561	15786	184	26071	8896	224	2558	135	115
18	60522	623338	141583	51994	966	68388	26336	1026	7177	543	425
19	148283	1619346	386865	165708	4330	179250	76310	4116	19660	1930	1396
20	*	4224993	1056815	517297	18291	471504	218570	15508	53864	6568	4440
21	910724	1741717	543896	466763	71728	271958	618978	54912	146180	21200	13470
22	2278657	1870473	7082742	1579860	268529	3541321	*	186792	396296	66497	*
23	1056131	2515449	729632	6953378	962461	314316	*	613477	1070296	202919	116140
24	793372	1706630	894989	5894661	594828	442424	249889	285324	1035075	608019	332827
25	3687776	*	6372846	*	5977592	3131423	*	1834149	*	167909	860608
26	*	*	*	*	1596391	*	*	655868	*	1585695	*

2.6 Transformation Methodology

2.6.1 Assumptions

The proposed methodology is based on two assumptions. One is that the molecular composition within each homologous series follows a statistical distribution against a certain property such as molecular weight or boiling point. The other assumption follows a general belief that the global properties of a petroleum fraction are close to the calculated from pure compounds based on mixing rules (Albahri, 2005).

2.6.1.1 Statistical Distribution Assumption

As reviewed in section 2.3.3.2, statistic distribution has been used to describe complex mixtures. Klein et al. (2005) recommends gamma distribution (eq. 2.1) because of its flexibility that it ranges from an exponential distribution to a delta function and can also approximate a normal distribution.

$$p(x) = \frac{(x - \eta)^{\alpha - 1} e^{-(x - \eta)/\beta}}{\beta^\alpha \Gamma(\alpha)} \quad (2.1)$$

where α , β , and η are three parameters of gamma distribution. x denotes the property, and p is the probability density function.

$$\Gamma(x) = \int_0^{\infty} t^{x-1} e^{-t} dt \quad (2.2)$$

To verify this assumption, gamma distribution is applied to fit the fractions of hydrocarbons with different carbon number within each homologous series for a FCC gasoline stream (Figure 2.12) and a middle distillate (Figure 2.13). The results show a good agreement between the predicted data from gamma distribution and the measured data. The data is from the literature (Chen, 1995; Fafet, 1995).

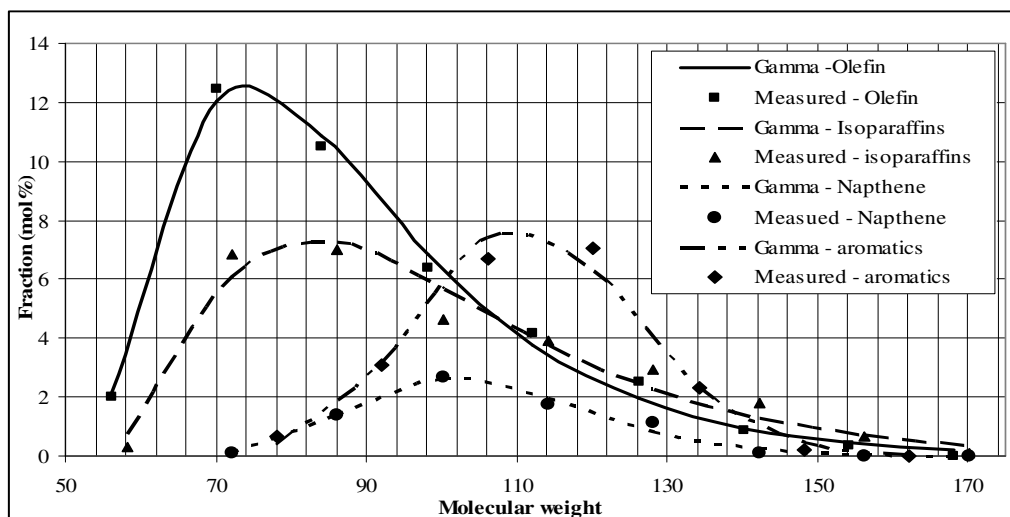


Figure 2.12 Gamma distribution fitted fractions within PONA homologous series of a FCC gasoline stream (Chen, 1995)

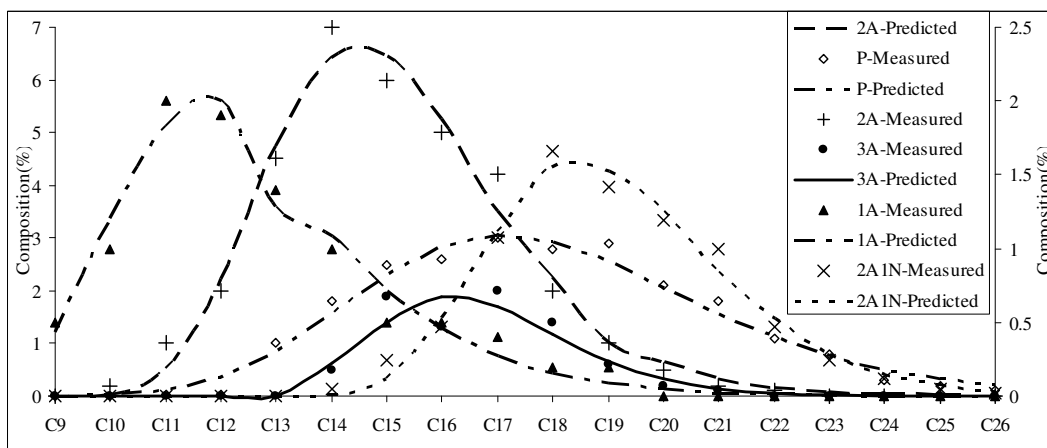


Figure 2.13 Gamma distribution fitted fractions within homologous series of a middle distillate (Fafet, 1995)

By assuming that compositions of the entries within each homologous series follow a gamma distribution with a certain property, some benefits are obtained. First of all, the need of the extremely-hard achievable sample matrices database has been removed, together with the limitation of the extrapolation capability. The most important benefit from this assumption is that the new methodology is capable of handling the challenge that the fractions with similar properties could have significantly different molecular compositions, because the distribution between molecules is taken into consideration. Furthermore, the shape of the distribution curve is easily controlled as integrated in mathematical model (section 2.6.2). Last but not least, the degrees of freedom to represent molecular

composition are reduced dramatically, such as from 18 to 4 for each homologous series regarding diesel fractions, including three parameters for the gamma distribution, and one fraction of each homologous series.

2.6.1.2 Property Estimation Assumption

The other assumption follows a general belief that the bulk properties of a petroleum fraction are close to the calculated from pure compounds based on mixing rules. The bulk properties could be measured in a laboratory or estimated by correlations based on the fundamental measured properties. In terms of characteristics of molecules, molecular energy and size are two important parameters, which in our case are used as the fundamental properties, represented by boiling point and density respectively.

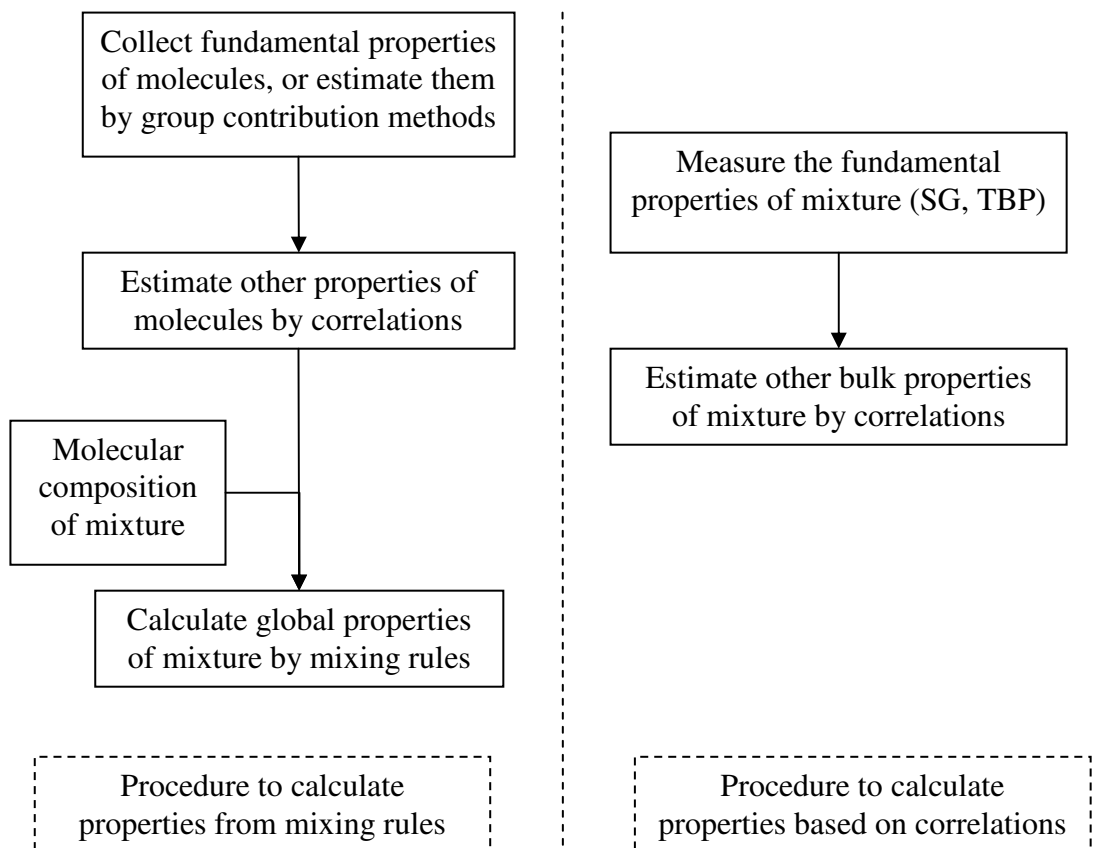


Figure 2.14 Calculation procedure based on the second assumption

Besides the measured properties such as distillation profile, specific gravity, etc., other derived bulk properties from correlations are also applied to capture the characteristics of each molecule in a petroleum fraction. Those properties are listed

in Table 2.7. The calculation procedure (Figure 2.14) following the assumption involves computing the properties of pure compounds and mixtures based on the fundamental properties, and those of mixtures based on mixing rules with molecular composition. Intensive correlations for mixture and pure compounds and mixing rules for these properties are developed in the past, and most are available from API TDB (1970) and Riazi (2005) as listed in Table 2.7, together with the deviations of the correlations.

Table 2.7 Properties estimation methodology for pure compounds and mixtures, mixing rules

Properties	Pure compounds	Correlations	Mixing Rules
Volume/weight/molar average boiling point (°C)	Experimental/Group contribution method	API 2B1.1	Eq 3.45
Molecular weight (g/mol)	Eq 2.40	API 2B2.1	Eq 3.45
Specific gravity	Experimental/Group contribution method	Experimental	Eq 5.126
Research octane number	Experimental	Experimental	(Ghosh, 2006)
Motor octane number	Experimental	Experimental	(Ghosh, 2006)
Reid vapour pressure (kPa)	Eq 3.102	Eq 3.103	API 5B 1.3
Refractive index	Eq 2.116	API 2B5.1	Eq 3.45
Aniline point (°C)	Eq 3.125	API 2B9.1	API 2-1.8/2-1.9
Kinematic viscosity(100 F) (cSt)	Eq. 2.128	(Wauquier,1995)	Eq. 3.45
Kinematic viscosity(210 F) (cSt)	Eq. 2.129	(Wauquier,1995)	Eq. 3.45
Critical pressure (kPa)	Eq. 2.40	API 4D4.1	API 4B2.1
Critical temperature (°C)	Eq. 2.40	API 4D3.1	API 4B1.1
Critical volume (m ³ /kg)	Eq. 2.40	Eq. 2.40	API 4B3.1

Properties	Pure compounds	Correlations	Mixing Rules
CH weight ratio (wt/wt)	Calculated	Eq. 2.120	Calculated
Watson K	Eq. 2.13	Eq. 2.13	API 2-0.9
Acentric factor	Eq. 2.105	API 2B3.1	Eq. 5.115
Heat of vaporisation at NBP (kJ/kg)	API 7C1.1	Eq. 7.54/7.56	API 7C2.1
Heat of combustion, 77 F (kJ/kg)	API 14A1.1/1.2	API 14A 1.3	Eq. 3.45
Liq heat capacity, 60 F, 1atm (kJ/kg·°C)	Eq 7.40	Eq. 7.43	Eq. 6.74
IG heat capacity, 60 F, 1atm (kJ/kg·°C)	Eq. 6.72	Eq. 6.72	Eq. 6.74
Critical compressibility Factor	Calculated	Calculated	Eq. 3.45
Liquid Thermal conductivity at 25 °C	Eq. 8.42/8.43	Eq. 8.46	API 12A 2.1
Cloud Point (°C)	API 2B12.1	API 2B12.1	Eq 3.117/3.121
Surface tension at 25 °C (dyne/cm)	Eq 8.85	API 10A3.2	Eq. 8.87

Eq: equations in the reference (Riazi, 2005), API: (API TDB, 1997)

To verify the assumption, the properties of a gasoline stream with the detailed molecular composition are calculated based on both correlations and mixing rules. The small deviations show a good agreement between them. This assumption is also verified in the literature (Albahri, 2005).

Table 2.8 Properties comparison of a gasoline stream based on both correlations and mixing rules

Properties	Mixing rules	Correlation	Error%
Volume average boiling point (°C)	112.48	113.23	0.67
Mole average boiling point (°C)	106.07	102.83	-3.06
Weight average boiling point (°C)	114.87	115.82	0.83
Molecular weight (g/mol)	102.01	103.99	1.94
Specific gravity	0.76	0.76	0.00
Reid vapour pressure (kPa)	13.31	13.17	-1.04
Refractive index	1.43	1.42	-0.70
Aniline point (°C)	37.24	37.26	0.06
Kinematic viscosity(100 °F) (cSt)	0.42	0.40	-4.76
Kinematic viscosity(210 °F) (cSt)	0.18	0.19	5.56
Critical pressure (kPa)	3312.10	3197.23	-3.47
Critical temperature (°C)	292.47	294.93	0.84
Critical volume (m ³ /kg)	0.0037	0.0037	0.0000
CH weight ratio (wt/wt)	6.66	6.31	-5.26
Watson K	11.58	11.55	-0.26
Acentric factor	0.30	0.29	-2.77
Heat of vaporisation at NBP (kJ/kg)	320.66	313.92	-2.10
Heat of combustion,77 °F (kJ/kg)	42961.64	43548.42	1.37
Liq heat capacity,60 °F,1atm (kJ/kg·°C)	1.97	2.01	2.13
IG heat capacity,60 °F,1atm (kJ/kg·°C)	1.38	1.42	3.03
Critical compressibility Factor	0.28	0.27	-3.57
Liquid Thermal conductivity at 25 °C	0.12	0.12	0.00
Cloud Point (°C)	-104.41	-102.66	-1.68
Surface tension at 25 °C (dyne/cm)	22.68	23.33	2.87

2.6.2 Mathematical Model

The mathematical model for the transformation methodology is as follows.

2.6.2.1 Objective Function

The objective function:

$$\begin{aligned}
 Obj = & \sum_T (w_{1,T} \times \frac{V_T^{msd} - V_T^{pred}}{V_T^{msd}})^2 + \sum_P (w_{2,P} \times \frac{P_P^{msd} - P_P^{pred}}{P_P^{msd}})^2 + \sum_{f \in PIONA} (w_{3,j} \times \frac{C_f^{msd} - C_f^{pred}}{C_f^{msd}})^2 \\
 & + \sum_C (w_{4,C} \times \frac{C_C^{msd} - C_C^{pred}}{C_C^{msd}})^2 + \sum_E (w_{5,E} \times \frac{C_E^{msd} - C_E^{pred}}{C_E^{msd}})^2 \quad (2.3)
 \end{aligned}$$

where subscripts of T , P , f , C , E stands for measured temperature of a distillation profile, properties listed in Table 2.7, the measurably-distinguished homologous series, carbon number, and atoms of sulphur, nitrogen, and oxygen respectively. Superscripts of msd and $pred$ denote the measured and the predicted respectively. w_1 - w_5 are weighting factors, determined as the inverse of the standard deviation of the experimentally determined value for the measured properties or the correlation calculated value for the derived properties respectively.

The chi-square statistic is a typical objective function used to optimise a representative feed to an actual feed by minimizing the objective function. The objective function is taken as the sum of the square of the percentage error between the observed and calculated properties. It consists of different kinds of differences. The first difference is between the measured distillation profiles and the calculated ones from the predicted molecular composition. An interpolation method is integrated into the optimisation program to determine the standard distillation profile. The second part of the objective function compares all the other properties excluding the distillation profile and the homologous series composition between the measured/estimated by correlations and the predicted from molecular composition. Homologous series composition difference is the third part of the objective function. Although several developed correlations could be employed to calculate homologous series composition, in the new methodology, homologous series composition would be determined experimentally. The fourth part of the objective function is the difference of molecular type composition between the measured if available and the predicted. The final term is the difference of composition for atoms such as sulphur, nitrogen, and this term is particularly

useful for diesel streams. If other data are available, other terms can easily be added into this flexible objective function as needed.

2.6.2.2 Constraints

The assumption that molecular compositions within each homologous series follow a gamma distribution against boiling point is as follows:

$$F(T_{i,j}^b) - F(T_{i-1,j}^b) = \frac{\gamma\left(\alpha_j, \frac{(T_{i,j}^b - \eta_j)}{\beta_j}\right)}{\Gamma(\alpha_j)} - \frac{\gamma\left(\alpha_j, \frac{(T_{i-1,j}^b - \eta_j)}{\beta_j}\right)}{\Gamma(\alpha_j)} = y_{i,j} \text{ for } i > 1 \quad (2.4)$$

$$F(T_{1,j}^b) = \frac{\gamma\left(\alpha_j, \frac{(T_{1,j}^b - \eta_j)}{\beta_j}\right)}{\Gamma(\alpha_j)} = y_{1,j}, \text{ for } i = 1 \quad (2.5)$$

$$\gamma(s, x) = \int_0^x t^{s-1} e^{-t} dt \quad (2.6)$$

where subscript i and j denote carbon number and homologous series of the MTHS matrix respectively. $\gamma(x,y)$ is incomplete gamma function as Equation 2.6, and $F(T_{i,j}^b)$ denotes cumulative distribution function of gamma distribution at $T_{i,j}^b$. $T_{i,j}^b$ is normal boiling point of the entry(i,j) of the MTHS matrix. $y_{i,j}$ stands for the fraction of the entry(i,j) within j homologous series of the MTHS matrix.

Therefore, the weight fraction of the entry(i,j) can be calculated according to the weight fraction x_j^w of homologous series j . x_j^w will be optimised. ε is the tolerance that allows small deviation of molecular composition between the optimal and the calculated based on a gamma distribution.

$$x_{i,j}^w = x_j^w \times \left(\frac{y_{i,j}}{\sum_{ii} y_{ii,j}} + \varepsilon \right) \quad (2.7)$$

$$x_j^w = \sum_i x_{i,j}^w \quad (2.8)$$

$$\sum_j x_j^w = 1 \quad (2.9)$$

The inter-conversion of weight, volume and molar fractions is as follows:

$$x_{i,j}^v = \frac{x_{i,j}^w / SG_{i,j}}{\sum_{ii} \sum_{jj} x_{ii,jj}^w / SG_{ii,jj}} \quad (2.10)$$

where $x_{i,j}^w, x_{i,j}^v, x_{i,j}^m$ denote the weight/volume/molar fraction of the entry(i,j) in the MTHS matrix. $SG_{i,j}, MW_{i,j}$ stand for specific gravity and molecular weight of the entry (i,j) of the MTHS matrix respectively.

The cumulative volume against the boiling point of each molecule is as follows:

$$x_{i,j}^{cv} = \sum_{jj} \sum_{ii} x_{ii,jj}^v, \text{ for } ii, jj \in \{ii, jj; T_{ii,jj}^b \leq T_{i,j}^b\} \quad (2.11)$$

The cumulative volume against some particular temperature $\{T_{TBP}\}$ is calculated through the linear interpolation as follows:

$$V_T^{pred} = x_{i',j'}^{cv} + \frac{x_{i'',j''}^{cv} - x_{i',j'}^{cv}}{T_{i'',j''}^b - T_{i',j'}^b} (T - T_{i',j'}^b) \text{ for } i', j', i'', j'' \in \{T_{i',j'}^b \leq T \leq T_{i'',j''}^b\} \quad (2.12)$$

The properties are calculated based on the fundamental properties by correlations are as follows:

$$p_P^{msd} = f_P(T_b, SG) \quad (2.13)$$

The properties are calculated based on mixing rule with the volume, weight or molar molecular composition as follows:

$$p_P^{pred} = f_P(x_{i,j}^v, P_{i,j,P}) \quad (2.14)$$

$$p_P^{pred} = f_P(x_{i,j}^w, P_{i,j,P}) \quad (2.15)$$

$$p_P^{pred} = f_P(x_{i,j}^m, P_{i,j,P}) \quad (2.16)$$

The molecular fractions in terms of the measurably-distinguished homologous series are as follows:

$$C_f^{pred} = \sum_{e(i,j) \in f} x_{i,j}^v \quad (2.17)$$

The molecular fractions in terms of carbon number are as follows:

$$C_C^{pred} = \sum_{i \in C} x_{i,j}^v \quad (2.18)$$

The weight contents of atoms excluding hydrogen and carbon such as sulphur, nitrogen and oxygen are as follows:

$$C_E^{pred} = \sum_{e(i,j) \in E} x_{i,j}^w \quad (2.19)$$

The application of gamma distribution to control the fraction distribution within each homologous series enables that some information could be utilised. For instance, in most circumstances, the fraction of C₈ or C₉ for gasoline streams is the maximum within aromatic homologous series, and that of C₁₆ or C₁₇ for diesel streams is the maximum within some homologous series. That information could be written as eq. 2.20 for gasoline, and eq. 2.21 for diesel respectively:

$$T_{C_{8,A}}^b \leq (\alpha_A - 1)\beta_A + \eta_A \leq T_{C_{9,A}}^b \quad (2.20)$$

$$T_{C_{16,j}}^b \leq (\alpha_j - 1)\beta_j + \eta_j \leq T_{C_{17,j}}^b \quad (2.21)$$

The listed equations and terms above are not necessarily the same for different cases, and could be changed depending on the available information. For example, regarding diesel streams, the fractions of different sulphur compound types lumped as SI, SII, SIII, SIV, SV, SVI are important if the predicted molecular composition is for kinetic models of processes. The distribution between different sulphur compound lumps sometimes is available in the literature or could be measured, and could be treated as constraints as well.

2.7 Optimisation Engines

The non-linear high dimensional problems with a complex search space can be solved by two classes of search methods: deterministic and stochastic ones. The deterministic methods, such as successive quadratic programming (SQP), are very efficient to solve the convex/concave problems, while require the computation of first and/or second order derivatives of the objective function and/or constraints, which makes these methods not applicable to a non-differentiable or discontinuous problem. Deterministic methods largely depend on the chosen initial solution in the search for the optimal solution.

Stochastic optimisation techniques have higher probability of escaping local optima and finding solutions in the vicinity of the global optimum for complex non-linear and non-convex problems compared to the deterministic methods (Arora, 2004). In the stochastic techniques, the problem is treated as a black-box. A black-box may be defined as a system that provides output for a given input and the information about internal calculations is not required. The optimisation algorithm makes use of the values of the objective function at randomly chosen points in the search space. The black-box treatment decouples the simulation and optimisation of the design problem and improves the performance of optimisation algorithm for complex problems.

Simulated annealing (SA) is a widely applied stochastic optimisation algorithm due to its robustness and simplicity to be implemented (Athier et al., 1997). Simulated annealing algorithm has been developed using the analogy to the physical annealing of metals where a metal in a molten state at a very high temperature is cooled down very slowly. In a molten state the metal atoms are distributed randomly. When the system, i.e. the metal, is cooled it reaches the state of minimum energy. If the annealing process is carried out slowly such that at any point in time the system is close to thermodynamic equilibrium then the system may reach stable crystalline structure with minimum energy. However, if the metal is not cooled sufficiently slowly or the initial temperature of the system is not high enough, then a glassy meta-stable structure, with energy higher than the desired minimum level, is formed.

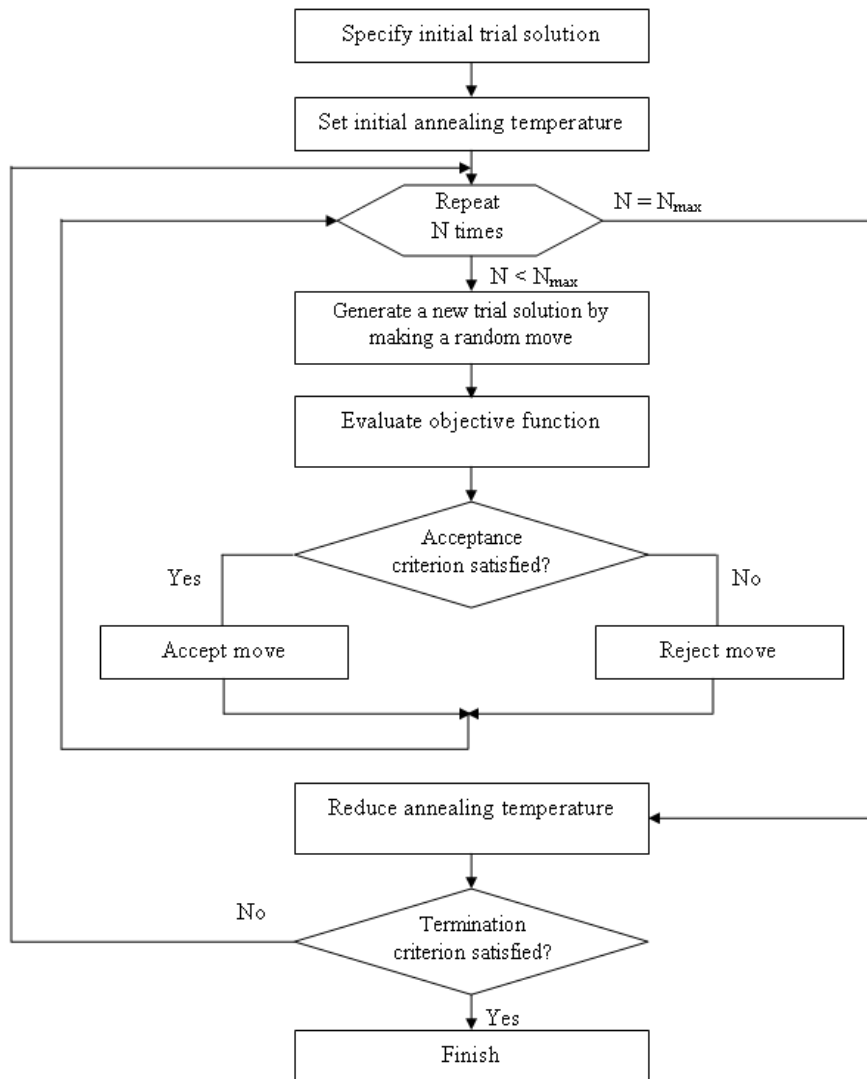


Figure 2.15 Simulated annealing algorithm (Kirkpatrick, 1983)

The simulated annealing algorithm (Kirkpatrick, 1983) represented in Figure 2.15 starts with an initial trial solution at an appropriate high value of the annealing temperature. The annealing temperature serves as a control parameter for the optimisation. The initial trial solution is modified by a random change, known as a random move; the objective function for this new prospective solution is evaluated against that of previous trial solution. The modification made to the current trial solution may be accepted or rejected based on the acceptance criterion employed. This process of modification, simulation and evaluation is repeated a number of times (N) determined by the parameter known as the Markov chain length (N_{\max}), to obtain a decent set of sample solutions. Once several candidate solutions have been obtained, the annealing temperature is reduced. This cycle is continued until

the termination criterion is satisfied. The annealing temperature, acceptance criterion, Markov chain length and termination criterion constitute the simulated annealing parameters.

2.8 Case Studies

Three cases are studied, including one FCC gasoline fraction previously used to demonstrate the shortcomings of the existing MTHS method, and two middle petroleum fractions: straight run gas oil (SRGO) and light cycle oil (LCO) stream.

2.8.1 FCC Gasoline Stream Case

To compare the existing and proposed methodology, the case in section 2.3.6 would be employed to get the molecular composition. Table 2.9 gives the measured molecular composition in terms of PIONA fraction.

Table 2.9 Measured molecular composition of a FCC stream (vol %)

vol%	nP	iP	O	N	A
C4	0.10	0.00	0.50	0.00	0.00
C5	1.00	5.52	9.84	0.89	0.00
C6	1.71	6.23	9.54	2.21	1.20
C7	0.40	5.22	6.33	1.31	4.02
C8	0.30	3.51	3.27	3.11	7.23
C9	0.20	2.21	1.81	0.56	11.15
C10	0.20	1.41	1.00	0.87	5.42
C11	0.30	0.70	0.70	0.02	0.00
C12	0.00	0.00	0.00	0.00	0.00

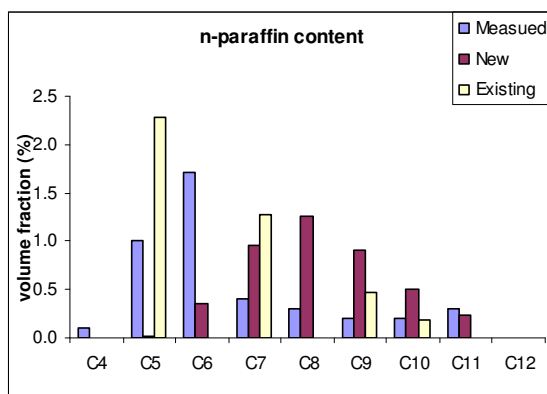
The input information such as distillation profile, specific gravity etc is given in the section 2.3.6. The generated new matrix for the FCC stream is as Table 2.10, while Table 2.11 compares the property difference between the measured and those calculated from both the existing and the proposed methodologies.

Table 2.10 Generated matrix for the FCC stream by the proposed methodology

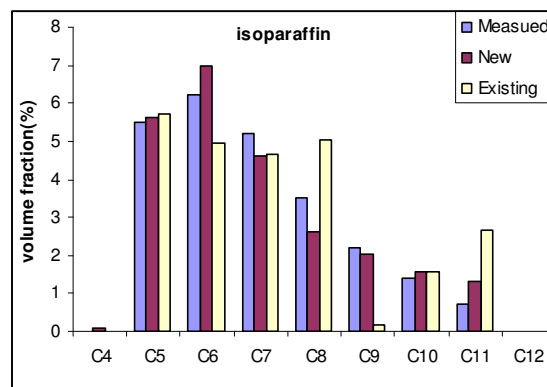
vol%	Iso-paraffin				Olefin		A	N	sum
	NP	MP	DP	TP	NO	BO			
C4	0.00	0.07			0.18	0.17			0.43
C5	0.02	4.70	0.91		8.13	1.85		2.03	17.63
C6	0.35	5.49	1.49		7.96	2.89	0.61	2.15	20.94
C7	0.96	2.89	1.68	0.04	3.97	2.80	3.60	1.79	17.72
C8	1.25	0.89	1.64	0.11	1.36	1.76	8.35	1.43	16.80
C9	0.90	0.21	1.61	0.20	0.30	0.93	9.91	0.85	14.91
C10	0.51	0.04	1.24	0.28	0.06	0.42	4.42	0.48	7.44
C11	0.23	0.01	0.96	0.32	0.01	0.16	2.18	0.25	4.12
C12	0.00	0.00	0.00	0.00	0.00	0.00	0.00	0.00	0.00
sum	4.22	14.30	9.53	0.95	21.97	10.99	29.07	8.97	100.00

Table 2.11 Comparison of properties

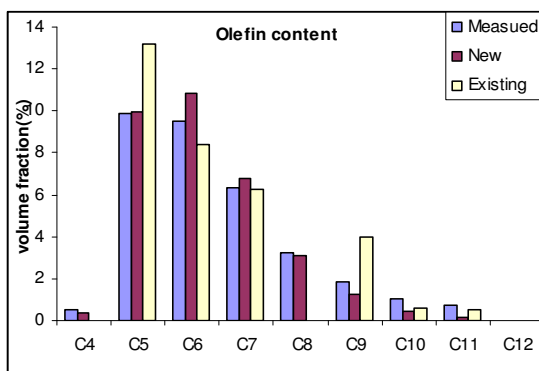
Properties Comparison					
	Measured	New App.	Error (%)	Existing	Error (%)
MW (g/mol)	97.49	97.41	-0.08	97.49	0.00
Specific Gravity	0.75	0.75	-0.07	0.75	0.00
RVP (psi)	6.17	6.16	-0.12	6.17	0.00
RON	90.89	90.86	-0.03	91.68	0.86
MON	78.06	78.23	0.22	77.73	-0.43
P (vol%)	4.22	4.22	-0.02	4.22	0.00
I (vol%)	24.80	24.77	-0.13	24.80	0.00
O (vol%)	32.99	32.94	-0.16	32.99	0.00
N (vol%)	8.97	8.97	0.00	8.97	0.00
A (vol%)	29.02	29.10	0.29	29.02	0.00



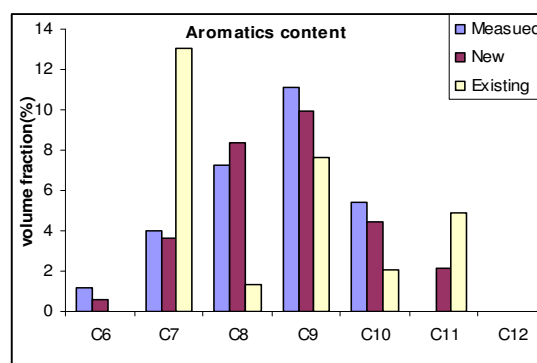
(a) paraffin content comparison



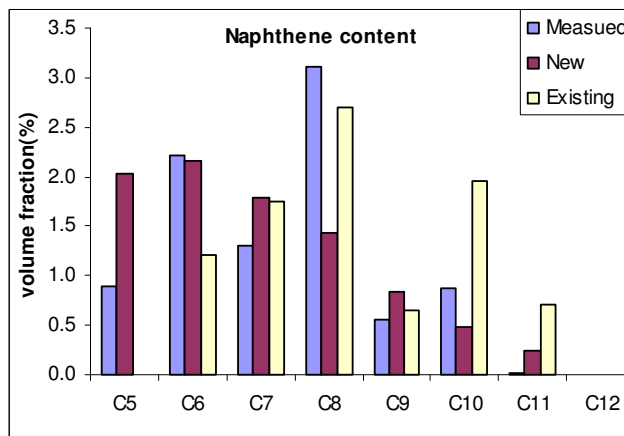
(b) isoparaffin content comparison



(c) olefin content comparison



(d) aromatics content comparison



(e) naphthene content comparison

Figure 2.16 Comparison of the detailed PIONA volume fraction between the measured and those based on the existing and proposed methodologies

Figure 2.16 exhibits the comparison of the detailed molecular composition between the measured and calculated by the existing and proposed methodologies. As seen in Figure 2.16 (a), the molecular composition from the proposed methodology has a little gap with the measured. The reasons may come from two points. One is the

normal paraffin content is relatively small with the total volume fraction of 4.22%, and the other is the measured composition does not follow with statistical distribution exactly possibly due to the inherent equipment and human errors. The consistency between the measured and the predicted distillation profile is shown in Table 2.12.

Table 2.12 Comparison of distillation profile between the measured and the predicted from the developed method

vol%	Measured (°F)	Predicted (°F)	Error(%)
5	74.85	74.84	-0.01
10	87.71	87.71	0.00
30	149.58	149.58	0.00
50	204.91	204.79	-0.06
70	281.51	281.31	-0.07
90	328.09	328.88	-0.24
95	347.15	347.38	0.01

2.8.2 SRGO Feed

In this section, two examples are present to illustrate the proposed methodology, for generating MTHS matrices of middle petroleum fractions. In the first example, a straight run gas oil from one of Kuwait crudes (Marafi, 2007) is applied to generate a MTHS matrix. The information available for the SRGO fraction regarding the physical properties and composition is shown in Table 2.13.

To follow the first assumption, it is supposed that the weight fractions of the MTHS matrix entries within each homologous series follow a gamma distribution against boiling point. The reason using boiling point rather than molecular weight is that the difference between two consecutive molecular weights within each homologous series is always the same, and not for boiling point. More importantly, boiling point is more common to be used. Since most of compounds locate between C12 and C21 (Bacon, 2009), the following constraints are applied.

$$T_{C12,j}^b \leq (\alpha_j - 1)\beta_j + \eta_j \leq T_{C21,j}^b \quad (2.22)$$

To avoid the distribution between molecules within each homologous series too narrow or too wide, the scale parameter β and the shape parameter α of gamma distribution has its individual limits.

$$1 \leq \alpha_j \leq 20 \quad (2.23)$$

$$19 \leq \beta_j \leq 100 \quad (2.24)$$

As known, there are no olefins in straight run gas oil, therefore, olefin homologous series is eliminated. Diesel streams are more complex than gasoline in terms of molecular species. To simplify the problem, in this case, the derived properties, if not measured, are excluded for the transformation methodology. Sulphur compound types are crucial to the hydrotreating process. Therefore, a distribution between different sulphur compound types – lumped as SII, SIII, SIV, SV in the MTHS matrix is applied from the literature (Depauw, 1997; Nylén, 2004). The applied weight distribution in this case is SII : SIII : SIV : SV = 7.5 : 2 : 1 : 0.4.

Table 2.13 Properties of SRGO Feed (Marafi, 2007)

Feed Properties	GO-LF
Density @ 15°C (g/cc)	0.8962
Sulphur (%wt)	3.22
Total aromatics (%wt)	45.68
Monoaromatics (%wt)	19.47
Polyaromatics (%wt)	26.21
Cetane index	38.2
ASTM D86 (°C)	
IBP	236
10 vol %	261
30 vol %	288
50 vol %	314
70 vol %	340
90 vol %	366
95 vol %	375

Table 2.14 MTHS matrix (wt %) generated for GO-LF SRGO by simulated annealing algorithm

	P	IP	N	A	AA	AN	NN	AAA	AAN	ANN	NNN	SII	SIII	SIV	SV
C9	0.00	0.00	0.00	0.00								0.00			
C10	0.00	0.00	0.00	0.00	0.00	0.00	0.00					0.01			
C11	0.02	0.00	0.10	0.00	0.00	0.00	0.00					0.39			
C12	0.08	0.01	0.68	0.02	0.12	0.04	0.02					1.99	0.04		
C13	0.22	0.12	1.88	0.04	1.07	0.24	0.09					3.67	0.37	0.03	
C14	0.44	0.54	2.48	0.09	2.65	0.58	0.23	0.04	0.03	0.00	0.00	3.73	1.62	0.21	0.03
C15	0.69	1.47	2.26	0.11	3.05	0.69	0.44	0.61	1.48	0.14	0.05	2.56	1.20	0.29	0.11
C16	0.91	2.73	1.47	0.09	2.16	0.60	0.60	0.49	2.22	0.79	0.29	1.34	0.47	0.29	0.13
C17	1.06	3.83	0.76	0.06	1.05	0.37	0.67	0.25	1.04	1.01	0.67	0.57	0.13	0.26	0.12
C18	1.11	4.31	0.32	0.04	0.43	0.20	0.61	0.10	0.32	0.69	0.89	0.21	0.03	0.22	0.10
C19	1.09	4.06	0.12	0.02	0.12	0.09	0.49	0.04	0.08	0.31	0.88	0.07	0.01	0.17	0.08
C20	1.00	2.98	0.04	0.01	0.05	0.03	0.33	0.02	0.02	0.12	0.69	0.02	0.00	0.14	0.06
C21	0.90	2.72	0.01	0.00	0.01	0.01	0.21	0.01	0.00	0.04	0.47	0.01	0.00	0.10	0.05
C22	0.77	1.55	0.00	0.00	0.00	0.00	0.11	0.00	0.00	0.01	0.29	0.00	0.00	0.08	0.03
C23	0.64	0.76	0.00	0.00	0.00	0.00	0.06	0.00	0.00	0.00	0.16	0.00	0.00	0.06	0.03
C24	0.53	0.54	0.00	0.00	0.00	0.00	0.03	0.00	0.00	0.00	0.08	0.00	0.00	0.04	0.02
C25	0.43	0.35	0.00	0.00	0.00	0.00	0.01	0.00	0.00	0.00	0.04	0.00	0.00	0.03	0.01
C26	0.35	0.12	0.00	0.00	0.00	0.00	0.01	0.00	0.00	0.00	0.02	0.00	0.00	0.02	0.01

The optimal parameters of the gamma distribution and fractions of homologous series are given in Table 2.15. As seen, normal paraffins and iso-paraffins have very close values of two parameters α and β , which means they have very similar distribution of molecules. Similarly, homologous series of N, A, 2A and AN have similar distributions. The molecular composition is shown in Table 2.14.

Table 2.15 Parameters of homologous series predicted for the gamma distribution and the distribution

	α	β	η	X
P	17.32	25.91	190.00	10.21
I	16.87	24.56	230.00	26.12
O	11.08	19.00	271.00	10.14
N	15.29	19.01	314.88	0.47
A	13.18	19.00	373.18	10.72
AA	12.18	19.00	376.12	2.85
AN	14.89	22.80	277.27	3.90
NN	2.01	42.37	590.25	1.56
AAA	4.89	19.01	583.93	5.20
AAN	7.17	19.02	552.30	3.11
ANN	6.09	30.55	520.00	4.53
NNN	10.72	19.00	414.50	14.56
SII	4.49	19.01	608.50	3.88
SIII	2.04	100.00	627.83	1.94
SIV	1.86	99.99	673.11	0.78
SV	17.32	25.91	190.00	10.21

Figure 2.17 shows the comparison of distillation profile between the measured and the predicted with some deviation of IBP, and also a comparison of the SRGO properties and compositions is given in Table 2.16 and shows a reasonable accuracy. Molecular weight, which value is calculated based on a correlation, is applied to ensure mass balance. Furthermore, to illustrate the accuracy of the achievable molecular composition, other properties, which are not applied in the

prediction, are predicted based on the optimal molecular composition and correlations respectively, and compared. The results are given as Table 2.17.

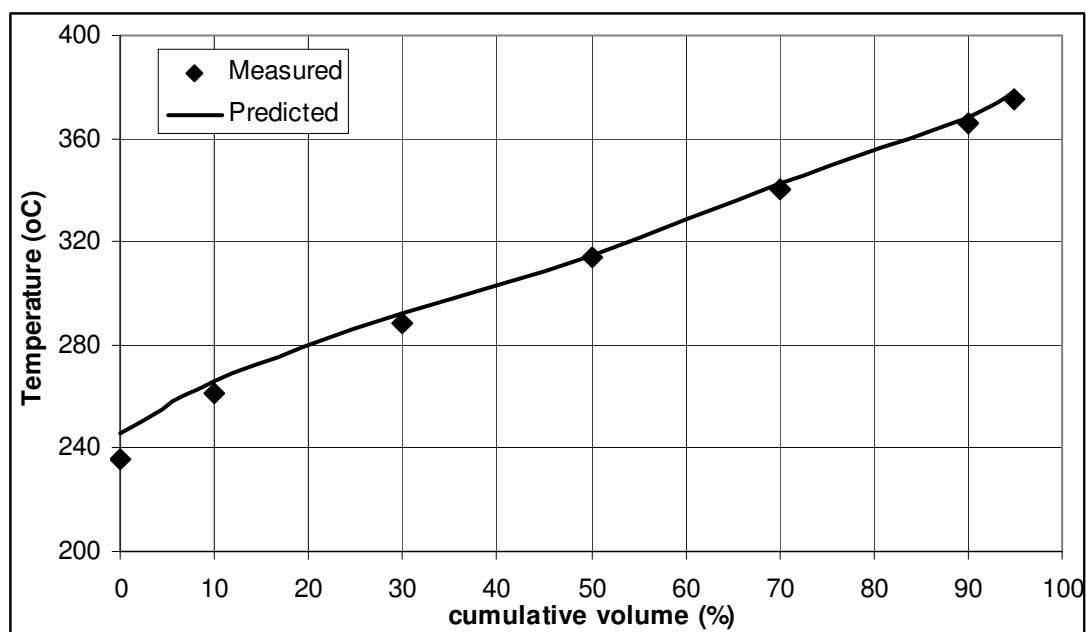


Figure 2.17 Distillation profiles of the SRGO from the measured and the predicted

Table 2.16 Comparison of the SRGO properties between the measured and the predicted

Feed Properties	Measured	Predicted	Error (%)
Density @ 15 °C (g/cc)	0.8962	0.8910	-0.58
Sulphur (%wt)	3.22	3.20	-0.62
Total aromatics (%wt)	45.68	45.08	-1.31
Monoaromatics (%wt)	19.47	21.00	7.86
Polyaromatics (%wt)	26.21	24.08	-8.13
Cetane index	38.2	37.8	-1.05
molecular weight (g/mol)	245.722*	243.460	-0.92

Table 2.17 Properties verification between calculated based on mixing rule and correlations

	mixing rule	correlation	Deviation (%)
Volume average Boiling point (°C)	322.65	317.84	-1.51
Mole average Boiling Point (°C)	313.57	308.66	-1.59
Weight Average Boiling Point (°C)	325.58	319.44	-1.92
Refractive Index	1.49	1.50	0.67
Aniline point (°C)	97.1	107.4	9.59
critical pressure (kPa)	1732.5	1742.7	0.59
critical temperature (°C)	539.2	512.5	-5.21
critical volume(m ³ /kg)	0.0038	0.0039	2.56
CH weight ratio (wt/wt)	7.09	6.97	-1.72
Watson K	11.54	11.37	-1.50
Acentric factor	0.723	0.733	1.36
heat of vaporisation at NBP(kJ/kg)	227.01	214.89	-5.64
heat of combustion,77 F(kJ/kg)	42015.5	42492.2	1.12
Liquid Thermal Conductivity at 25 °C	0.152	0.148	-2.70
Surface Tension at 25 °C (dyne/cm)	32.00	32.92	2.79

2.8.3 LCO Feed

In the second example of middle petroleum fractions, a light cycle oil (Ancheyta, 1999) is applied for the generation of a molecular composition used in chapter 6. The properties of the LCO are shown in Table 2.18.

Table 2.19 shows the comparison of the properties and composition between the predicted and the measured. API gravity has the biggest deviation of 2.5%, while others are within 0.5%.

Table 2.18 Measured properties of LCO

Feed Properties	GO-LF
API gravity	12.8
Sulphur (%wt)	3.50
Total aromatics (%wt)	72.0
Cetane index	26.2
Distillation (°C)	
IBP	182
10 vol %	257
30 vol %	276
50 vol %	295
70 vol %	327
90 vol %	368
EBP	399

Table 2.19 Comparison of LCO properties between the predicted and measured

Feed Properties	Measured	Simulated Annealing	Dif (%)
API gravity	12.8	13.12	2.500
Cetane index	26.2	26.20	-0.009
Sulphur (wt%)	3.5	3.50	0.001
Aromatics (wt%)	72	72.00	0.000
Distillation (°C)			
IBP	182	182.00	0.000
10 vol %	257	256.06	-0.365
30 vol %	276	276.14	0.049
50 vol %	295	295.03	0.011
70 vol %	327	327.17	0.053
90 vol %	368	368.36	0.098
95 vol %	399	398.96	-0.01

It can be concluded from the results of the two examples on the matrix generation that the proposed MTHS framework for the characterisation of diesel fractions can provide a reasonable approximation for the composition, by taking the consideration of isomers properly, integrating statistic distribution to set up the distribution between entries within each homologous series, and solving the problem with the simulated annealing methodology.

2.9 Summary

The conventional characterisation methods that are widely used in refinery process modelling cannot provide detailed information at the molecular level. Such information is needed for modelling of refinery processes to satisfy cleaner fuel specifications. The MTHS matrix characterisation approach is a systematic representation of detailed molecular information. In order to avoid expensive and time consuming chemical analysis of petroleum fractions, previous researchers developed methods for generation of MTHS matrices by minimising the difference between the calculated and the measured bulk properties of streams. However, the existing method has shortcomings, which prevent it from wide application.

A new methodology has been developed for molecular modeling of light and middle petroleum fractions. Composition of light and middle distillates can be characterised quickly without too much experimental effort. The method revolutionised the MTHS framework on both the representation matrix by considering isomers, and the transformation approach by introducing statistical distribution and extensive properties. One of the main advantages of this method over others is that the method not only focuses on minimising the difference of properties between the measured and the calculated, but also takes the distribution between molecules into account, which efficiently deals with the problem that different molecular compositions could be achieved based on the same bulk properties.

Chapter 3 Molecular Modelling of Gasoline Blending

3.1	Introduction	79
3.2	Gasoline Blending	79
3.2.1	A Brief Introduction of Gasoline Blending.....	79
3.2.2	Motivation of this Research on Gasoline Blending	85
3.3	A New Molecular Model for Property Prediction.....	86
3.3.1	Review of Previous Methodologies for ON.....	87
3.3.2	A New Methodology Correlating ON with Bulk Properties.....	87
3.3.3	Case Study.....	96
3.4	Gasoline Blending Model	101
3.4.1	Review of Gasoline Blending Models	101
3.4.2	Existing Blending Models for ON and RVP Properties	102
3.4.3	A New Molecular Gasoline Blending Methodology	106
3.4.4	Gasoline Blending Optimisation Model.....	108
3.4.5	Case Study.....	109
3.5	Summary	112
3.6	Nomenclature	112

3.1 Introduction

Product blending targets allocating available components in a way to meet product demands and specifications at the least cost and to produce incremental products which maximise the overall profit. The major refining products from blending are gasoline, diesel, jet fuels, lubricating oils, and heating fuels. The volume of products sold even by a medium-sized refiner, are so huge that savings of a fraction of a cent per unit will result in a substantial increase in profit over a period of one year. For example, if a refiner sells about one billion gallons of gasoline per year (about 65,000 BPCD; several refiners sell more than that in the United States), a saving of one one-hundredth of a cent per gallon results in an additional profit of \$100,000 per year. Moreover, the demand of refining products is increasing gradually, and will remain the increasing trend in the foreseeable future. On the other hand, the refining industry today has to comply with higher product quality specifications and more stringent environmental regulations, with more emphasis on the molecular composition of refining products, under the increased number of tighter environmental regulations from different agencies. These situations make product blending crucial in the competitive industry to increase or maintain the refining margin. However, many refiners used to treat product blending as a linear problem, combined with a trial-and-error procedure, which increases property giveaway with a huge profit loss (Gupta, 2008). Furthermore, the specifications concerning molecular composition and properties of refining products result in a large cost of instrument and maintenance. These scenarios lead to an aspiration for investigating the nonlinear blending nature of most specifications, as well as developing a methodology to predict properties based on easily obtained properties, which both ultimately increase refining profit.

3.2 Gasoline Blending

3.2.1 A Brief Introduction of Gasoline Blending

Gasoline blending is a process of mixing/blending various refinery streams produced by different refinery units along with additives to produce different grades of products. The blending ratio depends upon the amount and the cost of the

production of each stream, specifications, demand and the price of the final product. Selection of the blending components and their proportions in the product blend is a complex problem. Figure 3.1 shows a simplified refinery flowsheet related to gasoline blending.

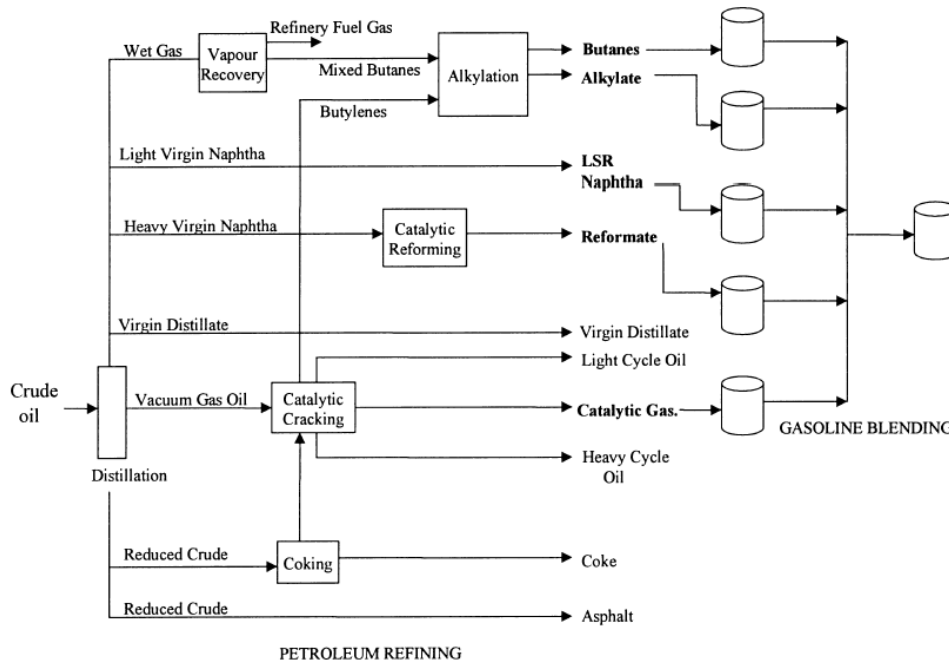


Figure 3.1 Simplified petroleum refinery flowsheet (Gupta, 2008)

3.2.1.1 Blending Process

3.2.1.2 Blending Type

Regarding operation types, in-line blending and batch blending are two general ways. In-line blending, also termed as continuous blending, involves mixing of various component streams in a blender continuously, and at the same time supplying products to a product storage tank. The in-line blender periodically samples the blend and automatically tests the properties of samples online. This information is used to adjust the feedstock flow rate so that the blend meets the quality specifications in spite of unanticipated fluctuation in the properties of feedstocks. This type of blending is very useful because of the fact that blending, quality analysis, loading and unloading can be done in a single run. However, techniques on on-line measurements, process control, as well as on-line optimisation are the keys to the success of this type of blending.

In batch blending, various component streams are fed to the blender one after another and converted to the product. Batch blending is a time consuming process and requires storage tanks for both pre-blended and final products. Batch blending is very cost effective when demand for a product is small. In batch blending the feed quality is fairly constant over the time as compared to in-line blending. In oil refineries, the batch blending is traditionally preferred but due to economic pressures for reducing on-site tankage and low inventory requirement for safety purposes, in-line blending is preferred (Singh et al., 2000).

3.2.1.3 Gasoline Blending Stocks

The incoming crude oil contains a wide range of materials, from light ones, such as gasoline, to the heaviest ones, such as industrial fuel oil and asphalt. The crude oil is split into various component streams by distillation according to their boiling point ranges. Only a small portion of the distillate can go directly to gasoline blending. Most of the output streams from the distillation unit are sent to other processing units where the molecules are reformed to improve their quality or are cracked and recombined into lighter, more valuable ones. These resulting products, of widely different qualities, are then sent to intermediate storage tanks from which they are blended into gasoline. A large refinery can have more than 20 blending feedstocks that are blended into several grades of gasoline. The refinery processes for producing gasoline blending streams are as follows:

- Catalytic reforming: converts saturated, low octane hydrocarbons into higher-octane products rich in aromatics.
- Fluidised catalytic cracking: breaks large hydrocarbon molecules into gasoline range products containing around 30% aromatics and 20-30% olefins.
- Isomerisation: raises gasoline fraction octane by converting straight chain hydrocarbons into branched isomers.
- Alkylation: reacts gaseous olefin streams with iso-butane to produce liquid high octane iso-alkanes, and only available in limited quantities in refinery.
- Others: other naphtha streams in a refinery can be from hydrocracking, visbreaking, coking and hydrotreating steps.

In addition to these streams, additives are blended to meet with the product specifications. The different types of additives are: oxygenates (used as octane

enhancers), anti-oxidants (to reduce gum formation), anti-rust agents (to inhibit rusting and protect the engine fuel system), detergents (to prevent deposits in the engine fuel system), lubricants (to lubricate piston rings and cylinders), dyes (to distinguish grades and brands), anti-icing agents (to retard icing and fuel line freezing), etc.

3.2.1.4 Gasoline Specifications

Table 3.1 Clean Air Act and CARB specifications (USA) (Aye, 2003)

	1990	Clean Air Act			CARB*			
		Simple	Complex		Phase 2		Phase 3	
			I	II	Limit	Average	Limit	Average
Benzene (max.vol.%)	2	1	1	1	1.0	0.8	0.8	0.7
Oxygen (min.mass %)	0.2	2	2	2	1.8	N/A	1.8	No change
(max.mass %)	-	2.7	-	-	2.2		2.2	
Sulphur (max.mass ppm)	150	-	-	-	40	30	20	15
Aromatics (max.vol.%)	32	-	-	-	25	22	No change	No change
Olefins (max.vol.%)	9.9	-	-	-	6.0	4.0	No change	No change
Reid vapour pressure (psi)	8.0	7.8	-	-	7.0	N/A	7.0	No change
(During VOC Control Period)	-	49.6	-	-				
50% evaporated (max.°F)	-	-	-	-	210	200	211	201
90% evaporated (max.°F)	170	-	-	-	300	290	305	295

*CARB = California Air Research Board

Product specifications are always a highly charged subject, due to the interests of environmental pressure groups, refiners, governments, consumers and engine manufacturers. However the interaction of these groups makes the predictions of future trends difficult. Table 3.1 gives the most stringent current specifications for gasoline under Clean Air Act and in California (U.S.A). New compositional measurements such as oxygenates, total aromatics, benzene and total olefins are being phased in since 1992 in addition to the traditional gasoline quality measurement. The increases in the environmental awareness and concerns are demanding refinery fuels to be cleaner. These specifications might be well above the restrictions imposed in many other countries but it is reasonable to postulate that the specifications in more countries around the world will be close or even stricter, as the reasons behind the strict regulations become apparent. As specifications tightened, the conventional refining technologies are challenged.

A number of properties are used to characterise automotive gasoline and the components that are blended to produce them, including octane number, Reid vapour pressure (RVP), ASTM distillation points, viscosity, flash point, and aniline point, as well as various properties from the concerns of environmental consideration.

The octane number of a fuel is defined as the percentage of iso-octane (with octane number 100) in a blend with n-heptane (having octane number of 0) that exhibits the same resistance to knocking as the test fuel under standard conditions in a standard engine. Antiknock properties of fuels for spark engines are characterised by two standard test procedures. Research Octane Number (RON) could be obtained from ASTM D-908, while ASTM D-357 gives the motor octane number (MON). RON represents antiknock properties under conditions of low speed and frequent accelerations while the MON represents engine performance under more severe high speed conditions. The main difference between automotive gasoline grades is their antiknock properties. For example, nowadays, in many parts of Europe, regular and premium gasolines are specified to have posted octane numbers of 95 and 97, respectively. Required octane number of gasolines vary with parameters such as air temperature, altitude, humidity, and engine speed. Improving the octane number of fuel would result in reducing power loss of the engine, improving fuel economy, and a reduction in environmental pollutants and engine damage (Bacon et al., 2009). For these reasons, octane number is one of the important properties related to the quality of gasolines. Usually the control of ON giveaway, having a great impact on the refining profitability, is one of the most challenging tasks in gasoline blending. The model with high accuracy for predicting ON of blending components, and ON of blends will be discussed in the late sections.

Reid vapour pressure is the absolute pressure exerted by a mixture at 37.8 °C at a vapour-to-liquid volume ratio of 4. RVP is one of most important gasoline properties, and it is used as a criterion for blending. For the specifications on vapour pressure of gasoline, there are six different classes according to locations and/or seasons. Vapour pressure limits for each class (54, 62, 69, 79, 93, 103 kPa) are also specified.

As gasoline is distilled, the temperatures at which various fractions are evaporated are calculated. Specifications define the temperatures at which various percentages of the fuel are evaporated. Distillation limits include maximum temperatures that 10% is evaporated (50-70 °C), 50% is evaporated (110-121 °C), 90% is evaporated (185-190 °C), and the final boiling point (225 °C). A minimum temperature for 50% evaporated is approximately (77 °C), and a maximum amount of residue after distillation is about 2%.

Benzene is carcinogenic, and it is required to be below a certain level in gasoline. Aromatics produce more smoke and smog, and produce benzene as a by-product on incomplete combustion. There are specifications for benzene content (maximum) and aromatics content (maximum). This restricts a refiner from using too much of reformat, one of the major octane provider blend stocks, in which benzene and aromatics are abundant. Benzene, overall aromatic and olefin contents in finished motor and aviation gasoline are determined by gas chromatography.

Table 3.2 California (USA) Phase 2 specifications for gasoline (Simon, 2007)

Sulphur (wt.% max)	0.004
RVP (kPa, max)	48.3
Benzene (vol% max)	1
Aromatics (vol% max)	25
Olefins (vol% max)	6
ASTM 90% (°C, max)	149

Sulphur compounds are corrosive, foul smelling, and increase sulphur dioxide/trioxide emissions. There are specifications for maximum sulphur in order to minimise air toxics and corrosive components. The 2007 specification of maximum sulphur content is 0.004 wt% in California (USA).

Oxygenates reduction is due to the recent findings that oxygenates such as methyl tertiary butyl ether (MTBE) are water soluble and contaminate water sources, and could also seriously harm the handler. Thus phasing out of water soluble oxygenates, which are very high in octane number, are on the way. This not only causes octane loss, it also reduces the amount of gasoline produced by 3-4% and

refiners lose the non-aromatic, non-olefinic, and low-sulphur blend stock (UOP 2000). Moreover, according to the studies done by various researches shows that the cost of production of gasoline would increase by about 30% with the oxygenate ban. Their future is uncertain from political standpoint.

Other properties include viscosity (maximum), API gravity, density, olefins (maximum vol%) and specific gravity. Table 3.2 shows the specification for gasoline in California (USA).

3.2.2 Motivation of this Research on Gasoline Blending

To achieve a successful operation in most petroleum refineries, gasoline blending is considered as a key process. This indicates the need to employ tight controls of blending operations on property giveaway as it can provide a crucial edge to the profitability of a refinery. As reviewed before, many refiners used to treat gasoline blending as a linear problem, sometimes as a non-linear one but still with a big giveaway due to the model accuracy, which leads to a significant profit loss. On the other hand, the compositional specifications such as benzene, aromatic and olefin contents, and other properties specifications need a demanding investment on the expensive instruments, constant maintenance, frequent standardisation, as well as consuming feedstock/product for analysis. Moreover, it is not suitable on-line monitoring. In the petroleum industry, measurement of the physical properties of hydrocarbons forms the basis of commodity pricing and the assessment of process parameters. The key measurement performed on gasoline is the calculation of octane number. The ASTM standard for reporting this measurement is an internal combustion engine in which octane is measured by interpolating between the nearest standards above and below the unknown sample. The procedure is time consuming, involves expensive (over \$100,000) and maintenance-intensive equipment, requires skilled labour and is not well suited to on-line monitoring. Although modern analytical technology is able to measure molecular information both online and offline, it cannot be used in a virtual environment, and will increase a large maintenance cost.

3.3 A New Molecular Model for Property Prediction

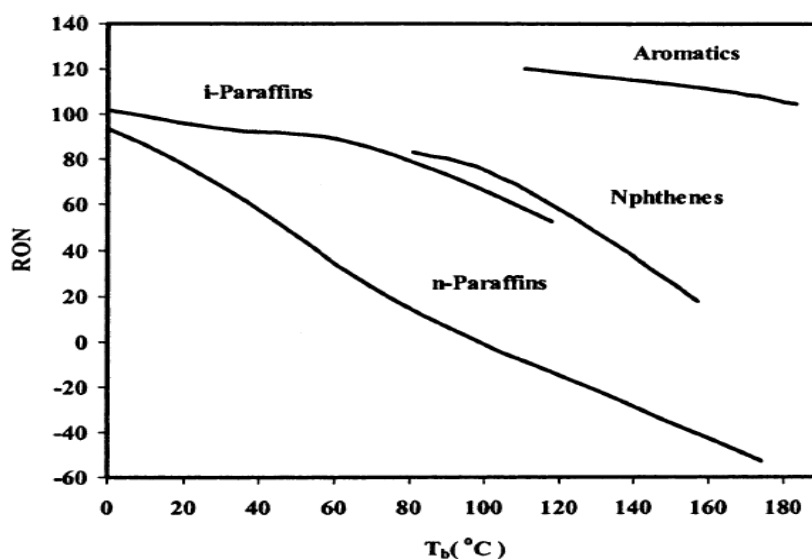


Figure 3.2 Research Octane Number of different families of hydrocarbons (Riazi, 2005)

As reviewed in chapter 2, numerous efforts have been put into developing correlations for predicting properties based on easily measured distillation profile and density in the past (see Table 2.7). However, some properties such as ON cannot be directly estimated from the boiling point and density, since ON very much depends on the chemical structure of components of the mixture. Figure 3.2 shows variation of RON with boiling point of pure hydrocarbons from different families. Knock results from the premature combustion of gasoline due to compression in the engine. As the fuel/air mixture is compressed in the internal combustion engine, certain molecules in gasoline tend to self-ignite even before they reach the ignition spark, thereby creating a resistive expansive motion in the compression stroke of the engine and hence the knock. Depending on the thermal stability of molecules and the ensuing radicals, certain molecules tend to combust sooner than others. Consequently, ON is a direct function of the molecular composition of gasoline fuel, and any modelling effort should explicitly acknowledge it.

3.3.1 Review of Previous Methodologies for ON

Previous studies have attempted to mathematically describe the ON as a function of gasoline composition. Anderson et al. (1972) developed a useful and simple method – an ideal model - for predicting the RON of different types of naphtha based on the gas chromatographic analysis of a sample by characterising a stream using 31 molecular lumps, and computing ON of the fuel as a linear addition of the contribution from each lump. Later on, more and more researchers (Rusin, 1981; Habib, 1989; Cotterman, 1989) found that the octane number is not generally a linear mixing property due to the interactions existing between the compounds of different chemical natures (olefins, paraffins, naphthenes, and aromatics). This can generate effects of synergy or inhibition and give the mixture a higher/lower octane number than its individual components. Lugo (1999) developed correlations between catalytic cracking naphtha ON and composition using a non-ideal model based on Anderson's lumps. Other relevant work in this includes the work by Twu and Coon (1997), and Albahri (2003). More recently, a detailed gasoline composition-based octane model (Ghosh, 2006) was presented with a total of 57 hydrocarbon lumps to predict ON of any type of gasoline fuels based on the analysis of 1471 gasoline fuels from different process streams. The model predicts the octane number within a standard error of 1 number for RON and MON for a broad range of ONs from 30 to 120.

All of these methods predict ON by correlating molecular composition, which obviously demand the molecular composition measured by different chemistry analytical methods.

3.3.2 A New Methodology Correlating ON with Bulk Properties

3.3.2.1 Assumptions

Published studies (API, 1997; Scott, 1958; Ghosh, 2006) reveal that hydrocarbons belonging to the same homologous series blend linearly on ON. That is to say that paraffins blend linearly with other paraffins, olefins blend linearly with other olefins, and so on. However, a blend of olefins and aromatics may exhibit

significant deviation from linearity. Such nonlinear interaction in a binary blend is qualitatively described in Figure 3.3.

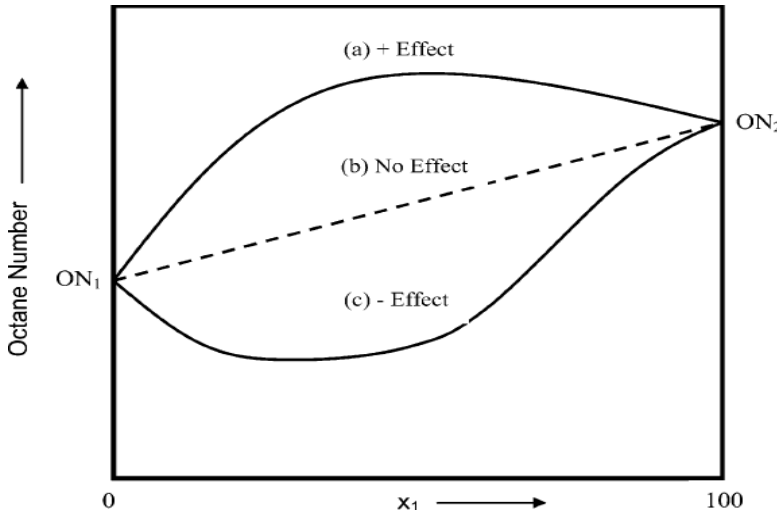


Figure 3.3 Nonlinear interactions between two molecules belonging to different homologous series (Ghosh, 2006)

According to this behaviour, an assumption is made that gasoline blending streams could be lumped as P, I, O, N, A, and the interaction between each lump is considered. Then, the proposed model could be expressed as Equation 3.1.

$$ON = f(x_i, ON_i) \quad \forall i \in PIONA \quad (3.1)$$

where x_i represents the fraction of i lump, and ON_i for ON of lump i .

The detailed gasoline composition-based octane model (Ghosh, 2006) will be applied to PIONA-lump model as Equation 3.2.

$$ON = f(x_i, ON_i) = \frac{\sum_{i \in PIONA} x_i^v \beta_i ON_i + I_{PI} \sum_{i \in PI} x_i^v \beta_i ON_i}{\sum_{i \in PIONA} x_i^v \beta_i + I_{PI} (\sum_{i \in PI} x_i^v \beta_i - \sum_{i \in PI} x_i^v)} \quad (3.2)$$

where β_i is the fixed coefficient.

$$I_{PI} = \frac{k_{PN}^a x_N^v + k_{PO}^a x_O^v}{1 + k_{PN}^b x_N^v + k_{PO}^b x_O^v} \quad (3.3)$$

In this model, the nonlinear interactions between paraffins and naphthenes and between paraffins and olefins are considered.

Based on the assumption made and the available molecular blending model, the problem switches to correlating PIONA volume fractions and PIONA ONs with easily obtained bulk properties through Equations 3.4 and 3.5 as Figure 3.4 shows.

$$x_i = f(TBP, d) \quad \forall i \in PIONA \quad (3.4)$$

$$ON_i = f(TBP, d) \quad \forall i \in PIONA \quad (3.5)$$

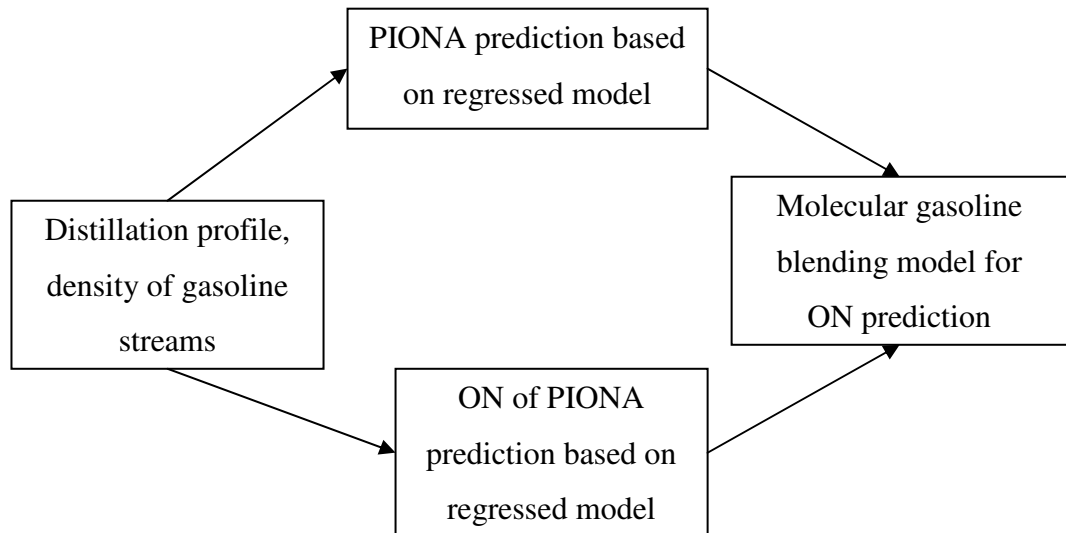


Figure 3.4 Simplified diagram for predicting ON of blending streams

The second assumption is made that fractions and ONs of PIONA lumps could be correlated with TBP curve and density of gasoline streams. Moreover, the correlations will depend on refining process type. As reviewed, straight run naphtha from atmospheric distillation unit, gasoline streams from FCC and CCR units, etc. are potential gasoline blending components, therefore the correlations of Equations 3.4 – 3.5 will be developed for each process. This assumption excludes the possibility that the streams from the same refining process with similar TBP and density could have quite different ONs.

The assumption of correlating fractions and ONs of PIONA lumps with bulk properties is aspired from the mostly commonly used correlation of ASTM D4737 for cetane number of diesel fuels illustrated as Equation 3.6.

$$CN = 45.2 + 0.0892T_{10N} + (0.131 + 0.901B_N)T_{50N} + (0.0523 - 0.42B_N)T_{90N} + [0.00049(T_{10N}^2 - T_{90N}^2)] + 107B_N + 60B_N^2 \quad (3.6)$$

where d is specific gravity at 60 °F, and T_x is the TBP temperature (in °C) at which x vol% of the sample has distilled.

$$B_N = e^{-3.5(d-0.85)} - 1 \quad (3.7)$$

$$T_{10N} = T_{10} - 215 \quad (3.8)$$

$$T_{50N} = T_{50} - 260 \quad (3.9)$$

$$T_{90N} = T_{90} - 310 \quad (3.10)$$

Despite its empirical nature, this simplified quadratic correlation has enjoyed enviable success in describing CN of various diesel fuels and their blends. It is used extensively within the petroleum industry. Therefore, the quadratic equations are proposed to correlate the fractions and ONs of PIONA lumps with bulk properties as Equations 3.11 and 3.12.

$$\begin{aligned} x_i^{pred} = & a_{1,i}^f B_N^2 + a_{2,i}^f T_{10N}^2 + a_{3,i}^f T_{50N}^2 + a_{4,i}^f T_{90N}^2 + a_{5,i}^f B_N T_{10N} + a_{6,i}^f B_N T_{50N} + a_{7,i}^f B_N T_{90N} \\ & + a_{8,i}^f T_{10N} + a_{9,i}^f T_{50N} + a_{10,i}^f T_{90N} + a_{11,i}^f B_N + a_{12,i}^f \quad \forall i \in PIONA \end{aligned} \quad (3.11)$$

$$\begin{aligned} ON_i^{pred} = & a_{1,i}^{ON} B_N^2 + a_{2,i}^{ON} T_{10N}^2 + a_{3,i}^{ON} T_{50N}^2 + a_{4,i}^{ON} T_{90N}^2 + a_{5,i}^{ON} B_N T_{10N} + a_{6,i}^{ON} B_N T_{50N} + a_{7,i}^{ON} B_N T_{90N} \\ & + a_{8,i}^{ON} T_{10N} + a_{9,i}^{ON} T_{50N} + a_{10,i}^{ON} T_{90N} + a_{11,i}^{ON} B_N + a_{12,i}^{ON} \quad \forall i \in PIONA \end{aligned} \quad (3.12)$$

where

$$B_N = e^{-3.5(d-\bar{d})} - 1 \quad (3.13)$$

$$T_{10N} = T_{10} / 100 \quad (3.14)$$

$$T_{50N} = T_{50} / 100 \quad (3.15)$$

$$T_{90N} = T_{90} / 100 \quad (3.16)$$

The coefficients in the correlations will be regressed by the proposed methodology.

3.3.2.2 Methodology

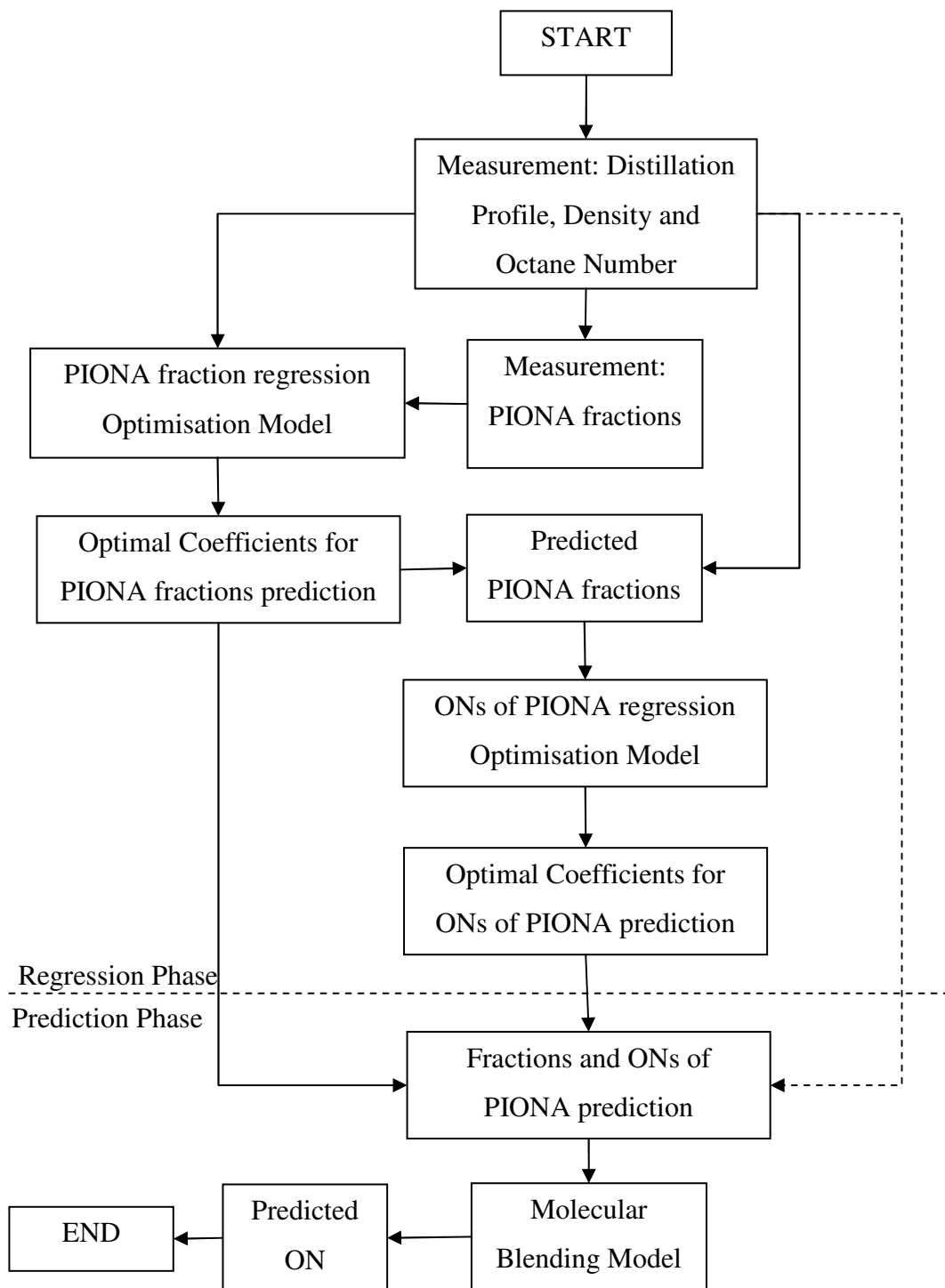


Figure 3.5 Diagram for the methodology of predicting ON of gasoline streams from one of refining process

The diagram for the proposed methodology used to predict ON based on easily obtained bulk properties is depicted in Figure 3.5. The whole procedure involves two phases, namely regression and prediction phases. The regression phase, as the

name implies, targets on achieving the optimal coefficients of the correlations for the prediction of the fractions and ONs of PIONA lumps, while the prediction phase will apply the optimal coefficients to predict the fractions and ONs of PIONA lumps, which are used to predict ON as Equation 3.2.

The first step in this scheme consists of information gathering about gasoline streams from the investigated refining process, including distillation profile, density, and ON, as well as compositional fractions of PIONA lumps. This experimental information provides the basic input for the regression models.

The second step is to use a regression optimisation model based on least square method for correlating the fractions of PIONA lumps by Equation 3.11. The mathematical model for this step is as follows.

Objective function is to minimise the difference of fractions between predicted and measured, in which the measured data is from the first step.

$$obj_i = \sum_j \left(\frac{x_{i,j}^{msd} - x_{i,j}^{pred}}{x_{i,j}^{msd}} \times 100 \right)^2 \quad (3.17)$$

Subject to

$$\begin{aligned} x_{i,j}^{pred} = & a_{1,i}^f B_{N,j}^2 + a_{2,i}^f T_{10N,j}^2 + a_{3,i}^f T_{50N,j}^2 + a_{4,i}^f T_{90N,j}^2 + a_{5,i}^f B_{N,j} T_{10N,j} + a_{6,i}^f B_{N,j} T_{50N,j} + \\ & a_{7,i}^f B_{N,j} T_{90N,j} + a_{8,i}^f T_{10N,j} + a_{9,i}^f T_{50N,j} + a_{10,i}^f T_{90N,j} + a_{11,i}^f B_{N,j} + a_{12,i}^f \\ & \forall i \in PIONA, \forall j \in J \end{aligned} \quad (3.18)$$

$$x_{i,j}^{pred} \geq 0 \quad (3.19)$$

where J stands for the all sample streams of the investigated refining process collected from the first step. The optimal coefficients of a^f will be used in the prediction phase.

The third step comprises of a regression optimisation model to correlate ONs of PIONA lumps with bulk properties. It cannot be implemented in the same way as the fractions regression model in the second step because ONs of PIONA lumps

are unknown. Therefore, an iterative procedure is proposed to implement it as Figure 3.6 shows.

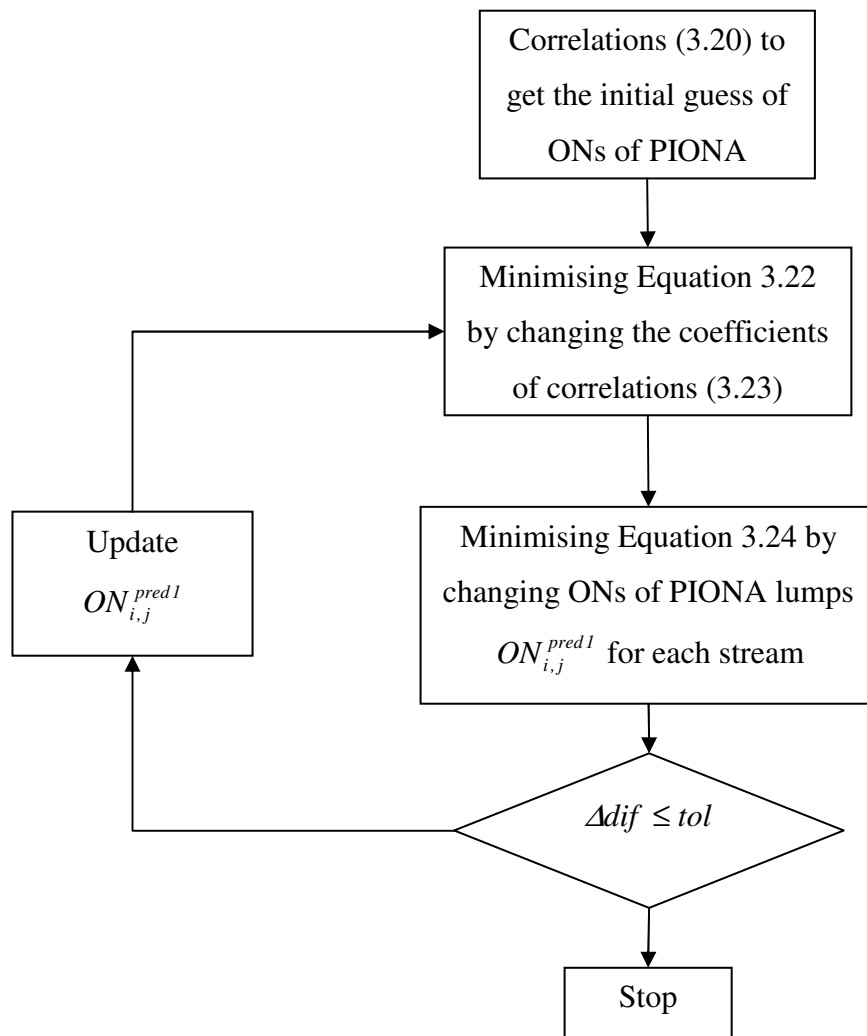


Figure 3.6 Series of procedures for achieving the optimal coefficients for predicting ONs of PIONA lumps

The first part of the step is to estimate ONs of PIONA lumps according to a correlation from the literature (Riazi, 2005) as Equations 3.20 and 3.21. These values are treated as the initial guess of $ON_{i,j}^{pred1}$.

$$RON_{i,j}^{init} = a_i + b_i T_{50,j} + c_i T_{50,j}^2 + d_i T_{50,j}^3 + e_i T_{50,j}^4 \quad (3.20)$$

$$MON_{i,j}^{init} = 22.5 + 0.83RON_{i,j}^{init} - 20.0d - 0.12(\%O) \quad (3.21)$$

The coefficients are given in Table 3.3. For isoparaffins, there are four sub-classes, and the ON of isoparaffins would be the average of these four.

Table 3.3 Coefficients of Equation 3.20 (Riazi, 2006)

RON	a	b	c	D	e
P	1514.964439	-3893.446054	1211.056162	3649.119954	-2507.33327
I	95.927	-157.53	561	-600	200
	92.069	57.63	-65	0	0
	109.38	-38.83	-26	0	0
	97.652	-20.8	58	-200	100
O	517.8532645	-1064.055902	181.0178314	1237.306636	-777.6732827
N	3.704079298	390.917866	-493.279582	98.66492226	82.24068859
A	145.668	-54.336	16.276	0	0

The following parts are within the iteration. The second part minimises the differences of ONs of PIONA lumps between the predicted based on Equation 3.23 and the predicted result from the first step for the first iteration or the updated result from the late iteration. The optimisation model is as follows.

The objective function:

$$obj_i = \sum_j \left(\frac{ON_{i,j}^{pred} - ON_{i,j}^{pred1}}{ON_{i,j}^{pred1}} \times 100 \right)^2 \quad (3.22)$$

where $ON_{i,j}^{pred1}$ is the result from the first step or the update result from the iteration.

Subject to

$$ON_{i,j}^{pred} = a_{1,i}^{ON} B_{N,j}^2 + a_{2,i}^{ON} T_{10N,j}^2 + a_{3,i}^{ON} T_{50N,j}^2 + a_{4,i}^{ON} T_{90N,j}^2 + a_{5,i}^{ON} B_{N,j} T_{10N,j} + a_{6,i}^{ON} B_{N,j} T_{50N,j} + a_{7,i}^{ON} B_{N,j} T_{90N,j} + a_{8,i}^{ON} T_{10N,j} + a_{9,i}^{ON} T_{50N,j} + a_{10,i}^{ON} T_{90N,j} + a_{11,i}^{ON} B_{N,j} + a_{12,i}^{ON} \quad \forall i \in PIONA, \forall j \in J \quad (3.23)$$

The third part of the step consists of minimising the difference of ON of the stream between the measured and the predicted from the molecular model as Equation 3.2 by changing the ONs of PIONA lumps of $ON_{i,j}^{pred1}$, and simultaneously remaining the optimal ONs of PIONA lumps close to the result from the second part of the step ($ON_{i,j}^{pred}$) as much as possible. The optimisation model is as follow.

Objective function

$$Obj_j = (ON_j^{pred} - ON_j^{msd})^2 + w \sum_{i \in PIONA} (ON_{i,j}^{pred1} - ON_{i,j}^{pred})^2 \quad \forall j \in J \quad (3.24)$$

Subject to

$$ON_j^{pred} = \frac{\sum_{i \in PIONA} x_{i,j}^{pred} \beta_i ON_{i,j}^{pred1} + I_{PI,j} \sum_{i \in PI} x_{i,j}^{pred} \beta_i ON_{i,j}^{pred1}}{\sum_{i \in PIONA} x_{i,j}^{pred} \beta_i + I_{PI,j} (\sum_{i \in PI} x_{i,j}^{pred} \beta_i - \sum_{i \in PI} x_{i,j}^{pred})} \quad (3.25)$$

$$RON_{P,j}^{pred1} \leq RON_{I,j}^{pred1} \quad (3.26)$$

$$RON_{O,j}^{pred1} \geq RON_{N,j}^{pred1} \quad (3.27)$$

$$RON_{A,j}^{pred1} \geq 100 \quad (3.28)$$

$$\left(\frac{ON_j^{pred} - ON_j^{msd}}{ON_j^{msd}} \times 100 \right)^2 \leq 0.25 \quad (3.29)$$

where w is the weighting factor, and the current value is 100. The first constraint in this optimisation model is the molecular model for predicting ON of the stream based on PIONA lumps. Equations 3.26 – 3.29 are applied to RON, and will be changed accordingly for MON. The last constraint is for the accuracy requirement of ON prediction, as the default of 0.5% deviation.

The iteration will be stopped until the change of the objective function is less than tolerance. From this step, the optimal coefficients for predicting ONs of PIONA based on bulk properties are achieved, which will be used in the prediction phase.

After achieving the optimal coefficients of correlations, ON of the stream could be predicted based on Equation 3.2 after calculating the fractions of PIONA from Equation 3.11 and ONs of PIONA lumps from Equation 3.12, which is termed as the prediction phase in Figure 3.5.

The proposed methodology can be applied to predict other properties as well, such as RVP. The difference in the methodology for different properties is that different molecular blending models instead of Equation 3.2 should be introduced. As for RVP, Equation 3.30 is introduced as the molecular blending model.

$$RVP = \frac{\sum_{i \in PIONA} x_i^v \beta_i RVP_i + I_A \sum_{i \in A} x_i^v \beta_i RVP_i}{\sum_{i \in PIONA} x_i^v \beta_i + I_A (\sum_{i \in A} x_i^v \beta_i - \sum_{i \in A} x_i^v)} \quad (3.30)$$

where

$$I_A = \frac{k_{AP}^a (x_P^v + x_I^v) + k_{AO}^a x_O^v + k_{AN}^a x_N^v}{1 + k_{AP}^b (x_P^v + x_I^v) + k_{AO}^b x_O^v + k_{AN}^b x_N^v} \quad (3.31)$$

The nonlinear interactions between aromatics and other homologous series (PION) are taken into account due to the well-known non-ideal blending behaviour of non-aromatics with aromatics (API, 1997). As for the initial value (Equation 3.20) of RVP, RVP of each entry of MTHS matrix is applied.

3.3.3 Case Study

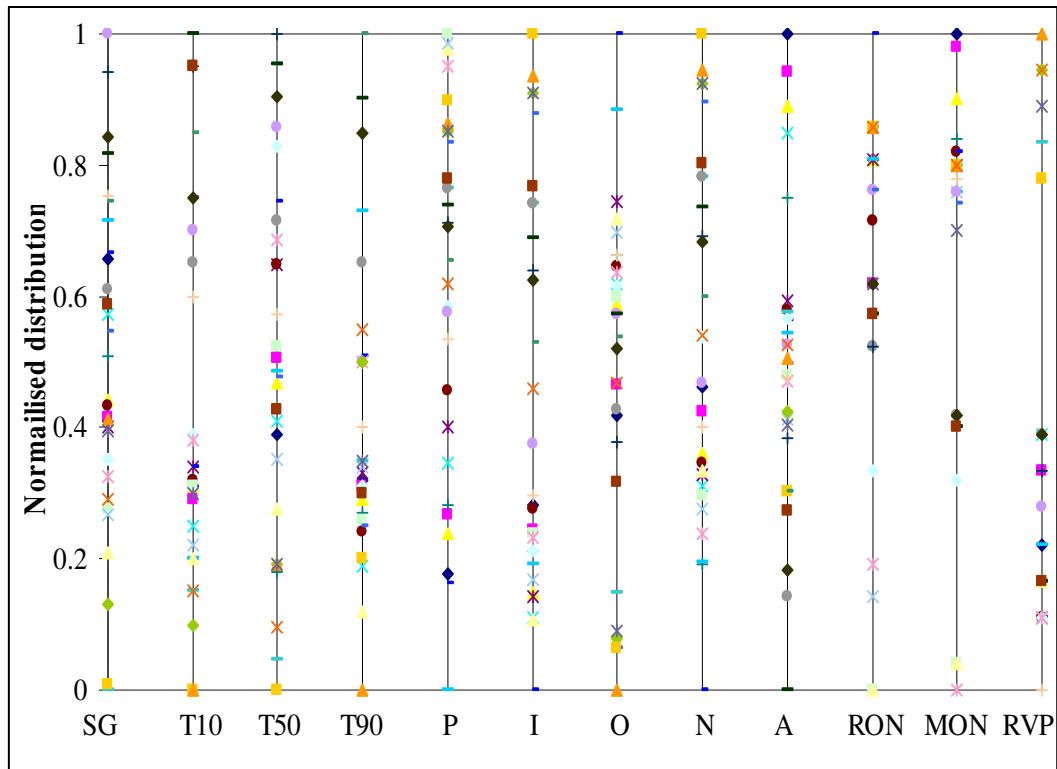


Figure 3.7 Normalised distributions of the related properties for the proposed methodology (Each dot stands for a different sample)

The proposed methodology will be applied to ON and RVP properties for the gasoline stream from a FCC unit in a plant. Historical data are obtained from the

report of the FCC units. Normalised distributions of properties including specific gravity, T_{10} , T_{50} , T_{90} , PIONA fractions, RON, MON and RVP are illustrated in Figure 3.7. 80% of the obtained dataset is used for the regression phase, and the rest to verify the accuracy of the proposed methodology. The proposed methodology is applied to ON/RVP properties. Many different initial guesses were assumed, and the parameters were re-optimised to ensure that the optimisation problem was not trapped in an inferior local solution.

3.3.3.1 Result of the Regression Phase

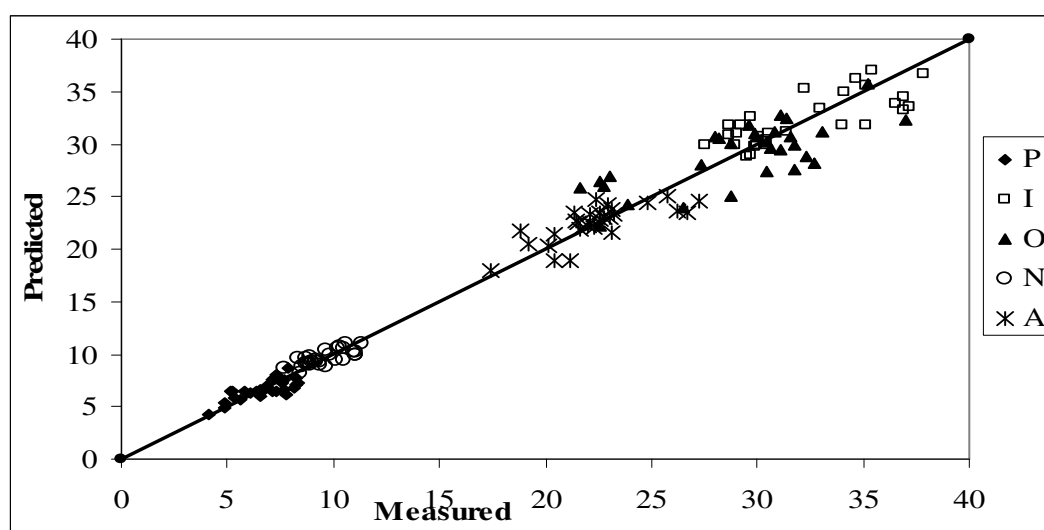


Figure 3.8 Comparison of PIONA volume fractions between the measured and predicted in regression phase

In the regression phase, the coefficients of the correlations will be optimised based on the proposed methodology. Figure 3.8 – 3.11 illustrate the results of the regression model for PIONA fractions, RON, MON and RVP respectively. Table 3.4 summarises the model performance. The overall standard error is defined as

$$\sqrt{\sum (meas - pred)^2 / n},$$

and the average represents the average of absolute errors between the measured and the predicted. The overall standard errors for RON, MON and RVP are 0.38, 0.51 number, and 0.24 psi. To have a comparison, direct quadratic correlations between properties including RON, MON and RVP and the easily obtained properties are applied, and the results are shown in Table 3.5. 0.25, 0.33 number of RON and MON, 0.16psi of RVP are improved in terms of the overall standard errors. This improvement may seem marginal, but even a 0.1

number improvement in the prediction error has a significant economic consequence (Ghosh, 2006).

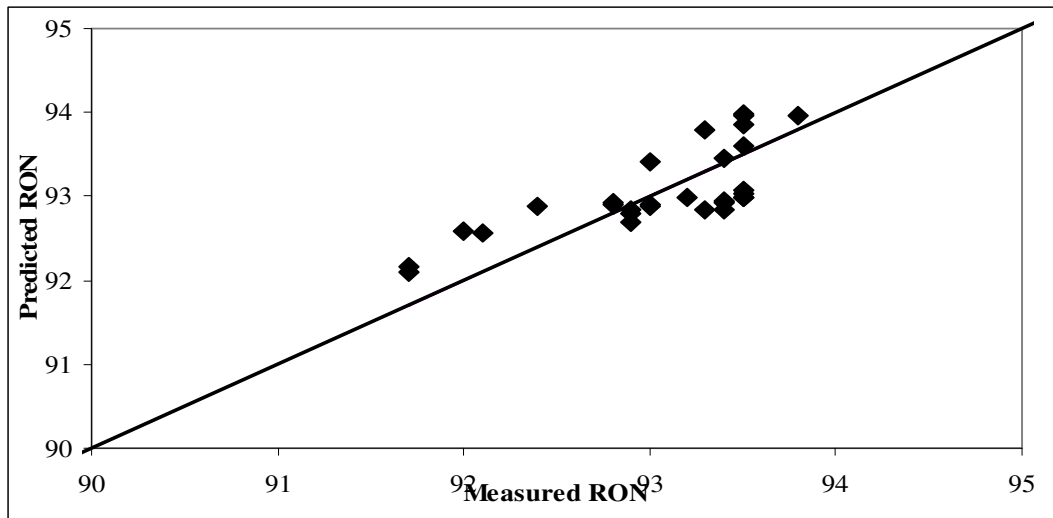


Figure 3.9 Comparison of RON between the measured and predicted in regression phase

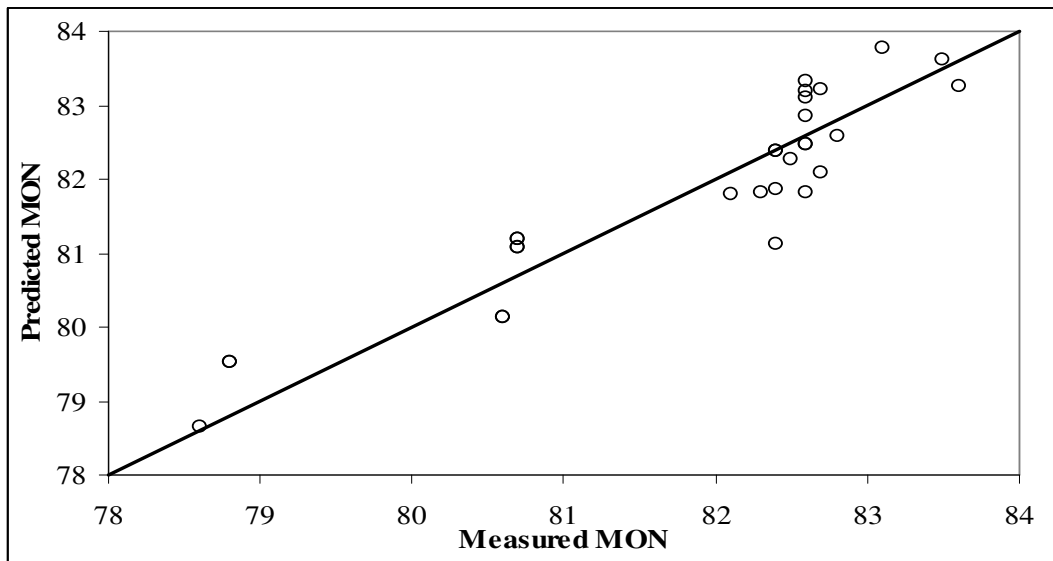


Figure 3.10 Comparison of MON between the measured and predicted in regression phase

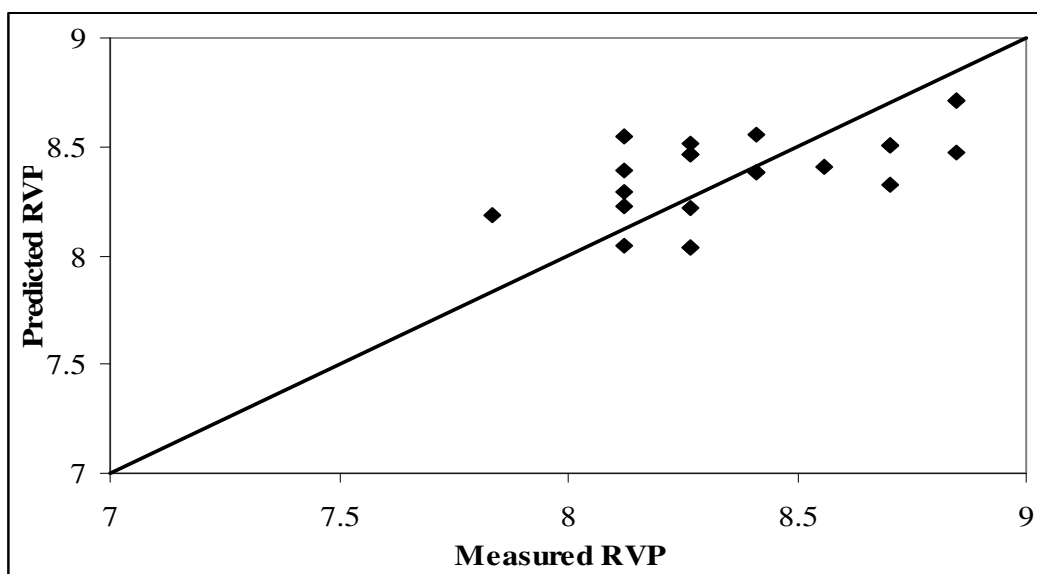


Figure 3.11 Comparison of RVP between the measured and predicted in regression phase

Table 3.4 Model performance in regression phase

	standard deviation	average	overall standard errors
P (vol%)	0.46	0.56	0.75
I (vol%)	1.19	3.94	1.99
O (vol%)	1.44	6.79	2.61
N (vol%)	0.38	0.41	0.64
A (vol%)	0.94	2.14	1.46
RON	0.18	0.34	0.38
MON	0.28	0.44	0.51
RVP (psi)	0.12	0.21	0.24

Table 3.5 Model performance of the direct correlated model (see section 3.3.3.1)

	standard deviation	average	overall standard errors
RON	0.43	0.47	0.63
MON	0.42	0.73	0.84
RVP (psi)	0.26	0.32	0.40

3.3.3.2 Result of the Prediction Phase

To investigate the performances of interpolation and extrapolation predictions, the prediction dataset includes the data both inside the range of properties and outside. To define the prediction type, if the dataset of the basic input information including density, T_{10} , T_{50} , and T_{90} all locate within the ranges of these properties for the regression phase, it's defined as interpolation prediction. Otherwise, if any of these properties of the dataset violates the ranges, it becomes extrapolation prediction.

Table 3.6 illustrates the good performance of the interpolation prediction, while Table 3.7 gives the result of an example of the extrapolation prediction, which sees bigger deviations of RON, MON and RVP properties. More investigation found that more gaps of the properties from the ranges of regression dataset, higher deviation will be generated, which is the common disadvantage of the regression based models. To enhance the accuracy of the prediction, the dataset outside of the regression range could be added for the regression to ensure the high accuracy of predicted results.

Table 3.6 Model performance of interpolation prediction in the prediction phase

	standard deviation	average	overall standard errors
RON	0.18	0.25	0.30
MON	0.17	0.36	0.39
RVP	0.24	0.42	0.46

Table 3.7 Result of an example of extrapolation prediction

	Measured	Prediction	Error
RON	91.80	92.88	1.08
MON	81.20	82.71	1.51
RVP	8.27	7.34	0.93

3.4 Gasoline Blending Model

3.4.1 Review of Gasoline Blending Models

In the previous section (section 3.3), a new methodology is proposed to predict the properties, which provides a fundamental information for gasoline blending. Since the process control objectives for the product blending are often framed in terms of meeting specifications on the properties of gasoline such as ON, RVP, viscosity, etc., process models in the form of component property mixing rules are required for effective process control.

The most simple and practical mixing rule (Riazi, 2005) that is applicable to most physical properties is as follows:

$$\theta_p = \sum_{k=1}^N x_k \theta_k \quad (3.32)$$

where x_k is the volume/weight/molar fraction of the blending component k , θ_k is a property for the blending component k , and θ_p is property of the product with N blending components. Equation 3.32 could be applied to any property, and has various modified versions when it is applied to different properties. The type of fraction used for x_k depends on the type of property. For example, to calculate molecular weight of a product, the most appropriate type of fraction is mole fraction. However, when it is applied to density, specific gravity, or refractive index, volume fraction should be used, or the modified version as Equation 3.33 with weight fraction can also be applied (Riazi, 2005).

$$1/\theta_p = \sum_{k=1}^N x_{wk} / \theta_k \quad (3.33)$$

Equation 3.32 can be applied to predict the properties blend linearly such as Aromatics, Benzene, Olefins, Oxygenates and sulphur contents. However, it has been widely recognised that some gasoline properties blend in a non-ideal and nonlinear fashion such as octane number, RVP, Aniline point, and viscosity, as well as distillation profile etc., necessitating the use of more complex blending models to predict these properties. Some of these properties can be converted to a

blending number or index to allow them to be blended linearly as Equation 3.34 shows.

$$BI_p = \sum_{k=1}^N x_k BI_k \quad (3.34)$$

where BI_k is the blending index/number of the property of blending component k which is the function of the property as Equation 3.35, and BI_p is the blending index/number of the property of the product, which can be inversely converted to the property of the product as Equation 3.36. x_k is the volume/weight/molar fraction of blending component k .

$$BI = f(P) \quad (3.35)$$

$$P = f^{-1}(BI) \quad (3.36)$$

The properties blended according to Equation 3.34 include RVP, viscosity, Aniline point, pour point and flash point (Riazi, 2005). However, one of serious disadvantages is that these blending indices/values only can be applied in a narrow property range, and will generate a big deviation for blending of streams with wide different properties. RVP and octane number are two most important properties of gasoline products with high non-linear blending nature. Several key factors are very important for the blending models: (1) predictive accuracy; (2) complexity; and (3) ease of implementation. The following section will firstly review the models specific for ON and RVP blending, followed by a new proposed methodology based on the molecular model, compared in these three key factors.

3.4.2 Existing Blending Models for ON and RVP Properties

3.4.2.1 Octane Number

Several blending models are available in the literature for the calculation of the blend octane rating and all these models recognise the nonlinear dependence of the blend octane number by modelling it with functions containing a linear part and a nonlinear correction term. A number of empirical blending models are available in the literature for predicting blended octane numbers given component properties which include the blending octane number method (Gary and Handwerk, 2001),

the transformation method (Rusin et al., 1981), the Ethyl RT-70 models (Healy et al., 1959), an olefins content based method from Stewart (1959), the interaction method (Morris, 1975) and the excess method (Muller, 1992).

Both the blending octane number approach and the transformation method attempt to convert the nonlinear blending problem to a linear problem by transforming RON and MON into quantities that blend ideally on a volumetric basis. The results of the blend calculations are then transformed back to an appropriate octane number. Although the blending octane number method requires fewer and simpler calculations than the far more complex transformation method, the blending octane numbers must be computed from experimental data.

The interaction method and the excess method are essentially regression analysis based approaches. In the interaction method, blending nonlinearity is accounted for via two-factor interaction (or bilinear) terms, whereas in the excess method, the deviation is accounted for using an excess (or bias) term. Both of these approaches require a considerable amount of data from laboratory blending studies to estimate the large number of parameters in the models.

For the transformation method, Rusin et al. (1981) have reported higher prediction accuracy for extrapolation than for interpolation. The excess method, being linear, is valid only within the vicinity of the nominal blend. Due to the fact that the transformation models and the interaction models require more feedstock quality data and contain more parameters, it is not very favourable though they seem to provide slightly better predictive accuracy than the Ethyl RT-70 models. Moreover, the Ethyl RT-70 models are much simpler and easier to use than the transformation models.

Despite the age, the Ethyl RT-70 blending models are widely used and have become a standard against which many of the newer models are compared. The Ethyl RT-70 approach consists of a linear blending part, and the blending nonlinearity is expressed in terms of the component sensitivity (RON-MON), olefins content, and the aromatic content of the blend components expressed as follow (Healy et al., 1959).

$$RON_b = RON_a + a_1[(RON \times S)_a - (RON_a \times S_a)] + a_2[(O^2)_a - (O_a)^2] + a_3[(A^2)_a - (A_a)^2] \quad (3.37)$$

$$MON_b = RON_a + b_1[(MON \times S)_a - (MON_a \times S_a)] + b_2[(O^2)_a - (O_a)^2] + b_3\{[(A^2)_a - (A_a)^2]/100\}^2 \quad (3.38)$$

where, a_i and b_i are standard coefficients and their values are given in Table 3.8, and S is the component sensitivity. The subscript a stands for the average.

Table 3.8 Coefficients in ethyl octane blending equations (Healy et al., 1959)

Coefficients for RON				Coefficients for RON		
	0.0 cc TEL/ gal	1.5 cc TEL/ gal	3.0 TEL/ gal	0.0 cc TEL/ gal	1.5 cc TEL/ gal	3.0 TEL/ gal
a ₁	0.03224	0.04600	0.05411	0.03224	0.04563	0.05242
a ₂	0.00101	0.00070	0.00098	0.00085	0.00066	0.00084
a ₃	0.00000	-0.00035	-0.00074	0.00000	-0.00042	0.00080
b ₁	0.0445	0.05122	0.03908	0.04285	0.04422	0.03532
b ₂	0.00081	0.00000	0.00000	0.00066	0.00000	0.00000
b ₃	-0.00645	-0.00539	-0.00703	0.00632	-0.00752	-0.00849

Although the Ethyl models are simple and easy to use, there are some disadvantages. Firstly, the predictive accuracy will reach 0.82 ON of standard deviation for the interpolation prediction with a narrow range of blending streams (Rusin et al., 1981). Secondly, the model is a regression based model with a limitation on the extrapolation prediction. Lastly, the model needs the measurement of RON, MON, olefin and aromatic contents of each blending streams.

More recently, molecular composition based octane blending models have been receiving significant attention to maintain/increase the refining margins with the serious forces from the environmental regulations. The main difference between the molecular blending models and traditional models is that the interactions between molecules/lumps are taken into account to achieve a high accuracy on ON prediction. The methods have been reviewed in section 3.31.

3.4.2.2 Reid Vapour Pressure

Two fundamental methods for predicting blended RVP are given in Stewart et al. (1959) and Vazques-Esparragoza et al. (1992). Stewart et al. (1959) presented one of the first theoretical approaches for predicting blended RVP's. The method uses component data (such as feedstock composition and component volatility), thermodynamic relationships, and a set of simplified assumptions to predict the blended RVP of a mixture. Vazques Esparragoza et al. (1992) presented an iterative procedure that extended Stewart's method. In this approach, the additivity of liquid and gas volumes is assumed and a different equation of state is used. Furthermore, the Vazques-Esparragoza et al. (1992) approach requires that the molar composition of the feedstocks to be known. The computations required in both of these methods are complex in comparison to those required in other approaches such as empirical approaches (Morris et al., 1975; Gary, J. H., 1994).

Comparisons of predictive accuracy of some of the methods can be found in Stewart (1959) who looked at the standard deviation of prediction error for 67 blends using different blended RVP prediction approaches. The latest method based on fundamental principles provides more accurate predictions. However, these theoretical methods are rather tedious due to their computational requirements. The interaction method requires numerous parameters to be updated. Although not as accurate as the theoretical methods, the simplicity of the blending index method makes it attractive for use in gasoline blending models. The equation used to calculate the RVP index for each blending component developed by Chevron Research Company is (Chevron, 1971):

$$RVPI = (RVP)^{1.25} \quad (3.39)$$

$$RVP_b = \left[\sum V_i (RVPI)_i \right]^{0.8} \quad (3.40)$$

However, the RVP blending values of pressurising agents increase with the aromatic content of the gasoline. The results of a comprehensive blending study (Morris, 2008) showed a considerable difference in RVP blending values of normal butane with different gasoline components (aromatics & non-aromatics), which cannot be handled by Chevron's model leading to a big RVP giveaway.

3.4.3 A New Molecular Gasoline Blending Methodology

3.4.3.1 Diagram

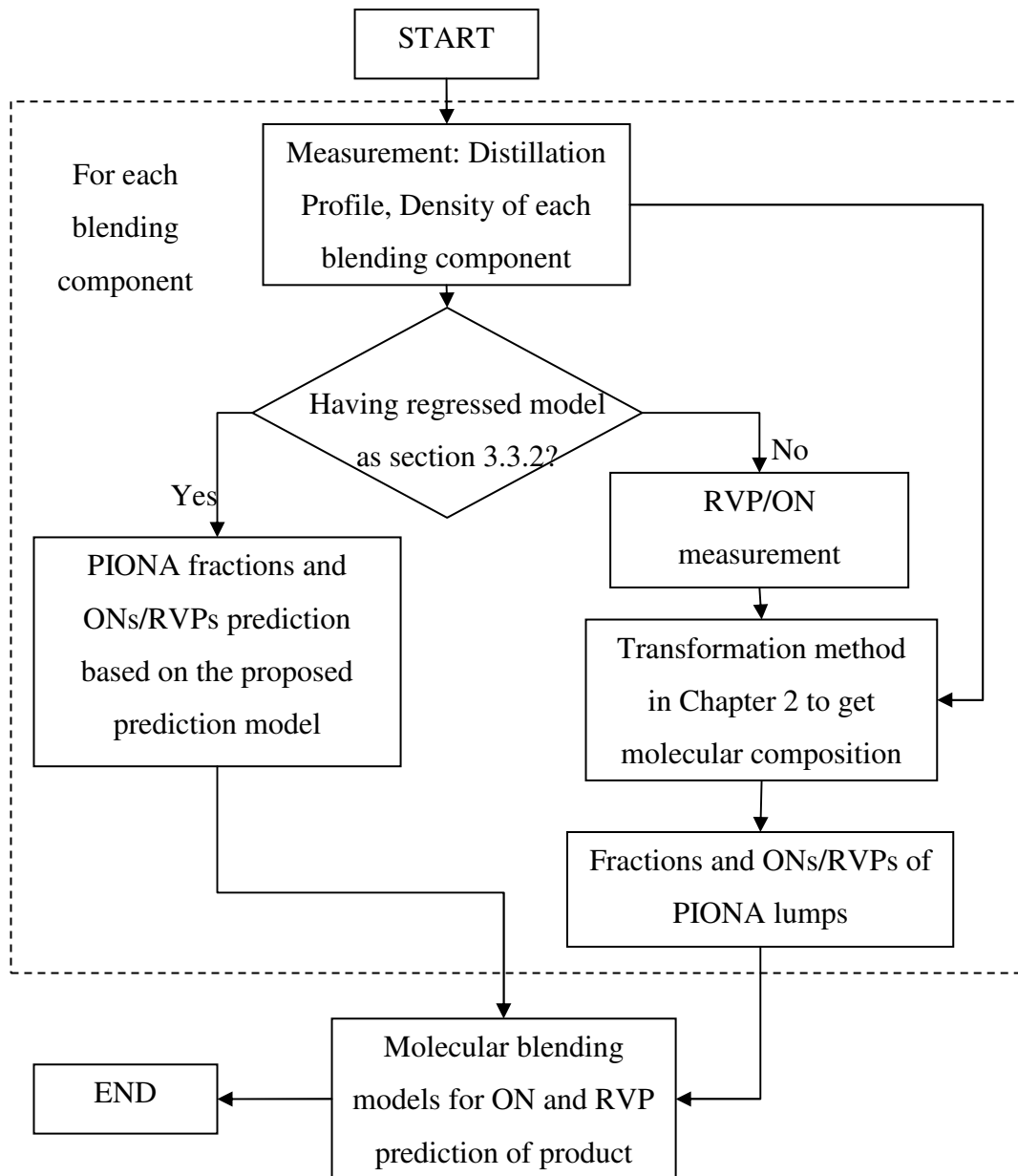


Figure 3.12 Proposed molecular gasoline blending methodology

The proposed new molecular gasoline blending methodology is illustrated in Figure 3.12, starting from the basic bulk properties information including distillation profile and density. If the regression based model described in section 3.3.2 is set up, the fractions and ONs/RVPs of PIONA lumps can be predicted according to the distillation profile and density. Otherwise, RVP/ON properties

should be measured for the transformation methodology investigated in Chapter 2 to achieve molecular composition of the blending stream in terms of MTHS matrix, which will be used to calculate the fractions and ONs/RVPs of PIONA lumps based on the assumption that the properties blend linearly within homologous series. These steps should be applied to each blending component, followed by the proposed molecular blending model for ON/RVP property prediction of gasoline products.

3.4.3.2 Mathematical Model

The volume fractions and ONs/RVPs of PIONA lumps of blending streams are predicted based on Equations 3.18 and 3.23, simplified as follows:

$$x_{i,j} = f(T_j, d_j) \quad \forall i \in PIONA, \forall j \in J \quad (3.41)$$

$$ON_{i,j} = f(T_j, d_j) \quad \forall i \in PIONA, \forall j \in J \quad (3.42)$$

$$RVP_{i,j} = f(T_j, d_j) \quad \forall i \in PIONA, \forall j \in J \quad (3.43)$$

The volume fractions and ONs/RVPs of PIONA lumps of blending products are calculated based on linear mixing rules in Equations 3.44 – 3.46.

$$x_{p,i} = \sum_j (y_j \times x_{i,j}) \quad \forall i \in PIONA, \forall j \in J, \forall p \in P \quad (3.44)$$

$$ON_{p,i} = \frac{\sum_j (y_j \times x_{j,i} \times ON_{j,i})}{\sum_j y_j \times x_{j,i}} \quad \forall i \in PIONA, \forall j \in J, \forall p \in P \quad (3.45)$$

$$RVP_{p,i} = \frac{\sum_j (y_j \times x_{j,i} \times RVP_{j,i})}{\sum_j y_j \times x_{j,i}} \quad \forall i \in PIONA, \forall j \in J, \forall p \in P \quad (3.46)$$

where y_j represents the blending ratio of component j .

The molecular models for ON/RVP prediction of products are defined as Equations 3.47 – 3.48, exactly the same as Equations 3.2 and 3.30.

$$ON = \frac{\sum_{i \in PIONA} x_i \beta_i ON_i + I_{PI} \sum_{i \in PI} x_i \beta_i ON_i}{\sum_{i \in PIONA} x_i \beta_i + I_{PI} (\sum_{i \in PI} x_i \beta_i - \sum_{i \in PI} x_i)} \quad (3.47)$$

$$RVP = \frac{\sum_{i \in PIONA} x_i \beta_i RVP_i + I_A \sum_{i \in A} x_i \beta_i RVP_i}{\sum_{i \in PIONA} x_i \beta_i + I_A (\sum_{i \in A} x_i \beta_i - \sum_{i \in A} x_i)} \quad (3.48)$$

3.4.4 Gasoline Blending Optimisation Model

The key component consideration introduces the nonlinearity in the blending problem and makes it an NLP formulation with constraints. The main constraints include: 1) product specifications, 2) the availability of blending stocks; 3) upper and lower bounds of market demand, 4) commodity prices, and 5) mass balance.

The objective function is to maximise the profit as Equation 3.49.

$$Profit = \sum_{p \in P} (F_p \times C_p) - \sum_{j \in J} (F_j \times C_j) \quad (3.49)$$

where F is the amount of stream, either product or blending component. C is the price of product/stock.

Subject to:

1) Product specifications

$$\theta_{p,k} = f(\theta_{j,k}, x_{i,j}) \quad \forall i \in PIONA, \forall j \in J, \forall p \in P, \forall k \in \theta \quad (3.50)$$

$$\theta_{p,k}^{min} \leq \theta_{p,k} \leq \theta_{p,k}^{max} \quad \forall p \in P, \forall k \in \theta \quad (3.51)$$

2) Availability of blending stocks

$$F_j^{min} \leq F_j \leq F_j^{max} \quad \forall j \in J \quad (3.52)$$

3) Market demands

$$F_p^{min} \leq F_p \leq F_p^{max} \quad \forall p \in P \quad (3.53)$$

4) Mass balance

$$F_p = \sum_{j \in J} F_{j,p} \quad \forall p \in P \quad (3.54)$$

$$F_j = \sum_{p \in P} F_{j,p} \quad \forall j \in J \quad (3.55)$$

3.4.5 Case Study

Table 3.9 Available feedstock properties and information about blending components

	RON	MON	RVP (psi)	A (%)	Olefin	Benzene	Availability (kbbl)	Price
Stream 1	91.3	78.8	4.02	32.1	26.6	0.18	150	-
Stream 2	99.2	88.0	4.41	63.2	0.00	1.52	150	-
Stream 3	110.2	97.2	1.75	89.1	0.00	2.01	250	-
Stream 4	78.3	71.9	5.67	11.7	0.205	0.49	230	-
Stream 5	72.9	67.6	3.42	15.2	0.00	0.64	200	-
isopentane	85.5	80	35.9	-	-	-	55	-
Ethanol	107.0	89.0	9.6	-	-	-	-	\$4.50/Gallon
Alkylate	93.7	83.9	9.40	-	20.14	0	150	\$2.95/Gallon

Table 3.10 Product specifications for two grades of gasolines

	RON	MON	RVP (psi)	Aromatics (%)	Olefin	Benzene (vol%)	Oxygenates (O wt%)	Price
Product1	98	86	6.9	33	5.5	0.8	4	\$4.11/Gallon
Product2	93	81	7.0	33	5.5	0.8	4	\$3.85/Gallon

The problem consists of five component streams along with iso-pentane stream to produce two different grades of gasoline. To meet with the product specifications, The additive of ethanol and alkylate can be blended with the component streams. Properties of blends are given in Table 3.9, and product specifications in Table 3.10. For ethanol, an additional constraint is considered that its concentration should not exceed 10% in the final gasoline product. Ethanol and alkylate can be purchased from the market at the price of 4.50\$/Gallon and 2.95\$/Gallon respectively. Final products product1 and product2 can be sold in the market at price of 4.11\$/Gallon and 3.85\$/Gallon respectively. The objective of the problem

is to maximise the profitability along with meeting the product specifications. Five blending components and iso-pentane should be used up.

3.4.5.1 Traditional Method

Optimisation is carried out based on the conventional approaches: Ethyl RT-70 and Chevron's correlations. The optimisation results are shown in Table 3.11 and Table 3.12. Table 3.11 shows detailed product distribution and Table 3.12 gives the blended product properties. Net revenue using the conventional approach is 172.0 MM\$..

Table 3.11 Detailed product distribution (the conventional approach)

	Product1 (kbbbl)	Product2 (kbbbl)
Stream 1	0.00	150.00
Stream 2	0.00	150.00
Stream 3	98.34	151.66
Stream 4	74.78	155.22
Stream 5	0.09	199.91
isopentane	6.19	48.81
Ethanol	33.67	120.73
Alkylate	79.00	71.00
Total	292.06	1047.34

Table 3.12 Blended product properties (the conventional approach)

	RON	MON	RVP (psi)	Aromatics (vol%)	Olefin (vol%)	Benzene (vol%)	Oxygenates (O wt%)
Product1	98.00	87.05	6.90	33.00	5.50	0.80	4.0
Product2	93.00	82.62	6.99	31.19	5.21	0.73	4.0

3.4.5.2 Molecular Blending Model

Table 3.13 Detailed product distribution (molecular modelling)

	Product1 (kbbbl)	Product2 (kbbbl)
Stream 1	-	150.00
Stream 2	-	150.00
Stream 3	137.50	112.50
Stream 4	111.43	118.57
Stream 5	-	200.00
iso-pentane	9.19	45.81
Ethanol	42.36	89.99
Alkylate	111.31	38.69
Total	411.78	905.56

Optimisation is carried out using the molecular information of the available feedstocks. Molecular models are implemented for ON/RVP using the proposed molecular blending model. Table 3.13 shows detailed product distribution while Table 3.14 illustrates the blend properties. Net revenue using the molecular models is 173.9 MM\$, a little higher profit.

Table 3.14 Blended product properties (molecular modelling)

	RON	MON	RVP (psi)	Aromatics (vol%)	Olefin (vol%)	Benzene (vol%)	Oxygenates (O wt%)
Product1	98.46	86.00	6.90	32.92	5.50	0.80	3.57
Product2	93.00	81.00	6.93	31.72	5.29	0.73	3.45

To summarise, molecular modelling of gasoline blending is capable of targeting molecules within the constraints of the regulations, and controls giveaway tightly to make more profit.

3.5 Summary

Firstly, to decrease the huge amount of cost for the instruments used to measure the properties, a new methodology is proposed to predict ON/RVP properties based on the easily obtained properties including distillation profile and density. The developed method is on the basis of regression models, and shows a good performance of interpolation prediction, illustrated by a case study that the overall standard errors for RON, MON and RVP are 0.38, 0.51 number, and 0.24 psi. However, the inherent disadvantage of the regression based model shows a bad performance of the extrapolation prediction, which could be improved by adding the extrapolated dataset in the regression process.

To tightly control on the property giveaway of gasoline blending, particularly with nonlinear blending nature such as RON, MON and RVP, a novel molecular model of gasoline blending on PIONA lumps is developed based on a detailed gasoline composition-based octane model (Ghosh, 2006). The previously proposed property prediction methodology is successfully applied to obtain the basic information for the molecular blending model. Thereafter, the molecular blending model is integrated into the recipe optimisation, demonstrated by a case study showing the economic improvement from the tighter control on property giveaway compared with the conventional approaches. The significance of this work is that the detailed property consideration during optimisation helps to find better solutions and meet with the product specifications more closely, and the proposed methodology can be integrated into more complex overall site-level optimisation.

3.6 Nomenclature

List of sets

i	<i>PIONA</i>
j	sample stream
p	product
k	properties
ON	RON and MON

List of symbols

ON_i	MON/RON of i
x_i	fraction of i
β_i	coefficient of i in the model
I_p	interaction term of paraffins with olefins and aromatics
$k_{PN}^a, k_{PN}^b, k_{PO}^a, k_{PO}^b$	coefficients in the developed model
d	density
TBP	boiling point
T_{10}, T_{50}, T_{90}	temperature of distillation profile at volume of 10%, 50%, and 90% respectively
CN	cetane number
$a_{i,j}$	coefficients of the developed correlation
y_j	blending fraction of stream j
RVP	Reid vapour pressure
F	amount of a stream

Chapter 4 Molecular Modelling of Semiregenerative Catalytic Reforming

4.1	Introduction	116
4.1.1	Catalytic Reforming Process.....	117
4.1.2	Feed Characteristics	119
4.1.3	Operating Conditions	120
4.1.4	Product Specifications.....	122
4.1.5	Review of Previous Work	123
4.1.6	Motivation of Molecular Modelling of Catalytic Reforming	126
4.2	Chemical Reactions Network and Kinetics.....	127
4.2.1	Dehydrogenation of Naphthenes to Aromatics	128
4.2.2	Isomerisation of Paraffins and Naphthenes	129
4.2.3	Dehydrocyclisation of Paraffins.....	129
4.2.4	Hydrocracking and Dealkylation	130
4.2.5	Kinetics	131
4.3	Process Model	131
4.4	Case Study.....	134
4.4.1	Simulation of the Process.....	135
4.4.2	Sensitivity Analysis of Operating Conditions.....	139
4.5	Catalyst Deactivation	142
4.5.1	Mathematical Model of Catalyst Deactivation	142
4.5.2	Multi-period Process Model.....	144
4.6	Catalytic Reforming Process Optimisation.....	146
4.6.1	Mathematical Model	147
4.6.2	Optimisation Approach	148
4.7	Case Study – Multi-period Process Simulation and Optimisation.....	148

4.7.1 Multi-period Process Simulation	148
4.7.2 Sensitivity Analysis of Operating Temperatures	150
4.7.3 Process Optimisation.....	151
4.8 Summary	153
4.9 Nomenclature	154

4.1 Introduction

Traditionally, catalytic reforming is a very important process for octane improvement with 50 vol% contribution to the gasoline pool, and the production of aromatic feedstock for the petrochemical industry, while a modern catalytic reforming process is gradually treated as one of important sources of precious hydrogen. The process converts gasoline-boiling-range low-octane hydrocarbons consisting of C₅-C₁₂ with a research octane number of 50-60, into high-octane gasoline compounds of 90-105 for use as high-performance gasoline fuel. This is achieved by transforming *n*-paraffins and naphthenes into the corresponding isoparaffins and aromatics, which means high content of aromatics in the reforming product. Recent environmental legislations established by different agencies such as the Clean Air Act demand the reduction in emissions of volatile, toxic, and polluting components in gasoline, such as benzene and aromatics. Coupled with these stricter environmental regulations, there has been a consistent increase in the demand for higher fuel efficiency standards of engines, and therefore motor fuel with an even greater octane number. Higher-octane-number products can be achieved under more severe conditions, but this will also cause the violation of environmental regulations, and the reduction of cycle lengths of catalyst, resulting in the higher operating cost. This scenario has continuously forced the improvement of different aspects, such as reactor configurations, catalyst, etc. One of most important strategies is to explore the trade-offs between high-octane-number and the specification of aromatics limit. A proper selection of operating conditions within plant constraints is essential to maximise the profitability of a reformer. Advanced optimisation of such a complex process requires a detailed mathematical model capable of accurately predicting the reformat composition, the product quality, and the catalyst life cycle over a wide range of operating conditions.

This chapter firstly briefly introduces catalytic reforming process, along with a short review of previous works on modelling of catalytic reforming. To build up a molecular model of a catalytic reformer, chemical reactions and modelling of the reactor are described respectively. A case study demonstrates the accuracy of the proposed model, together with the sensitivity analysis of the operating conditions.

Another important issue of catalyst deactivation, which has a serious impact on the economic performance, is also considered. Finally, a multi-period process level optimisation model is developed with the consideration of catalyst deactivation, well illustrated in the case study.

4.1.1 Catalytic Reforming Process

Reforming processes are classified as continuous, cyclic, or semiregenerative depending upon the frequency of catalyst regeneration. The continuous type is able to maintain high catalyst activity and selectivity by continuous catalyst regeneration as increased coke laydown and thermodynamic equilibrium yields of reformat are both favoured by low pressure operation. This advantage has to be evaluated with respect to higher capital cost and possible lower operating cost due to lower hydrogen recycle rates and pressures needed to keep coke laydown at an acceptable level.

The semiregenerative unit is at the other end of the spectrum and has the advantage of lower capital cost. Regeneration requires the unit to be taken off-stream. Depending upon severity of operation, regeneration is required at intervals of 3 to 24 months. High hydrogen recycle rates and operating pressures are utilised to minimise coke laydown and consequent loss of catalyst activity.

The cyclic process is a compromise between these extremes and is characterised by having a swing reactor in addition to those on-stream in which catalyst can be regenerated without shutting the unit down. When the activity of catalyst in one of the on-stream reactors drops below the desired level, this reactor is isolated from the system and replaced by a swing reactor. The catalyst in the replaced reactor is then regenerated by admitting hot air into the reactor to burn the carbon off the catalyst. After regeneration it is used to replace the next reactor needing regeneration.

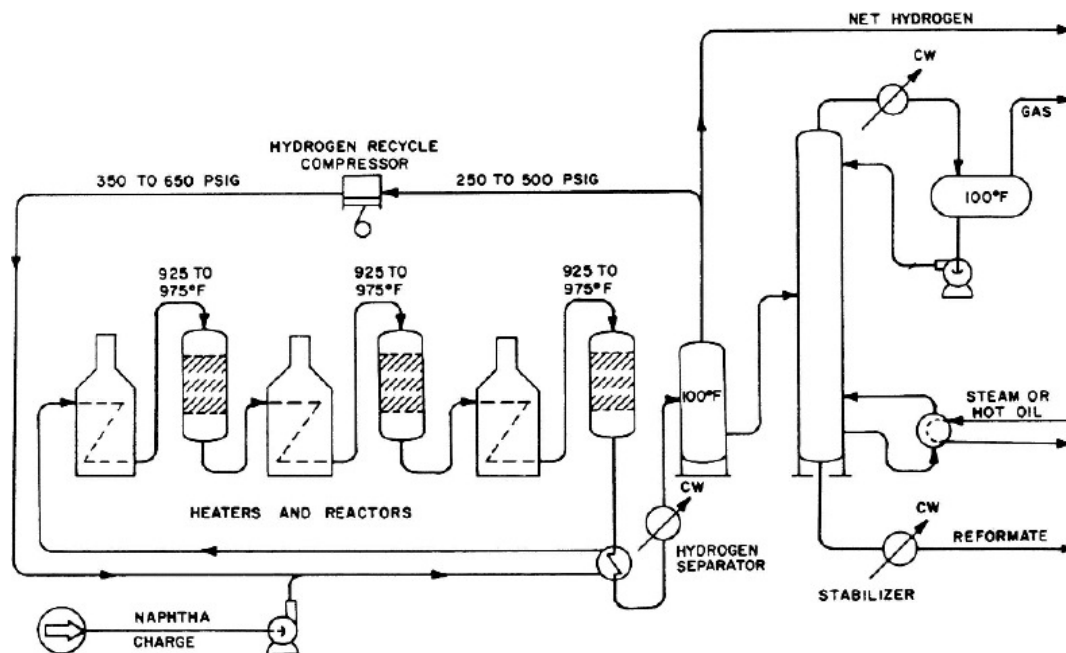


Figure 4.1 Simplified semiregenerative process of catalytic reforming (Gary and Handwerk, 2001)

The semiregenerative reforming process is typical of fixed-bed reactor reforming operations and will be discussed in this work. Figure 4.1 shows a simplified semiregenerative process diagram. The mixture of the feed and recycle hydrogen is heated first by reactor effluent for energy saving. Then the mixture is further heated up to a reactor inlet temperature before fed to the fixed-bed adiabatically operated reactors in series, in which quantities of reactions take place in the presence of catalyst. The major reactions in the first reactor are strongly endothermic and very fast, causing a sharp temperature drop. To maintain the reaction rate, the gases are reheated before being passed over the catalyst in the second reactor. As the total reactor charge proceeds through the sequence of heating and reacting, the reactions become less and less endothermic and the temperature differential across the reactors decreases. Usually three or four reactors are sufficient to provide the desired degree of reaction and heaters are needed before each reactor to bring the mixture up to reaction temperature. In practice, either separate heaters can be used or one heater can contain several separate coils. The reaction mixture from the last reactor is cooled and the liquid products condensed. The hydrogen-rich gases are separated from the liquid phase in a drum separator, and the liquid from the separator is sent to a fractionator to be stabilised, and finally sent to storage for gasoline blending. The hydrogen-rich gas

stream is split into a hydrogen recycle stream, passed to a compressor and then circulated to join the naphtha charge, and a net hydrogen by-product which is used in hydrotreating or hydrocracking operations or as a fuel.

There are numerous issues to be addressed for the performance of a reformer, including feed characteristics, catalyst formulation, process configuration, reactor design, operating conditions, and product specifications etc. The study of some of these depends totally or partially on experimental work, such as catalyst formulation, reactor design. However others can be undertaken theoretically via modelling and simulation. These factors (feed characteristics, operating conditions, and product specifications) would be briefly investigated in the following section.

4.1.2 Feed Characteristics

The typical feed to catalytic reforming process is heavy straight run gasoline or naphtha (90 to 160 °C). The reason for the use of heavy naphtha as a feed is that the ease of cyclisation and isomerisation reactions in the process increases with the increase of carbon atoms. Light naphtha tends to crack forming butane and light gases causing the lost in yield, hence it is not economical. Heavier feeds cause formation of carbon deposits on the catalyst and partially deactivate it.

Table 4.1 Compositions of two typical feeds (Gary, 2001)

	Paraffinic (Arabian Light)	Naphthenic (Nigeria)
RON	50	66
Average MW	114	119
Sulphur (wtppm)	500	350
Paraffins (vol%)	66.8	29.3
Naphthenes (vol%)	21.8	61.85
Aromatics (vol%)	11.4	8.85

Table 4.1 gives the composition of two typical feeds: paraffinic and naphthenic. RON is low with 50 for the paraffinic feed with very high paraffin content of more than 60 vol%, and 66 for the naphthenic with naphthene content of more than 60 vol%. The average molecular weight is about 115, around C₈. Sulphur is present in the feed in the range of 500 and 350 wtppm, which are representative of straight

run gasolines coming from atmospheric distillation of crude. But values lower than 100 wtppm are found in a few particular crudes. These SR feeds contain limited amounts of nitrogen in the form of amines, or oxygenated compounds in the form of phenol or carboxylic acid. In some cases, traces (<1 ppm) of metals or metalloids can be found, depending on the origin of the crudes. Feed pretreating, in the form of hydrotreating, is usually employed to remove these materials.

Other feeds rather than SR naphtha can be sent to reforming as well. These are cuts distilled in the same range of SR naphtha which is produced from conversion units and have low octane numbers. For instance, visbreaking or coking gasolines can be sent to reforming which are characterised by, in comparison with SR feeds, a high olefin and acid sulphur content and larger amounts of nitrogen compounds. Hydrocracking gasoline is another feed free of sulphur and nitrogen compounds because the use of hydrogen in the hydrocracking process works as a hydrotreating process, but such a feed is mainly made up of cyclopentane-structure naphthenes and isoparaffins. FCC gasoline is another possible feed, characterised by significant olefins and aromatics concentrations as well as the presence of molecules containing heteroatoms such as S or N.

4.1.3 Operating Conditions

The key operating conditions, which affect the performance of reforming, are reactor temperatures, reactor pressures, space velocity (SV), and hydrogen/hydrocarbon ratio.

The operating temperature is the principal parameter of reactors that operators need to watch carefully and adjust frequently through the entire run cycle. The typical range of operating temperature is from 490 to 520 °C. In practice, temperatures can be chosen to balance the advantage of increased reformate quality (octane number) and disadvantage of increased deactivation rate as well as aromatics content as temperature increased. The operating temperature will impact yield of reforming depending on the catalyst type: monometallic catalysts show a drop in yield as soon as the temperature rises, while bimetallic catalysts remain same until the end of a run.

The operating pressure is one of the key operating parameters, which will affect on product yield and cycle length. Low pressure shows a trend of catalytic reforming since it favours the increase of yield with high quality although with increase of coke content as illustrated in Figure 4.2 (Meyers, 2004). To compensate the loss of catalyst activity because of coke content, the operation type depending on catalyst regeneration evolves from semiregenerative to continuous including cyclic. In the beginning, the pressure used was greater than 50 bar, and pressure drop had little influence in comparison with total pressure drop. The evolution allows operation at pressure lower than 25 bar, therefore pressure drop in reactors became significant in relation to the total pressure drop. In addition, the cost of recycle hydrogen compression became a non-negligible item.

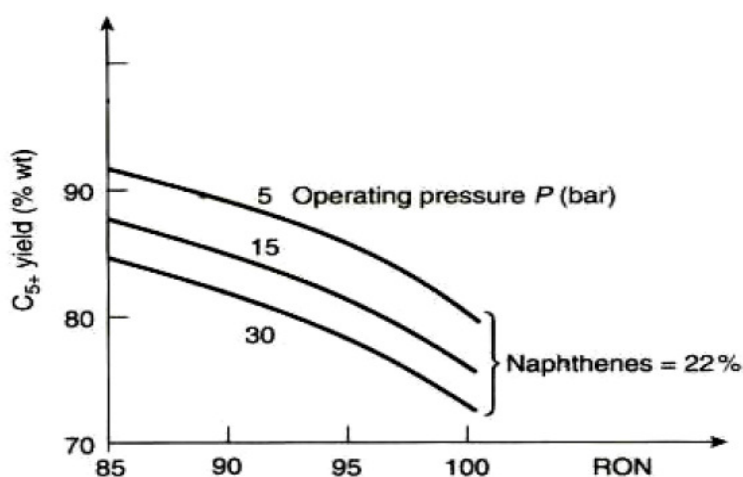


Figure 4.2 Pressure influence (Robert, 2003)

Space velocity is a measure of the contact time between reactants and catalyst, and expressed as liquid hourly space velocity (LHSV) or weight hourly space velocity (WHSV). The choice represents a compromise between allowable hydrocracking and desired dehydrocyclisation. Aromatisation and isomerisation are not affected by changes in space velocity because these reaction approach equilibrium even at high space velocity. Modern reformers usually operate between 1.0 and 2.0 h^{-1} (LHSV). As below 1.0 h^{-1} undesired side reactions hydrocracking are increased, and therefore reduce reformate yield.

H_2/HC ratio is one of crucial operating parameters having impact on catalyst deactivation. The advantage of increasing H_2/HC ratio is that hydrogen will react with coke precursors, removing them from catalyst before they form significant

amount of polycyclic aromatics, therefore, leading to a longer catalyst life. On the other hand, increasing H_2/HC ratio will affect aromatization, and increase hydrocracking resulting in the decrease of reformate yield. A lower hydrogen partial pressure favours dehydrogenation of naphthenes and dehydrocyclisation of paraffins. The typical H_2/HC ranges from 3 to 8 on molar basis.

4.1.4 Product

Table 4.2 Typical product distribution from paraffinic feed at 15 bar with RON of 98 (George, 2004)

Product	Yield (wt%/feed)
H_2	2.5
CH_4	1.7
C_2H_6	3.1
C_3H_8	4.2
$(n+i) C_4H_{10}$	6.0
C_5^+	82.5

As mentioned before, catalytic reforming produces C_5^+ reformate, hydrogen, also a little amount of methane, ethane, propane and butanes. In the last few decades the importance of the production of hydrogen, besides C_5^+ , has risen gradually with pressures going down to 10 bar and less as a result of catalyst improvement. Table 4.2 gives an average product distribution from a paraffinic feed on a bimetallic at 15 bar. The desired products account for 85% weight and the ones with lower added value represent less than 5% weight (methane and ethane).

Olefins and naphthenes concentrations are lower than 1% wt except for low pressure which approach 1%. Table 4.3 shows a typical analysis for a low pressure reformate. It should be noted that to achieve RON of 98, the aromatic content is close to 70% wt. The octane rating in a reformate is generally provided by C_7 to C_{10} aromatics and by light iso-paraffins, especially C_5 . This is because C_6 , C_7 and C_8 isoparaffins are not very branched and so they have a low RON.

Table 4.3 Typical composition (wt %) of reformates with low operating pressure (George, 2004)

	nP	iP	O	N	A	sum
4	0.57					0.57
5	1.51	2.37	0.1			3.98
6	1.69	3.97	0.16	0.19	2.34	8.35
7	2.5	8.42	0.35	0.4	14.16	25.83
8	1.16	4.91	0.44	0.34	26.28	33.13
9	0.26	1.04	0.08	0	21.08	22.46
10	0.07	0.28	0	0	4.76	5.11
11	0	0.02	0	0	0.55	0.57
sum	7.76	21.01	1.13	0.93	69.17	100

Reformate is basically made up of C₇ to C₁₀ aromatics, directly related to the desired research octane number. It is also important to note that reformates do not contain any sulphur (S ≤ 0.1 ppm). High pressure reformates contain few olefins. However, in modern units running at low hydrogen partial pressure, there are more and more olefins. These olefins lower MON of gasoline and often make hydrogen purification more complicated.

4.1.5 Review of Previous Work

The effects on investigating catalytic reforming have three aspects: kinetic models, catalyst deactivation, as well as process optimisation. The main issue related to kinetic models is the representation of reactants and corresponding products, which falls in three ways: lumped model, pathways level and mechanistic level models. Various kinetic models to represent catalytic reforming have been reported in the literature, which have different levels of sophistication. The first significant effort was made by Smith (1959), where the complex naphtha mixture is idealised so that each of three hydrocarbon classes: paraffins, naphthenes, and aromatics, is represented by a single compound having the average properties of that class. With this simplified model, a kinetic analysis was developed which described the reforming operation with satisfactory accuracy. However, the fact remains that it oversimplifies the nature of the process, which cannot handle the operation over a

wide range of operating conditions. However, all the models up to that time were pseudohomogeneous in nature.

Kmak (1972) presented the first endeavour to incorporate catalytic nature. By deriving a reaction scheme with Hougen-Watson Langmuir-Hinshelwood (HWLH) type of kinetics, the model explicitly accounts for the interaction of chemical species with the catalyst. The developed model was limited to the representation of isothermal operation at some points within the experimental temperature range in which they fitted the parameters.

Marin et al. (1983) refined the Kmak (1972) model, developed the reaction network covering the whole naphtha in the carbon number from C₅ to C₁₀. The network included 23 pseudocomponents and used HWLH rate equations. Marin and Froment (1982), and Van Trimont et al. (1988) also conducted separate studies on C₆ and C₇ carbon number fractions respectively, and developed the corresponding HWLH rate equations. Various possible reaction paths and mechanisms were systematically evaluated before choosing the one that best fits the experimental data on a laboratory-scale reactor. Taskar et al. (1997) applied the kinetic scheme, and extended carbon number fractions from C₈ to C₁₀ based on using rate expressions that have the same form as the C₆ and C₇ rate expression from Marin and Froment (1988). Finally, it contains 35 pseudocomponents connected together by a network of 36 reactions. Moreover, isoparaffins had been further broken down into single-branched paraffins and multi-branched paraffins because the physical properties of two paraffins are different.

Padmavathi et al. (1997) developed a simulation model to monitor commercial plant performance, given as the lumping details of the feed and reacting scheme, parameter estimation and model validation details. The results of the model were validated for 4 different commercial reactor performances with a good accuracy. Ancheyta et al. (2000) proposed a model that utilises lumped mathematical representation of the reactions that take place, which are written in terms of isomers of the same nature. These groups range from 1 to 11 atoms of carbon for paraffins, and from 6 to 11 carbon atoms for naphthenes and aromatics. The cyclohexane formation via methylcyclopentane isomerisation and paraffins isomerisation reactions were considered in the model. Additionally, an Arrhenius-

type variation was added to the model in order to include the effect of pressure and temperature on the rate constants. The kinetic parameters were estimated using experimental information obtained in a fix-bed pilot plant in which three reforming reactors were loaded with different amounts of catalyst.

Mechanistic level models are also developed. Quann and Jaffe (1996) developed a structure oriented lumping model, with a large number of key molecules generated by assembling 22 structural groups in various ways. This synthetic feed has to satisfy the observable characteristics, both chemical and physical. Klein and co-workers (Wei and Klein, 2008) reduced the complexity of the feed by introducing a number of representative pseudocomponents by Monte-Carlo simulation and generated the reaction network of this synthetic feed by computers using graph theory. Forment and his colleagues (Sotelo-Boyas and Froment, 2009) developed a kinetic model based on a detailed description of the fundamental chemistry of the transformation of each hydrocarbon, and applied single event concept for rate expressions. The results showed excellent agreement between the experimental and estimated yield.

Catalyst deactivation has been investigated intensively. De Paulw and Froment (1974) developed a methodology of characterising the deactivation of a catalyst by coke deposition in the isomerisation reaction of *n*-pentane. The approach proposed that the deactivation functions are related to the real cause of deactivation, which is the actual amount of coke formed on the surface of the catalyst and not the process on-stream time as is usually done. Marin and Froment (1982) and Van Trimont et al. (1988) applied the same methodology for C₆ and C₇.

Because of the new legislation of benzene and aromatics content in commercial gasoline, refiners have to investigate the operating condition properly by process optimisation recently. Taskar and Riggs (1997) investigated different operating strategies of time-invariant and time-optimal modes by optimising a semiregenerative catalytic naphtha reformer with catalyst deactivation. The time-optimal mode demonstrated significant economic improvement over the time-invariant mode. Hu (2004) integrated catalytic reforming into an overall refinery optimisation problem, and investigated the economic performance with the optimisation of catalytic reforming process.

4.1.6 Motivation of Molecular Modelling of Catalytic Reforming

As mentioned previously, recently there has been a renewed interest in reforming processes. Because reformate is a major source of aromatics due to the new regulations on the commercial gasolines. In this sense, the operating severity has to be reduced to decrease the amount of aromatics, which however adversely affects the reformate octane number. Besides this, catalyst deactivation also plays a very important role on economic performance. Olefinic intermediates are the main cause of forming carbonaceous deposits on catalyst, which is suppressed by high hydrogen partial pressure (De Pauw and Froment, 1974). However, high pressure reduces the selectivity to aromatics in the desired product. Overall, high temperature and low pressures would seem most desirable for the main reforming reactions, but the same conditions favour deactivation of catalyst. For this reason, the process operating conditions have to be a compromise.

To achieve this, optimisation plays a key role, which demands an appropriate kinetic model combined with a suitable reactor model capable of predicting the detailed reformate composition. Besides, the kinetic model should include the impact of changing operating conditions on the process performance. A Lumped model has its inherent disadvantages of rate coefficients depending on the feed composition, while a mechanistic level model has too many details and takes a very long computation time, which is not suitable for optimisation. A pathway level model contains most of the observed species explicitly, and describes the molecule-to-molecule transitions in a reaction network. The corresponding mathematical model is numerically friendly and can be solved quickly. The model developed by Ancheyta et al. (2000, 2001) considered the whole range of naphtha, and the cyclohexane formation via methylcyclopentane isomeration, as well as paraffins isomerisation. Additionally, the pressure effect on rate constants was also included, which enhances the prediction accuracy. To include the cost of power consumption due to the pressure drop of recycle hydrogen, the Ergun equation (Fogler, 1992) for computing the differential pressure drop in a fixed bed is applied in this work, which is not considered in Ancheyta's work (2000; 2001). The previous investigation on the optimisation of catalytic reforming (Taskar, 1997) limited three periods for run cycle due to the enormously increased computational

burden if more periods were included at that time. However, along with the development of computation capacity, it is possible to implement the investigation on a monthly or even smaller period, which possibly achieves better economic performance.

4.2 Chemical Reactions Network and Kinetics

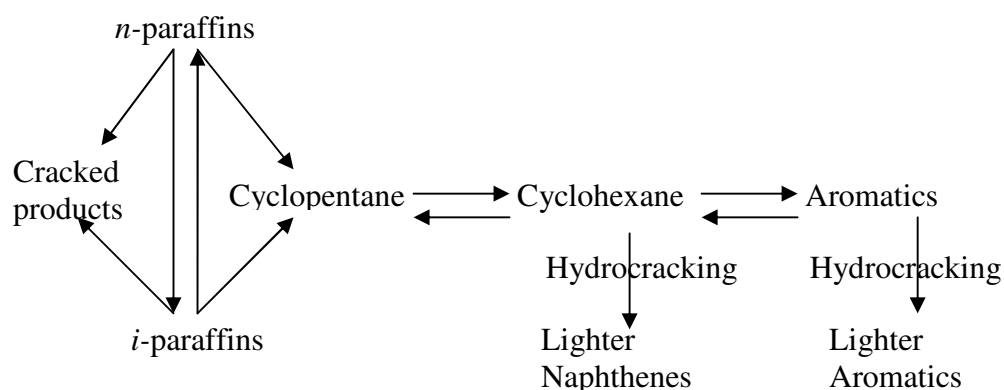


Figure 4.3 Generalised reaction network

Reactions mainly involve four categories: dehydrogenation, isomerisation, dehydrocyclisation, and hydrocracking. Every reaction produces an increase in octane number, and except isomerisation of paraffins, results in a decrease in reformat yield. The fastest reaction is dehydrogenation, and isomerisation is moderately fast, while dehydrocyclisation and hydrocracking are the slowest. The reactions are promoted by two kinds of active sites on catalyst, acidic and metallic. The generalised reaction network is illustrated in Figure 4.3.

As in any series of complex chemical reactions, reactions occur which produce undesirable products in addition to those desired. Reaction conditions have to be chosen those favour the desired and inhibit the undesired reactions. Desirable reactions lead to the formation of aromatics and isoparaffins as follows:

- Paraffins are isomerised and to some extent converted to naphthenes, subsequently converted to aromatics,
- Olefins are saturated to form paraffins which then react as the first,
- Naphthenes are converted to aromatics,
- Aromatics are left essentially unchanged.

Reactions leading to the formation of undesirable products include:

- Dealkylation of side chains on naphthenes and aromatics to form butane and lighter paraffins,
- Cracking of paraffins and naphthenes to form butane and lighter paraffins.

4.2.1 Dehydrogenation of Naphthenes to Aromatics

The principle reforming reaction in producing aromatics from naphthenes is dehydrogenation of alkylcyclohexanes. The pathways of reactants and products in terms of the MTHS matrix elements are as follows.



where n ranges from 6 to 12.

The dehydrogenation reactions are highly endothermic and cause a decrease in temperature as the reaction progresses, which necessitates the use of inter-heaters between catalyst beds to keep the mixture at sufficiently high temperatures for the reactions to proceed at practical rates. Because this reaction proceeds rapidly and produces hydrogen as well as aromatics, naphthenes are the most desirable components in the feedstock.

Aromatics have a higher liquid density than paraffins or naphthenes, so volume of the produced aromatics will be reduced. In addition, the conversion to aromatics increases the gasoline end point because the boiling points of aromatics are higher than those of paraffins and naphthenes. The yield of aromatics is increased by:

- High temperature (increases reaction rate but adversely affects chemical equilibrium),
- Low pressure (shifts chemical equilibrium “to the right”),
- Low space velocity (promotes approach to equilibrium),
- Low hydrogen-to-hydrocarbon mole ratios (shifts chemical equilibrium “to the right”, however, a sufficient hydrogen partial pressure must be maintained to avoid excessive coke formation).

4.2.2 Isomerisation of Paraffins and Naphthenes

The isomerisation reactions occur moderately fast catalysed by acid sites at commercial operating temperatures with small heat effects. Thermodynamic equilibrium, however, slightly favours the isomers that are more highly branched. Isomerisation of paraffins and cyclopentanes usually results in a lower octane product than does conversion to aromatics. However, there is a substantial increase over that of the un-isomerised materials. For isomerisation of paraffins, it is common to assume that the isomerisation reactions are rapid enough to closely approach thermodynamic equilibrium at normal reforming conditions (Gates, 1979). Therefore, the distribution of paraffins in the MTHS matrix classified as NP, MP, DP, and TP will be calculated by known equilibrium in this work. The isomerisation of methylcyclopentane (MCP) to cyclohexane, which is further dehydrogenated to benzene, is considered for the naphthenes isomerisation. Isomerisation yield is increased by high temperature (which increases reaction rate), low space velocity, and low pressure.

4.2.3 Dehydrocyclisation of Paraffins

The most difficult reaction to promote is the dehydrocyclisation of paraffins, consisting of molecular rearrangement of paraffins to naphthenes as shown in Equation 4.2 in terms of MTHS matrix elements.

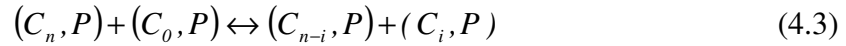


where n ranges from 6 to 12.

For cyclisation to occur, a paraffin with at least a six-carbon straight chain is needed. The reaction becomes easier with increasing molecular weight of paraffins because the probability of ring formation increases, however partially offset by hydrocracking to lighter paraffins. The produced naphthenes are easily further converted to aromatics by dehydrogenation. Dehydrocyclisation is favoured by low pressure and high temperature, and requires both the metal and acid functions of catalyst.

4.2.4 Hydrocracking and Dealkylation

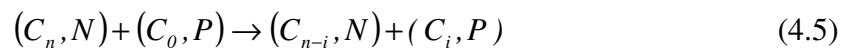
The reactions of paraffins hydrocracking are given as Equation 4.3 in terms of MTHS matrix elements.



where $1 \leq i \leq 5$, and $n \geq 5$.

The hydrocracking reactions are exothermic and result in the production of lighter liquid and gas products. They are relatively slow reactions and therefore most of hydrocracking occurs in the last section of the reactor. The major hydrocracking reactions involve the cracking and saturation of paraffins. In order to obtain high product quality and yield, it is necessary to carefully control the hydrocracking reactions. As paraffins crack into lighter paraffins, the reactions consume the specious hydrogen and reduce the net liquid yield, although the remaining aromatics become concentrated, thereby, increasing octane number. The concentration of paraffins in the charge stock determines the extent of the hydrocracking reaction, but the relative fraction of isomers produced in any molecular weight group is independent of the charge stock, relying on the thermodynamic equilibrium as mentioned previously.

Dealkylation of aromatics and naphthenes includes both making the alkyl group – a side chain on the aromatic or naphthene ring – smaller and removing the alkyl group completely. Equations 4.4 and 4.5 show the dealkylation of aromatics and naphthenes respectively in the form of MTHS matrix elements.



where $n \geq 7$, and $i \leq 3$.

Hydrocracking and dealkylation yields are increased by high temperature, high pressure and low space velocity.

4.2.5 Kinetics

All reactions are presumed to be pseudo-first order with respect to the hydrocarbon, given as Equation 4.6.

$$\frac{dC}{dt} = kC \quad (4.6)$$

To consider the effects of pressure and temperature on kinetic constants, Ancheyta (1994) integrated an Arrhenius-type variation for temperature consideration and a factor for pressure into Krane's model (1960). More improvements were made thereafter (Ancheyta, 2000). The reaction rate constant is as Equation 4.7.

$$k_i = k_i^0 \times \exp\left[\frac{E_{Aj}}{R} \times \left(\frac{1}{T_0} - \frac{1}{T}\right)\right] \times \left(\frac{P}{P_0}\right)^{\alpha_k} \quad (4.7)$$

where k_0 is the rate constant with the 300 psig of pressure, and 766 K of temperature. E_{Aj} is the activation energy, R is ideal gas constant, and α_k is the factor for pressure effect. The activation energy for each reforming reaction and the factor for pressure effect are given in Appendix B, as well as the kinetic constants of the model.

4.3 Process Model

The mathematical equations are developed based on the following assumptions:

- Gas velocity is constant across the reactor section;
- The reactor is operated with an adiabatic and steady-state condition;
- No radial deviation of concentrations exists within the reactor.

The kinetic model described in the previous section was incorporated in a fixed-bed one-dimensional pseudohomogeneous adiabatic reactor model. Under the general reactor operating conditions, radial and axial dispersion effects were found to be negligible. Therefore, a perfect plug-flow behaviour assumption is reasonable (Taskar, 1997). The ordinary differential Equations 4.8 and 4.9, which describe the reformate composition and temperature profiles at the steady state (Froment, 1990), are integrated through each reactor bed.

$$\frac{dF_i}{dw} = \sum_{j \in J} \gamma_{j,i} r_j \quad \forall i \in I \quad (4.8)$$

$$\frac{dT}{dw} = \frac{\sum_{j \in J} r_j (-\Delta H_j)}{\sum_{i \in I} F_i C_{pi}} \quad (4.9)$$

where F_i stands for molar flow rate of component i , and w is catalyst weight. $\gamma_{j,i}$ is stoichiometric coefficient of component i in reaction j . r_j is reaction rate of reaction j . T is reactor temperature along with catalyst weight, and ΔH_j represents reaction heat of reaction j . C_{pi} is specific heat capacity of component i .

Because reactor pressure is being reduced gradually due to the improvement of catalyst, the cost for compressing recycle hydrogen to the reactor pressure is not negligible any more. The equation describing the pressure drop as Equation 4.10, the Ergun equation (Fogler, 1992), is integrated into the process model.

$$\frac{dP}{dw} = -\frac{G}{\rho d_p \varepsilon^3} \left[\frac{150(1-\varepsilon)\mu}{d_p} + 1.75G \right] \frac{1}{A_c \rho_c} \quad (4.10)$$

where P stands for pressure along with the catalyst weight, and G is superficial mass velocity of gas mixture. d_p is diameter of catalyst particle, while ρ describes density of gas mixture. ε is for void fraction of catalyst bed, and μ for viscosity of the gas mixture. A_c is cross sectional area of the bed, and ρ_c is density of catalyst.

The power consumption of compressor was estimated on the basis of calculated adiabatic head and flow rate of recycle gases as Equation 4.11.

$$\Delta H_{adiabatic} = FZRT \frac{k}{k-1} \left[\left(\frac{P_{out}}{P_{in}} \right)^{\frac{k-1}{k}} - 1 \right] \quad (4.11)$$

where F is molar flow rate of recycle gas, and Z is compressibility factor, which value is 1 for ideal gas. T stands for temperature of recycle gas, and k is specific heat ratio. P_{out} , P_{in} are pressures after compressor and before respectively. $\Delta H_{adiabatic}$ is power consumption for recycle gas with molar flow rate F .

Besides, the cost for heating up feed to the inlet temperature of reactors between beds is also needed to be considered. The energy balance of the system can be described as Equation 4.12.

$$\Delta H_{heating} = \sum_{r \in R} \Delta H_r - \Delta H_{effluent} \quad (4.12)$$

where r stands reactors, and ΔH_r is the energy consumption to heat up feed from the outlet temperature of previous reactor or the ambient temperature for the first reactor to the inlet temperature of the next reactor. $\Delta H_{effluent}$ is the energy of cooling effluent from the outlet temperature of the last reactor to the ambient temperature. Since fuel cost is of the interest, the rigorous modelling of heat exchanging is not necessary, and macroscopic energy balance is used.

Another issue is that usually the analysis of feed naphtha is reported in terms of bulk properties such as distillation profile and density, rather than molecular composition. Therefore, the developed methodology in Chapter 2 will be employed to transform bulk properties into molecular information. Moreover, the developed methodology for the prediction of properties such as octane number in Chapter 3 is also integrated to improve the accuracy of the prediction as Equation 4.13 which appears as Equation 3.47 in Chapter 3.

$$ON = \frac{\sum_{i \in PIONA} x_i \beta_i ON_i + I_{PI} \sum_{i \in PI} x_i \beta_i ON_i}{\sum_{i \in PIONA} x_i \beta_i + I_{PI} \left(\sum_{i \in PI} x_i \beta_i - \sum_{i \in PI} x_i \right)} \quad (4.13)$$

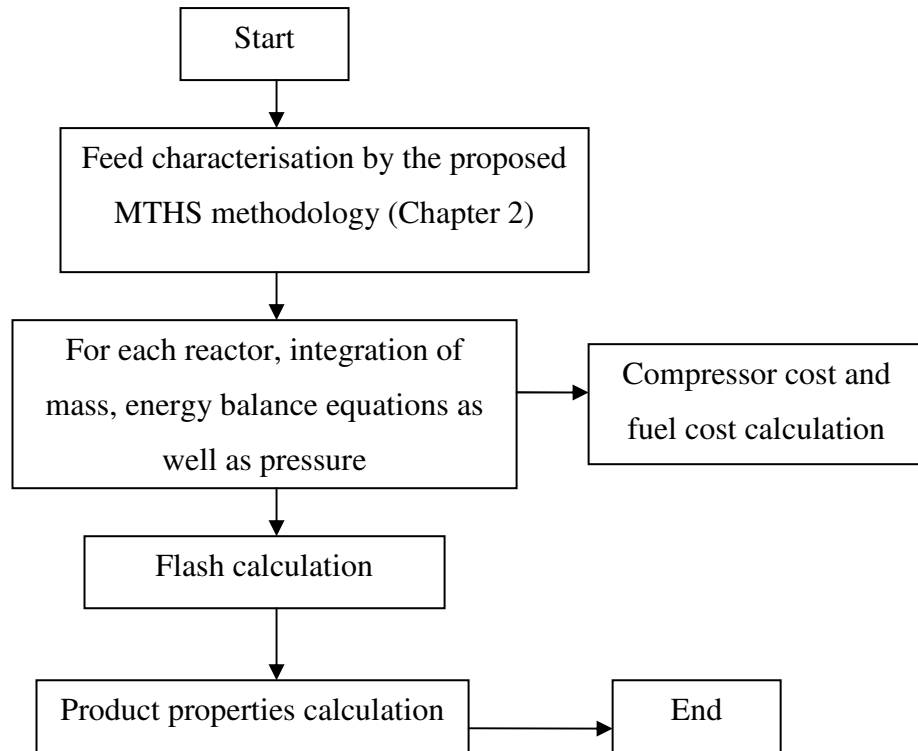


Figure 4.4 Diagram of the simulation of catalytic reforming

The 4th Runge-Kutta integration method with adaptive step size is applied for the integration. The whole simulation procedure is illustrated in Figure 4.4.

4.4 Case Study

The studied case (Ancheyta, 2000) is used to investigate the proposed model. The semiregenerative catalytic reforming process consists of three fixed bed reactors. Each reactor is operated in isothermal mode by independent temperature control. The detailed operating condition is listed in Figure 4.5 with the flowsheet.

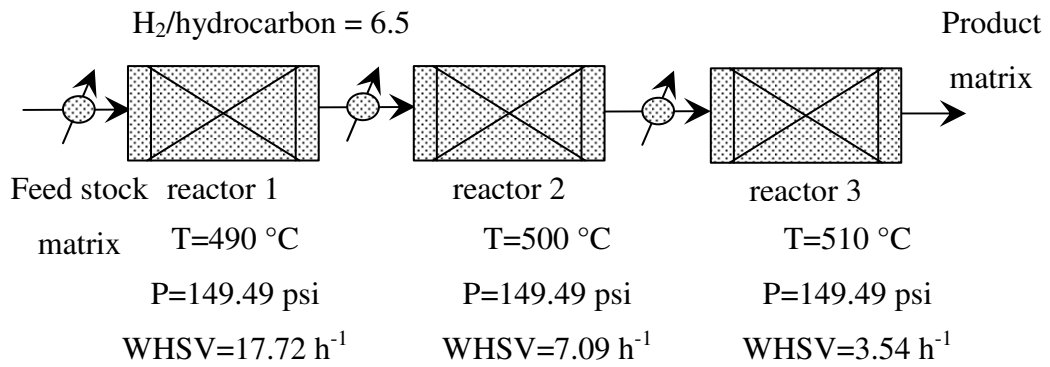


Figure 4.5 Reactors configuration and operating conditions

Table 4.4 Molecular composition of feedstock (mol %) (Ancheyta, 2000)

	P	I	N	A	sum
C4	0	0			0.00
C5	3.8	3.4	0.42		7.62
C6	4.4	6.7	3.21	0.8	15.11
C7	3.2	6.2	5.8	3.22	18.42
C8	6.36	6.52	4.71	4.71	22.30
C9	5.09	8.32	3.56	4.21	21.18
C10	2.97	6.22	0.6	2.7	12.49
C11	2.2	0	0.4	0.3	2.90
sum	28.02	37.36	18.70	15.94	100.02

Table 4.4 gives the detail molecular composition of feedstock. Reformate samples were collected in a high-pressure product receiver. The remaining C_4^- cracking products are removed by distillation afterward.

4.4.1 Simulation of the Process

To illustrate the capability and accuracy of the proposed methodology, the measured molecular composition of the feedstock is converted to bulk properties firstly. Then based on the predicted properties, a new molecular composition for the feedstock is predicted. By applying the kinetic models, the stabilised product molecular composition and its corresponding bulk properties are determined sequentially, which are compared with those results from the experimental data.

Table 4.5 Comparison of the properties between the measured and predicted for feedstock and product

Properties	Feedstock		Product	
	Measured*	Predicted	Measured*	Predicted
SG	0.74	0.74	0.79	0.79
RVP(psi)	3.11	3.10	4.32	4.61
RON	62.98	63.15	97.38	97.45
MON	58.95	58.63	86.84	87.00
Benzene (vol%)	0.48	0.64	4.59	4.82
P (vol%)	69.24	69.27	39.21	38.83
N (vol%)	17.11	17.09	1.71	2.45
A (vol%)	13.65	13.63	59.08	58.72

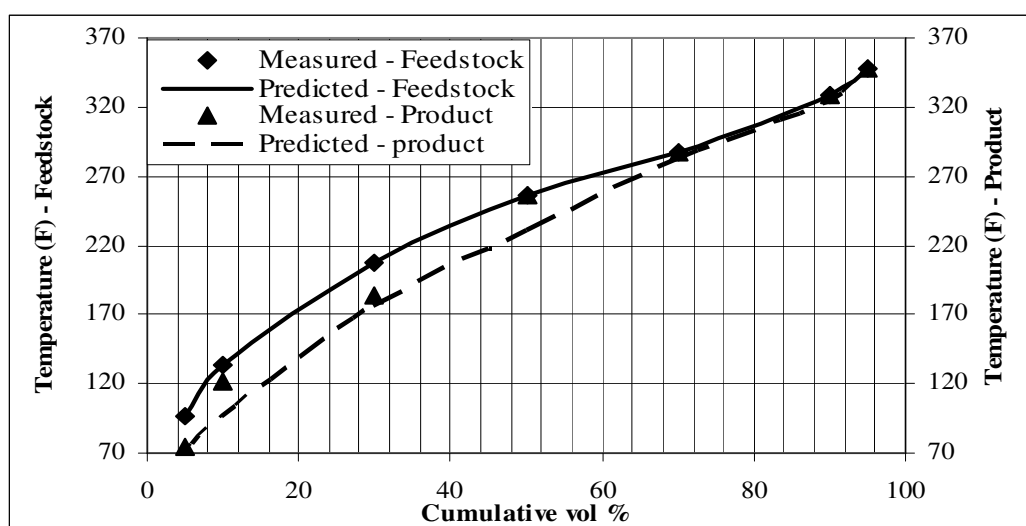


Figure 4.6 Distillate profiles of feedstock and product from the measured and the predicted

Table 4.5 compares the properties of the feedstock and product between the measured and predicted, while Figure 4.6 gives distillation profile. Figure 4.7 gives a view of the agreement of molecular composition of product between the measured and the predicted. For the feedstock, the most deviations between the measured and the predicted are less than 1% except for benzene with a small fraction. Regarding the product, it sees a bigger deviation, especially 10 vol% of distillate profile, while as the two key properties, ON and RVP see small gaps. It is

also safely concluded that A₇-A₉ are the major molecules produced, which contribute the majority of ON.

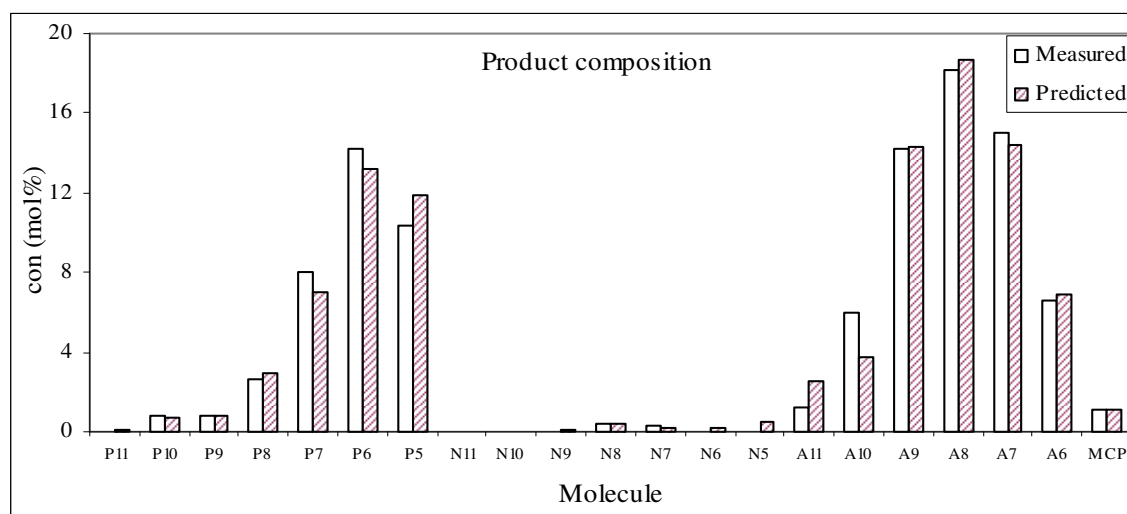


Figure 4.7 Comparison of the product molecular composition

Table 4.6 shows a good consistence of product distribution between the predicted and the measured.

Table 4.6 Product distribution based on 100 mol feedstock

	Measured	Predicted
Product	96.12 mol	96.32 mol
P ₄	8.18 mol	8.42 mol
P ₃	9.57 mol	9.20 mol
P ₂	6.63 mol	6.81 mol
P ₁	4.22 mol	4.18 mol
H ₂	128.93 mol	129.33 mol
H ₂ purity (mol %)	81.84	81.88

Reformate composition profiles are presented in Figure 4.8. The reaction of dehydrogenation of naphthenes to aromatics mostly takes place in the first reactor, leading to the big increase of aromatics. Paraffin content is gradually reduced because of dehydrocyclisation and cracking reactions. Cracked products including C₁ to C₄ see an increase. Due to the isothermal operating mode, the composition between continuous reactors changes smoothly.

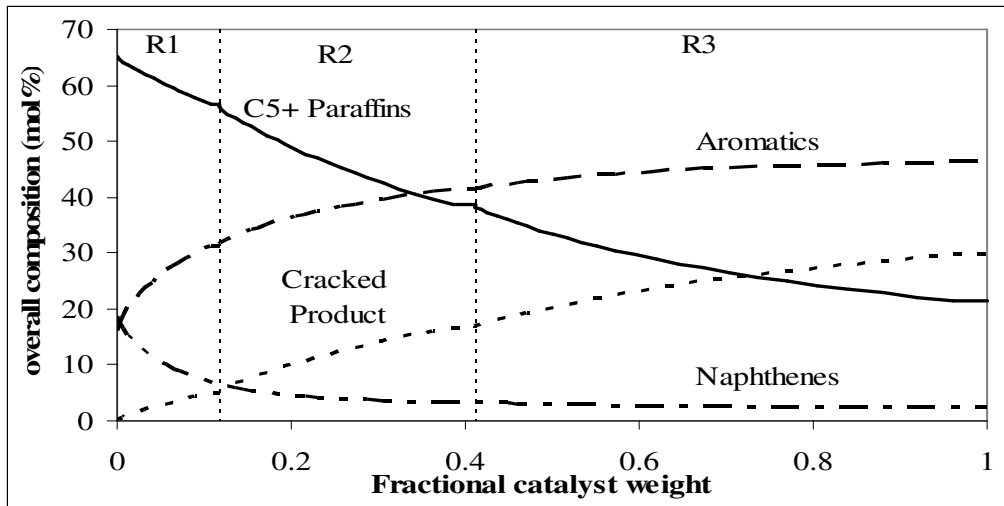


Figure 4.8 Profiles of composition through the reactors

In this case, the temperature and pressure profile are not taken into account, therefore, it is changed to operate in the adiabatic mode with the consideration of pressure drop in the following section.

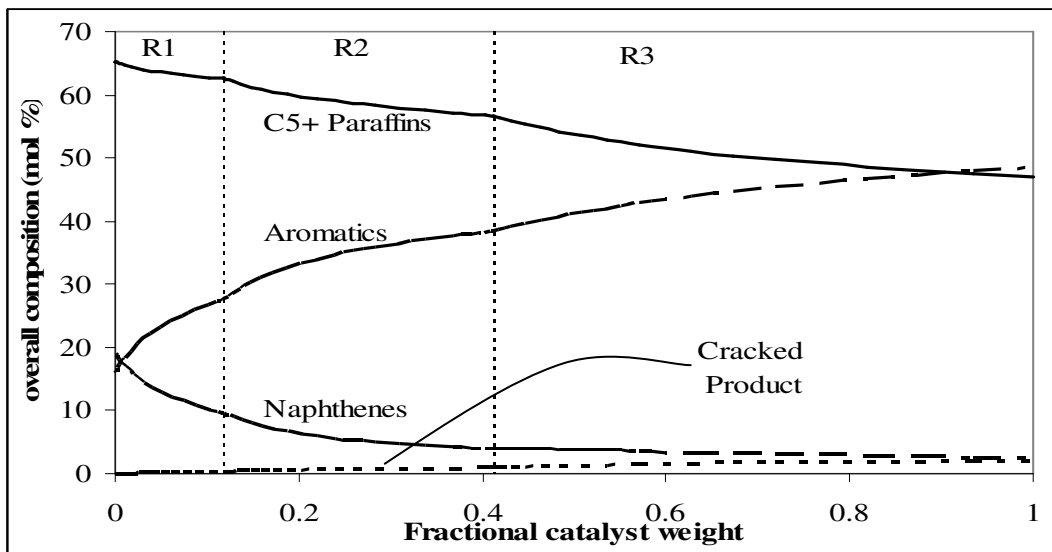


Figure 4.9 Composition profiles under the adiabatic operating mode

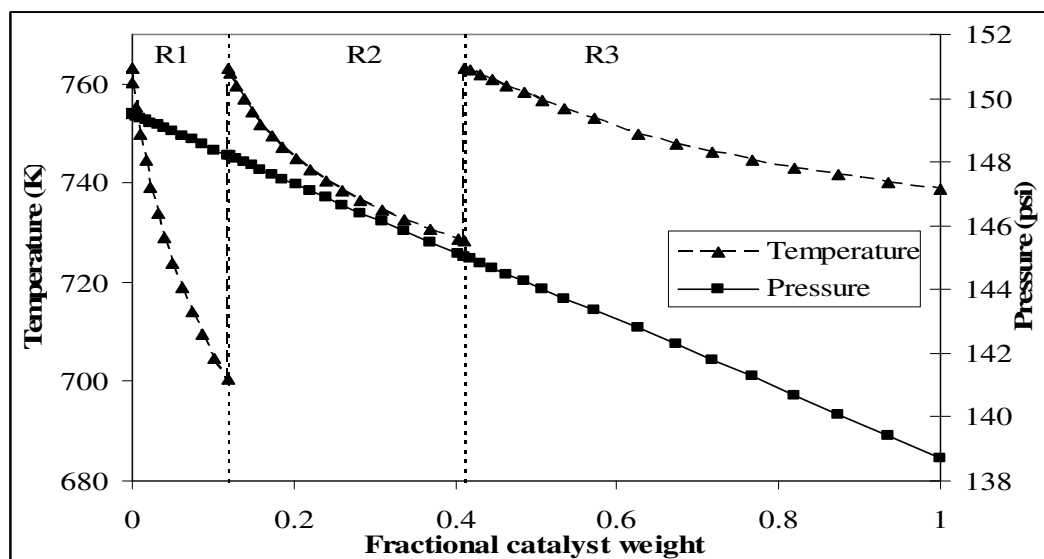


Figure 4.10 Temperature and pressure profile under the adiabatic operating mode

On the overall, the reactions taken place in catalytic reforming are endothermic, which is illustrated in Figure 4.10 as the temperature will drop across the reactors. The reactions of dehydrogenation of naphthenes to aromatics are very fast (as Figure 4.9), and endothermic, causing the temperature drop by around 60 K in the first reactor. In the second reactor, mostly the isomerisation takes place, and the remaining naphthenes are dehydrogenated, which makes a moderate temperature drop by around 30K. The temperature drop across the third reactor is relatively low due to the exothermic hydrocracking of paraffins and dealkylation of naphthenes and aromatics. Due to the temperature drop across reactors, the aromatic yield is less than that with the isothermal operating model, as well as the cracked product. The pressure drop across three reactors is 10.8 psi, by 7.2% of the reactor pressure.

4.4.2 Sensitivity Analysis of Operating Conditions

Effects of the operating conditions such as temperature, WHSV, and pressure are analysed as well. Figure 4.11 gives the influence of the operating temperature on the reformate yield and quality, and product distribution in Figure 4.12. It is assumed that all three reactors are operated in the same inlet temperature. High temperature will improve octane number of reformate, with the increase of aromatics content, together with the reformate yield reduction due to the hydrocracking reactions also favoured by high temperature. Therefore, to balance the reformate yield and its quality, the temperature should be properly controlled.

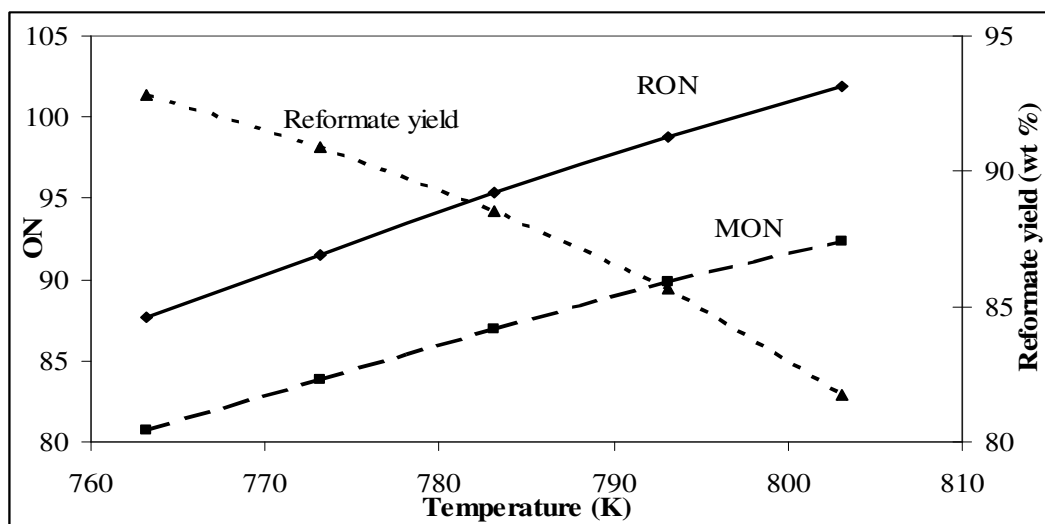


Figure 4.11 Influence of temperature on quality of reformate and yield (Pressure of 150 psi)

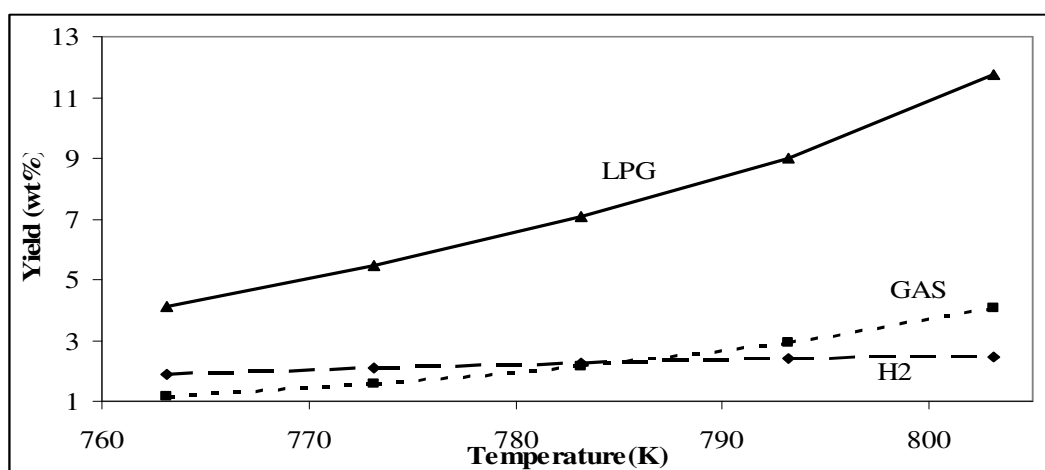


Figure 4.12 Influence of temperature on product yields (Pressure of 150 psi)

Figure 4.13 presents the influence of reactor pressure on the reformate yield and its quality, as well as product distribution and yield in Figure 4.14. With the increase of pressure, both reformate yield and quality decrease. High pressure favours hydrocracking reactions, which reduces the reformate and hydrogen yield, and slows down the other reactions such as dehydrogenation, dehydrocyclisation reactions, which reduces reformate octane number.

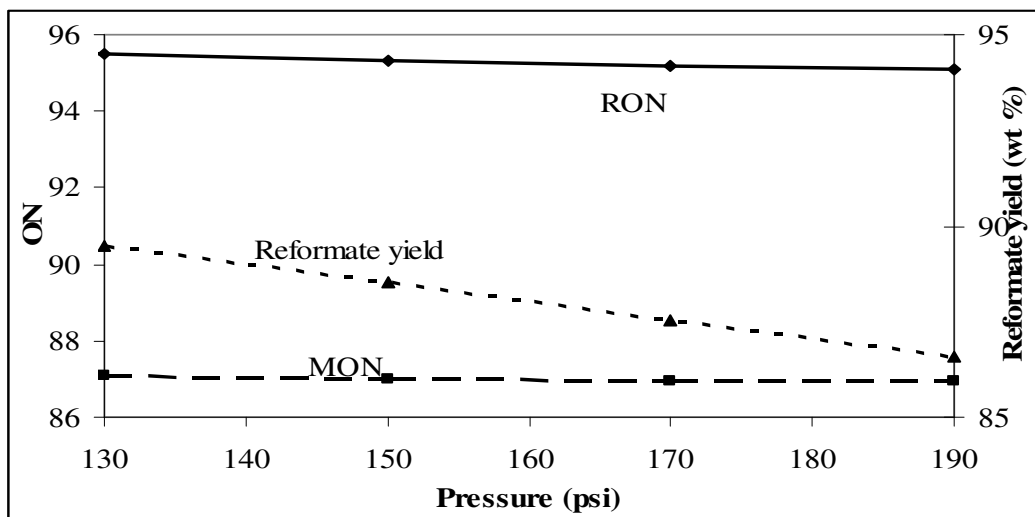


Figure 4.13 Influence of pressure on reformate yield and quality (T: 783.15K)

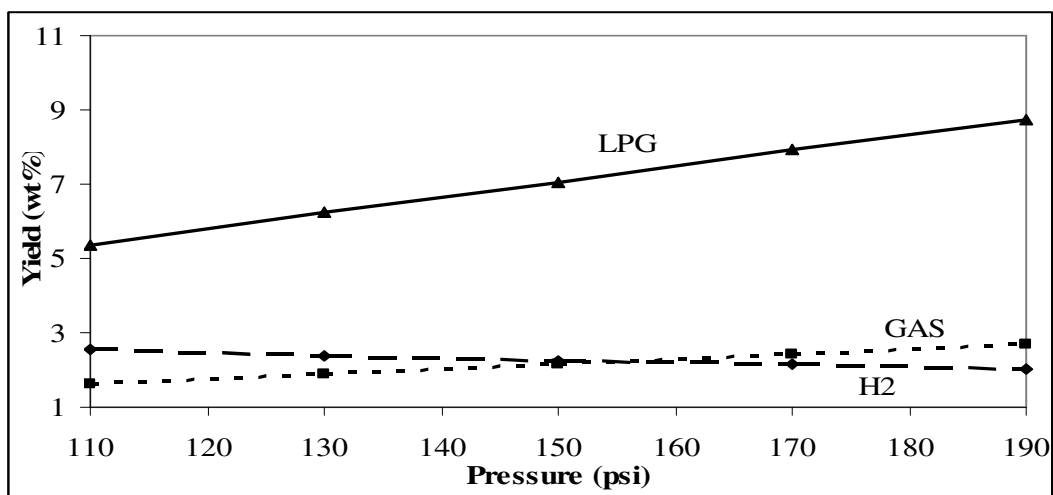


Figure 4.14 Influence of pressure on product distribution and yield (T: 783.15K)

The influence of WHSV on product distribution and quality, considering the fixed catalyst weight and varying feed throughput, is also investigated as shown in Figure 4.15 and Figure 4.16. Along with the increase of the throughput, the reformate octane number is reduced, and the reformate yield is increased, while the yields for other product such as hydrogen and cracked products are reduced.

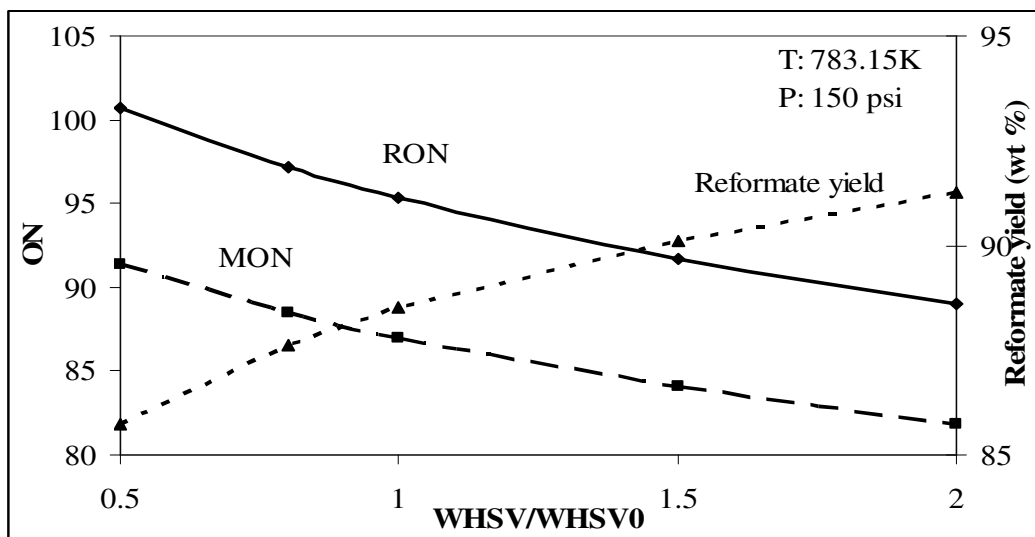


Figure 4.15 Influence of WHSV on reformate yield and quality

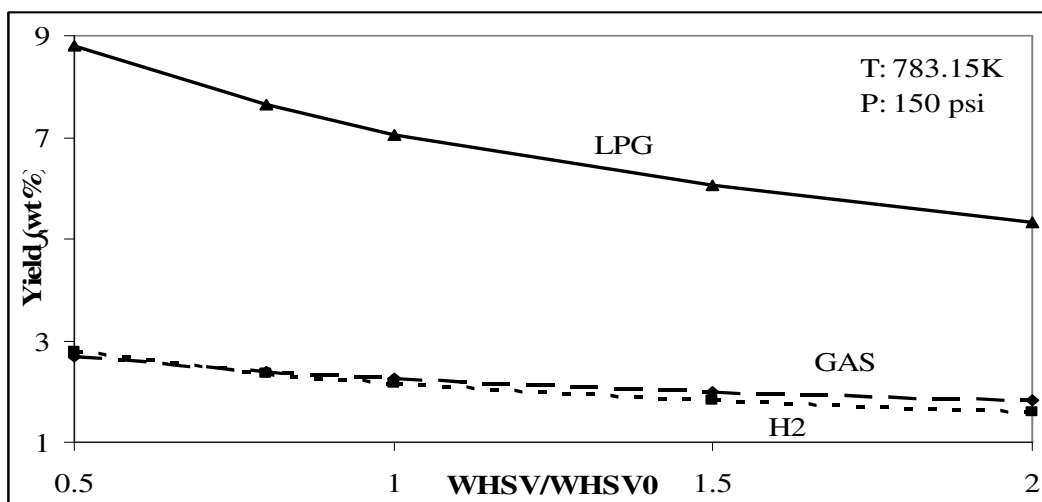


Figure 4.16 Influence of WHSV on product distribution

4.5 Catalyst Deactivation

4.5.1 Mathematical Model of Catalyst Deactivation

In refinery, the deactivation of catalyst by carbonaceous deposits is an important technological problem. Deactivation in a reforming process is attributed to coke formation and deposition. In reforming reactions of naphtha, the thermodynamics are such that it would be desirable to work at high temperature and low pressure. Such operating conditions favour coke formation, and many reforming units operate under high pressure in order to increase the life time of catalyst.

The coke amount increases with the increasing temperature, and this evolution can be explained by the effect of high temperature on the unsaturated products which are coke precursors. Generally, heavier feedstock of catalytic reforming produces more coke, but the cut with the lowest boiling range having a high content of cyclopentanic compounds are great coke producers as well.

The model developed by De Pauw and Froment (1974) is applied in this work because the model is related to the real cause of catalyst deactivation which is the amount of coke formed on the catalyst surface. A deactivation function ϕ_c also termed as the catalyst activity, is given as Equation 4.14.

$$\phi_c = \frac{r}{r_0} \quad (4.14)$$

where r_0 is the reaction rate without deactivation, and r is the reaction rate affected by deactivation. ϕ_c ranges from 0 to 1.

The catalyst activity is related to the coke content by an exponential function as follows.

$$\phi_c = e^{-\alpha C_c} \quad (4.15)$$

where α is the deactivation constant, and C_c stands for the coke content described as the weight of coke per unit catalyst weight calculated as Equation 4.16.

$$C_c = \int r_c dt \quad (4.16)$$

where r_c describes the rates of coking reactions.

To simplify the problem, it is assumed that the coke generation is related to the content of coke precursor including aromatics and cyclopentanic compounds, and follows a pseudo-first-order equation with respect to the content of the coke precursor as Equation 4.17.

$$r_c = kC_{pr} \quad (4.17)$$

where k is the rate constant, and related to temperature by the Arrhenius equation. C_{pr} stands for the concentration of coke precursor.

$$k = k_0 e^{-E_a / RT} \quad (4.18)$$

where k_0 and E_a are regressed based on the experimental data.

4.5.2 Multi-period Process Model

The semiregenerative unit of catalytic reforming requires plant to be shut down for catalyst regeneration every 3 to 24 months. The period between catalyst regenerations is called cycle life of catalyst. During the run of the period, the operating conditions, normally reactor inlet temperature will be changed to compensate the catalyst activity loss caused by coke deposition. The operating action can be described as changing temperature along with a series of running periods of the process. In each running period, operators make a decision on how many degrees of temperature should be changed, which will enhance the quality of reformat for further gasoline blending, and simultaneously balance the quality and deactivation of the catalyst to maximise the refining margins. Generally, the running length of a reformer will meet the schedule of the refinery. Therefore, the principle of changing temperature is to maximise the refining profit while meeting the schedule.

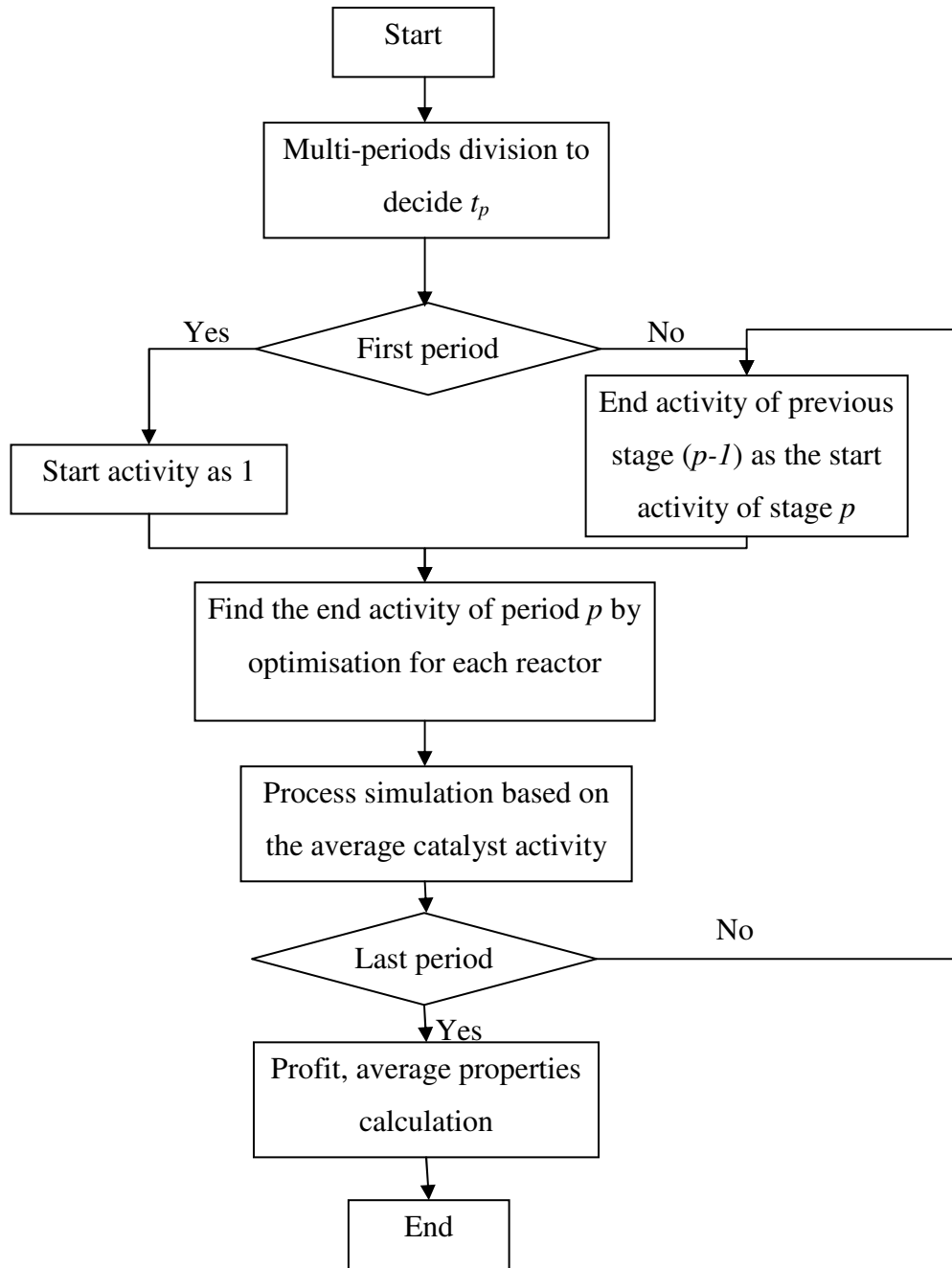


Figure 4.17 Simulation procedure of the proposed multi-period process model

Based on this acknowledgement, a new multi-period process model of catalytic reforming is proposed as Figure 4.17. The running length, which is fixed in advance to meet the schedule, is divided into multiple periods as the length of each period t_p is known. The catalyst activity of the very first period of the running starts from 1 ($\phi_{c,p}^s$) for every reactor, assumed as totally activated by regeneration. To find the end activity ($\phi_{c,p}^e$) of catalyst of the period for individual reactor, a sub-optimisation problem is applied respectively, which targets minimising the

difference of the time length from the prefixed (t_p) and that based on the varying end activity $\phi_{c,p}^e$. An average catalyst activity $(\phi_{c,p}^s + \phi_{c,p}^e)/2$ is assumed for the simulation of the process in the period p as Equation 4.14, to calculate the content of coke precursor in the product. The average content of coke precursor, taking the contents at the inlet of reactor and outlet, is used in Equation 4.17 for the reaction rate of coke formation. The bisection method is used to find the end activity, which is the start activity of the next period. The calculation continues until the last period. Finally, the economic performance or the overall product quality can be calculated for the whole run length.

4.6 Catalytic Reforming Process Optimisation

The performance of catalytic reforming largely depends on the operating conditions. Based on the results of sensitivity analysis, operating temperature plays a key role determining the product yield and quality, as well as the life cycle of catalyst. Therefore, a new optimisation model is proposed to target four different objectives by optimising the operating temperature in each period. Four objectives include maximum profit, gasoline yield, octane number, and hydrogen yield.

The rigorous process model is with the non-linearity and high dimensionality, which makes optimisation even more complicated. In order to simplify the problem regarding the degrees of freedom, it is assumed that the temperatures of different periods are functions of the time as Equation 4.19.

$$T_{r,p} = a_r + b_r t_p + c_r t_p^2 + d_r t_p^3 + e_r t_p^4 \quad (4.19)$$

where $T_{r,p}$ is the inlet temperature of reactor r in period p , and t_p is the time of period p . a_r, b_r, c_r, d_r, e_r are the coefficients of reactor r of the function.

The advantage of the assumption, first of all, is that the degrees of freedom are reduced to 15 for three reactors, and any number of periods. Secondly, the temperatures would change smoothly, which is more reasonable in practice.

4.6.1 Mathematical Model

The objectives are listed as follows. The max profit (Equation 4.20) consists of the income of selling products including reformat, hydrogen, gas and etc, the cost for heating fuel, and power consumption for the compressor. Only the terms that could be influenced by changing the operating temperatures are included, which means the cost for the feedstock will be excluded because it is fixed.

$$\max profit = \sum_{p \in P} \left(\sum_{product} (C_{product} F_{p,product}) - C_{fuel} \Delta H_{heating} - C_{power} \Delta H_{adibatic} \right) \quad (4.20)$$

where $C_{p,product}$ stands for the price of product (reformat, hydrogen, gas and etc.) in period p , which is related to the quality of product as Equation 4.21 for the reformat. $F_{p,product}$ is the product quantity in period p . C_{fuel} is the price of fuel, and C_{power} is the price of every unit of power for compressor. $\Delta H_{heating}$, $\Delta H_{adibatic}$ are defined previously.

$$C_{p,reformat} = C_0 + (ON_p - ON_0) C_{coef} \quad (4.21)$$

where C_0 is the reference price of reformat with ON_0 . C_{coef} is the coefficient for the substantial price because of the increased ON.

$$\max hydrogen = \frac{1}{N_p} \sum_p F_{p,H2} \quad (4.22)$$

$$\max ON = \frac{1}{N_p} \sum_p ON_p \quad (4.23)$$

$$\max gasolineyield = \frac{1}{N_p} \sum_p yield_{p,reformat} \quad (4.24)$$

Equation 4.22, 4.23, and 4.24 describe the other three objectives. N_p is the interval number.

In this work, the only constraints are taken into account are the lower and upper bounds of the operating temperature.

$$T^L \leq T_{r,p} \leq T^U \quad (4.25)$$

4.6.2 Optimisation Approach

Since there is no explicit expression between the objectives and the coefficients of the operating temperature functions, the optimisation is the simulation-based methodology, which normally requires a large number of simulations. Therefore, it is necessary to choose an optimiser that, in general requires fewer functional evaluations for convergence. Sequential quadratic programming (SQP), which typically needs a smaller number of iterations than other comparable methods, is used to solve this nonlinear programming problem by introducing NAG MATLAB library subroutine e04ue.

4.7 Case Study – Multi-period Process Simulation and Optimisation

4.7.1 Multi-period Process Simulation

A multi-period process simulation is investigated on the case in section 4.4, which does not consider the catalyst deactivation, based on the proposed multi-period process model. The cycle length is scheduled as 1 year (12 months), and each period as 1 month. Therefore, there are 12 periods. All three reactors are operated at the inlet temperature of 783.15 K and the pressure of 150 psi. These would be used as base case.

As Figure 4.18 and Figure 4.19 illustrate, along with the time progressing, the profit and reformate quality octane number in each period will decrease, since the inlet temperatures remain same. Although the reformate yield will increase shown in Figure 4.19, reformate RON is decreased from around 95 to 80, which has a significant negative effect on the economic performance, decreased by almost half of the profit. The cracked products, hydrogen and C₄⁻ hydrocarbon are gradually reduced.

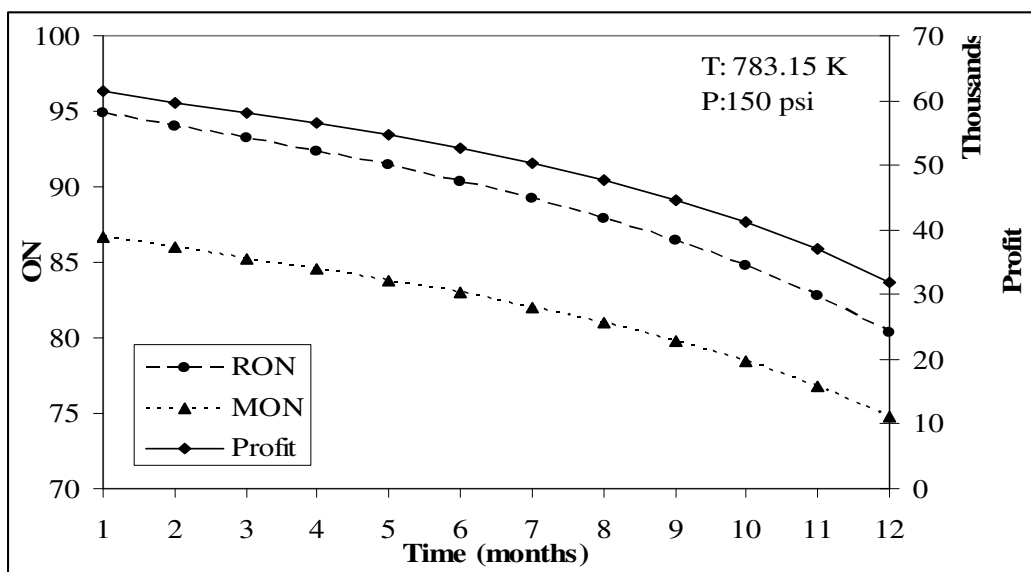


Figure 4.18 Profit and reformat ON through running cycle

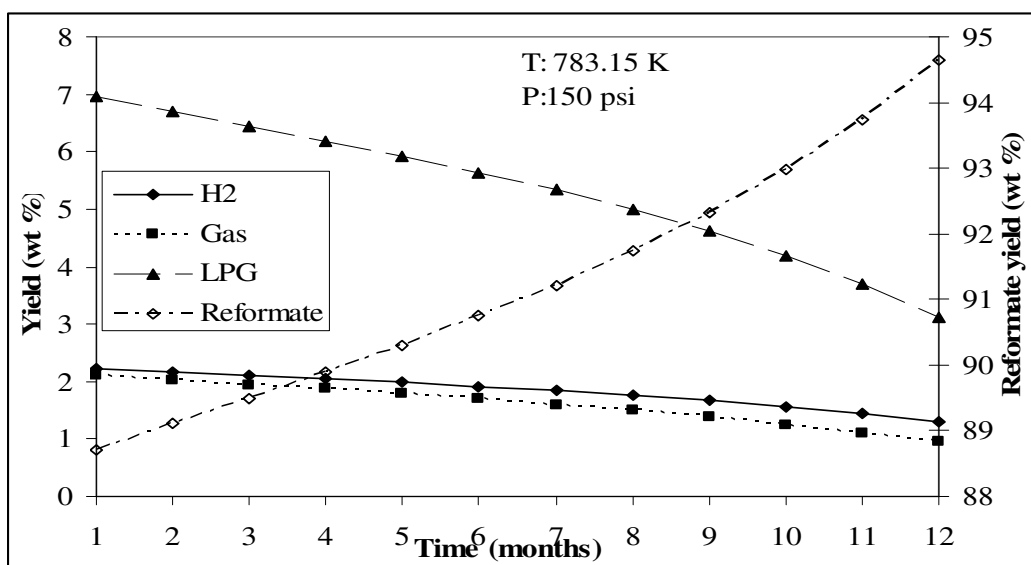


Figure 4.19 Product distributions through running cycle

All the impacts come from the loss of catalyst activity, illustrated in Figure 4.20, with final activity of 0.26, 0.18, and 0.12 for three reactors respectively. The reason that the activity of the last reactor is least is that the content of coke precursor (olefin and aromatic compounds) will increase across the reactors.

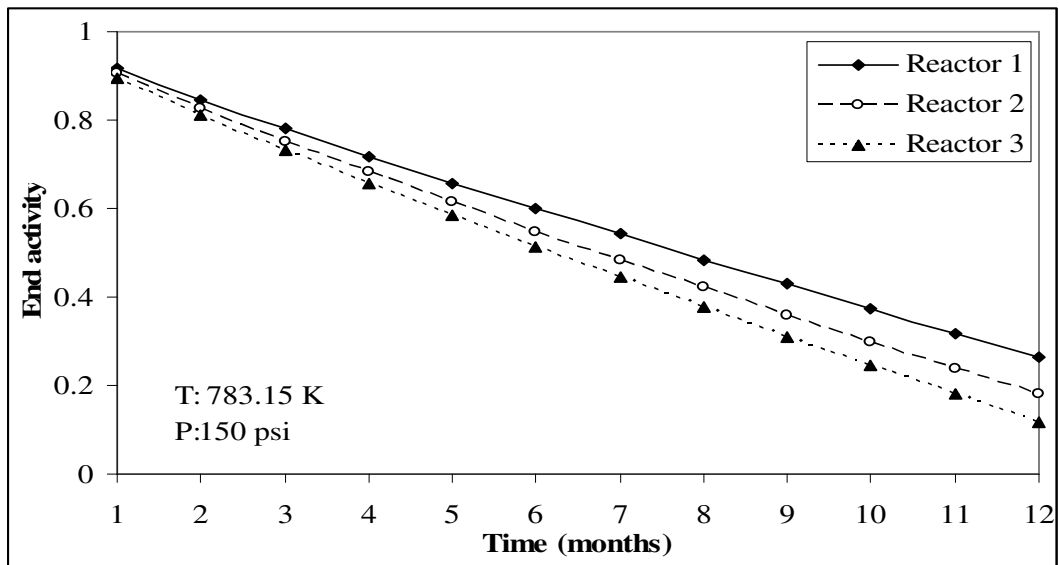


Figure 4.20 Catalyst activities of three reactors through running cycle

4.7.2 Sensitivity Analysis of Operating Temperatures

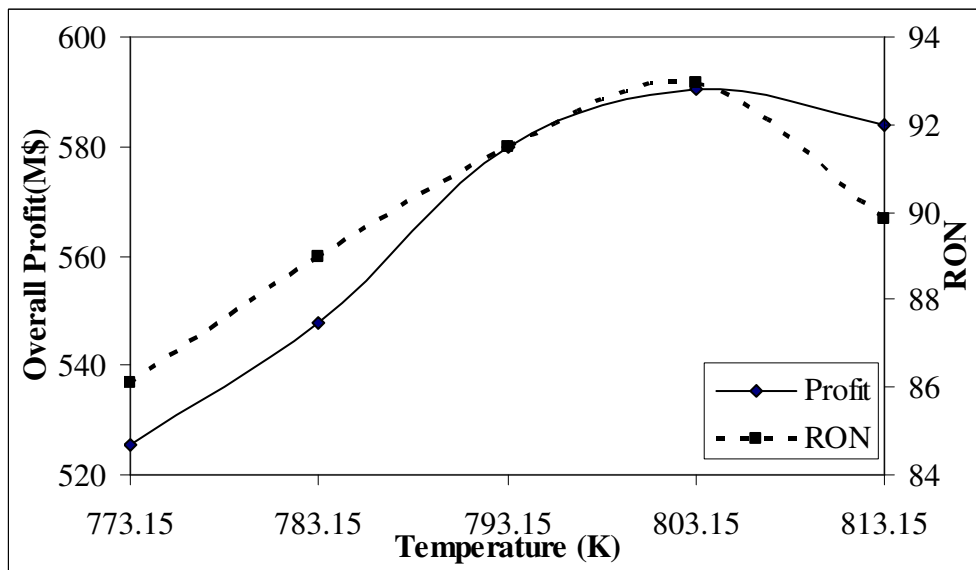


Figure 4.21 Influence of temperature on overall profit and RON

The impacts of operating temperature on process performances, including overall profit, octane number, hydrogen and reformat yields, are analysed as Figure 4.21 and Figure 4.22. The operating temperatures of three reactors are the same in any of period for the simplification of sensitivity analysis. The overall profit shows a similar trend with temperature as RON as Figure 4.21 shows because of the major contribution of profit from the reformat related to its quality. The overall profit and average RON are increased rapidly with the temperature increase at the

beginning, and then the substantial increase decreases along with high temperature because of reformat yield decreases. Due to the fixed run cycle length, the optimiser would choose the low temperatures in the later periods leading to low reformat quality, if high temperatures are selected in the first periods. Therefore, how to determine the operating temperature profile through the periods is not obvious without the process optimisation.

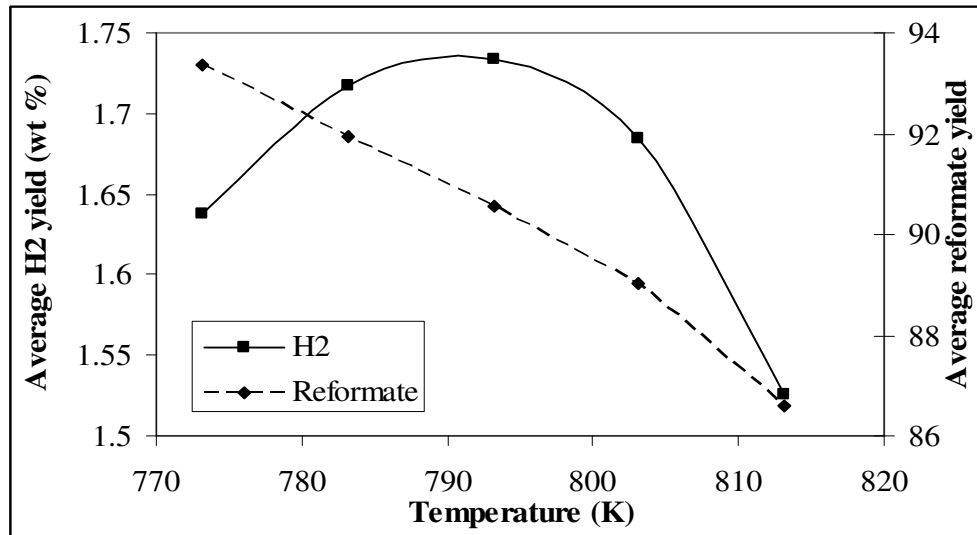


Figure 4.22 Influence of temperature on the overall hydrogen and reformat yields

Figure 4.22 presents the influence of temperature on the overall reformat and hydrogen yields. As known, the reformat yield will increase with the decrease of operating temperatures, along with the deteriorating of reformat quality. But for hydrogen yield, high temperature favour both hydrocracking reactions, which consumes hydrogen, and dehydrogenation, which produces hydrogen. As Figure 4.22 shows that the hydrogen yield would be maximised if operated at the temperature of 790 – 800K with all same inlet temperatures for reactors.

4.7.3 Process Optimisation

The proposed process optimisation methodology is applied for the base case in the section 4.4 for the optimal operating temperature of each period. Different objectives including maximising profit, reformat yield, and hydrogen yields are employed. The major impact on the profit is the reformat quality, therefore, the optimal operating temperatures for maximising profit and RON is similar. The lower and upper bounds for temperature are 760K and 803.15K respectively.

Table 4.7 presents the results of different process performances by adapting different objectives. The mode of maximising reformat yield has the lowest profit because of the low reformat quality of octane number with the average 75.7.

Table 4.7 Objectives of base case

	Base case	Max profit	Max hydrogen	Max reformat
Profit(M\$)	427963	600441	596602	253467
RON	82.26	89.45	89.18	75.70
MON	76.26	82.19	81.98	70.81
Hydrogen (wt%)	1.52	1.80	1.81	1.18
Reformat (wt %)	94.68	90.47	90.86	97.34

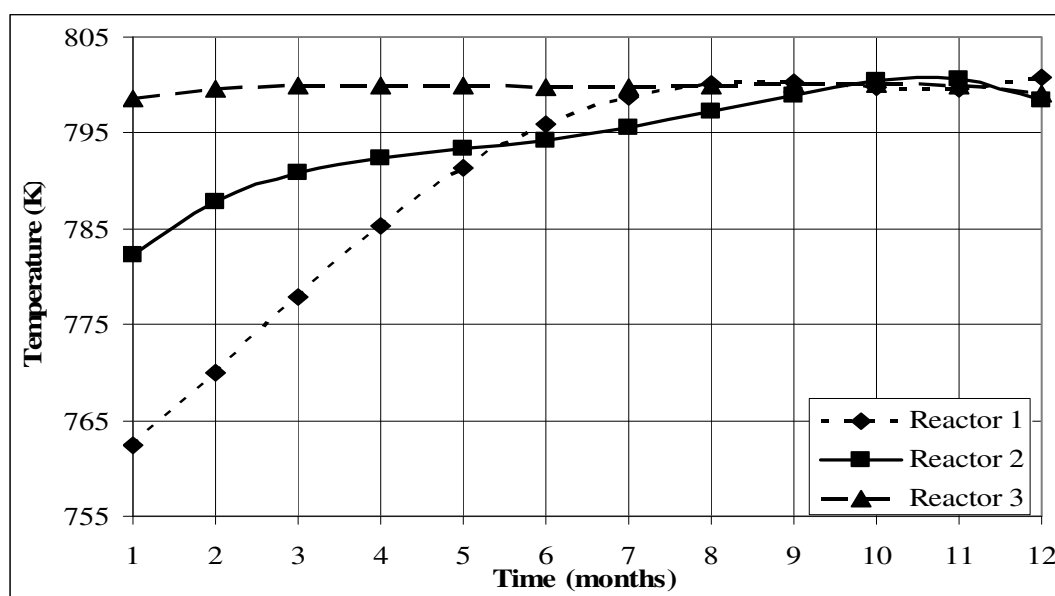


Figure 4.23 Optimal operating temperature through the running periods targeting the maximal profit

Figure 4.23 gives the temperature profiles of three reactors, in which the objective function is maximising the profit. The first reactor is operated at the lowest temperature compared with the other two, and gradually increased, finally to the upper bound. The operating temperature of the second reactor shows the similar trend, while it is close to the upper bound for the third reactor. The characteristics of the temperature profiles possibly is determined by that dehydrogenation, mainly in the first reactor, is very fast, and the rate of reactions taken place in the following reactors is relatively slow.

Figure 4.24 presents the product distribution through the running periods for the maximal profit operating mode. Although the operating temperatures are always increased gradually, the reformate yield is reduced first because of the high operating temperature, followed with the gradual growth because of catalyst deactivation.

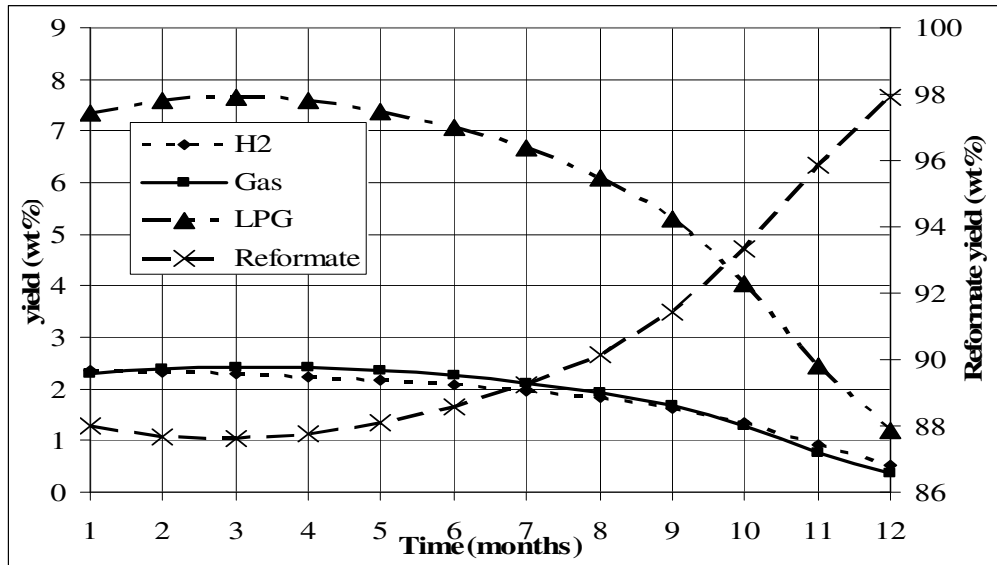


Figure 4.24 Product distribution through the running periods targeting the maximal profit

4.8 Summary

A rigorous molecular model of a semiregenerative catalytic reforming process has been developed based on the developed MTHS matrix for feedstock and product streams. The process model includes a kinetic model which takes into account the most important reactions of the catalytic reforming process. Pressure drop has been taken into account due to the non-negligible cost for the power consumption of compressing the recycle hydrogen gas. Composition, temperature and pressure have been obtained to provide information about the extent of conversion in the reactors. The case study has compared the results from the proposed molecular model with the measured data. The results not only demonstrate that the developed model is capable of simulating the reactions in a catalytic reformer and being applied in the process optimisation, but also illustrates the accuracy of the proposed characterisation methodology on naphtha streams. Furthermore,

sensitivity analysis of operating conditions exhibits different characteristics impact on the process performance.

A process level optimisation model has been developed with the consideration of catalyst deactivation. Firstly, the model of catalyst deactivation correlating coke amount on catalyst with reaction rate is performed. Secondly, a multi-period process model of catalytic reforming has been developed based on time-division intervals of the running cycle. Lastly, the optimisation model targeting different objectives by varying the operating temperatures of the reactors in the periods is successfully implemented assuming the temperature profile follows a smooth function with respect to time. The case study shows the capability of the proposed optimisation model, which will be integrated into the site-level optimisation in the later chapter.

4.9 Nomenclature

List of sets

i	component index
j	reaction index
r	reactor index
p	period index of multi-period model

List of symbols

t	time
k, k_0	rate constant with temperature T and pressure P , rate constant with temperature of 766 K and 300 psi
EA_j	activation energy
R	ideal gas constant
α_k	factor for pressure effect
T	operating temperature
P	operating pressure
F_i	molar flow of the component i
w	catalyst weight
$\gamma_{j,i}$	stoichiometric coefficient of component i in reaction j

r_j	reaction rate of reaction j
ΔH_j	reaction heat of reaction j
C_{p_i}	specific heat capacity of component i
G	superficial mass velocity
d_p	diameter of catalyst particle
ρ, ρ_c	density of gas mixture, density of catalyst
ε	void fraction of catalyst
μ	viscosity of the gas mixture
A_c	cross section area of the bed
Z	compressibility factor
P_{in}, P_{out}	inlet and outlet pressure of compressor
$\Delta H_{adiabatic}$	power consumption of the compressor

Chapter 5 Molecular Modelling of Diesel Hydrotreater

5.1	Introduction	157
5.1.1	Diesel Hydrotreating Process	157
5.1.2	Feed Characteristics	159
5.1.3	Operating Conditions	159
5.1.4	Product Specification	161
5.1.5	Motivation of a Molecular Model for Diesel Hydrotreater.....	162
5.2	Reactions Network and Kinetics	163
5.2.1	Hydrodesulphurisation (HDS)	164
5.2.2	Hydrodearomatisation (HDA).....	171
5.3	Modelling of a Trickle – bed Reactor	174
5.3.1	Mathematical Equations.....	175
5.3.2	Estimation of Physical Properties	177
5.3.3	Mathematical Methodology and Solving Procedure.....	179
5.4	Case Study – Modelling of Diesel Hydrotreater	181
5.4.1	Simulation of a Diesel Hydrotreater	181
5.4.2	Sensitivity Analysis of Operating Conditions.....	183
5.5	Catalyst Deactivation	186
5.5.1	Mathematical Model of Catalyst Deactivation	186
5.5.2	Multi-period Model of Catalyst Deactivation	188
5.6	Diesel Hydrotreater Optimisation	189
5.6.1	Mathematical Model	190
5.7	Case Study – Optimisation of Diesel Hydrotreater.....	191
5.8	Summary	192
5.9	Nomenclature	193

5.1 Introduction

Current trend of dieselisation is because of the higher efficiency in diesel fuel consumption and lower CO₂ emissions. However, increasing concerns about the environmental issues have led to the stricter legislation on the quality of diesel, such as ultra-low sulphur diesel (ULSD), even sulphur free diesel. Therefore, refiners must increase their hydrotreating capability by revamping existing processes or building new processes to meet the future scenarios. As the margins decrease, refiners also want to enhance it through process optimisation. However, the traditional lumped process model is not capable of predicting the behaviors of deep hydrotreating because different sulphur compounds have quite different reaction characteristics. These scenarios lead to an aspiration for a detailed kinetic model of diesel hydrotreating processes on a molecular level.

In this chapter, firstly, diesel hydrotreating process is briefly introduced, along with the issues to the performance of a hydrotreater. To build up a molecular model of a diesel hydrotreater, chemical reactions and the modelling of a reactor are described respectively. In the chemical reactions part, hydrodesulphurisation (HDS) and hydrodearomatisation (HDA) are included, and investigated with three aspects: compounds taking reactions, reactions network and kinetic models, as well as the method to obtain kinetic parameters. Regarding the reactor modelling, mathematical equations are given firstly, followed by the estimation of the required physical properties, and the mathematical solving procedure. A case is simulated with the proposed model, together with the sensitivity analysis of the operating conditions. Catalyst deactivation, which has a serious impact on the economic performance, is also considered in this research. Finally, a multi-period process level optimisation model is developed, and applied in a case study.

5.1.1 Diesel Hydrotreating Process

Diesel hydrotreating process (DHT) is usually used to remove sulphur in diesel oil to produce the qualified products. In addition to sulphur reduction, diesel hydrotreating can also help to improve other qualities such as cetane number, oxidation stability, polynuclear aromatic content and color.

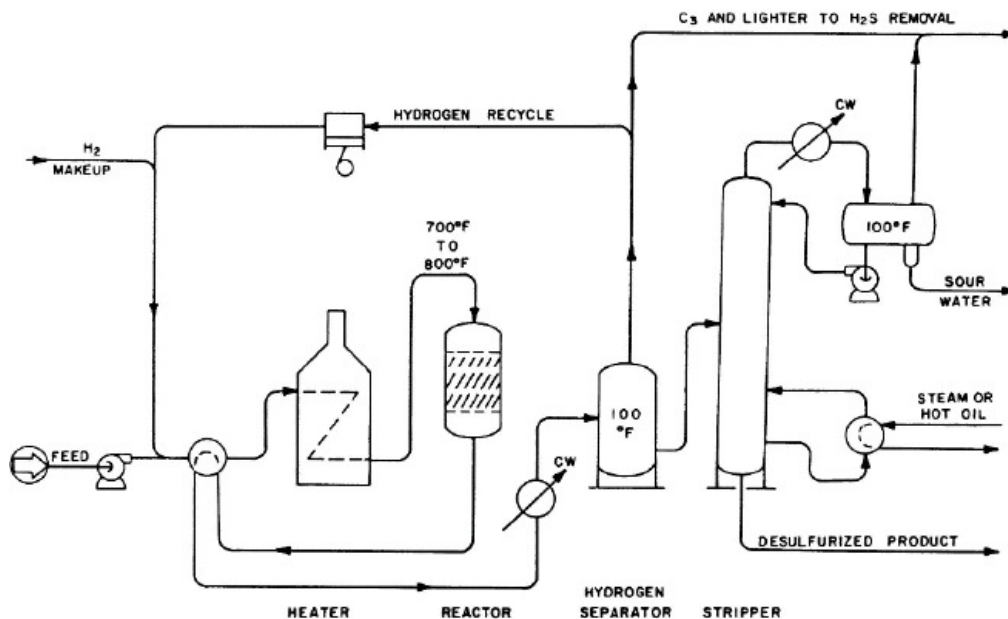


Figure 5.1 A simplified diesel hydrotreating process flowsheet (Gary, 2001)

Figure 5.1 shows a simplified diesel hydrotreating process flowsheet (Gary, 2001). The mixture of a feed and hydrogen gas is heated first by reactor effluent, because usually hydrotreating reactions are exothermic and release a huge amount of heat, which can be integrated for the energy saving. Then the mixture is further heated up to the reactor inlet temperature before fed to a reactor, in which quantities of reactions take place in the presence of catalysts. Sulphur in the form of hydrogen sulphide, and nitrogen as ammonia accumulates through the reactor in the vapour phase. Hydrogen is separated first from the streams out of the reactor, and then recycled or purified to remove the light hydrocarbon accumulated in the streams. To decrease the inhibition of hydrogen sulphide and ammonia on the hydrotreating reactions, hydrogen sulphide and ammonia usually are removed from the vapour phase. Makeup hydrogen stream must be present to maintain the partial pressure of hydrogen, which has a great impact on the hydrotreating reactions.

There are numerous issues to be addressed for the performance of a hydrotreater, including feed characteristics, catalysts formulation, process configuration, reactor design, operating conditions, and product specifications etc.

5.1.2 Feed Characteristics

Sulphur, nitrogen and aromatic contents are the most important feed characteristics. Usually, the aromatic content of a feed will govern the chemical hydrogen consumption at low space velocities and high hydrogen partial pressures required for a very low sulphur diesel production.

Generally, cracked stocks can be included in the feed up to the level limited by the product cetane or gravity without a significant impact on hydrotreater performance. There is a small increase in API gravity and cetane index after the hydrotreating reactions. If a significant improvement in cetane or gravity is required, a multi-stage design using aromatics saturation catalysts in the second stage may be the more economical option. Table 5.1 gives typical characteristics for potential diesel blending stocks, including yields, sulphur contents and cetane etc.

Table 5.1 Typical characteristics of feed to diesel hydrotreaters (Heinrich et al, 2001)

Feedstock:	Paraffinic crude			Naphthenic crude		Vacuum distillate		Vacuum residue	
Process:	Atmospheric distillation			Atmospheric distillation		FCC LCO	Hydro-cracking	Vis-breaking	Coking
Yield, wt%	30.2	32.8	36.7	29.2	47.2	10-15	30-40	5-15	35
Density @15°C, kg/l	0.83	0.82	0.84	0.827	0.856	0.930	0.814	0.845	0.900
Distillation, °C									
IBP	170	180	170	180	170	170	220	170	170
FBP	370	375	400	350	370	370	370	370	370
Cloud point, °C	5	-2	1	-10	-20	-5	-17	-4	-8
Pour point, °C	-12	-9	-6	-18	-33	-14	-20	-18	-20
Cetane number	50	51	54	45	43	24	64	40	28
Sulphur, wt%	0.12	0.04	0.83	0.80	0.09	2.8	0.001	2.33	2.10

5.1.3 Operating Conditions

The key operating conditions of a diesel hydrotreating unit are liquid hourly space velocity (LHSV), hydrogen partial pressure, make-up hydrogen purity, hydrogen/oil ratio, cycle length, and reactor temperature.

For a given cycle length and treating severity, reactor space velocity, and hydrogen gas quantity as well as hydrogen partial pressure are the variables optimised along

with reactor temperature. As the hydrogen partial pressure is increased, the catalyst deactivation rate is reduced. Thus, space velocity can be increased accordingly for a constant cycle length. However, this is at the expense of higher hydrogen consumption. Another important variable is the ratio of total hydrogen supplied to a reactor bed to the chemical hydrogen consumption for that bed.

For the revamp designs, the achievable hydrogen partial pressure is restricted by the existing equipment and piping mechanical design, and hydraulics in the reactor loop. A higher treat gas rate can be used to increase the hydrogen partial pressure, but this is usually limited because of the associated increase in the reactor loop pressure drop and the corresponding maximum operating pressure of the various system components. Make-up hydrogen purity impacts the hydrogen partial pressure for a fixed reactor operating pressure. Lower purity make-up hydrogen requires higher hydrogen circulation rates to maintain the target hydrogen partial pressure and may even require a purge stream from the cold separator. If the make-up hydrogen purity is too low, there is no combination of recycle rate and purge that can be used to achieve the target reactor outlet partial pressure. For a revamp design, increased make-up hydrogen purity is the most effective means of increasing the hydrogen partial pressure.

For new designs, cycle lengths have typically been set at 24–36 months. This has been based on the logic that, at some point, the cycle will be limited by factors other than catalyst activity: namely, reactor pressure drop (Korsten, 1996). Hydrogen partial pressure has a major impact on cycle length from a catalyst activity standpoint. For a fixed space velocity, the cycle length increases with hydrogen partial pressure. Maximum reactor outlet temperature at end-of-cycle catalyst conditions is generally set at 725–750 °F to avoid aromatics saturation equilibrium constraints. This is also influenced by the quantity of cracked stocks in the feed and the crude source. Hydrotreating catalyst performance correlations for reactor temperature are usually based on the weighted average bed temperature (WABT). The temperature rise is usually limited to 40–50 °F per bed by quenching. Thus, for a 50°F temperature rise and a 725 °F maximum reactor outlet temperature, the end-of-run WABT would be $(725-50) + 2/3(50) = 708$ °F. The start-of-run WABT has to be sufficient to obtain the required removal of sulphur

and nitrogen. Cycle length is determined by the catalyst deactivation rate at the design space velocity and hydrogen partial pressure. During the cycle, the increase in WABT will be 30– 50 °F, with lower deactivation rates occurring at higher hydrogen partial pressures.

5.1.4 Product Specification

Table 5.2 EN 590 diesel fuel requirements – date introduced: 1/1/2005

Diesel specification parameter	Units	Limits
Cetane Number		51.0 minimum
Cetane Index		46.0 minimum
Density at 15 °C	kg/m ³	820 – 845
Polycyclic Aromatic Hydrocarbons	% (m/m)	11 maximum
Sulphur Content	mg/kg	10 maximum
Flash Point	°C	>55
Carbon Residue (on 10% Dist. Residue)	% (m/m)	0.3 maximum
Ash Content	% (m/m)	0.01 maximum
Total Contamination	mg/kg	24 maximum
Copper Strip Corrosion (3 Hours at 50 °C)		
Oxidation Stability	g/m ³	25 maximum
Lubricity, WSD at 60 °C		460 maximum
Viscosity at 40 °C	mm ² /sec	2 – 4.5
Distillation Vol. Recovered at:		
250 °C	% (v/v)	<65
350 °C	% (v/v)	85 minimum
95 % Point	°C	360 maximum
Fatty Acid Methyl Esters (FAME) Content	% (v/v)	5 maximum

Sulphur content is one of the most important specifications of diesel fuel. Recently, the constraint on the aromatic content has become a legal issue in some areas. The higher the cetane number, the shorter is the delay interval of an engine. Generally, diesel engines will operate well on fuels with cetane numbers above 50. The flash point temperature of diesel fuel is the minimum temperature at which the fuel will ignite on application of an ignition source under specified conditions. Minimum

flash point temperatures are required for proper safety and handling of diesel fuel. Table 5.2 gives diesel fuel specifications in the European Union.

5.1.5 Motivation of a Molecular Model for Diesel Hydrotreater

To fulfil the stringent environmental requirements on diesel fuel, it is necessary to have a deep understanding on the behaviour of DHT process from different points of view as reviewed in the last section: feed characteristics, operating conditions and product specifications etc. Conventional models usually lump sulphur compounds as one or two pseudo compounds, and the pseudo order of reaction rate could vary from first order to second according to different feedstocks and operating conditions (Landau et al., 1998; Beuttner and Schmid, 1963; Cotta et al., 2000). As the parameters are derived from the specific hydrodesulphurisation conditions, the models have a restricted application for deep desulphurisation. Another important factor is that the well-known inhibitory effect of H₂S and nitrogen compounds on the hydrodesulphurisation rate is not accounted for in the conventional models (Korsten, 1996). Therefore, in order to have a deep understanding of diesel hydrotreater behaviour, a detailed kinetic model on the basis of molecular information is required.

For light feeds, the reactions are frequently performed in two-phase (gas –solid) fixed-bed reactors. However, when the installation range of the feed increases, hydrogen, a liquid–gas mixture of the partially vaporised feed, and solid catalyst are commonly found. This latter system is called a trickle-bed reactor (TBR), which is referenced in the literature as a reactor in which a liquid phase and a gas phase flow concurrently downward through a fixed-bed of catalyst particles while reactions occur (Rodríguez, 2004). Therefore, in nature, diesel hydrotreating reactions take place in a three-phase reactor. Moreover, the investigation of the hydrodesulphurisation especially shows a large inhibiting effect of hydrogen sulphide on conversion (Gates et al., 1979; Vrinat, 1983). Since the concentration of H₂S increases along with the reactor, the pseudohomogeneous plug-flow model cannot yield satisfying results, because a change of the gas-phase concentrations and the mass transfer between the phases are neglected. For a reliable result achievement, a three-phase reactor should be considered.

This research tries to develop a detailed kinetic model for hydrotreating process with a three-phase reactor based on feedstocks and products in terms of the MTHS matrix representation. Beyond the molecular modelling of a diesel hydrotreater, a multi-period model of run cycle is proposed to take the catalyst deactivation into account, and a process optimisation model is developed to help the refiners increase margins as well. Furthermore, the developed model will be integrated into hydrogen network management detailed in chapter 6.

The work consists of four aspects: reactions network and kinetics, modelling of a trickle-bed reactor, modelling of catalyst deactivation, and the optimisation model.

5.2 Reactions Network and Kinetics

Reactions in diesel hydrotreating processes are complex, generally involving tens of thousands of reaction steps and species. Girgis and Gates (1991) have provided a detailed literature review of the early studies on the hydrotreating chemistry, including thermodynamics, reactivities, reaction networks, and reaction kinetics. These studies provide molecular information and mechanism of the hydrotreating reactions of various species in middle distillates. The reactions are classified as hydrodearomatisation (HDA), hydrodesulphurisation (HDS), hydrodenitrogenation (HDN), and hydrodeoxygenation (HDO). Based on the classification, Sun (2004) successfully introduced reaction family to build up molecular modelling of a diesel hydrotreater based on the MTHS framework, with a pseudohomogeneous reactor model. Each group includes the reaction families that show similar reactions. The molecular level pathways of these reaction families can be expressed as the inter-conversions of the matrix elements. However, kinetic parameters obtaining is not solved properly. In this work, HDN and HDO are not considered due to two reasons. One is that the fractions of nitrogen compounds and oxygen compounds are very low, while sulphur content in products is ultra low. HDA is the main hydrogen consumption reaction which would impact the hydrogen partial pressure in the vapor phase and the hydrogen concentration in the liquid phase. The other is that the research on HDO and HDN is not as mature as that on HDS and HDA.

Obtaining kinetic parameters is a crucial step for a kinetic model. As mentioned before, hydrotreating process involves tens of thousands of reactions, in which a

set of kinetic parameters are corresponded. For instance, Froment (1994) concluded that 1133 parameters are needed to be determined for HDS of DBT and methyl-DBT, not including other reactions. Therefore, it is a big challenge of how to obtain kinetic parameters properly.

5.2.1 Hydrodesulphurisation (HDS)

Sulphur atoms tend to be bound in the oil as “sulphur bridges” between two carbon atoms or to be contained in a saturated ring structure. Removal of these sulphur atoms usually requires only the breaking of the two sulphur-carbon bonds per sulphur atom and the subsequent addition of four atoms of hydrogen to cap the ends of the bonds that were broken. When the part of a molecule that contains sulphur can access catalyst surface, sulphur removal is relatively easy.

5.2.1.1 Sulphur Compounds

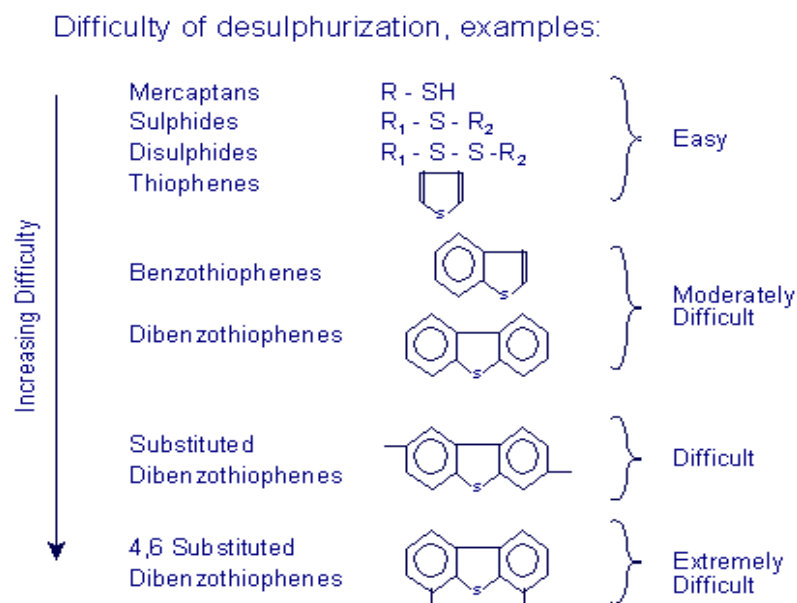


Figure 5.2 Difficulties of desulphurisation of different sulphur compounds (Froment, 2007)

The types of sulphur compounds present in different fractions of petroleum distillates may be different with each type, exhibiting different relative reactivities. The operating severity needed for different types of sulphur compounds are considerably different as Figure 5.2 shows. A clear understanding of the nature of sulphur compounds present in different petroleum fractions as well as the kinetics

and mechanism of their desulphurisation processes under hydrotreating conditions is of interest to refiners for proper choice of feedstocks for the production of low sulphur diesel fuels cost effectively. In addition, the understanding of sulphur compounds in petroleum fractions also helps the optimisation of operating conditions for deep desulphurisation.

Table 5.3 Sulphur distribution in various LCO fractions (Depauw, 1997; Carcía, 2002; Nylén, 2004)

Sulphur compound	Sulphur distribution (%)		
	Depauw	Carcía	Nylén
BT	1.9	0.4	1.5
C1-BT	9.5	4.3	10.2
C2-BT	15.1	12.7	19.1
C3-BT +	22.1	19.9	29.3
DBT	2.2	3.8	3.3
C1-DBT	11.8	16.5	12.5
C2-DBT	15.9	22.2	11.8
4,6 – DMDBT	1.1	-	1.3
C3 – DBT +	20.6	20.2	12.4
Total sulphur (ppm)	7809	11911	~ 11750

C1-: substitute with one carbon, C2- substitute with two carbons, C3+- substitute with three and more than three carbons

Efforts have been made to monitor and identify traces of sulphur compounds in various petroleum fractions, using methods mainly based on capillary gas chromatography equipped with various types of detectors such as GC-AED (Atomic Emission Detector), GC-MS, GC-FPD (Flame Photometric Detector), and GC-SCD (Sulphur Chemiluminescence Detection). Andari (1996) quantitatively estimated sulphur compounds in different cuts from Kuwait crude oil, and found that thiophene and its alkyl derivatives constituted about 60% of the total sulphur compounds in the naphtha fraction, while the remaining 40% was composed of mercaptanes and alkyl sulphides. Regarding the gas oil boiling point range (210 – 340 °C), the alkyl benzothiophenes (BT) account for the major portion in the fraction boiling in the narrow range 235 – 257 °C, and alkyl dibenzothiophenes

(DBT) are highly concentrated in a fraction boiling between 280 – 325 °C, and both are absent in the fraction boiling above 330 oC. Detailed characterisation of sulphur components present in light cycle oils were also performed (Depauw and Froment, 1997; Carcía, 2002; Nylén, 2004) as Table 5.3 illustrates. According to the difficulty of desulphurisation, sulphur compounds are classified into five categories in the MTHS matrix for middle distillate: SI, SII, SIII, SIV, and SV.

5.2.1.2 Reactions Network and Kinetics

The fundamental transformations in HDS for sulphur compounds are similar and summarised as follows:

1. Adsorption (coordination) of the sulphur compound to the active site
2. Hydrogenation of unsaturated C=C bonds
3. Cleavage of two carbon-sulphur bonds (sequential or simultaneous)
4. Addition of hydrogen to the broken bonds of both sulphur and carbon
5. Release of the hydrocarbon product from the catalytic site
6. Release of H₂S from the site

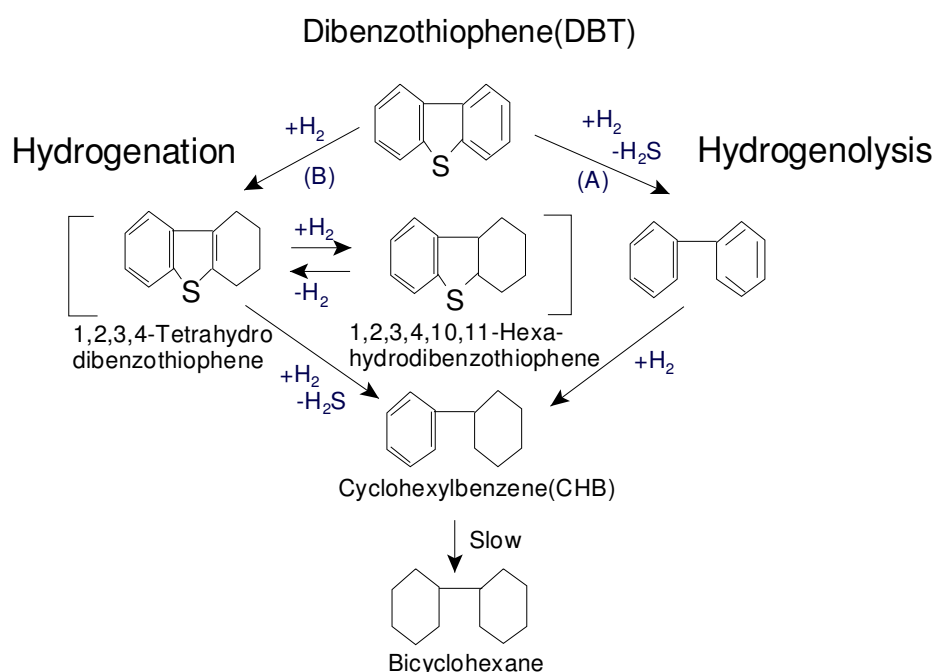


Figure 5.3 Reaction Network for the HDS of DBT

For HDS reactions of thiophenic species, it is suggested that two reaction pathways take place on two different types of sites on the catalyst, denoted σ for hydrogenolysis and τ for hydrogenation (Van Parijs et al., 1986; Duayne et al.,

2001). As Figure 5.3 shows the proposed reaction mechanism for dibenzothiophene HDS, it involves two parallel pathways: hydrogenation and hydrogenolysis, inferred to occur on two different kinds of sites (Houalla et al., 1978; Vanrysselberghe and Froment, 1996).

Froment et al had investigated the reaction network and kinetics of hydrodesulphurisation for different sulphur compounds, including thiophene (Van Parijs and Froment 1986), benzothiophene (Van Parijs and Froment 1986), dibenzothiophene (Vanrysselberghe and Froment, 1996) and 4-methyldibenzothiophene and 4,6-dimethyldibenzothiophene (Vanrysselberghe and Froment, 1998), and concluded that the surface reaction between absorbed reactants and two competitively absorbed hydrogen atoms was the rate-determining step for hydrogenation and hydrogenolysis reactions. Therefore, a uniform kinetic model of HDS for various sulphur compounds was suggested as follows (Vanrysselberghe and Froment, 1998).

Hougen-Waston rate equation:

$$r_s = \frac{k_{s,\sigma} K_{H,\sigma} K_{s,\sigma} C_s C_{H_2}}{DEN_\sigma} + \frac{k_{s,\tau} K_{H,\tau} K_{s,\tau} C_s C_{H_2}}{DEN_\tau} \quad (5.1)$$

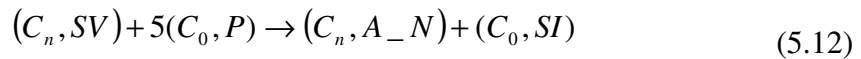
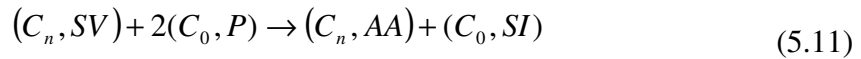
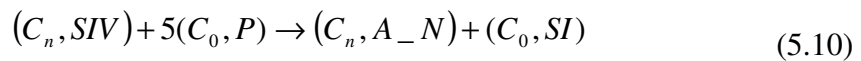
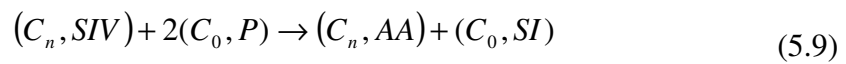
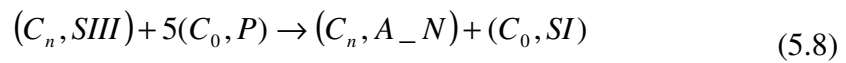
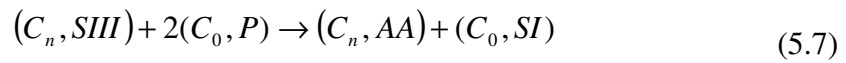
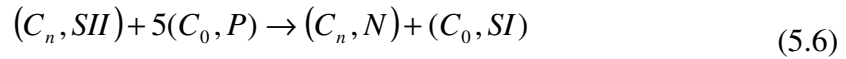
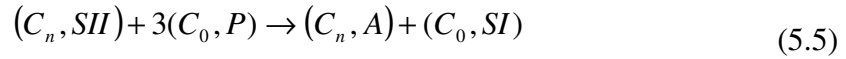
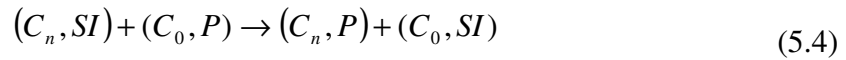
with

$$DEN_\sigma = \left(1 + \sum_i K_{i,\sigma} C_i + \sqrt{K_{H,\sigma} C_{H_2}} \right)^3 \quad (5.2)$$

$$DEN_\tau = \left(1 + \sum_i K_{i,\tau} C_i + \sqrt{K_{H,\tau} C_{H_2}} \right)^3 \quad (5.3)$$

where r_s is the reaction rate of sulphur compound s , $k_{s,\sigma}$ $k_{s,\tau}$ are the rate coefficients for the reactions of sulphur compound s on σ and τ sites respectively, $K_{i,\sigma}$ $K_{i,\tau}$ are the adsorption coefficient of component i on σ and τ sites, C_i is the liquid concentration of component i .

The HDS pathways of various sulphur compounds in terms of the MTHS matrix elements implemented by Sun (2004) are applied in this research outlined as follows.



5.2.1.3 Obtaining Kinetic Parameters – Structure Contribution Approach

Table 5.4 gives the information about the kinetic parameters number to build up the kinetic model of HDS with the stream representation of the MTHS matrix. Take SIII reaction family as an example, in a diesel fraction, SIII class of carbon number ranges from 12 to 26 which means 15 sulphur lumps of SIII exist in diesel fraction. For each sulphur lump of SIII, both hydrogenation and hydrogenolysis take place on different sites, therefore leading to two sets of reaction parameters (rate coefficient and activation energy) and adsorption parameters. SI class could be eliminated for diesel fractions because SI is negligible as in the 5.2.1.1 section.

Table 5.4 kinetic parameters number needed for the kinetic model of HDS with molecules represented by the MTHS matrix

	k_{σ}	k_{τ}	K_{σ}	K_{τ}
SI	18×2		18×2	18×2
SII	18×2	18×2	18×2	18×2
SIII	15×2	15×2	15×2	15×2
SIV	14×2	14×2	14×2	14×2
SV	13×2	13×2	13×2	13×2
P			18×2	18×2
A			18×2	18×2
N			18×2	18×2
AA			15×2	15×2
AN			15×2	15×2
H ₂ S			1×2	1×2
H ₂			1×2	1×2
Sum	156	120	328	328

Total number of 932 prohibits the way of parameter estimation based on the experimental data. Some simplifications and different strategies to achieve these parameters are needed. Structural contributions approach was firstly introduced to handle this particular problem by Froment (1994). Based on the observation of the hydrogenolysis rate coefficients of thiophene, benzothiophene and selected methyl-substituted dibenzothiophenens, Froment concluded that the position of the methyl substituent is more important than their number. The hydrogenolysis reactions involve vertical adsorption of the molecules through the S-atom on the σ -sites (Houalla et al., 1978). Then several assumptions are made (Froment, 1994):

1. In the adsorption electronic and steric effects are to be considered separately;
2. Methyl groups at a distance from the sulphur atom beyond the α -position only exert electronic effects on the adsorption;
3. Only methyl groups on the aromatic ring exert an electronic influence;
4. Methyl groups in the 4- and 6- positions also sterically hinder the adsorption;
5. Once a molecule is adsorbed, only the electronic effects of the methyl groups are of importance.

Based upon these assumptions, the equilibrium constant for the adsorption of the various substituted DBT on the σ -sites is related to that of the parent molecule through the following expression (Froment, 1994):

$$K_{sDBT,\sigma} = K_{DBT,\sigma} K_{EL,\sigma}^{sDBT}(m;n;p) K_{ST,\sigma}^{sDBT}(m;n;p) \quad (5.13)$$

m , n and p indicate the position of the methyl group in mono-, di-, and tri-substituted DBT. Only three structural contributions are required to account for the electronic effect of the substituents and two for the steric hindrance effect when there are substituents in α -position with respect to the S-atom. If there is one substituent in 4- or 6- position, $K_{ST,\sigma}^{sDBT}(m;n;p)$ is written $K_{ST,\sigma}^{sDBT}(4;0;0)$ or $K_{ST,\sigma}^{sDBT}(6;0;0)$. For substituents in both 4- and 6-positions, it is $K_{ST,\sigma}^{sDBT}(4;6;0)$.

The simplification of the rate coefficients for the hydrogenolysis reactions of the substituted DBT follows the same pattern:

$$k_{sDBT,\sigma} = k_{DBT,\sigma} k_{EL,\sigma}^{sDBT}(m;n;p) k_{ST,\sigma}^{sDBT}(m;n;p) \quad (5.14)$$

For the adsorption of species on τ -sites, which is considered to be flat, only the number of substituents and not their position has to be taken into account, so that the electronic and steric hindrance effects may be lumped. In this case, the adsorption equilibrium constant is simplified as follows:

$$K_{sDBT,\tau} = K_{DBT,\tau} K_{ST+EL,\tau}^{sDBT}(m;n;p) \quad (5.15)$$

Regarding to the hydrogenation reaction rate coefficients, the expression is described:

$$k_{sDBT,\tau} = k_{DBT,\tau} k_{ST+EL,\tau}^{sDBT}(m;n;p) \quad (5.16)$$

The final result regarding HDS of (s)DBT is given in Appendix C, as well as the way to apply structural contribution approach for (s)BT.

5.2.2 Hydrodearomatisation (HDA)

HDA reactions consist of the addition reactions of hydrogen with aromatic species existing in a petroleum feedstock, and are reversible and exothermic with equilibrium conversions of hydrocarbons under practical processing conditions (Girgis and Gates, 1991). The extent of these reactions at equilibrium decreases with the increase of temperature. HDA is different from HDS and HDN owing to thermodynamic equilibrium limitations, so a clear understanding of the effects of catalyst type, and process variables on the chemistry and thermodynamic equilibrium of different types of aromatic compounds present in petroleum feedstock is necessary for determination of optimum operating strategies.

5.2.2.1 Aromatic Compounds

Analysis of petroleum fractions shows that the aromatic compounds in petroleum mixtures mainly fall into four groups, namely monoaromatics, diaromatics, triaromatics and polycyclic aromatics (Stanislaus and Cooper, 1994). The polycyclic aromatics with four or more condensed benzene rings are usually present in high-boiling fractions (Boiling range > 350°C), while the first three types are present in middle distillates. It is seen that diaromatics constitute a major portion of the total aromatic content in straight run gas oil. Therefore the MTHS matrix representation, of middle distillate fractions, excludes polycyclic aromatic compounds in this work, represented by A, AA, AAA, AN, AAN, and ANN.

5.2.2.2 Reactions Network and Kinetics

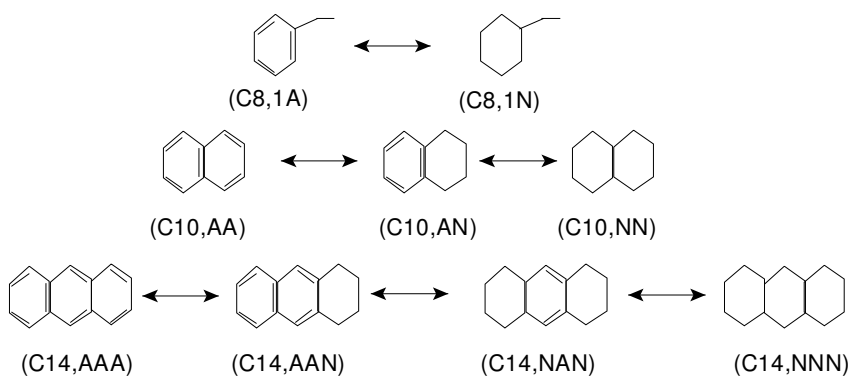
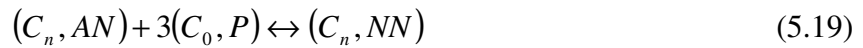
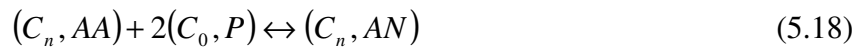


Figure 5.4 HDA reactions in diesel hydrotreater (Neurock, 1990)

The reaction networks for the above mentioned aromatic compounds of diesel hydrotreating feedstocks are obtained from the literature (Girgis and Gates, 1991; Korre et al., 1995) and presented as Figure 5.4. The hydrogenation of aromatic compounds shows several qualitative trends:

1. Polynuclear aromatics hydrogenation proceeds in a ring-by-ring manner;
2. Hydrogenation reactivity increases with the number of aromatic rings;
3. For groups with the same number of fused aromatic rings, hydrogenation reactivity increases with the presence of alkyl branches and naphthenic rings;
4. For multi-ring aromatics, polynuclear aromatics proceed in a ring-by-ring manner. Hydrogenation of the ring located at the end of the molecule is faster than hydrogenation of the ring in the middle.

The pathways for HDA of these aromatic compounds in terms of the conversion between the elements of the MTHS matrix are shown as follows.



Various kinetic models were developed for different class of aromatic compounds. The Langmuir-Hinshewood-Hougen-Waston (LHHW) (Froment and Bischoff, 1990) rate expression (eq 2.23) was widely used and simplified.

$$r_{ij} = \frac{k_{sr}^{ij} K_i (P_{H_2}^n C_i - C_j / K_{eq}^{ij})}{1 + \sum_m K_m C_m} \quad (5.23)$$

where r_{ij} is the rate of conversion of compound i to compound j , C_i is the concentration of compound i , K_m is the adsorption parameters of compound m , k_{sr}^{ij} is the surface reaction rate parameter, K_{eq}^{ij} is the overall hydrogenation equilibrium constant, P_{H_2} is the hydrogen partial pressure in the reactor, n is the reaction stoichiometry with respect to hydrogen. Korre (1994) lumped some parameters and simplified the equation as follows.

$$r_{ij} = \frac{k_{ij}(C_i - C_j / K_{ij})}{1 + \sum_m K_m C_m} \quad (5.24)$$

where k_{ij} is the combined numerator rate parameter, including surface reaction and adsorption parameter contributions, and hydrogen pressure. K_{ij} is the equilibrium ratio.

5.2.2.3 Obtaining Kinetic Parameters

The quantitative structure-reactivity correlations concept is applied to account for the effect of substituent carbon atoms on reactivity using representative model compounds as base structures. In order to reflect the effect of molecular structure on reactivity of a species quantitative structure-reactivity correlations (QS/RC) can be explored to relate the reactivity of components with their molecular properties for a homologous series of reactions (Klein et al., 2006).

Based on the experimental data of reaction pathways, kinetics, and mechanisms for catalytic hydrogenation of one-, two-, three-, and four-fused aromatic ring compounds, Korre (1994) used 7 parameters for QS/RC that characterised the associated set of series of homologous reactions to represent the rate law parameters for hydrogenation and dehydrogenation. LHHW adsorption constants is correlated with the number of aromatic rings and the number of saturated carbons, surface reaction rate constants correlates with the enthalpy of hydrogenation and the highest bond order (HBO) in the aromatic ring being saturated. Semiempirical molecular orbital calculations provided acceptable estimates of the enthalpy of reaction, which, via compensation, provided estimates of the entropy of reaction,

and thus equilibrium constant. A combination of three correlations is recommended (eq 5.25 – 5.27).

$$\ln K_i = 1.04 + 0.654N_{AR} + 0.0964N_{SC} \quad (5.25)$$

$$\ln k_{sr} = -15.0 - 7.91n + 0.133|\Delta H_R^0| + 8.22HBO \quad (5.26)$$

$$\ln K_{eq} = -3.91 - 6.63n + 0.289|\Delta H_R^0| \quad (5.27)$$

where NAR is the number of aromatic rings in a PNA molecule, NSC is the number of saturated carbons in a PNA molecule, HBO is the highest bond order in an aromatic ring. The bond order (as calculated in MOPAC/AMI, Dewar, 1985) is the scaled sum of squares of the electronic density matrix overlap between two atoms. n is reaction stoichiometry with respect to hydrogen, ΔH_R^0 is the difference between gas-phase heats of formation of products and reactants under the standard condition.

An alternative way is that Sun (2004) regressed the data available for benzene, some alkylbenzenes, and the products of their hydrogenation based on the data (Stull et al. 1969), and obtained a set of correlations particularly for equilibrium constants of aromatic compound in terms of the MTHS matrix.

5.3 Modelling of a Trickle – bed Reactor

Recently, the research on modelling a hydrotreater with three-phase trickle-bed reactor is intensive. An adiabatic multiphase reactor was simulated with a one-dimensional heterogeneous model (Froment, 1994), the calculation of the concentration profile within the catalyst particle, and the consideration of pressure drop. Korsten (1996) developed a simplified three-phase reactor model by assuming a constant catalyst effectiveness factor down through the reactor, and only hydrogen and hydrogen sulphide existing in vapor phase with the fixed temperature and pressure. Mederos (2007) compared the behaviors of tricked-bed reactors with cocurrent and countercurrent operation modes by developing a dynamic plug-flow heterogeneous one-dimensional reactor model.

In commercial applications, trickle and pulse flow are the most likely flow regimes. Trickle flow features a continuous gas phase and a dispersed liquid phase flowing as a laminar film or as rivulets over the particles. The pulse flow regime is obtained at higher liquid and gas throughputs (Froment, 1994). According to Wammes et al. (1990), the pulse flow regime is not attained at high pressures and realistic liquid flow rates, if the molecular weight of the gas phase is of the order of that of nitrogen. In a hydroprocessing unit operating, for example, at 310 °C and 50 bar, the molecular weight of the gas phase is approximately 20 g/mol. Therefore, strong indications exist that trickle flow is the dominating flow regime. Besides, it is commonly accepted that in commercial hydroprocessing reactors, all the particles are completely wetted when the gas and liquid are adequately distributed (Shah, 1979). Deviations from trickle flow can be neglected for both phases, which is confirmed by Korsten (1996). Therefore, the developed reactor model is a one-dimensional heterogeneous model with both the gas and liquid phase in plug flow.

Regarding the modelling of a diesel hydrotreater, there are three issues: mathematical equations, the estimation of physical properties, and the mathematical methodology for solving the complex model.

5.3.1 Mathematical Equations

The mathematical equations are developed based on the following assumptions:

1. Reactions only take place on the catalyst;
2. Gas and liquid velocities are constant across the reactor section;
3. The reactor is operated isothermally under isobaric and steady-state condition;
4. No radial deviation of concentration exists within the reactor;
5. The catalyst particles are completely wetted.

Although the model by Korsten (1996) is simpler, and easier to be solved, the assumption that the catalyst effectiveness factor is constant down through the reactor prevents the application in this research. Because the reactor configuration would impact the catalyst effectiveness factor and it is different for different reactors and operating conditions. Therefore, the model developed by Froment (1994) is applied in this research.

The steady state continuity equation for component i of the gas phase is written as

$$\frac{u_G}{RT} \frac{dp_{ig}}{dz} = -K_L a_L \left(\frac{p_{ig}}{H_i} - C_{iL} \right) \quad i = 1, \dots, N \quad (5.28)$$

$$\text{at } z = 0, \quad p_{ig} = p_{ig}^0$$

where u_G is the superficial velocity of the gas, R is the gas constant, T represents the reactor temperature, p_{ig} is the partial pressure of compound i , $K_L a_L$ describes the mass transfer between the gas and the liquid phases, and the liquid-phase concentration of compound i in equilibrium with the bulk partial pressure is represented by the term p_{ig}/H_i . C_{iL} represents the concentration in the liquid phase of compound i . The partial pressure of component i in the gas phase can only change by transfer to or from the liquid phase. The interphase mass transfer rate is described as follows.

$$N_i = K_L \left(\frac{p_{ig}}{H_i} - C_{iL} \right) \quad (5.29)$$

The liquid phase contacts the gas phase and the solid phase, which is reflected in the continuity equations for the reacting species by two terms, accounting respectively for the liquid-solid and the gas-liquid interphase mass transfer:

$$u_L \frac{dC_{iL}}{dz} = K_s a_s (C_{iS}^S - C_{iL}) + K_L a_L \left(\frac{p_{ig}}{H_i} - C_{iL} \right) \quad (5.30)$$

$$\text{at } z = 0, \quad C_{iL} = C_{iL}^0$$

where u_L is the superficial velocity of the liquid, and $K_s a_s$ describes the mass transfer between the liquid and the solid phases, C_{iS}^S represents the concentration of component i on the catalyst surface.

The concentration gradients inside the catalyst particles where the reactions take place are accounted to calculate the effectiveness factor. The pores are considered

to be completely filled with liquid. The continuity equation for component i inside a spherical catalyst is written:

$$\frac{D_{ie}}{\xi^2} \frac{d}{d\xi} \left(\xi^2 \frac{dC_{is}}{d\xi} \right) = \rho_s \sum_{j=1}^{N_r} S[j,i] r_j(C_{is}, \dots, T_s) \quad (5.31)$$

with boundary conditions:

$$\begin{aligned} \text{at } \xi = 0, \quad & \frac{dC_{is}}{d\xi} = 0 \\ \text{at } \xi = \frac{d_p}{2} \quad & K_s a_s (C_{is}^S - C_{iL}) = \rho_B \sum_{j=1}^{N_r} \eta_j S[j,i] r_j(C_{is}^S, \dots, T_s) \end{aligned} \quad (5.32)$$

where C_{is} represents the concentration of component i inside the solid, ξ is radial coordinate, D_{ie} is the effective diffusivity of component i for transport in a pseudocontinuum, d_p is the equivalent particle diameter, ρ_s , ρ_B are the catalyst density and bulk density, N_r represents the number of reactions, η_s is the effectiveness factor of reaction j for solid particle, T_s is the temperature of the catalyst solid, r_j is the reaction rate of reaction j per unit catalyst mass for heterogeneous reaction, $s[j,i]$ represents the stoichiometric coefficient of component i in reaction j .

The effectiveness factor for a general nonlinear reaction rate is defined as

$$\eta = \frac{\int r dV}{\int r^0 dV} \quad (5.33)$$

As for the spherical catalyst, eq 5.33 could be written as

$$\eta = \frac{3}{r(C^0)R^3} \int_0^R r(C) \xi^2 d\xi \quad (5.34)$$

5.3.2 Estimation of Physical Properties

The mathematical model needs quantities of physical properties of pure compounds and the gas and liquid mixtures as Table 5.5 shows. Regarding pure

compounds/lumps in terms of the MTHS matrix elements, physical property could be separated into temperature-independent properties and temperature-dependent properties. The physical properties for both gas and liquid phases obviously depend on the composition of streams and operating conditions.

Table 5.5 Physical property of the model

Type		Property
Pure compounds/lumps	Temperature-independent properties	MW, T_b , T_C , P_C , V_C , Z_C , ω , C_p^0 , H_f^0 , ΔG_f^0 , SG
	Dependent properties	V_m , μ , k , D , H , C_p , $K_L a_L$, $K_S a_S$, ΔH
Phase	Gas	ρ , C_p , μ , k , $K_L a_L$, D , V_m ,
	Liquid	ρ , C_p , μ , k , $K_S a_S$, D , V_m

Table 5.6 Properties estimation methods

Properties	Estimation method
Basic properties(T_C , P_C , T_B , etc)	Joback group contribution
Heat of reaction	Peng Robinson Equation of state
Heat of vaporization	
Heat capacity of both phases	
Density of both phases	
Henry coefficients	Chung et al (1988)
Viscosity of both phases	
Thermal conductivity of both phases	Reid et al. (1987)
Diffusion coefficients	
Mass transfer coefficients for gas-liquid phase	Goto and Smith (1975)
Mass transfer coefficients for liquid-solid phase	Froment and Bischoff (1990)

Table 5.6 gives the estimation methods. Basic properties including critical temperature (T_C), critical pressure (P_C), critical compressibility factor (Z_C), boiling point (T_b), heat of formation (H_f^0), Gibbs free energy of formation (ΔG_f^0), and

ideal gas heat capacity (C_p^0), etc are estimated by Joback group contribution method, which has been introduced in the previous chapter. These properties would be used to calculate some of other properties based on correlations such as acentric factor. Then Peng Robinson equation of state is applied to estimate some properties including enthalpy of all compounds, heat of reactions, heat of vaporisation, densities of both phases, Henry coefficients ($H_i = p_{ig} / C_{iL}$). Detailed calculation of some physical properties could be found in Appendix D.

5.3.3 Mathematical Methodology and Solving Procedure

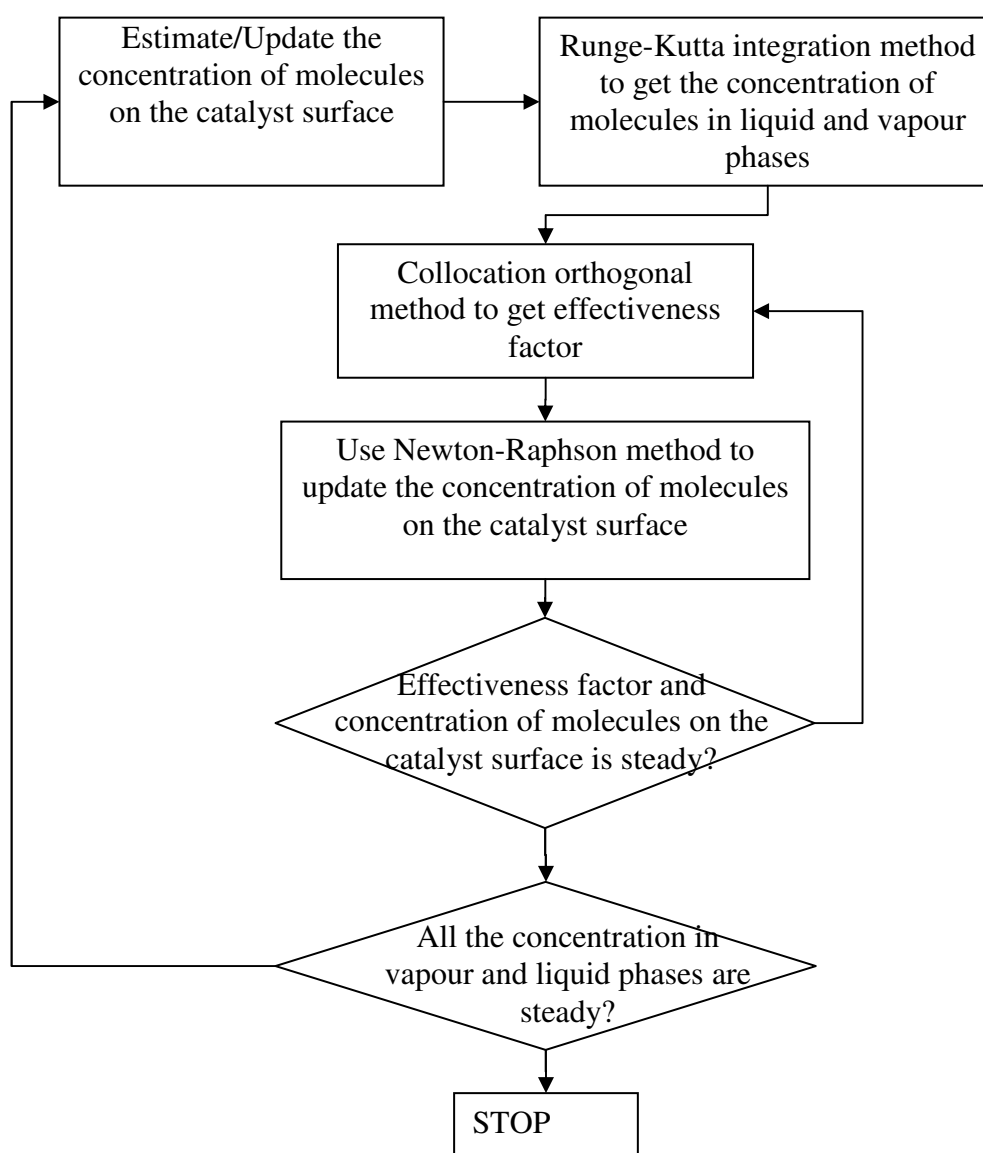


Figure 5.5 Solving procedure for a diesel hydrotreater trickle-bed reactor

The mathematical model involves ordinary differential equations with the initial value type, in which conditions are specified at only one position such as eq. 5.28, eq. 5.30 and eq. 5.32 etc., and with boundary value type as well, in which conditions are specified at two different points in domain such as eq. 5.31. Different mathematical techniques are needed to handle these two different types of differential equations. Usually, for the first type – ordinary differential equations with initial value, a fourth order Runge-Kutta method is widely used. To solve boundary value problem, detailed information could be found in Appendix E.

The surface concentration is unknown, since resistance of mass transfer is accounted for at the catalyst surface. Therefore, an initial guess of the surface concentration has to be made first, which is used in the orthogonal collocation method to perform the intraparticle integration to get the effectiveness factor. The effectiveness factor is used to update the concentration in the liquid. Iterations are performed between these two steps until the change of the concentrations in the liquid and on the catalyst surface are in the tolerance. Those values provide the basis of the fourth-order Runge-Kutta integration method with variable step size.

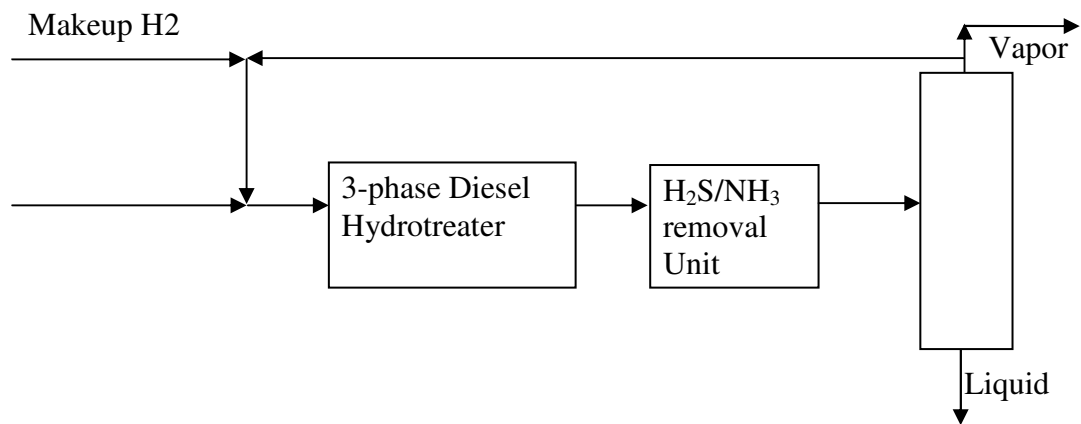


Figure 5.6 simulated process integrated with H₂S scrubber and flash

A flash (Figure 5.6) is also integrated into the process in order to get the molecular composition of vapour phase, which considers the impact of the recycle hydrogen stream. An initial guess of the molecular composition of the recycle hydrogen stream is made, and iterations are performed to update the molecular composition of the recycle stream until the criteria is satisfied. The developed framework for the modelling of a diesel hydrotreater is implemented in FORTRAN.

5.4 Case Study – Modelling of Diesel Hydrotreater

5.4.1 Simulation of a Diesel Hydrotreater

To verify the developed model and the solving methodology, sets of the experimental data (Marafi, 2007) on hydrotreating diesel streams are applied. Table 5.7 gives the configuration of the reactor and its operating conditions. The properties and the MTHS matrix of straight run gas oil are listed in the section 3.5 of chapter 3. Thermodynamic equilibrium was assumed between the gas and liquid phases at the reactor inlet.

Table 5.7 Configuration of the reactor and operating conditions

Reactor configuration	
Diameter (m)	1
Length (m)	20
Density of bed (kg_{cat}/m_r^3)	710
Catalyst characteristics	
Equivalent diameter (m)	1.3×10^{-3}
Density(kg/m^3)	1420
Porosity(m_f^3/m_p^3)	0.6
Operating condition	
Temperature(K)	610, 625, 640
Pressure(bar)	40
LHSV($m_l^3/(m_{cat}^3 h)$)	1.30
H2/oil	200
Flash temperature(K)	298.15
Hydrogen purity(mol/mol)	0.91

Table 5.8 compares the composition and the properties of the hydrotreated product between the measured and the predicted at the reactor temperature of 625K, which shows a good agreement. Table 5.9 compares sulphur contents and monoaromatics contents of the products with three different operating temperatures, which also shows a good consistence.

Table 5.8 Composition and properties of the product of the measured and predicted

	Measured	Predicted
Total aromatics (wt%)	37.91	37.62
Monoaromatics (wt%)	29.45	29.67
Polyaromatics (wt%)	8.45	7.95
Density @ 15 °C (g/cc)	0.8609	0.86
Sulphur content (wtppm)	689.00	695.83

Table 5.9 Monoaromatics content and sulphur content of the products with three different reactor temperatures

Temperature	Monoaromatics (wt%)		Sulphur (wtppm)	
	Measured	Predicted	Measured	Predicted
610K	30.70	31.06	1380.00	1302.54
625K	29.45	29.67	689.00	695.83
640K	28.80	28.82	490.00	482.79

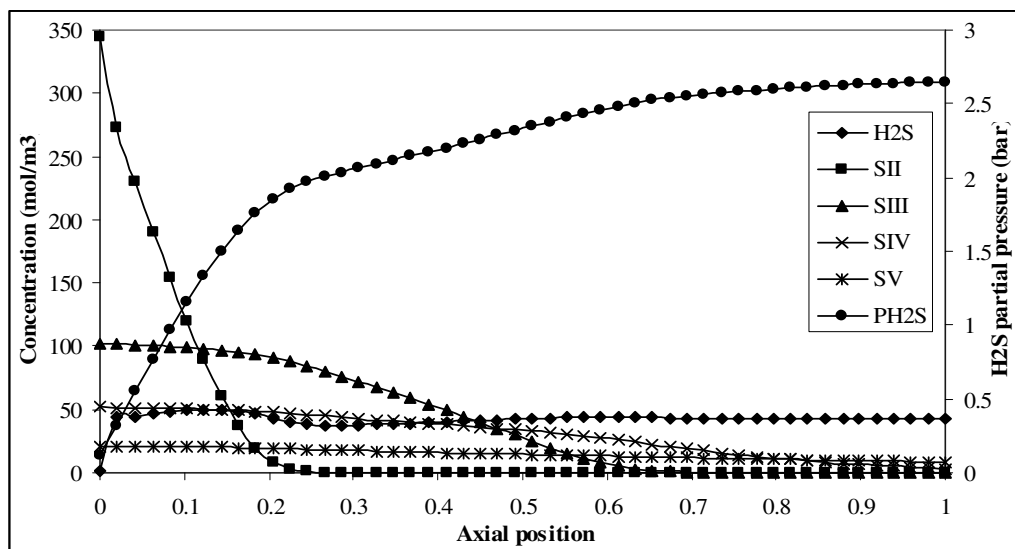


Figure 5.7 Axial profiles of the sulphur compound content and the partial pressure of H₂S (625 K)

The evolution of sulphur contents of SII, SIII, SIV, and SV through the reactor is shown in Figure 5.7. As seen, the major fraction of the sulphur removal is taken place in the initial part of the reactor – 0.2 length comparable ratio of the reactor, and in the left part of the reactor, sulphur is removed slowly. That is because

benzothiophene (SII) reacts fastest. The slowest reaction is the removal of 4,6-dimethylidibenzothiophene and its substituted 4,6-diDBT (SV), which comprise the major components of sulphur compound in hydrotreated products. The sulphur removal rate order follows: SII > SIII > SIV > SV.

The partial pressure of H₂S in the gas phase increases dramatically at the beginning of the reactor due to the fast removal of sulphur from SII. The fast consumption of hydrogen in the initial part of the reactor is also reflected in Figure 5.8. The concentration of hydrogen in the liquid phase at the initial part of the reactor is far from the saturation, which makes the hydrogen concentration in the liquid phase at the initial part of the reactor become the key of the reaction rate.

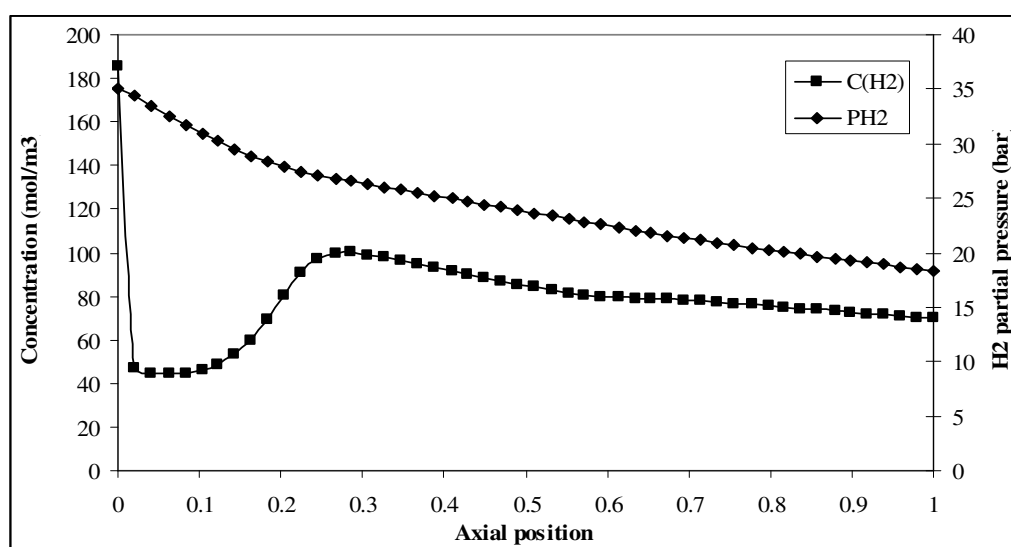


Figure 5.8 Axial concentration of hydrogen in the liquid phase and partial pressure of hydrogen in the vapour phase (625 K)

5.4.2 Sensitivity Analysis of Operating Conditions

Effects of operating conditions such as temperature, LHSV, pressure, and H₂/oil are analysed as well. The operating condition with the temperature of 625K is used as the basis for the sensitivity analysis.

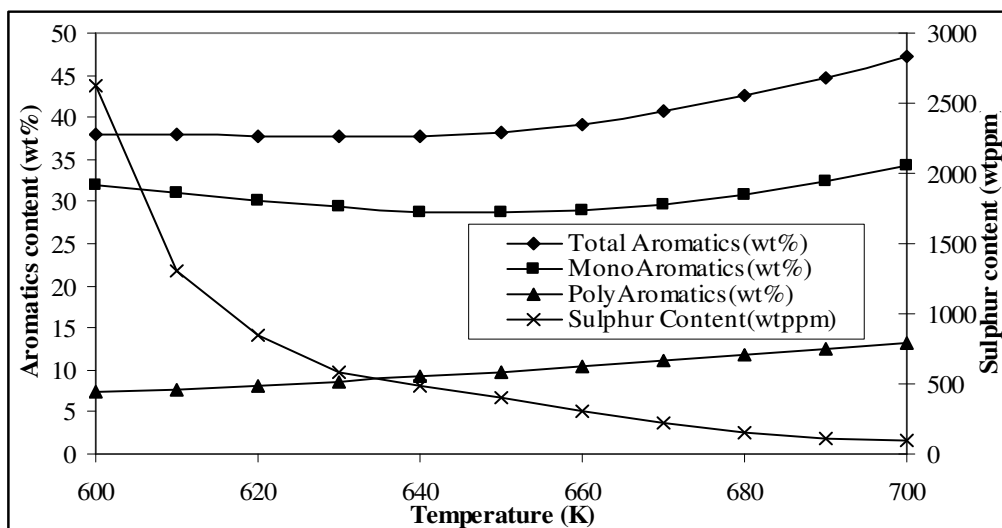


Figure 5.9 Influence of temperature on the product compositions

Figure 5.9 illustrates the influence of the operating temperature on the product composition. High temperature favours the reactions of both HDS and HDA. However, HDA reaction is controlled by thermodynamic equilibrium, and too high temperature will prevent it. As for HDS, the increased efficiency of sulphur removal is decreased with the increase of the operating temperature, which means that only increasing operating temperature may be not efficient to meet the sulphur conversion requirement.

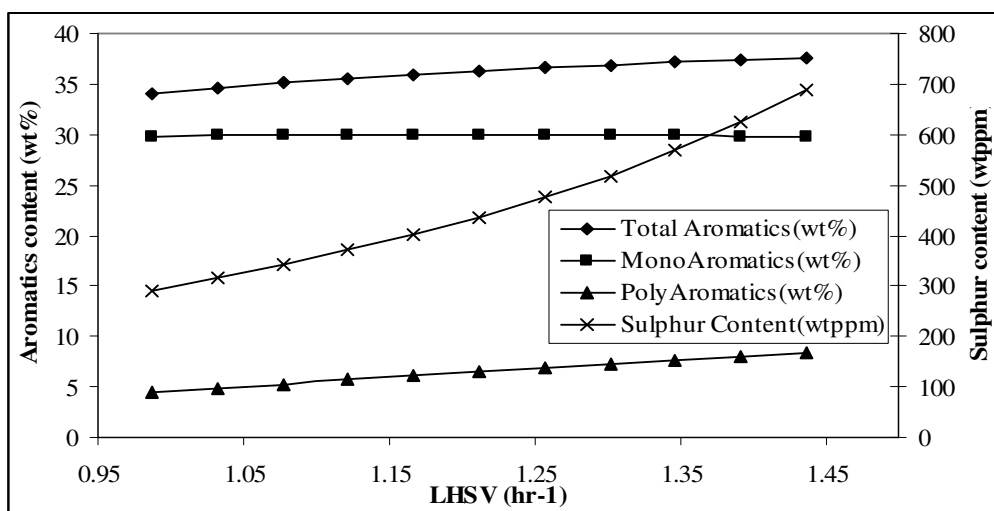


Figure 5.10 Influence of the LHSV on the product compositions

Figure 5.10 shows the influence of LHSV on the product compositions. As feed flow rate is increased, sulphur and aromatics contents in the product are increased

as well. To balance between the ultra low sulphur requirement and profit margins, LHSV is necessarily an important parameter to be optimised for the design.

Figure 5.11 shows the influence of the reactor pressure on the product composition. As the reactor pressure increases, the concentration of hydrogen in the liquid would be increased as well, which impacts the reactions seriously. As for HDS, the increased efficiency of sulphur removal is decreased with the increase of the reactor pressure. Reactor pressure is one of important design parameters.

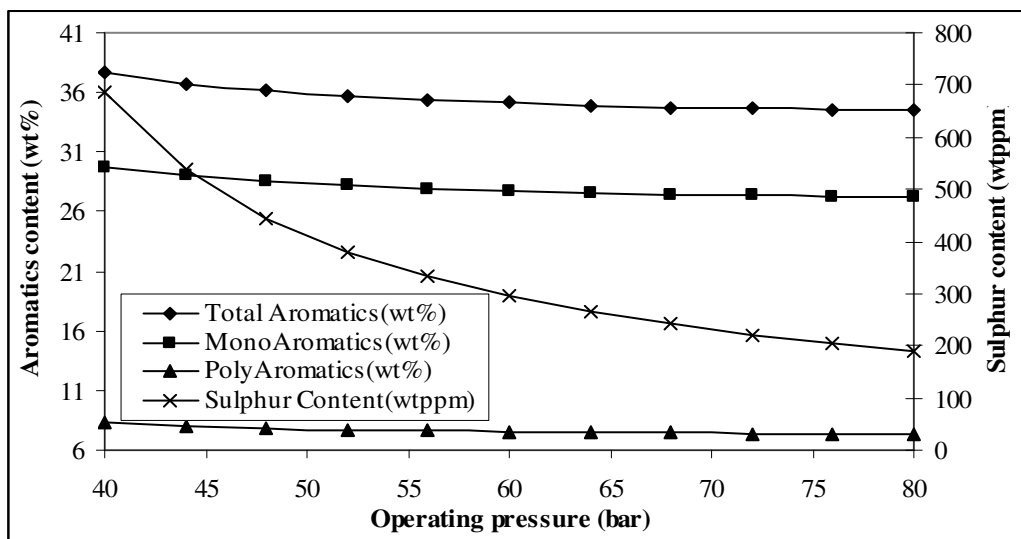


Figure 5.11 Influence of the pressure on the product composition

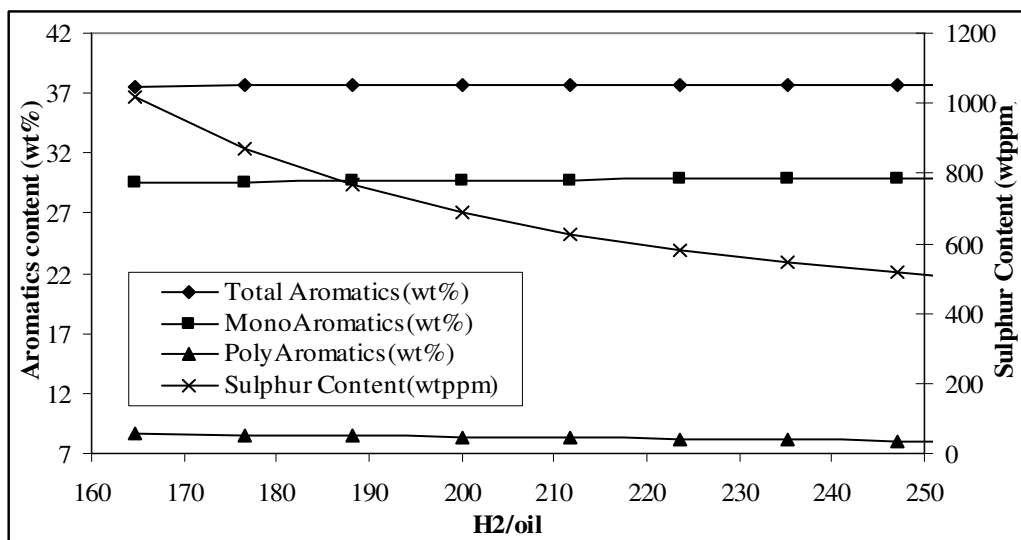


Figure 5.12 Influence of the H₂/oil ratio on the product composition

Figure 5.12 presents the influence of H₂/oil ratio on the product composition. As the ratio increases, the partial pressure of hydrogen and the concentration of hydrogen in the liquid are increased as well, which favors all the reactions. As for HDS, the increased efficiency of sulphur removal is decreased with the increase of H₂/oil, therefore H₂/oil should only be increased to a certain extent considering the balance between the efficiency and cost.

The impact of catalyst activity on sulphur reactions is also performed. As Figure 5.13 shows, sulphur content in the liquid product is increased dramatically with the loss of catalyst activity. Therefore changing operating condition such as increasing operating temperature or hydrogen flow rate to compensate catalyst deactivation is necessary.

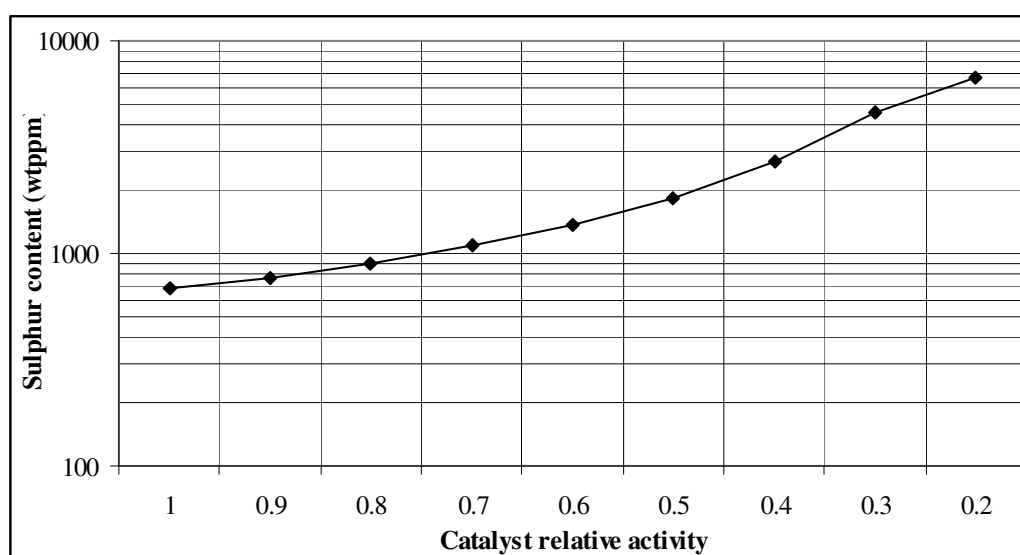


Figure 5.13 Influence of catalyst activity on the sulphur removal

To summarise, the trend of changing operating condition is obvious, but the extent of these changes should be optimised properly.

5.5 Catalyst Deactivation

5.5.1 Mathematical Model of Catalyst Deactivation

Catalyst deactivation has a strong effect on the run length of a hydrotreating reactor, and consequently the margins. Therefore, a deep understanding on the mechanism of catalyst deactivation could help increase the profitability.

The mechanism for catalyst deactivation has three different stages (Tamm and Harnsberger, 1981):

- Stage 1 – rapid formation of initial coke with significant loss in catalyst activity;
- Stage 2 – gradual build-up in pore by continuous accumulation of coke, causing further loss in the intrinsic activity of the catalyst;
- Stage 3 – constriction or blockage of pores by coke with complete loss of catalytic activity due to diffusion limitation.

The model developed by Sun (2004) is applied in this work. Equation 5.35 is a quantitative description of catalyst activity.

$$\alpha = \frac{r}{r_0} \quad (5.35)$$

where r_0 is the reaction rate of catalyst at the start of the run, r is the rate of reaction after a determined time-on-stream.

De Jong et al. (1997) correlated the activity of catalyst with the coke content on the catalyst as equation 5.36.

$$\alpha = 1 - a(W_c)^b \quad (5.36)$$

where a , b are the coefficients regressed by the experimental data, and W_c is the weight content of coke on catalyst calculated as equation 5.37.

$$W_c = \int_0^T r_{coke} dt \quad (5.37)$$

The reaction includes a coke formation model and a reactivity-coke content relationship (De Jong, 1994): (i) thermal condensation reactions of aromatic moieties and (ii) catalytic dehydrogenation reactions. Equation 5.38 describes the total rate of coke deposition that includes thermal and catalytic coke.

$$r_{coke} = r_c + r_t \quad (5.38)$$

where r_c is the catalytic coking rate, and r_t is the thermal coking rate.

The mathematical models for thermal and catalytic coking are shown as follows.

$$r_c = \frac{k_c K_{adsp} C_p}{1 + K_{adsp} C_p} \quad (5.39)$$

$$r_t = \frac{k_t C_p}{P_{H_2}} \quad (5.40)$$

where k_t is the rate constant for thermal coking, P_{H_2} is the hydrogen partial pressure, K_{adsp} is the adsorption constant of coke precursor, C_p is the concentration of coke precursor, can be set as the aromatic content in the feedstock.

5.5.2 Multi-period Model of Catalyst Deactivation

During the run of a diesel hydrotreater, operating conditions are needed to be changed to compensate the activity loss caused by coke to satisfy the product specification. Under industrial operating conditions, catalytic conversion activity of a diesel hydrotreater is maintained by constantly raising the temperature (Tamm and Harnsberger, 1981). Sun (2004) developed a model for the operation involving making multi-stage decisions, and these decisions are inter-related by dividing the whole run length into multiple periods in terms of time. In each period, the minimum increase of reactor temperature that can meet the sulphur specification would be raised.

However, as reviewed previously, not only reactor temperature is the important parameter that can help meet the product specification, but also other parameters such as pressure, LHSV, and hydrogen/oil ratio. As known, the increase of temperature would help the removal of sulphur content, but also prevent HDA reactions, and shorten catalyst life leading to the increase of operating cost. Low LHSV is preferred to remove sulphur content, but consequently leads to the loss of the income. As for hydrogen/oil ratio, high value favours the removal of sulphur content, but also increases the operating cost. How to compensate the loss of the catalyst activity is not obvious considering the economic performance.

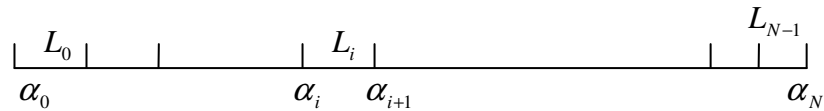


Figure 5.14 Multi-period of run length on the catalyst activity basis division

Another shortcoming of the model (Sun, 2004) is that the decision of each period, the minimal increased temperature, depends on the history of operations, which makes the problem quite complex and being solved sequentially. Moreover, multi-stage on the time-basis division cannot accurately present the physical meaning of catalyst activity. A multi-period model on the catalyst activity basis division of run length is proposed as Figure 5.14 shows.

The activity of catalyst starts from α_0 , which is 1 for catalyst without any deposit of carbon, or a certain value for the regenerated catalyst with a certain deposit of carbon on catalyst. The end activity is that catalyst with it cannot satisfy the product specification with any compensation by changing operating conditions. Since the reaction rate of each period would depend on the start and end activities of catalyst, and its operating conditions in the stage, the simulation with catalyst deactivation in each period will no longer depends on the history of operations. Therefore, the simulation in each period could be performed simultaneously.

The length of each period is calculated using the model of catalyst deactivation. The coke deposit on catalyst can be calculated according to the activity of catalyst based on Equation 5.36. Then according to Equation 5.37, the time length of each period could be calculated. The run length of a diesel hydrotreater is the sum of all these intervals.

5.6 Diesel Hydrotreater Optimisation

Due to the non-linearity and high dimensionality of a rigorous diesel hydrotreater model, little information about the process level optimisation is published. A decision support tool for process optimisation of sulphur free diesel production is developed with a simplified model for a hydrotreater on the site-wide level in industry, which targets the maximal of the margin by adapting the process operation to changes in the specification requirements without capital investments,

taking account of blend values, deactivation costs of the catalyst, shutdown margin losses, product specifications and quality margins (Lukszo, 2006). The model is a site-wide level model, which cannot handle the change of feedstock. Abbasi (2009) employed genetic algorithm (GA) to handle the no-linearity and high dimensionality of a complex model of a three-phase trickle-bed reactor, which leads to the convergence problem through conventional algorithms as the author reported. The variables to be optimised are gas and liquid superficial velocity, the reactor temperature and pressure, and the length of reactor. The optimisation objective of the work is to find out the appropriate operational conditions at steady state that lead to the highest amount of sulphur removal in presence of conditions that will minimise the gas make. However, the model has not considered the catalyst deactivation, which has a serious impact on the economic data. Moreover, stochastic optimisation usually takes a huge amount of CPU resources.

The proposed optimisation model would integrate the developed multi-period hydrotreater model, targeting the minimal operating cost by changing the operating temperature, hydrogen stream quantity, with the constraints of product specification and practices.

5.6.1 Mathematical Model

The annualised operating cost is shown as equation 5.41.

$$obj = \frac{365}{\sum_{k=1}^N L_k + L_{shutdown}} \left(c_{H2} \sum_{k=1}^N F_k^{H2} L_k + C_{cat} + C_{loss} L_{shutdown} \right) \quad (5.41)$$

The operating cost includes hydrogen utility cost, catalyst cost, and the economic lost because of shutdown.

The molecular composition of product from a diesel hydrotreater is calculated through the simulation expressed as Equation 5.42.

$$C_{iV}^P = f(C_j^F, T, P, r_r, L_r, \alpha_c, \dots) \quad (5.42)$$

The constraints include the product specification such as sulphur content limit, temperature/hydrogen allowable change range, and run length illustrated as Equations 5.43 – 5.46.

$$S_k^{prod} \leq S_{spec} \quad (5.43)$$

$$T_{Min} \leq T_k \leq T_{Max} \quad (5.44)$$

$$F_{Min} \leq F_k^{H2} \leq F_{Max} \quad (5.45)$$

$$L_{Min} \leq \sum_{k=1}^N L_k \leq L_{Max} \quad (5.46)$$

Deterministic algorithm rather than stochastic algorithm is employed because of large amount of simulations demanded by stochastic algorithm leading to the huge CPU time. Successive quadratic programming (SQP) algorithm is successfully applied in the optimisation by introducing NAG FORTRAN library function E04UCF without any difficulty of convergence problem.

5.7 Case Study – Optimisation of Diesel Hydrotreater

Diesel product of the simulation case in section 5.4 never reaches the specification with the maximum sulphur content of 50 wtppm. The proposed optimisation model is applied to upgrade the straight run gas oil with the satisfaction of the sulphur specification, and remaining the throughput. Due to the consideration of catalyst deactivation and high sulphur content, only increasing operating temperature and hydrogen flow rate would not meet the product specification, therefore, the reactor pressure is increased to 60 bar, and fixed. The whole run length is split into three stages shown as Table 5.10 with the constraint given in Table 5.11.

Table 5.10 Activity division of catalyst for three stages

Stage	Start activity	End activity
S	1	0.75
M	0.75	0.6
E	0.6	0.4

Table 5.11 Constraints of the optimisation case

Property	Bound
Sulphur content (wtppm)	≤ 50
Temperature(K)	≤ 700
Hydrogen (t/day)	≤ 15
Catalyst life (days)	≥ 300

Table 5.12 presents the optimal operating conditions, the sulphur content of product, the time length of each period and aromatic conversion as well. Both the reactor temperature and the hydrogen flow rate are increased to compensate the loss of catalyst activity along with the time. The sulphur content of product is satisfied at the bound. The run length of the diesel hydrotreater is 350 days. Aromatics conversion decreases significantly through stages because of the increase of the operating temperature and the loss of activity.

Table 5.12 Optimal operating conditions and results

	S	M	E
Temperature (K)	685.01	689.77	700.00
Hydrogen (t/day)	11.93	12.47	12.40
Sulphur (wtppm)	50.00	50.00	49.80
Duration(days)	39.40	127.01	184.22
Aromatic conversion (wt%)	17.20	13.28	5.51

5.8 Summary

A molecular model of hydrotreating reactions with a three-phase trickle-bed reactor has been developed based on the developed MTHS matrix for feedstock and product streams. First of all, structural contribution approach is applied for kinetics and adsorption parameters, which is tailored for the MTHS matrix. Secondly, correlations and models are employed to calculate a big number of the properties for pure compounds and the phases of gas and liquid. Lastly, a simulation method is proposed to solve the model, combining a fourth order Runge-Kutta integration method for integration in the axial direction and an orthogonal collocation method for the intraparticle integration within catalyst

sphere. The result under the different operating conditions between the calculated and the measured is compared in a case study, and shows that the developed model is capable of simulating a diesel hydrotreater.

A process level optimisation model has been developed with the consideration of catalyst deactivation. Firstly, the model of catalyst deactivation correlates coke amount on catalyst with reaction rate. Secondly, a new division of catalyst life is proposed to make stages independent with each other. Lastly, the optimisation model targeting minimising the operating cost with the satisfactions of product specifications is successfully implemented. This step also provides the possibility to explore the interactions between hydrotreaters and hydrogen network.

5.9 Nomenclature

List of symbols

r	reaction rate
k	reaction rate constant
K	adsorption constant
Keq	equilibrium constant
N_{AR}	number of aromatic rings in a PNA molecule
N_{SC}	number of saturated carbons in a PNA molecule
HBO	highest bond order in an aromatic ring
ΔH_R^0	difference between gas-phase heats of formation of products and reactants under the standard condition
n	reaction stoichiometry with respect to hydrogen
u_g	superficial velocity of the gas
u_L	superficial velocity of the liquid
R	gas constant
T	represents the reactor temperature
P	represents the reactor pressure
p_{ig}	partial pressure of compound i
K_{LaL}	the mass transfer between the gas and the liquid phases
K_{SaS}	mass transfer between the liquid and the solid phases
H_i	Henry coefficient of the entry i in the MTHS matrix

C_{iL}	concentration in the liquid phase of compound i
C_{iS}^S	concentration of component i on the catalyst surface
C_{iS}	concentration of component i inside the catalyst
D_{ie}	effective diffusivity of component i for transport in a pseudo continuum
d_p	equivalent particle diameter
ρ_s	catalyst density
ρ_B	catalyst bulk density
Nr	number of reactions
η_j	effectiveness factor of reaction j for solid particle
$S[j,i]$	stoichiometric coefficient of component i in reaction j
R_c	radius of spherical catalyst
a, b	coefficients
W_c	weight content of coke on the catalyst
L_k	the time length of the interval k of catalyst life length
$L_{shutdown}$	time length for the shutdown because of catalyst replacement
C_{H2}	price of hydrogen
C_{cat}	catalyst cost of one life cycle
F_k^{H2}	vapour flow rate fed to DHT
S	sulphur content

Subscripts

s	hydrodesulphurisation
τ	hydrogenation site
σ	hydrogenolysis site
i, j	entries of the MTHS matrix
k	interval of catalyst life cycle
m	reactions taking place in hydrotreater, including HDS, HDA
ST	steric effect for structure group contribution method
EL	electronic effect for structure group contribution method
m, n, p	the position of substituents on DBT
ξ	radial coordinate of spherical catalyst

Chapter 6 Integrated Site and Process Optimisation with Molecular Modelling

6.1	Introduction	196
6.1.1	Challenges of Refinery Optimisation.....	196
6.1.2	Decomposition Strategy for Refinery Optimisation (Zhang, 2000).....	198
6.2	Incorporating Molecular Management into Refinery Optimisation.....	199
6.3	Application I: Exploitation of Interaction between Refinery Material Processing Network and Processes	199
6.3.1	Introduction	199
6.3.2	Site Level Model	200
6.3.3	Site Optimisation with Process Simulation.....	202
6.3.4	Integrated Site and Process Optimisation	204
6.3.5	Case Study.....	205
6.4	Application II: Exploitation of Interactions between Hydrogen Network and Hydroprocesses	215
6.4.1	Introduction	215
6.4.2	Integrating Hydrogen Network and Hydroprocesses.....	220
6.4.3	Site Level Model	220
6.4.4	Site Optimisation with Process Simulation.....	226
6.4.5	Integrated Site and Process Optimisation	227
6.4.6	Case Study.....	228
6.5	Summary	232
6.6	Nomenclature	233
6.6.1	Application I.....	233
6.6.2	Application II	233

6.1 Introduction

A typical refinery involves a wide spectrum of activities, starting from crude oil operations, refining operations, and final product blending. The nature of value chain is such that its economics are extremely complex and heavily linked, consisting of so many decisions making in different levels. From the managerial level, managers need to decide which crudes to buy, which products to produce, which operating route to follow, etc. From the process level, operators have to determine the detailed operating conditions for equipments. All decisions are highly inter-related and the interactions have large impact on the overall profit. Besides the internal complex nature of refining operations, the current external picture of refining industry is characterised by fluctuating markets, heavier, sourer, costly crude oils, higher product quality specifications, and more stringent environmental regulations with more emphasis on the molecules of products. Therefore, smarter operation strategies based on molecular management are very necessary to maintain margin while simultaneously following the regulations. Refinery optimisation targets on making right decisions of the highly interacted operations on different levels to achieve the maximal profit or the minimal cost.

This chapter firstly introduces the challenges of refinery optimisation, followed by a brief review of the optimisation techniques. Then, a decomposed strategy (Zhang, 2000), which effectively and efficiently handles the complexity of refinery optimisation on both site and process levels, is incorporated with molecular management. The integrated framework firstly is applied in an overall refinery optimisation focusing on the material processing system. Secondly, an exploitation of interaction between hydroprocesses and hydrogen network is investigated. The goodness of both applications is well illustrated in the case studies respectively.

6.1.1 Challenges of Refinery Optimisation

There are generally two types of mathematical formulations in refinery optimisation: linear programming (LP) or mixed integer linear programming (MILP), and nonlinear programming (NLP). LP formulation is that all the

objective and constraints are in linear form, while NLP formulation is that any of the objective and constraints is nonlinear.

The state-of-the-art of LP/MILP is widely used in the overall refinery optimisation for planning purpose. The advantages of LP/MILP are its robustness, speed and the ease with which important solutions such as the complete value structure in terms of marginal prices can be obtained. However, problems can be formulated as LP/MILP only if the algebraic relationships between variables are linear or can be closely approximated by linear equations. It is normally not the case for process operations with highly nonlinear kinetics, thermodynamics, and hydromechanics, etc. As a result, this kind of models cannot describe the nonlinear aspects accurately. To mimic nonlinear behaviour while maintaining linear formulation, recursion techniques in LP are commonly used, which requires sequential execution of a number of LPs. Although recursion gives more accurate solutions, it not only increases computing time, but also reduces the transparency of LP's value structure and its economic driving forces, and therefore reduces the confidence (Hartmann, 1998). These in turn are restricted to long-term planning for plant-wide optimisation, and not suitable for day to day operations. These LP based models are well implemented in some commercial software packages, like RPMS (Honeywell Hi-Spec Solutions), PIMS (Aspen Technology).

In principle, NLP models for the overall refinery optimisation can be formulated by lumping all the rigorous process models. However, there is no established commercial NLP software existing due to the great difficulties involved in mathematics and computation to handle such complexities in the overall plant modelling (Grossmann, 1995). In practice, normally NLP models are applied in the process optimisation for the optimal operating conditions, which has a result close to the reality. However, the process optimisation is with a stand-alone mode, without the guidance from the overall refinery LP optimisation. Consequently, the synergy between plant-wide aspects and process operations cannot be exploited properly, which greatly limits the economic contribution of process optimisation.

6.1.2 Decomposition Strategy for Refinery Optimisation (Zhang, 2000)

In an effort to improve the accuracy and ability to tackle the nonlinear aspects while maintaining the robustness and the speed in overall refinery optimisation, a decomposition approach for overall refinery optimisation has been developed (Zhang, 2000). The approach consists of two-level optimisation, namely the site-level and process level, and more importantly, a strategy to coordinate two levels. In this decomposition approach, all non-linear and discrete aspects are allowed to be tackled in different levels with precise details and solvable mathematics.

In the site level, with given process performances, alternatively speaking, with fixed operating conditions, the objective is to maximise the overall profit by taking into account major aspects associated with plant-wide operations, which are basically about how to manage resource distributions among processes. These aspects have major impacts on overall economic performance, which include selection of feeds and products, distribution of intermediate products, connections between different processes and allocations of utilities. These aspects feature nonlinear and/or discrete nature. In this level, processes are modelled with linear yield correlations without the information of detailed process operating conditions.

In the process level optimisation, with given resource distribution, the objective is to maximise process profit by optimising operating conditions. In this level, non-linear and discrete aspects related to individual processes are fully addressed. The main feature of this level optimisation is that feed conditions are fixed the same as those determined from the current run of the site level optimisation.

The state-of-the-art of the approach is to coordinate two level models. To match the real performance of refining processes, an iterative procedure is applied to update the simplified linear yield correlations by the rigorous process simulation. To guide the process optimisation, the marginal value of the intermediate product is calculated to be used as the economic insight from the site level.

With this decomposition and coordination scheme, the problem of overall plant optimisation can be modelled efficiently without the need of building an overall plant model, and be solved efficiently without losing accuracy and interaction

between different systems. Furthermore, the rigorous process models can be effectively integrated in the framework without the need of making simplifications.

6.2 Incorporating Molecular Management into Refinery Optimisation

Based on the two-level decomposition approach (Zhang, 2000), molecular modeling of refining streams and processes will be incorporated into the refinery optimisation to investigate the benefits of the molecular techniques. The integrated framework will be applied in two applications. The first is to explore the integration of site and process level optimisation mainly focusing on material processing system. In this application, molecular modelling technique are applied in both site and process level models to monitor and control the molecular specification of products properly, and simultaneously achieve the maximal economic performance. The second application is to develop a method on how to manage hydrogen utility more efficiently to improve economic performance rather than saving hydrogen. Both applications include the basic idea of the two-level decomposition approach: site level modelling, site level optimisation with simulation/optimisation, and integration of site and process optimisation. The developed methodologies are finally well illustrated in case studies.

6.3 Application I: Exploitation of Interaction between Refinery Material Processing Network and Processes

6.3.1 Introduction

Obviously, material processing network has a strong interaction with each process. The network will allocate materials to processes, while the process operating conditions will determine the product quantity and quality fed back into the network. By adopting the decomposition framework, the strong connection between the network and processes can be fully exploited. To enhance the accuracy of process models, simultaneously monitor and control molecules, molecular modelling will be incorporated in both site and process levels.

6.3.2 Site Level Model

In the site level, the important aspects include the selection of crude oil (C), and the allocation of intermediate refining streams (S) to refining units (U), as well as refining products (P), together with the composition (K) represented by MTHS matrix and properties (PP) of refining streams.

To differentiate the contribution from different crude oils, each flow is decomposed into several flows based on their origins from the crude oils. For instance, if a refinery has two crudes to choose from, VGO from AVU is decomposed into two streams: VGO from Crude 1 and VGO from Crude 2 respectively. In this way, each crude is traced to its final products, and the economical contribution of different crudes can be evaluated precisely.

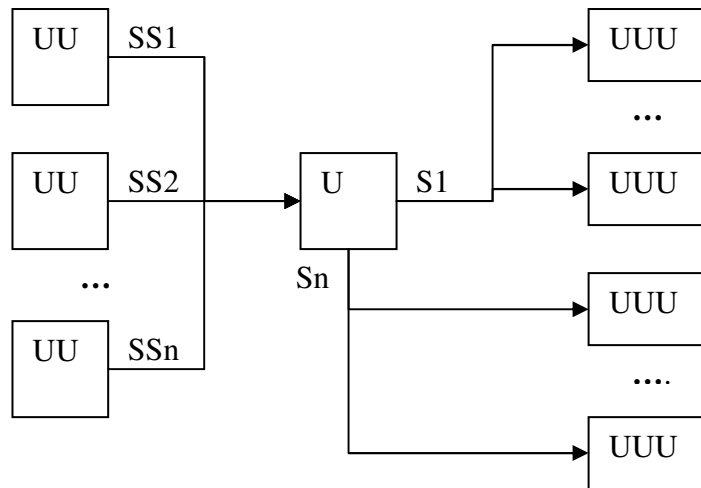


Figure 6.1 A general connection

Figure 6.1 shows a general connection in a refinery. Streams (SS1, SS2... SSn) from different processes (UU1, UU2... UUn) are fed into process U to produce different products (S1... Sn), and then products such as S1 will be fed to different processes (UUU1, UUU2... UUU3). The mass balance of these connections is:

$$\sum_{uu} \sum_{ss} (F_{c,uu,ss,u} \times \bar{R}_{c,ss,u,s}) = \sum_{uuu} F_{c,u,s,uuu} \quad \forall c \in C, \forall u \in U, \forall s \in S \quad (6.1)$$

As mentioned, a process is modeled as simplified yield linear correlations. $\bar{R}_{c,ss,u,s}$ is the yield coefficients representing that one unit of feed *ss* will produce *R* of

product s through process u from crude oil c . This general connection includes splitters. Decomposition of all process flows is based according to their crude oil origin. The composition of the stream into a splitter has to be the same as that of the streams leaving the splitter in all splitter operation, which is indicated as:

$$\frac{F_{c,u,s,uuu}}{\sum_{uuu} F_{c,u,s,uuu}} = \frac{F_{cc,u,s,uuu}}{\sum_{uuu} F_{cc,u,s,uuu}} \quad \forall c \in C, \forall cc \in C, \forall u \in U, \forall s \in S \quad (6.2)$$

The mass balance on each molecular composition of streams represented by MTHS matrix can be written as:

$$y_{c,u,s,k} = \frac{\sum_{uu} \sum_{ss} (F_{c,uu,ss,u} \times \bar{R}_{c,ss,u,s} \times \bar{y}_{c,ss,u,s,k})}{\sum_{uu} F_{c,u,s,uu}} \quad \forall c \in C, \forall u \in U, \forall s \in S, \forall k \in K \quad (6.3)$$

The composition in a blending process is as:

$$y_{s,k} = \frac{\sum_c \sum_{uu} \sum_{ss} (F_{c,uu,ss,u} \times \bar{R}_{c,ss,u,s} \times \bar{y}_{c,ss,u,s,k})}{\sum_c \sum_{uu} F_{c,u,s,uu}} \quad \forall c \in C, \forall s \in P, \forall k \in K \quad (6.4)$$

Properties blending nonlinearly:

$$Pt_{s,p} = f(y_{s,k}) \quad \forall s \in P, p \in NP \quad (6.5)$$

Properties blending linearly:

$$Pt_{s,p} = \sum_k y_{s,k} Pt_{k,p} \quad \forall s \in P, p \in LP \quad (6.6)$$

Utility consumption:

$$Q_{ut} = \sum_c \sum_{uu} \sum_s \sum_u F_{c,uu,s,u} \times \alpha_{c,uu,s,u,ut} \quad \forall ut \in UT \quad (6.7)$$

Crude oil usage:

$$F_c = \sum_s \sum_u F_{c,uu,s,u} \quad \forall c \in C, \forall uu \in CS \quad (6.8)$$

Crude oil is assumed to be loaded from a storage tank (CS).

Product quantity:

$$F_p = \sum_c \sum_{uu} \sum_s F_{c,uu,s,u} \quad \forall u \in PS \quad (6.9)$$

Products are assumed to be fed to products tank (PS).

Inequalities associated with limits on throughputs, product specifications, market demands, etc. give the constraints associated with refinery operation.

Unit capacity:

$$F_u^L \leq \sum_c \sum_{uu} \sum_s F_{c,uu,s,u} \leq F_u^U \quad \forall u \in U \quad (6.10)$$

Product specification:

$$Pt_{s,p}^L \leq Pt_{s,p} \leq Pt_{s,p}^U \quad \forall s \in P, p \in PP \quad (6.11)$$

Market constraints:

$$F_c^L \leq F_c \leq F_c^U \quad \forall c \in C \quad (6.12)$$

$$F_s^L \leq F_p \leq F_s^U \quad \forall p \in P \quad (6.13)$$

The objective of the site-level optimisation is to maximise the net profit that arises from the sale of products and utilities minus the cost of purchasing raw materials and utilities e.g. fuel, power, etc. This objective is a linear function of material and utility requirements for given product prices and raw material and utility costs.

$$profit = \sum_p F_p \times C_p - \sum_c F_c \times C_c - \sum_{ut} Q_{ut} \times C_{ut} - \sum_u \sum_c \sum_{uu} \sum_{ss} (F_{c,uu,s,u} \times C_u) \quad (6.14)$$

6.3.3 Site Optimisation with Process Simulation

To improve the feasibility of the overall solution, simulation is introduced in the site level to form an iterative procedure to correct the error caused by the simplified linear yield correlations. Based on the current operating scenario, the first step is to carry out process simulation. Streams represented by MTHS matrix

in the site level will be transformed into molecular information according to the bulk properties from the simulation. The developed methodology in Chapter 2 will be applied. Besides that, the simulation also provides the initial linear correlations, which are used in the site-level optimisation to determine the optimal material allocation for processes. The new and improved operation may deviate from the previous operating scenario on which the linear correlations are updated. This indicates that although the overall profit may have risen, the point has deviated from the actual operation. In other words, the correlations do not correspond with current site-level results. In order to return to a feasible point, process simulation is again carried out, in which the linear correlations are updated for the subsequent site level optimisation. This iteration, between the site-level optimisation and the process simulation is repeated until the differences between consecutive yields are within the set tolerance. The whole iteration procedure is illustrated in Figure 6.2.

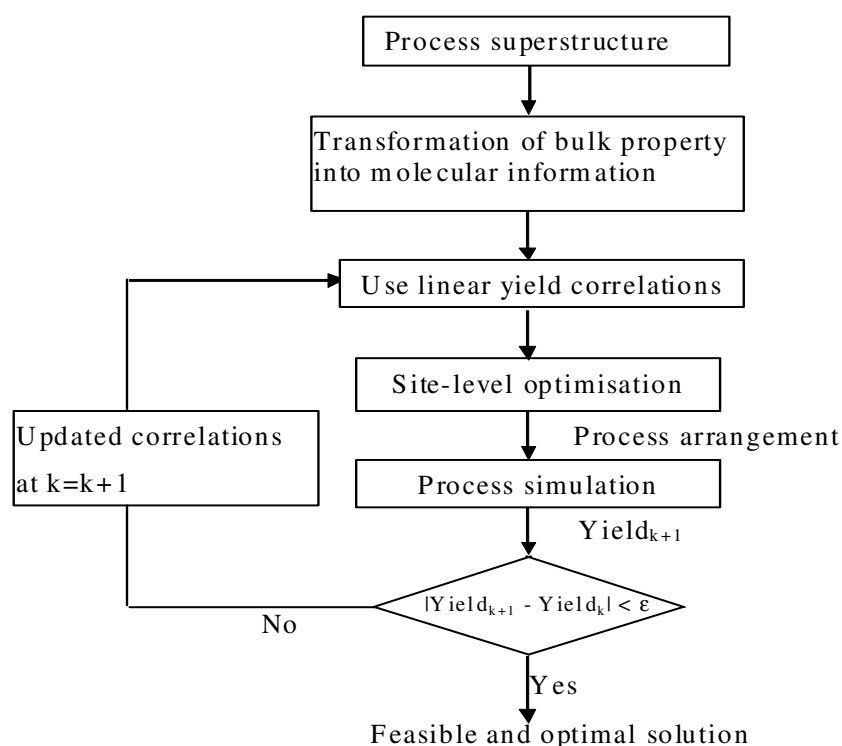


Figure 6.2 Site level optimisation with process simulation

It is important to note that at this stage, simulation is carried out under fixed process operating conditions. The only change is in the distribution of feeds and intermediate products determined via the site-level optimisation.

6.3.4 Integrated Site and Process Optimisation

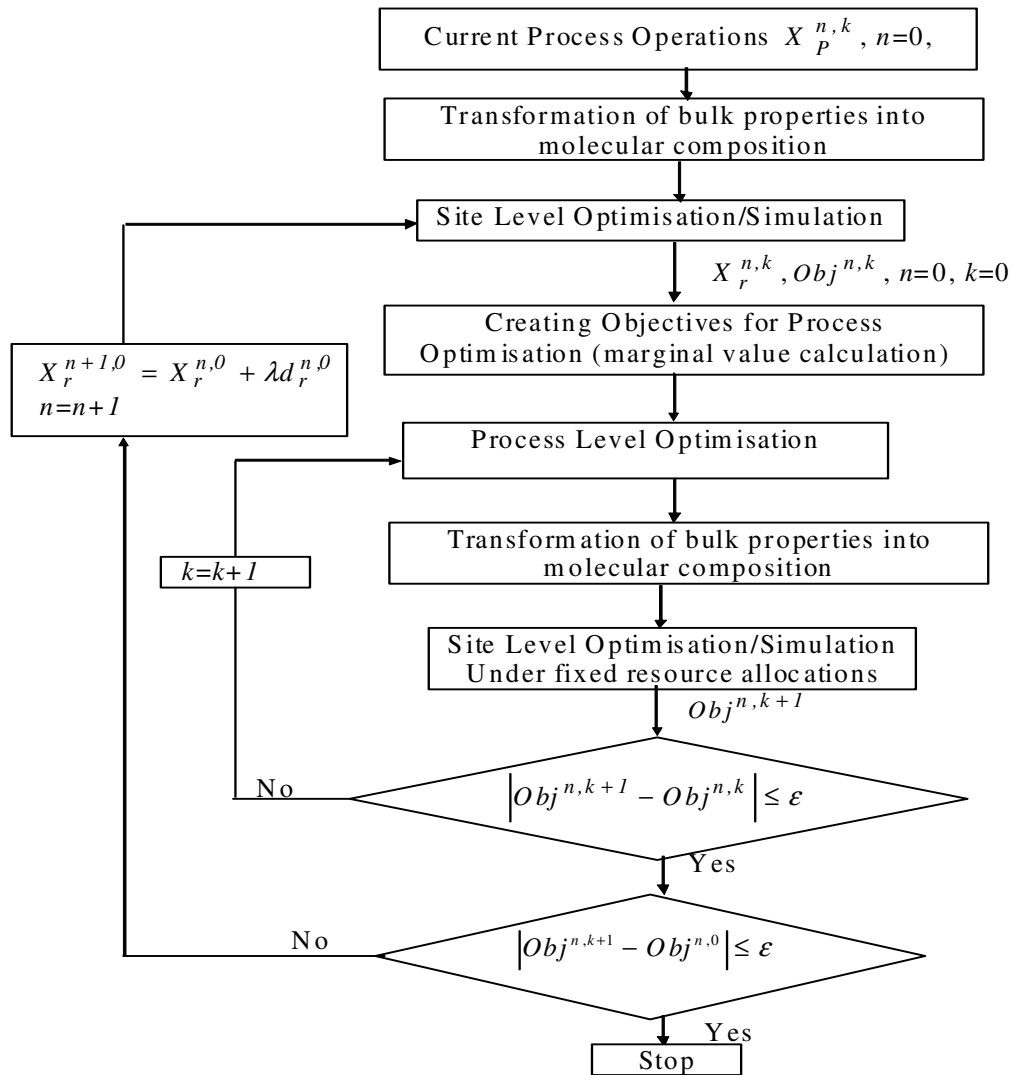


Figure 6.3 Integration of site level optimisation and process optimisation

Site level optimisation determines the optimal allocation of materials and utilities based on the fixed operating conditions of processes, which means it does not consider the interaction between site level issues and individual processes, and thus lose some opportunities to further improve the overall economic performance. The developed approach (Zhang, 2000) integrated process optimisation with site level optimisation. Marginal values of intermediate products obtained from site level optimisation are used in process optimisation to maximise the process profit. The changes of operating conditions from process optimisation are updated through the simplified linear correlations, which are used in site optimisation. In this way, a

loop is created effectively to incorporate site and process optimisation together. Figure 6.3 shows the diagram of integration of site and process optimisation.

6.3.5 Case Study

6.3.5.1 Problem Definition

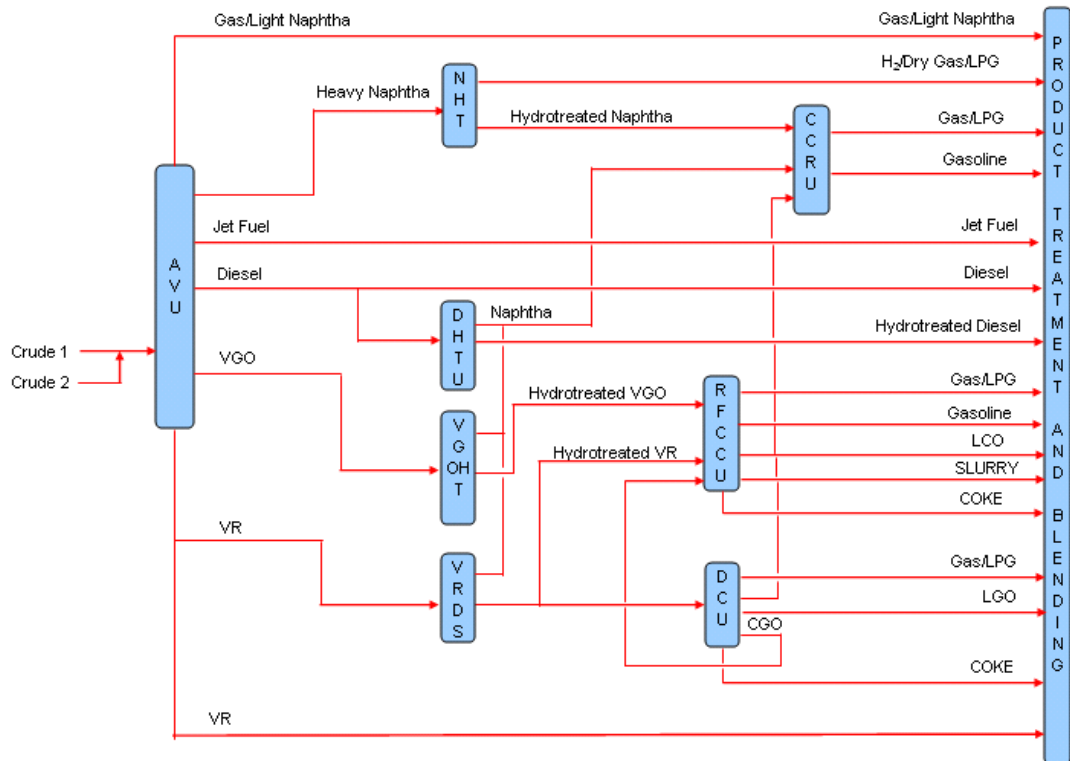


Figure 6.4 Flowsheet of a refinery

Table 6.1 Unit capacity

Process Capacity, bpd	Low Limit	High Limit
AVU	120,000	200,000
CCRU	8,000	24,000
RFCCU	50,000	80,000
DCU	50,000	80,000
CNHTU	6,000	20,000
DHTU	12,000	140,000

To investigate the benefit of integrating process optimisation with site optimisation and molecular modelling techniques, a case is studied. Figure 6.4 shows the flowsheet of a refinery, consisting of an Atmosphere/Vacuum Distillation Unit (AVU), a Catalytic Reforming Unit (CRU), a Residue Fluid Catalytic Cracking Unit (RFCCU), a Delayed Coker Unit (DCU), several hydrotreating units and product blending units. The capacity of each unit is listed in Table 6.1.

Table 6.2 Properties of two crudes

	Crude 1	Crude 2
API	33.1	24.9
Viscosity @50 C, mm ² /s	20.19	83.36
Freeze Point, C	30	28
Wax, wt%	26.2	14.6
Gum, wt%	8.9	19
Conradson Carbon Residue, wt%	2.9	6.4
Element Analysis, wt%		
Carbon	85.87	86.26
Hydrogen	13.73	12.2
Surphur	0.1	0.8
Nitrogen	0.16	0.41
Ni, ppm	3.1	26

Table 6.3 Availability of crudes

Crude Selection, bpd		
	Low Limit	High Limit
Crude 1	0	120,000
Crude 2	0	120,000

There are two crudes for the refinery to select from. Both of the crudes are heavy sweet with crude 2 being slightly heavier and sourer than the crude 1. The properties of these two crudes are listed in Table 6.2, as well as the availability of these two crudes in Table 6.3. The major products of the refinery are four grades of gasolines (including gasoline90, gasoline93, gasoline 95 and gasoline 97), diesel,

liquefied petroleum gas (LPG), jet fuel, fuel oil and coke. Table 6.4 shows the market conditions of gasoline and diesel products.

Table 6.4 Major market conditions of refining products

Major Market Conditions, bpd	Low Limit	High Limit
Gasoline 90#	20,000	30,000
Gasoline 93#	4,000	10,000
Gasoline 95#	4,000	10,000
Gasoline 97#	2,000	10,000
Diesel	40,000	62,000

6.3.5.2 Modelling of Refining Streams and Processes

The developed molecular models of gasoline blending and CRU in Chapter 3 and Chapter 4 will be applied in the case study. For the rest units, the non-linear models are based on the correlations published by HPI Consultants, Inc. (1999) in Appendix F. As for the streams, they are lumped in terms of the products generated and feedstock depending on processes. For instance, the distillation products will be lumped into the main fractions e.g. gas, light and heavy naphtha, jet fuel, diesel, vacuum gas oil and vacuum residue, and for fluid catalytic unit, these include dry gas, gasoline, liquefied petroleum gas (LPG), light cycle oil, coke and slurry, etc. In the stage of process optimisation, the corresponding developed molecular optimisation models are applied.

Since both the traditional lumped models and molecular models are preset, the streams connecting these two kinds of units should have a proper interface to incorporate both. MTHS matrix representation will be applied as the developed molecular process models are also based on MTHS matrix, and they are easily transformed to bulk properties, which the conventional model needs. Therefore, streams flowing from units with conventional models to units with molecular modelling are needed to transform into molecular composition by the developed approach in Chapter 2, and vice versa. For instance, naphtha from DHT will be transformed into molecular information before fed into CRU, and gasoline from CRU in the form of MTHS matrix is directly used in gasoline blending units.

6.3.5.3 Strategy of Case Study

Table 6.5 Investigation modes of case study

	Case 1	Case 2	Case 3	Case 4
Simulation	Yes	Yes	Yes	Yes
Site level optimisation		Yes	Yes	Yes
Specification		Yes	Yes	Yes
Raw material allocation			Yes	Yes
Process level optimisation				Yes

Not only will the benefits from the integration of site and process optimisation be illustrated, but also the benefits of incorporating molecular management. The case study is investigated in four scenarios as Table 6.5.

Case 1, also base case, is applying rigorous molecular models to simulate current operation. With only considering octane specification for gasolines and cetane number for diesels, the products may violate the specifications on the molecular information such as olefin, aromatic and benzene contents. In this step, RFCCU is operated in the maximal gasoline mode with 70% of the conversion level.

Table 6.6 Gasoline specification

Gasoline Type	G90	G93	G95	G97
RON (min)	90	93	95	97
RVP(psi) (max)	7.8	7.8	7.8	7.8
Sulphur(wt ppm) (min)	100	100	100	100
Aromatics (vol%) (max)	55	55	55	55
Olefins (vol%) (max)	25	25	25	25
Benzene (vol%) (max)	5.5	5.5	5.5	5.5

Table 6.7 Diesel specification

CN (min)	50
Sulphur(wt ppm) (max)	300

In case 2, given the same crude oil selections as case 1, the product specifications (given as Table 6.6 and Table 6.7) are considered, which will reallocate the intermediate products between processes to maximise the profit with the product specifications. In this step, molecular modelling techniques show its advantages to monitor and control the molecular contents in the products.

Based on case 2, the degree of freedom of site level optimisation is increased by allowing the changes of crude oil selection to demonstrate it is crucial to the overall economic performance. Finally, process optimisation is integrated based on case 3 to form case 4, to fully investigate the maximal profit.

In this refinery, the RFCC unit is the key process for the plant economics, since it can convert low-value VGO and part of VR to high-value gasoline and diesel. It is necessary to optimise RFCC operation in the overall refinery. The optimised variable of RFCCU is the conversion level for HPI correlations. On the other hand, the gasoline from CRU has desired high octane number, but also with the high restricted aromatic and benzene contents. Therefore, the proper control of operating conditions of CRU is crucial to gasoline blending, and should be considered in process optimisation. The operating temperature and pressure of CRU will be optimised in the process level.

6.3.5.4 Optimisation Results

Table 6.8 Total profit of the refinery in the different modes

	Total profit of the refinery, MM\$/yr	Improvement (%)
Case 1	152.19	0.00
Case 2	114.37	-24.85
Case 3	126.63	-16.79
Case 4	156.36	2.74

Table 6.8 compares the total profit of the refinery of these four cases. Compared with base case, the profit is reduced dramatically by 24.85% from 152.19 MM\$ to 114.37 MM\$ after imposing environmental constraints on product quality, if with the fixed operating conditions and crude selection. The total profit then is increased

to 126.63 MM\$ after allowing crude selection, further to 156.36 MM\$ with a great improvement by integrating process optimisation.

Because of low sulphur, crude 1 is favored with the configuration of the refinery as Table 6.9 shows the crude selections. Crude 1 favoring is also well illustrated as the throughput of DHT reaches the maximal capacity showed in Table 6.10. Due to the high aromatic/benzene content of product from CRU and aromatic/benzene specification of gasoline, the throughput of CRU is reduced.

Table 6.9 Crude oil selection in the different modes

Crude oil selection, bpd	Crude 1	Crude 2
Case1	54000	120000
Case2	54000	120000
Case3	120000	54095
Case4	120000	55922

Table 6.10 Process utilisation in the different modes

Process Utilisation, bpd				
	Case1	Case2	Case3	Case 4
AVU	174000.00	174000.00	174095.05	175922.82
CCR	18172.85	13748.63	14166.05	16215.89
RFCC	60247.33	52488.49	54811.65	75527.54
DCU	50000.00	50000.00	50000.00	50000.00
DHT	124968.00	140000.00	140000.00	140000.00
CNHT	20000.00	17096.89	17501.49	19857.89

Table 6.11 gives the main product distribution in different cases. Table 6.12 and

Table 6.13 selectively present the properties of gasoline90 and gasoline97 respectively. Without the restriction of environmental specification, gasoline90 product in base case has 34.53% of the olefin content, and gasoline97 has 57.76% of aromatic content, higher than the maximal specified contents. Table 6.14 shows that sulphur content of diesel product of base case also violates the specification. Therefore, 152.19 MM\$/yr of the overall profit for base case is unrealistic,

producing high profitable product gasoline⁹⁷ as much as maximal market demand, but with violated quality. Table 6.11 also exhibits that the production of diesel reaches the maximal market demand since low sulphur crude oil is available.

Table 6.11 Main product distribution in different modes

Main product, bpd	Case 1	Case 2	Case 3	Case 4
Light Naphtha	787.87	0.00	0.00	0.00
Jet Fuel	6870.00	10560.98	11391.95	9239.40
Fuel Oil	0.00	6531.85	0.00	0.00
LPG	11099.78	9711.60	10199.12	11862.94
Coke	3359.43	2926.40	2904.39	4363.74
G90	27620.03	30000.00	30000.00	29407.57
G93	4000.00	4137.94	5637.93	10000.00
G95	4402.55	4000.00	4000.00	8731.65
G97	10000.00	2000.00	2000.00	2000.00
Diesel	55343.85	53492.73	53954.76	62000.00
Gas	8091.06	7756.97	5869.25	6288.91

Table 6.12 Gasoline⁹⁰ product properties in different modes

G90 Product property				
	Case 1	Case 2	case 3	case 4
RON	90.00	90.00	90.00	90.00
MON	77.33	77.77	77.82	77.74
RVP	3.99	4.73	4.96	4.82
Sulphur(wt ppm)	81.13	59.64	68.27	82.91
Nitrogen(wt ppm)	179.31	129.44	197.98	209.53
Aromatics(vol%)	32.72	34.60	34.14	34.83
Olefin(vol%)	34.53	25.00	25.00	25.00
Benzene(vol%)	0.62	1.59	1.55	1.43

Table 6.13 Gasoline97 product properties in different modes

G97 Product property				
	Case 1	Case 2	case 3	case 4
RON	97.00	97.00	97.00	97.00
MON	86.80	87.08	87.05	87.14
RVP	5.23	5.53	5.50	5.76
Sulphur(wt ppm)	0.27	0.30	0.30	0.36
Nitrogen(wt ppm)	0.14	0.18	0.12	0.09
Aromatics(vol%)	57.76	55.00	55.00	55.00
Olefin(vol%)	0.00	0.00	0.00	0.00
Benzene(vol%)	4.35	5.05	4.85	4.49

Table 6.14 Diesel product properties in different modes

Diesel property				
Diesel	Case 1	Case 2	Case 3	Case 4
CN	54.45	54.81	55.16	53.72
Sulphur(wt ppm)	1150.64	300.00	300.00	300.00

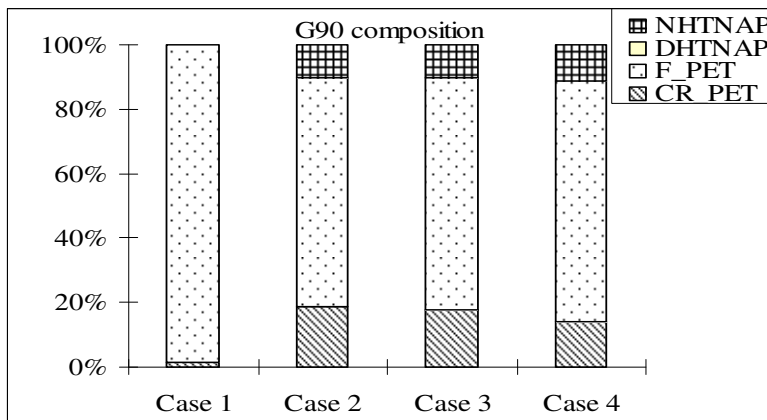


Figure 6.5 Composition of gasoline90 in different modes

Figure 6.5 - Figure 6.8 give the components of gasoline products. In the refinery, gasoline from RFCCU and RCU comprises the major contribution of gasoline products. For example, in base case, around 97% of gasoline90 is from RFCC, which also explains the violated high olefin content. Along with the increase of octane specification, the percentage of gasoline from CRU is increased as well.

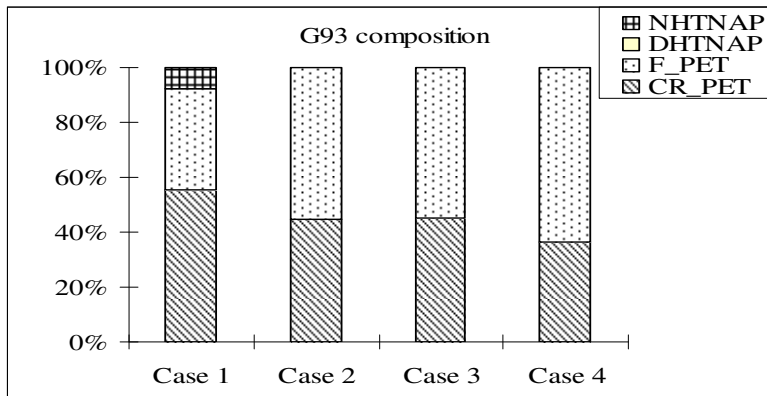


Figure 6.6 Composition of gasoline93 in different modes

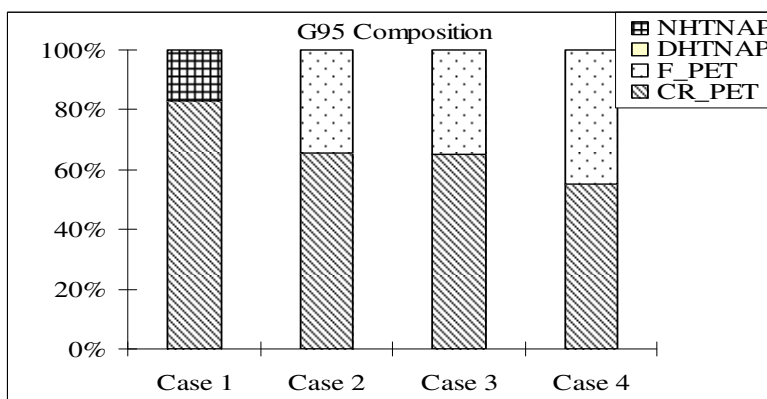


Figure 6.7 Composition of gasoline95 in different modes

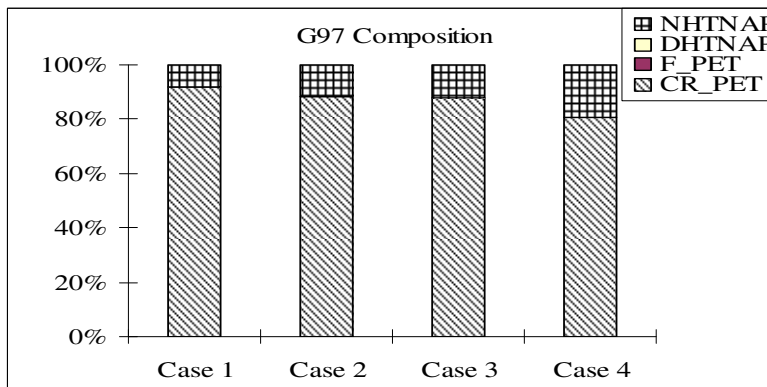


Figure 6.8 Composition of gasoline97 in different modes

Figure 6.9 shows the components of diesel products. Straight run diesel, which has 2900 wt ppm sulphur content, is the main contribution to diesel product with 1150 wt ppm in base case.

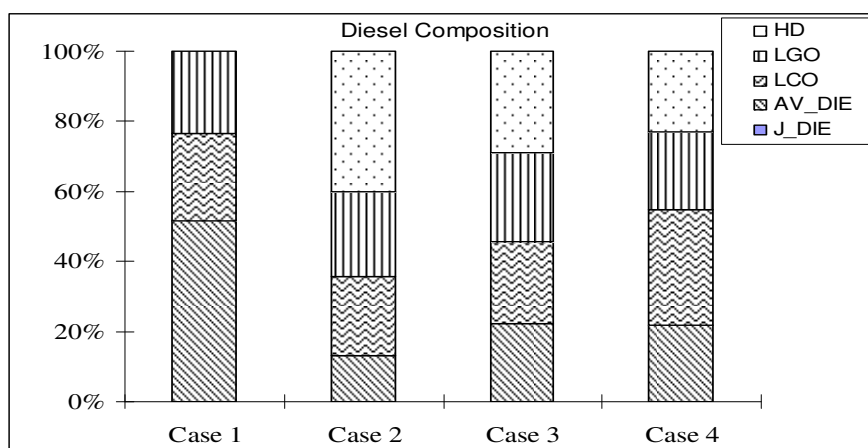


Figure 6.9 Composition of diesel in different modes

The large increase in profit is achieved by exploiting the synergies between the site level aspects and process operating details. In this case, RFCC operation is no longer fixed at the maximum gasoline mode. Instead, the best compromise between different operation modes is exploited with the integrated optimisation. As a result, the RFCC conversion level is changed from 70 LV% to 64.71 LV%. As for CRU, the operating temperature is decreased to lower aromatic contents in products. Table 6.15 shows the optimal operating conditions of RFCCU and RCU respectively.

Table 6.15 Operating conditions of processes in different modes

	Case 1	Case 2	Case 3	Case 4
Temperature -Reactor1(K)	783.50	783.50	783.50	763.15
Temperature -Reactor2(K)	793.50	793.50	793.50	763.15
Temperature -Reactor3(K)	793.50	793.50	793.50	763.15
Pressure(psi)	120.00	120.00	120.00	80.00
FCC Conversion Level	70.00	70.00	70.00	64.71

6.4 Application II: Exploitation of Interactions between Hydrogen Network and Hydroprocesses

6.4.1 Introduction

A hydrogen network may be described as a system of these refinery processes interacting with each other through a hydrogen distribution system. The refinery processes operating with hydrogen as a shared commodity constitute the components of a hydrogen network.

The existing tools and methods for design of refinery hydrogen networks target minimising the hydrogen utility of a given hydrogen network by assuming constant operating conditions of refinery processes. The operating conditions of refinery processes are changing from time to time depending on the feedstock and market demands. Therefore, the hydrogen balance of a given hydrogen network may also vary resulting in changing performance of refinery processes. A window of opportunity that requires further research is the improvement of performance of hydrogen consuming processes by utilising the hydrogen freed-up using hydrogen management techniques. The hydrogen consumption of refinery processes is bound to keep increasing in this era of cleaner transportation fuels, and consequently design approaches are needed that can provide not only flexible hydrogen distribution systems but also optimal utilisation of hydrogen for increasing the overall profit margins of refineries.

6.4.1.1 Hydrogen Network in Refinery

Hydrogen network in refinery usually involves hydrogen producers that supply hydrogen such as hydrogen plant and catalytic reforming process, hydrogen consumers that consume hydrogen such as diesel hydrotreater and hydrocracker, compressors that assure the pressure of hydrogen sink is met, and purifiers that purify the hydrogen streams, as well as pipelines that transport hydrogen between units. Figure 6.10 shows a typical hydrogen network (Singh, 2004) without the consideration of pressure difference between processes.

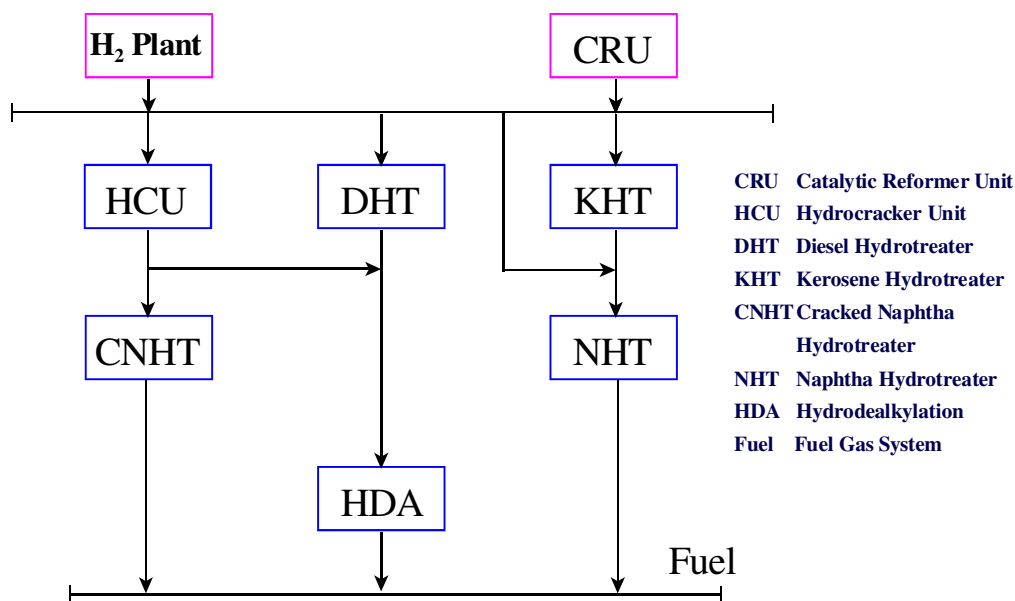


Figure 6.10 A typical hydrogen network

Hydrogen is supplied as a product of steam reformers (H_2 plant in Figure 6.10), and a by-product of catalytic reformers (CRU), and a number of offgas or purge streams in a refinery that contain hydrogen. There are various hydrogen consumers in a refinery, which possibly include hydrocracking (HCU), diesel hydrotreater (DHT), kerosene hydrotreater (KHT), cracked naphtha hydrotreater (CNHT), naphtha hydrotreater (NHT) and hydrodealkylation (HDA) as Figure 6.10 shows. Normally, the purities and pressures of these hydrogen consumers are different because of the process characteristics, and the hydrogen source streams coming out of the different units also have different pressures and purities. The difference in operating pressure and hydrogen purity in the various hydroprocessing units can be arranged in a downward sequence as Figure 6.10.

6.4.1.2 Hydrogen Network Management

Refinery hydrogen network management refers to the optimal allocation of hydrogen distribution network. The methodology for hydrogen network management has been developed intensively in this decade due to the stricter environmental regulations on the transportation fuels. A brief review of these methodologies would be present, together with some concepts used in this work.

Alves (1999) developed a framework of sinks and sources for classification of components of a hydrogen distribution system. A sink is a stream that consumes

hydrogen from the hydrogen distribution system while a source is defined as a stream supplying hydrogen to the system. The hydrogen producing processes form the sources of a hydrogen distribution system with given purities and pressure levels. The hydrogen consuming processes are represented in the framework of sinks and sources as shown in Figure 6.11.

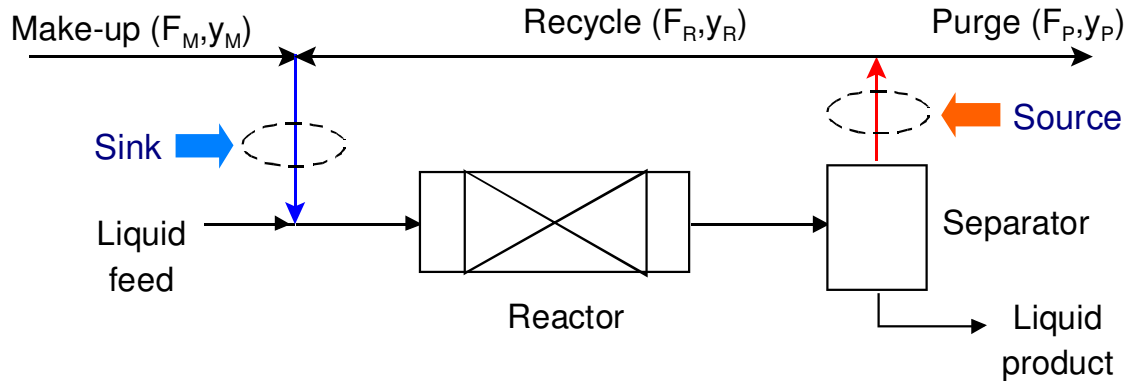


Figure 6.11 Simplified diagram of a hydrogen consumer (Alves, 1999)

Hydrogen pinch approach (Alves, 1999) to target the minimal hydrogen utility is based upon the pinch technology and takes advantage of an analogy with heat exchanger network synthesis (Linnhoff, 1993). In this method, sources and sinks of hydrogen are similar to hot and cold streams in heat exchanger networks.

Sources and sinks of a hydrogen network can be plotted in a two-dimensional graph by the flowrate and the purity as composite curves. Figure 6.12 displays a hydrogen demand profile and a supply profile plotted in the order of decreasing purity. There are regions where the source profile lies above the sink profile indicating an excess of hydrogen available in that particular range of purity (marked as +). On the other hand if the source profile is beneath the sink profile then we have a deficit of available hydrogen in that purity range (marked as -). The availability of hydrogen at different purity levels is represented as the hydrogen surplus which is defined as the net cumulative excess of hydrogen in the purity profile at a given flow rate (Alves et al., 2002). A hydrogen surplus diagram is a plot of the hydrogen surplus against different purity levels of a hydrogen network. Figure 6.13 shows a hydrogen surplus diagram generated by plotting the hydrogen surplus or deficit, from purity profiles, at different purity levels.

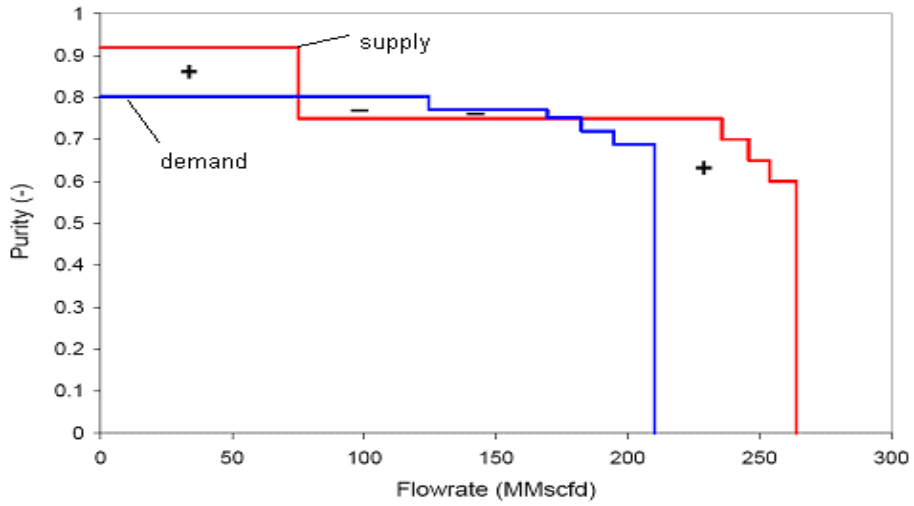


Figure 6.12 Composite curves (Liu, 2002)

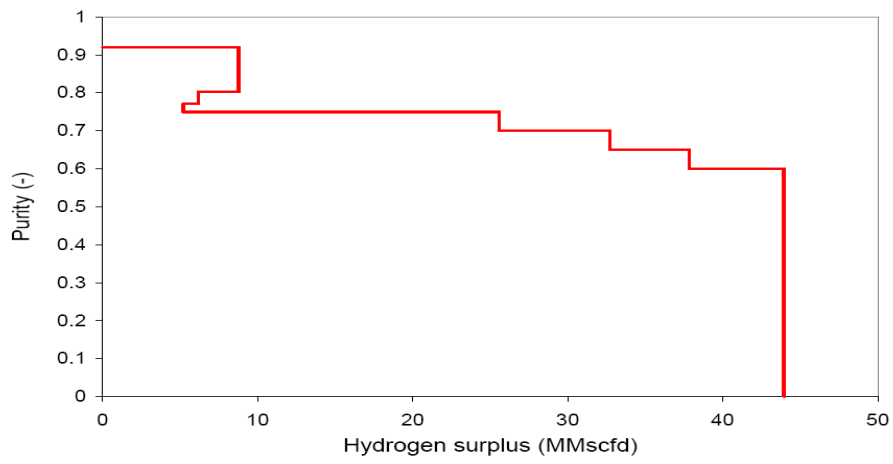


Figure 6.13 A hydrogen surplus diagram (Liu, 2002)

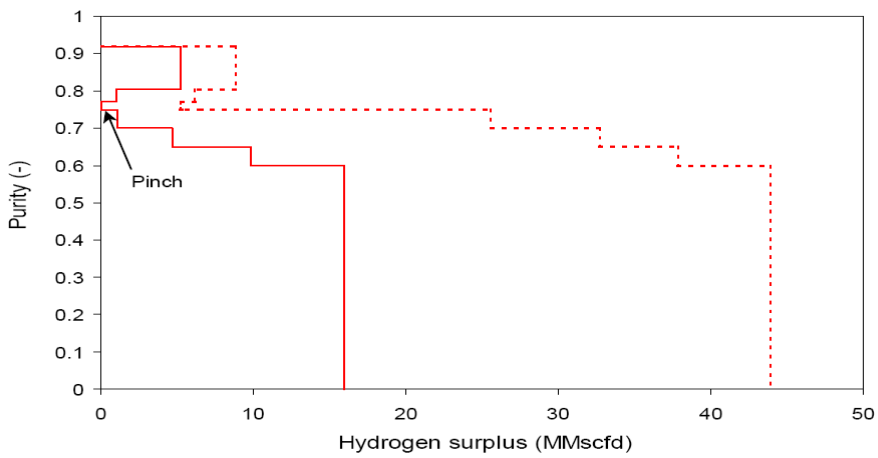


Figure 6.14 Balanced hydrogen surplus cascade diagram (Liu, 2002)

The hydrogen pinch is determined by moving this surplus curve towards the vertical axis that is minimising the surplus amount of hydrogen available in the hydrogen network. The sink in the segment touching the vertical axis is defined as the hydrogen pinch. In this way, the minimum demand of hydrogen is determined. If the hydrogen surplus curve passes the purity axis, the supply of hydrogen sources can not satisfy the demand of hydrogen sinks.

The hydrogen network approaches discussed do not provide a framework for optimal utilisation of hydrogen to improve the economic performance of refinery processes (Hallale et al., 2002). The change of operating conditions plays an important role in product quality as well as hydrogen consumption. For example, increasing hydrogen partial pressure may enhance the reactor conversion, throughput, product yields and catalyst life of hydrogen consuming processes. The interaction between a hydrogen network and hydroprocessing processes could be described as:

- Hydrogen sources affect hydrogen consumers by providing hydrogen at different flowrates and purities;
- Changes of sources result in different process performance;
- Hydrogen consumers affect hydrogen sources by requiring certain amounts of hydrogen at certain purities;
- Changes of operating conditions result in different hydrogen consumption;

Sun (2004) developed a series of procedures to investigate the interaction between hydrogen network and diesel hydrotreater. The approach (Sun, 2004) is far from systematic. First of all, the effect of purity of hydrogen source was not investigated, which has a significant impact on both a hydrogen network and diesel hydrotreaters. Secondly, the effect of the change of operating conditions of diesel hydrotreater on the economic performance is a complex problem, and not easily identified by analysing the results from the different combinations of operating conditions of a diesel hydrotreater. Last, a multi-period hydrogen network due to catalyst deactivation was not considered yet.

6.4.2 Integrating Hydrogen Network and Hydroprocesses

The reason that the approach (Sun, 2004) to investigate the interaction between hydrogen network and diesel hydrotreater is based on the analysis of the results from the different combinations of operating conditions, is that the model relating to process operations of a diesel hydrotreater are highly non-linear. This then led to the great difficulty to handle the non-linearities related to the kinetics, thermodynamics, etc. The challenge of this work then was to develop a model that can account for both highly non-linear process models (containing detailed descriptions of operating conditions) and at the same time optimise the overall performance of a multi-period model of a hydrogen network.

The framework developed by Zhang (2000) forms the basic idea of the proposed approach for the investigation of the interaction. The site-level optimisation is the management of a multi-period hydrogen network, which is built to find the optimal operations in each period: the changes of feeds fed to the processes, the hydrogen purities and amounts, and the allocation of hydrogen between hydrogen sources and sinks. In this level of optimisation, processes are modelled with linear correlations and the information of detailed operating conditions is not needed. The detailed procedure about these correlations building is explained in the late section.

The process-level optimisation tries to improve process performances based on the allocated resources. Take diesel hydrotreater as an example, the process-level optimisation would target on maximising the process profit based on the allocated feed flowrate and hydrogen purity by changing the operating temperature and hydrogen flowrate satisfying the product specifications. In this level of optimisation, non-linear and discrete aspects related to individual processes are fully addressed, and the rigorous process model can be employed. The main feature of this level optimisation is that feed conditions and the hydrogen purity determined on the site level are fixed.

6.4.3 Site Level Model

The target of this work is to switch the objective from saving hydrogen to improving the economic performance by utilising hydrogen more efficiently. There

are several potential ways to increase the economic performance: feeding cheaper feedstocks, increasing throughput, and reducing hydrogen and catalyst cost. To include these potential ways, the representation of a hydrogen consuming process is changed as illustrated in Figure 6.15, which allows the consideration of changing feedstock composition and flowrate, as well as the hydrogen flowrate and purity.

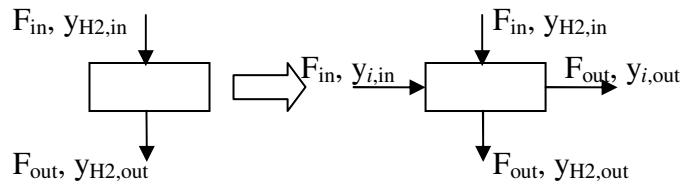


Figure 6.15 Representation change of a process for new method

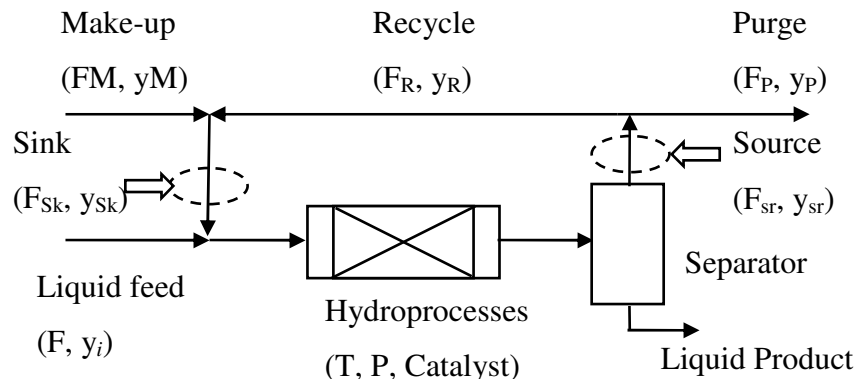


Figure 6.16 Modified diagram of a hydrogen consuming process

For a process, the operating condition such as temperature and pressure is changeable to satisfy the product specifications as Figure 6.16 shows.

In this research, to simplify the problem, the practical constraints are not considered such as pressure differences between hydrogen sources and sinks, and compressors, purifiers are not included. The constraints on hydrogen network are the overall mass balance and hydrogen mass balance. The proposed model can be easily integrated with the consideration of practical constraints.

A nonlinear programming model is formulated to account for the mass balance of a hydrogen distribution network. The important aspects related to the multi-period hydrogen network include processes to be optimised (CPO), hydrogen sinks (SK) and hydrogen source (SR), different types of (FD), multi-stage because of catalyst deactivation (ST), hydrogen utility (HU). In the following mathematical model, the

symbol with an over-bar represents a parameter, which value is fixed in the current site-level optimisation, and may be different in different iterations, and a symbol without an over-bar is a variable.

The objective function of site-level optimisation is the annualised overall profit.

$$profit = \frac{365}{\sum_{s=1}^{N_s} L_s + \bar{L}_{shutdown}} (C_{income} - C_{feed\ cost} - C_{H_2} - \bar{C}_{cat}) \quad (6.15)$$

where L_s is the run length of period s , $\bar{L}_{shutdown}$ represents the duration for replacing catalyst, N_s is the period number in one run. C_{income} is the income of selling products, $C_{feed\ cost}$ stands for the cost of the consumed feedstock, C_{H_2} is the operating cost of hydrogen utility, and \bar{C}_{cat} is the catalyst cost for one run.

$$L_s = \bar{L}_{0,s} + \sum_{f \in FD} \bar{\alpha}_{s,f}^L \Delta F_{s,f} \quad \forall s \in ST \quad (6.16)$$

$$C_{income} = \sum_{s \in ST} c^P F_s^P L_s \quad (6.17)$$

$$C_{feed\ cost} = \sum_{s \in ST} \sum_{f \in FD} c_f^F F_{s,f}^F L_s \quad (6.18)$$

$$C_{H_2} = \sum_{s \in ST} c^{H_2} F_s^{H_2} L_s \quad (6.19)$$

where c^P, c_f^F, c^{H_2} are the prices of product, feedstock f of CPO, and hydrogen utility respectively. $F_s^P, F_{s,f}^F$ are the flowrates of product and feedstock f of CPO respectively, given as:

$$F_s^P = \bar{F}_{0,s}^P + \sum_{f \in FD} \bar{\alpha}_{s,f}^P \Delta F_{s,f} \quad \forall s \in ST \quad (6.20)$$

$$F_{s,f}^F = \bar{F}_{0,s,f}^F + \Delta F_{s,f} \quad \forall s \in ST, \forall f \in FD \quad (6.21)$$

$$F_s^{H_2} = \sum_{j \in SK} F_{u,j,s} \quad \forall s \in ST, \forall u \in HU \quad (6.22)$$

where $\bar{F}_{0,s}^P$ is the product flowrate of CPO at stage s from the previous iteration. $\bar{\alpha}_{s,f}^P$ is the coefficient updated from the process optimisation. $\Delta F_{s,f}$ stands for the change of feed f at stage s . $F_{u,j,s}$ is the hydrogen flowrate fed to hydrogen sink j from hydrogen utility u at stage s .

As mentioned previously, the process models on the site level are simplified linear correlations, which are derived from the process optimisation (explained later) based on the rigorous models by using finite difference approximation. These aspects include the period length, product yields, flowrate and hydrogen purity of offgas, as well as the demand hydrogen flowrate.

Hydrogen distribution is constrained by overall hydrogen stream mass balance and hydrogen mass balance. The overall mass balance on a hydrogen sink is as:

$$\sum_{i \in SR} F_{i,j,s} + \sum_{ii \in CPO} F_{ii,j,s} = \bar{F}_j^{sink} \quad \forall s \in ST, \forall j \in SK \quad (6.23)$$

$$\sum_{i \in SR} F_{i,jj,s} + \sum_{ii \in CPO} F_{ii,jj,s} = F_{jj,s}^{sink} \quad \forall s \in ST, \forall jj \in CPO \quad (6.24)$$

where $F_{i,j,s}, F_{ii,j,s}, F_{i,jj,s}, F_{ii,jj,s}$ all stand for the flowrates of hydrogen from the sources i or ii to the sinks j or jj . \bar{F}_j^{sink} is the demand flowrate of hydrogen for sink j which is fixed in all periods, and $F_{jj,s}^{sink}$ stands for the demand flowrate of hydrogen of CPO in period s , which would be changed depending on the selected feedstock and hydrogen purity.

By assuming the demand hydrogen quantity remains same for different hydrogen purity, the flowrate of hydrogen stream is calculated as:

$$F_{jj,s}^{sink} = \frac{F_{0,jj,s}^{sink} \bar{y}_{0,jj,s}^{sink}}{y_{jj,s}^{sink}} \quad \forall s \in ST, \forall jj \in CPO \quad (6.25)$$

where $\bar{y}_{0,jj,s}^{sink}$ is the hydrogen purity from the previous iteration, and $y_{jj,s}^{sink}$ is the hydrogen purity (to be optimised) of CPO at stage s . $F_{0,jj,s}^{sink}$ is the flowrate of hydrogen if with $\bar{y}_{0,jj,s}^{sink}$ of the hydrogen purity for the change of feed as:

$$F_{0,jj,s}^{sink} = \bar{F}_{0,jj,s}^{sink} + \sum_{f \in FD} \bar{\alpha}_{s,f}^{H2} \Delta F_{s,f} \quad \forall s \in ST, \quad \forall jj \in CPO \quad (6.26)$$

where $\bar{F}_{0,jj,s}^{sink}$ is the result of flowrate of hydrogen stream from previous iteration, and $\bar{\alpha}_{s,f}^{H2}$ is the coefficient standing for the flowrate change of hydrogen stream with feed f change at stage s of CPO.

Consequently, the purity of hydrogen sink is allowed to be changed leading to another degree of freedom. The change of sink hydrogen purity will impact the hydrogen purity of the offgas, which is also affected by changing feed.

$$y_{jj,s}^{Sr} = \bar{y}_{0,jj,s}^{Sr} + \sum_{f \in FD} \bar{\alpha}_{s,f}^y \Delta F_{s,f} + \Delta y_{jj,s}^{Sk} \frac{\bar{y}_{0,jj,s}^{Sr}}{\bar{y}_{0,jj,s}^{sink}} \quad \forall s \in ST, \quad \forall jj \in CPO \quad (6.27)$$

where $\bar{y}_{0,jj,s}^{Sr}$ is the hydrogen purity of offgas from the previous iteration, $\bar{\alpha}_{s,f}^y$ is the coefficient that represents the impact of feed f change on the hydrogen purity of offgas at stage s of CPO.

$$\Delta y_{jj,s}^{Sk} = y_{jj,s}^{sink} - \bar{y}_{0,jj,s}^{sink} \quad \forall s \in ST, \quad \forall jj \in CPO \quad (6.28)$$

The hydrogen mass balance on sinks is described as:

$$\sum_{i \in SR} F_{i,j,s} \bar{y}_i^{Sr} + \sum_{ii \in CPO} F_{ii,j,s} y_{ii,s}^{Sr} = \bar{F}_j^{sink} \bar{y}_j^{sink} \quad \forall s \in ST, \quad \forall j \in SK \quad (6.29)$$

$$\sum_{i \in SR} F_{i,jj,s} \bar{y}_i^{Sr} + \sum_{ii \in CPO} F_{ii,jj,s} y_{ii,s}^{Sr} = F_{jj,s}^{sink} y_{jj,s}^{sink} = F_{0,jj,s}^{sink} \bar{y}_{0,jj,s}^{sink} \quad \forall s \in ST, \quad \forall jj \in CPO \quad (6.30)$$

where \bar{y}_i^{Sr} is the hydrogen purity of the source i , which is fixed.

The overall mass balance on hydrogen sources is given as:

$$\sum_{j \in SK} F_{i,j,s} + \sum_{jj \in CPO} F_{i,jj,s} + F_{i,s}^{Fuel} = \bar{F}_i^{Sr} \quad \forall s \in ST, \quad \forall j \in SR \quad (6.31)$$

$$\sum_{j \in SK} F_{ii,j,s} + \sum_{jj \in CPO} F_{ii,jj,s} + F_{ii,s}^{Fuel} = F_{ii,s}^{Sr} \quad \forall s \in ST, \forall ii \in CPO \quad (6.32)$$

where \bar{F}_i^{Sr} is the flowrate of hydrogen source i , which is fixed. $F_{i,s}^{Fuel}$ is the flowrate from source i to fuel at stage s .

$$F_{ii,s}^{Sr} = \bar{F}_{0,ii,s}^{Sr} + \sum_{f \in FD} \bar{\alpha}_{s,f}^{Sr} \Delta F_{s,f} \quad \forall s \in ST, \forall ii \in CPO \quad (6.33)$$

where $\bar{F}_{0,ii,s}^{Sr}$ is the offgas flowrate of CPO at stage s from the previous iteration, $\bar{\alpha}_{s,f}^{Sr}$ is the coefficient representing the effect of feed f change on the offgas flowrate of CPO at the stage s .

Some practical constraints can be considered such as the capacity of processes, the run length of process etc.

$$L^{Feed} \leq \sum_{f \in FD} F_{s,f}^{Feed} \leq U^{Feed} \quad \forall s \in ST \quad (6.34)$$

$$L^{run} \leq \sum_{s \in ST} L_s \leq U^{run} \quad (6.35)$$

As discussed previously, the process model on the site-level optimisation is a simplified linear model. These correlations could only be applied for a small change of variables. Otherwise it could lead to big deviations from the reality. Therefore, all independent variables are allowed to be changed in a certain range.

$$\beta_{s,f}^L \sum_{f \in FD} F_{s,f}^{Feed} \leq \Delta F_{s,f} \leq \beta_{s,f}^U \sum_{f \in FD} F_{s,f}^{Feed} \quad \forall s \in ST \quad (6.36)$$

$$\beta_s^L y_s^{sink} \leq \Delta y_{ii,s}^{sink} \leq \beta_s^U y_{ii,s}^{sink} \quad \forall s \in ST, \forall ii \in CPO \quad (6.37)$$

The coefficient β is controlled depending on the previous iterations with a maximum and minimal value. The way to update the bounds of variation follows:

- If $\Delta F_{s,f}, \Delta y_{ii,s}^{sink}$ has changed sign from the last site-level optimisation and the latest one is positive,

$$\beta_{i+1}^L \leftarrow \beta_i^L / 2$$

- If $\Delta F_{s,f}, \Delta y_{ii,s}^{sink}$ has changed sign from the last site-level optimisation and the latest one is negative,

$$\beta_{i+1}^U \leftarrow \beta_i^U / 2$$

- If $\Delta F_{s,f}, \Delta y_{ii,s}^{sink}$ has touched the upper bound for the three consecutive iterations,

$$\beta_{i+1}^U \leftarrow 2\beta_i^U$$

- If $\Delta F_{s,f}, \Delta y_{ii,s}^{sink}$ has touched the lower bound for the three consecutive iterations,

$$\beta_{i+1}^L \leftarrow 2\beta_i^L$$

6.4.4 Site Optimisation with Process Simulation

Since the site level uses the simplified correlations to model process operation, it is expected to cause obvious errors to realistic results. Therefore, it is necessary to combine a rigorous process simulation/optimisation with the site level optimisation, which can correct these errors. The stage is named as stabilisation. To satisfy product specifications on process level, the process optimisation based on a rigorous process model is needed. Then, hydrogen flowrate and reactor temperature will be optimised to achieve the product specification. The main feature in this stage is that the process optimisation is performed with the fixed feed selection, and the site-level optimisation is with the fixed hydrogen purity. What the site-level optimisation gets from the process-level optimisation is the update of the simplified correlations. To simplify, the site-level optimisation in the stabilisation is just a traditional hydrogen network distribution optimisation with the fixed hydrogen source and purity, hydrogen sink and purity.

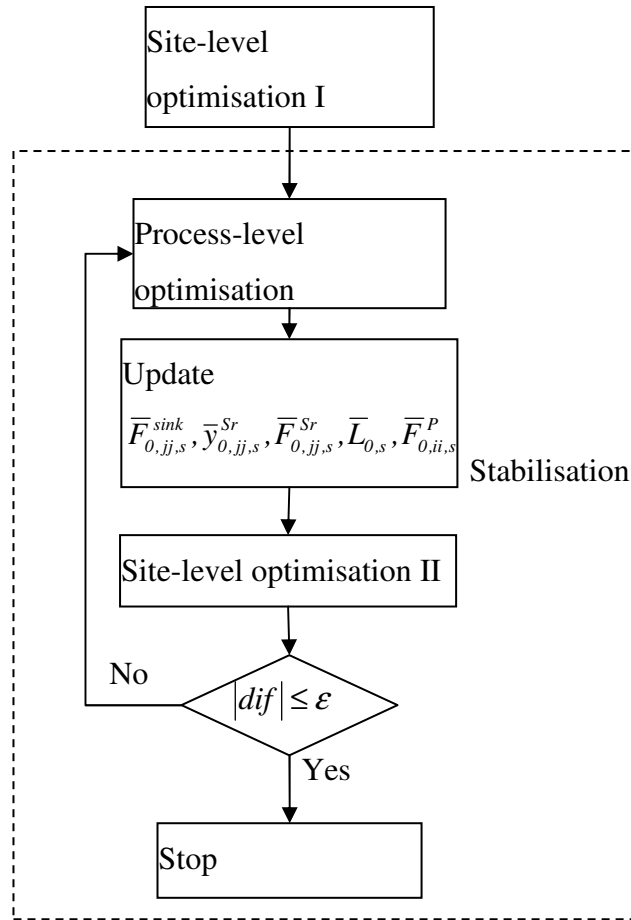


Figure 6.17 Site optimisation with process simulation/optimisation

The stabilisation is performed in an iterative procedure as Figure 6.17. To differ the optimisation in different stages, site-level optimisation I represents site-level optimisation with the allowable change on feed selection and hydrogen purity, and site-level optimisation II stands for the traditional hydrogen network optimisation.

6.4.5 Integrated Site and Process Optimisation

The procedure of integrating site-level and process-level optimisation starts with a base case, which is the current operation. Based on current feed selection, a small deviation on different types of feed is performed. Then, a process optimisation is performed to update the linear correlations for process model. Thereafter, the site-level optimisation I is applied to optimise the hydrogen distribution network, and simultaneously the feed selection and hydrogen purity of sinks, followed by stabilisation step to correct the unrealistic errors. The new value of objective function, as well as the feed selection and hydrogen purity is compared with the

previous one. If the difference between these two results is within the specified tolerance, the procedure would terminate, otherwise, a new iteration will start.

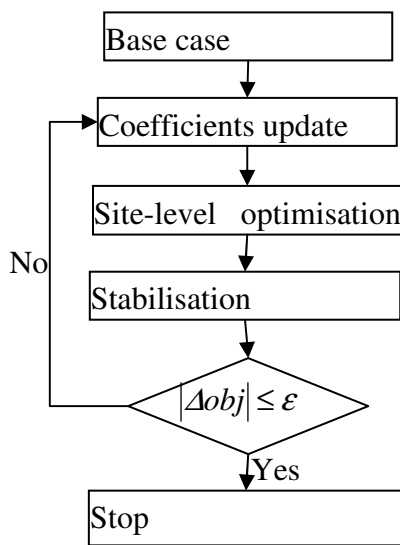


Figure 6.18 Integration of hydrogen network and hydroprocesses

It is worthy to note about the feasibility of site-level optimisation. The optimal hydrogen sinks (optimised from process-level optimisation) and the hydrogen purity of sinks (from the previous site-level optimisation) possibly cannot be satisfied by the available hydrogen sources. Therefore, to avoid the infeasibility of hydrogen distribution network, one pure hydrogen source if without any hydrogen utility in system and one zero hydrogen source (the hydrogen purity is zero) are introduced. The penalty strategy is applied to make the site-level optimisation use these two introduced hydrogen sources as little as possible.

6.4.6 Case Study

The case employed by Sun (2004) would be used to demonstrate the performance of the proposed framework. The developed process level optimisation model of diesel hydrotreater in Chapter 5 would be applied.

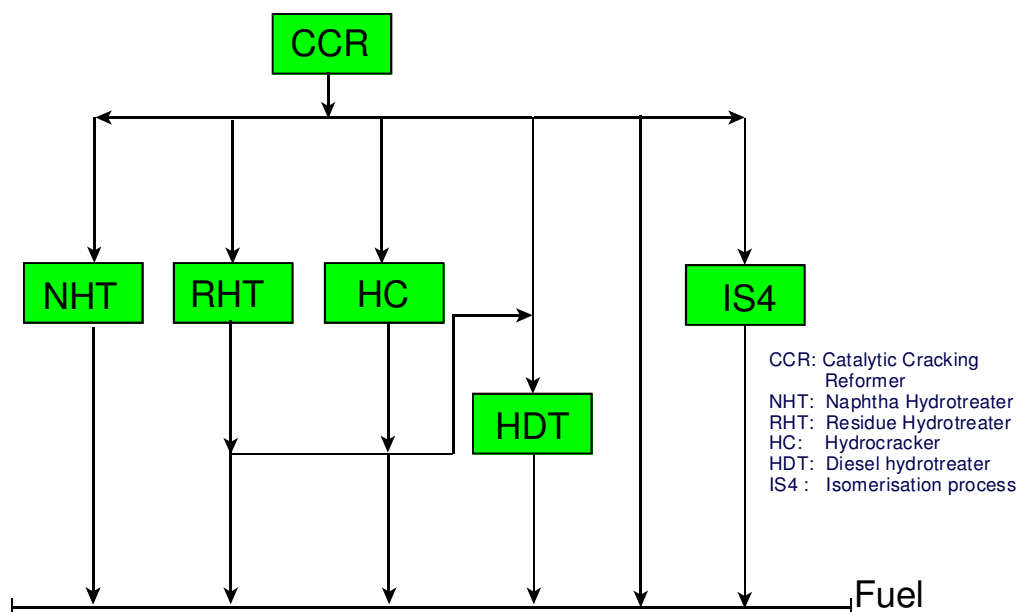


Figure 6.19 The hydrogen network of the case (Sun, 2004)

Table 6.16 Calibrated data of hydrogen sinks (Sun, 2004)

Unit	Flowrate (t/day)	Purity (mass fraction)
NHT	3.108	0.2620
RHT	5.081	0.2624
HC	3.251	0.2624
ISOM	5.913	0.2596
CCR fuel	0.446	0.2624

Figure 6.19 shows the hydrogen network. There is only one hydrogen producer – CCR, and five hydrogen consumers: NHT, RHT, HC, HDT, and IS4. The calibrated data about hydrogen network is listed as Table 6.16 and Table 6.17, which give the information about hydrogen sources and sinks respectively.

Table 6.17 Calibrated data of hydrogen sources (Sun, 2004)

Unit	Flowrate (t/day)	Purity (mass fraction)
CCR	13.73	0.2624
NHT	2.24	0.2857
RHT	4.95	0.2436
HC	3.16	0.2436
ISOM	4.58	0.2588

Due to the catalyst deactivation, the run cycle of DHT is divided into three stages, and only temperature is increased to compensate the loss of activity of catalyst. The throughput remains same along stages. Table 6.18 shows the related operating conditions of DHT. Hydrogen surplus diagram of base case, which is current operation, and balanced hydrogen surplus given as Figure 6.20 based on pinch analysis, shows a positive surplus. The balanced hydrogen cascade diagram shows that the pinch concentration is 0.2015, which corresponds to the DHT sink concentration shown in Table 6.18. That means DHT is most likely to become the bottleneck within the system. The overall profit of base case is 13.03 M\$/yr.

Table 6.18 Operating conditions of DHT for base case

Stage	Purity (wt)	Sink flowrate(t/d)	SRGO(t/d)	Temperature(K)
S	0.2015	28.58	350	677.1
M	0.2015	28.58	350	687.5
E	0.2015	28.58	350	700.0

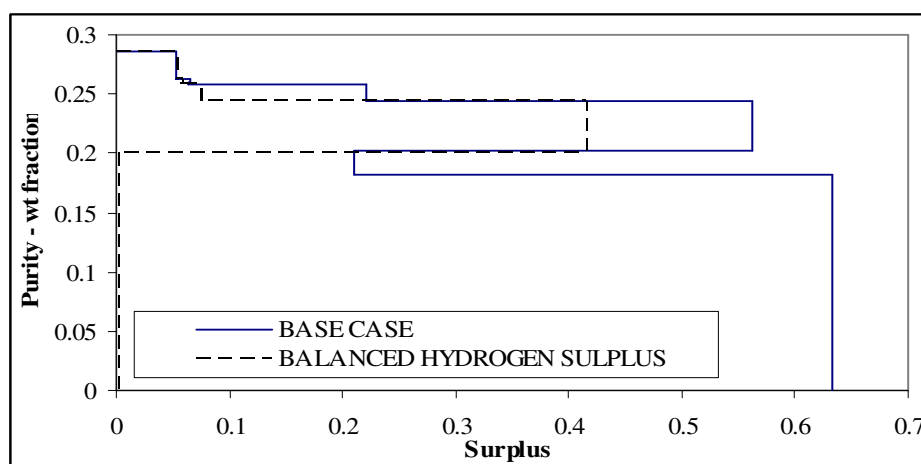


Figure 6.20 Hydrogen surplus diagram

To utilise hydrogen in system more efficiently, light cycle oil (LCO), cheaper than SRGO, is allowed to be used as another feedstock of DHT but remaining the same throughput. The hydrogen purity and flowrate fed to DHT, as well as operating temperature can be changed to satisfy the product specification of the maximum 50wt ppm sulphur content. The proposed integration methodology is applied to exploit the maximum profit, together with the developed rigorous model of DHT on molecular level. Some practical constraints are given in Table 6.19.

Table 6.19 Constraints of operating conditions for DHT

Constraint	Bound
Maximum reactor Temperature (K)	700
Minimum catalyst life(days)	300
Maximum product sulphur content (wtppm)	50

Table 6.20 Optimal operating conditions of diesel hydrotreater in each period

Stage	Purity	Flowrate	SRGO	LCO	Temperature
S	0.155	94.062	90.4	259.6	700
M	0.192	101.267	133.4	216.6	700
E	0.236	78.785	215.1	134.9	700

The achieved overall profit is increased to 17.60 M\$/yr, by 35.1% compared with the profit of base case. The big increase in profit indicates that if the degrees of freedom in the process level are exploited together with the degrees of freedom in the site level, it provides significant synergy for economic improvement. The optimal operating conditions for DHT are given in Table 6.20, which are quite different from those of base case. The hydrogen purity is increased to compensate the activity loss, and the operating temperatures reach the upper bound, which may be because of the higher hydrogen consumption of aromatic hydrogenation reactions and hydrodesulphurisation favoured by higher temperature.

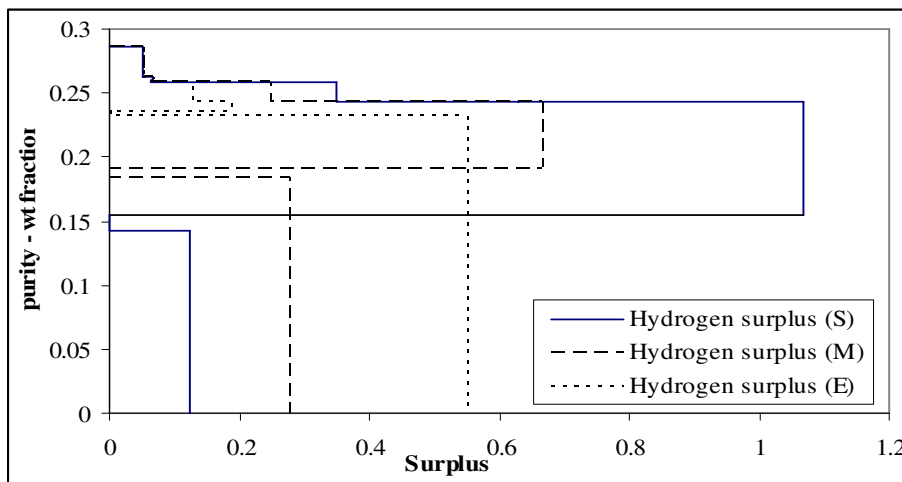


Figure 6.21 Hydrogen surplus diagrams of periods

The run cycle length of DHT is decreased dramatically from 707 to 339 days due to higher operating temperature and higher aromatic contents of LCO. Cheaper feedstock of LCO is blend as feedstock of DHT, which enhances the economic performance. LCO blend ratio decreases along with the loss of catalyst activity from 259 to 134 t/day. The hydrogen surplus diagrams of the optimal result in three periods (Figure 6.21) all show that the hydrogen purity of DHT sink is the pinch point, which means that hydrogen is utilised efficiently in each period.

6.5 Summary

Molecular modelling is firstly integrated into the two-level decomposition optimisation approach (Zhang, 2000), and then the incorporated framework is successfully applied in two exploitations, the interaction between material processing network and refining processes, and the interaction between hydrogen network and hydrogen consuming processes. With the integration of the process and the site-level models, a better perspective is obtained with regard to material processing system. By applying molecular modelling of the refining streams and processes, the integrated approach not only controls the molecules in products properly, but also increases the overall refinery performance.

In the second application, a novel framework for the integration of hydrogen network with hydroprocesses is developed to target the maximum profit. It allocates hydrogen on the hydrogen network level and utilise hydrogen efficiently on the process level. The proposed methodology switches the objective from saving hydrogen to improving the economic performance. Throughput could be increased to make full use of hydrogen surplus, and cheaper feedstock could be blended into feedstock of hydroprocesses to reduce the cost. The hydrogen purity fed to hydroprocesses, which significantly impacts sulphur/nitrogen conversion, throughput, and catalyst life, is optimised as well. The case study demonstrates that the proposed methodology is capable of not only handling the complexity of non-linearity of rigorous process models, but also improving the economic performance greatly. Consequently, the extent of achieving the maximum profit could be fully exploited with optimal hydrogen utilisation.

6.6 Nomenclature

6.6.1 Application I

List of sets

C	crude oil
U, UU, UUU	refining unit
S, SS	refining stream
P	refining products
K	component represented by MTHS matrix
PP	property of refining streams
UT	utility

List of symbols

$\bar{R}_{c,ss,u,s}$	yield coefficients representing that one unit of feed ss will produce R amount of product s through process u from crude oil c
$F_{c,uu,ss,u}$	mass flow from unit uu to unit u through stream ss from crude oil c
$y_{c,u,s,k}$	composition of component k in the stream s produced by unit u from crude oil c
$\bar{y}_{c,ss,u,s,k}$	composition of component k in the stream s produced by unit u from the feedstock ss coming from crude oil c
F_p, F_c	flow rate of product p and crude oil c
$Pt_{s,p}$	blending property p of stream s
$y_{s,k}$	composition of component k in blending component s
C_p, C_c, C_{ut}, C_u	prices of product p, crude oil c, utility ut, and the operating cost of unit u

6.6.2 Application II

List of sets

S	stage of multi-period
CPO	hydrogen consuming process to be optimised
P	product

F	feedstock
i	hydrogen source
j	hydrogen sink
u	hydrogen utility

List of symbols

Ls	run length of period s
$\bar{L}_{shutdown}$	duration for replacing catalyst
Ns	period number in one run
Cincome	income of selling products
Cfeedcost	cost of the consumed feedstock
CH2	operating cost of hydrogen utility
\bar{C}_{cat}	catalyst cost for one run
c^P, c_f^F, c^{H2}	prices of product, feedstock f of CPO, and hydrogen utility respectively.
$F_s^P, F_{s,f}^F$	flowrates of product and feedstock f of CPO respectively
$\bar{F}_{0,s}^P$	product flowrate of CPO at stage s from the previous iteration
$\bar{\alpha}_{s,f}^P$	coefficient updated from the process simulation/optimisation
$\Delta F_{s,f}$	change of feed f at stage s
$F_{u,j,s}$	hydrogen flowrate fed to hydrogen sink j from hydrogen utility u at stage s
$F_{i,j,s}, F_{ii,j,s}, F_{i,jj,s}, F_{ii,jj,s}$	flowrates of hydrogen from the sources i or ii to the sinks j or jj
\bar{F}_j^{sink}	demand flowrate of hydrogen for sink j which is fixed in all periods
$F_{jj,s}^{sink}$	demand flowrate of hydrogen of CPO in period s
$\bar{y}_{0,jj,s}^{sink}$	hydrogen purity from the previous iteration
$y_{jj,s}^{sink}$	hydrogen purity to be optimised, of CPO at stage s
$F_{0,jj,s}^{sink}$	flowrate of hydrogen if with $\bar{y}_{0,jj,s}^{sink}$ of the hydrogen purity for the change of feed

$\bar{F}_{0,ij,s}^{sink}$	result of flowrate of hydrogen stream from previous iteration
$\bar{\alpha}_{s,f}^{H2}$	coefficient standing for the flowrate change of hydrogen stream with feed f change at stage s of CPO
$\bar{y}_{0,ij,s}^{Sr}$	hydrogen purity of offgas from the previous iteration
$\bar{\alpha}_{s,f}^y$	coefficient that represents the impact of feed f change on the hydrogen purity of offgas at stage s of CPO
\bar{y}_i^{Sr}	hydrogen purity of the source i , which is fixed
\bar{F}_i^{Sr}	flowrate of hydrogen source i , which is fixed
$F_{i,s}^{Fuel}$	flowrate from source i to fuel at stage s
$\bar{F}_{0,ii,s}^{Sr}$	offgas flowrate of CPO at stage s from the previous iteration
$\bar{\alpha}_{s,f}^{Sr}$	coefficient representing the effect of feed f change on the offgas flowrate of CPO at the stage s

Chapter 7 Conclusions and Future Work

7.1	Conclusions	237
7.2	Future Work	239

7.1 Conclusions

In this work, four aspects of molecular management in oil refineries are investigated respectively.

First of all, a novel methodology to characterise light and middle distillates into the molecular level is developed on the basis of MTHS matrix framework. The method comprises of the enhancements of both representation matrix construction and transformation methodology of bulk properties into molecular composition. To improve the accuracy and adequacy of the representation model, different strategies are set up separately for light and middle distillates for the consideration of isomers. By introducing statistical distribution and applying extensive bulk properties, the transformation approach is revolutionised to increase the usability, and tackle the challenge of possibly achieving significantly different molecular compositions from the same bulk properties of refining streams by the existing transformation approach.

Regarding molecular modelling of refining processes, gasoline blending, catalytic reforming, and diesel hydrotreating are investigated in the representative of MTHS matrix for feedstocks and products, together with the consideration of critical issues related to each process. Based on the developed molecular models, process level optimisation is also presented, which is integrated into overall refinery optimisation.

On the modelling of gasoline blending processes, firstly a new methodology is proposed to predict ON/RVP properties of blending components based on easily obtainable properties. To tightly control the property giveaways in gasoline blending, a molecular model of gasoline blending on PIONA lumps is developed based on a detailed composition-based octane model, and then integrated into the recipe optimisation. A case study demonstrates the economic improvement from the tighter control on property giveaways compared with the conventional approaches. The significance of this work is that the detailed property consideration during optimisation helps to find better solutions and meet with the

product specifications more closely, and the proposed methodology can be integrated into the overall site-level optimisation.

As for the molecular modelling of catalytic reforming, a rigorous molecular model of a semiregenerative catalytic reforming process has been developed. Pressure drop is taken into account due to the non-negligible cost for the power consumption of compressing the recycle hydrogen gas. Composition, temperature and pressure have been obtained to provide information about the extent of conversion in the reactors. A case study demonstrates that the developed model is capable of simulating the reactions in a catalytic reformer accurately. Furthermore, sensitivity analysis of operating conditions exhibits different characteristics on the process performances. Thereafter, a multi-period process level optimisation model has been formulated with the consideration of catalyst deactivation, by correlating coke yield with reaction rate. The optimisation model targeting different objectives by varying the operating temperatures of the reactors in the periods is successfully implemented by assuming the temperature profile follows a smooth function with respect to time.

Regarding a diesel hydrotreater, firstly a molecular model of hydrotreating reactions with a three-phase trickle-bed reactor has been developed. Structural contribution approach is used to obtain kinetics and adsorption parameters. The concept of reaction family is applied. A case study shows that the developed model is capable of simulating the reactions in a diesel hydrotreater accurately. Furthermore, a process level optimisation model is developed with the consideration of catalyst deactivation in stages independent from each other. The optimisation model targeting the minimum operating cost with production specifications is successfully implemented. The developed model enhances the possibility to explore the interactions between hydrotreaters and a hydrogen network by the integration of the site and the process level optimisation.

After the build-up of the molecular models of individual refining processes and streams, the overall refinery optimisation can be taken into account. Molecular modelling is integrated into the two-level decomposition optimisation approach (Zhang, 2000), and then the incorporated framework is applied in two aspects. Firstly, with the integration of the process and the site level models, a better overall

perspective is obtained with regard to material processing system. Together with molecular modelling of the refining streams and processes, the integrated approach not only provides better controls over molecular flows in products properly, but also increases the overall refinery performance. In the second application, a novel framework to integrate hydrogen network with hydroprocesses is developed, which allocates hydrogen at the hydrogen network level, and utilise hydrogen efficiently at the process level. The proposed methodology targets improving the economic performance, rather than saving hydrogen. Case studies illustrate that the incorporated framework can help improve the overall refinery performance significantly.

In summary, systematic molecular management is successfully implemented step by step, which hence efficiently tackles the stricter environmental regulations, and more importantly, enhances the refining profitability and competitiveness through managing molecules effectively.

7.2 Future Work

The present work mainly focuses on molecular management of streams and refining processes related to gasoline and diesel. There is still a massive to enhance and expand the work done in this thesis, as a few outlined as follows.

First of all, as the basis of molecular management, the proposed methodology of molecular characterisation need to be properly extended to heavier fractions, and integrated to characterise a refining stream covering a broader list of properties. As expected, the number of molecular species as well as the possible structural arrangements in molecules increases exponentially as boiling point increases. Therefore, the MTHS representative matrix could be modified based on boiling point rather than carbon number for very heavy fractions due to the difficulties of dealing with high carbon numbers for process modelling.

Secondly, in this work, although process modelling is constrained to the processes handling gasoline and diesel streams, the methodology can be extended to other refining processes. With the proper modelling of refining processes, they can be applied in the overall refinery modelling at a molecular level to track the path of

each individual molecule as it is processed, which provides a better understanding of a refinery configuration, and therefore the possibility to get the most value out of any molecular species through proper process design and operation.

Last but not least, refinery optimisation can be done in many aspects. As a molecule can be tracked as it is processes, the target of molecular management, allocating the right molecule to be at the right place at the right time and at the right price could be explored potentially. On the other hand, the integration of utility systems into plant-wide operation can be investigated. In this work, hydrogen management are incorporated with hydroprocessing processes to find more opportunities of enhancing the economic performance. More opportunities can be found with the consideration of energy system.

References

Abbasi, R., Fatemi, S., Mathematical Modeling of Gas Oil HDS and Optimization of Operational Conditions in Trickle Bed Reactor by Genetic Algorithm, *International Journal of Chemical Reactor Engineering*, 7, 2009

Albahri. T.A., Molecularly Explicit Characterization Model (MECM) for Light Petroleum Fractions. *Industrial & Engineering Chemistry Research*, 44, pp9286 – 9298, 2005

Altgelt, K.H., Gouw, T.H., *Chromatography in petroleum analysis*, Marcel Dekker, New York, 1979

Alves, J. J.: *Analysis and design of refinery hydrogen distribution systems*. Department of Process Integration, UMIST, Manchester, 1999

Alves, J. J., Towler, G.P.: *Analysis of refinery hydrogen distribution systems*. *Industrial and engineering chemistry research* 41. pp5759-5769, 2002

Ancheyta, J. J.; Aguilar, R. E. *Oil Gas J.*, 1994, Jan. 31, pp93 – 95

Ancheyta, J. J., E. V., *Kinetic Modeling of Naphtha Catalytic Reforming Reactions*, *Energy & Fuels*, 14, pp1032 – 1037, 2000

Ancheyta, J., E., Aguilar-Rodriguez, D. Salazar-Sotelo, G., Betancourt-Rivera, M., *Hydrotreating of straight run gas oil-light cycle oil blends*. *Applied Catalysis A - General*, 180, pp195-205., 1999

Andari, M. K., Behbehani H., Stanislaus, A., *Sulfur compound type distribution in Naphtha and gas oil fractions of Kuwaiti crude*. *Fuel Science & Technology International*, 14, pp939-961, 1996

Anderson, P. C. , Sharkey, J. M.,Walsh, R. P., Calculation of the research octane number of motor gasoline from gas chromatographic data and a new approach to motor gasoline quality control, J. of Inst. of Pet. 58, pp83, 1972

American Petroleum Institute. Technical Data Book-Petroleum Refining; 6th Ed, Washington, D.C., 1997

Arora, J. S., Introduction to Optimum Design. 2nd Edition: Academic Press, 2004

Ascher, Steven J. R., Raymond J. S., Implicit-explicit Runge-Kutta methods for time-dependent partial differential equations, 25, pp151 – 167, 1997

Athier, G., Floquet, P., Pibouleau, L., Domenech, S., Process optimization by simulated annealing and NLP procedures. Application to heat exchanger network synthesis. Computers & Chemical Engineering 21: ppS475-S480, 1997

Aye, M.: Molecular modelling for cleaner fuel production. Department of Process integration, UMIST, Manchester, 2003

Aye, M. S.; Zhang, N., A Novel Methodology in Transformation Bulk Properties of Refining Streams into Molecular Information. Chem. Eng. Sci., 60, pp6702-6717, 2005

Bacon, J.; et al., Motor Gasolines Technical Review, Chevron, 2009

Baird, C., Petroleum refining process correlations, HPI Consultants, Inc., 1999

Baltanas, M.A., Forment, G.F., Computer generation of reaction networks and calculation of product distribution in the hydroisomerisation and hydrocracking of paraffins on Pt-containing bifunctional catalyst, Computers & Chemical Engineering, 9, pp71-81, 1985

Beuttner, H., Schmid, B.K., Proc. 6th world Petroleum Congress, Vol. 3, p.197, 1963

Boduszynski, M.M., Composition of Heavy Petroleum. Energy and Fuels, Page 2, Vol.1, 1987, Page 597, Vol. 2, 1988, Page 68, Vol. 6, 1992 and Page 72, Vol. 6, 1992

Briesen H, Marquardt W, New approach to refinery process simulation with adaptive composition representation, *AIChE Journal*, 50(3): pp634–645, 2004

Brown, J.K., Ladner, W.R., A study of the hydrogen distribution in coal-like materials by high-resolution nuclear magnetic resonance spectroscopy II- A comparison with infra-red measurement and the conversion to carbon structure, pp87-96 in *Fuel*, 39, 1960

Campbell, D.M., Stochastic Modeling of Structure and Reaction in Hydrocarbon Conversion, doctoral dissertation, University of Delaware, Newark, 1998

Chen, J. W., Process and Engineering of Fluid Catalytic Cracking; Chinese Petrochemical Publisher: China, 1995

Chilton, T. H., Colburn, A. P., Mass transfer (absorption) coefficients. Prediction from data on heat-transfer and fluid friction, *Ind. Eng. Chem.*, 26, pp1183, 1934

Chung, T., Ajlan, M., Lee, L. L., Starling, K. E., Generalized Multi-parameter Correlation for Non-polar and Polar Fluid Transport Properties, *Industrial & Engineering Chemistry Research*, 27, pp671, 1988

Clymans, P.J. Froment, G.F., Computer generation of reaction paths and rate equations in thermal cracking of normal and branches paraffins, pp137-142, *Computers & Chemical Engineering*, Vol. 8, 1984

Costa, C.B.B., Wolf-Maciel, M. R., Maciel F., R., Factorial design technique applied to genetic algorithm parameters in a batch cooling crystallization optimisation, *Computer and Chemical Engineering*, 29, pp2229-2241, 2005

Cotta, R.M., Wolf-Maciel, M.R., Maciel F., R., A Cape of HDT Industrial Reactor for Middle Distillates, *Computers and Chemical Engineer*, Vol. 24, pp1731, 2000

Cotterman, R. L.; Plunkee, K. W., Effects of Gasoline Composition on Octane Number. The ACS Symposium Division of Petroleum Chemistry, Miami, FL, Sep pp10-15, 1989

Couch, K.A. and Bell L.E., Concepts for an Overall Refinery Energy Solution through Novel Integration of FCC Flue Gas Power Recovery, National Petrochemical & Refiners Association (NPRA) Annual Meeting, Paper AM-06-10, 2006

Dente, M., Ranzi, E., Goossens, A.G., Detailed prediction of olefin yields from hydrocarbon pyrolysis through a fundamental simulation model (SPYRO), *Comput. Chem. Eng.*, 3, pp61 – 75, 1979

De Pauw, R. P., Froment, G. F., Deactivation of a Platinum Reforming Catalyst in a Tubular Reactor, *Chem. Eng. Sci.*, 30, pp789,1974

Depauw, G. A., Froment, G. F., Molecular analysis of the sulphur components in a light cycle oil of a catalytic cracking unit by gas chromatography with mass spectrometric and atomic emission detection, *Journal of Chromatography A*, 761, pp231-247, 1997

Desai, Characterisation of Gasoline Fraction of Refinery Process Streams, Msc thesis, the University of Manchester, 2008

Dewar, M. J. S.; Zerbisch, E. G., Healy, E. F., Stewart. J. J. P., AM1: A new general purpose quantum mechanical molecular model. *J Am Chem. Soc* 107:pp3902-3909, 1985

Dong, D., Jeong, S., Massoth, F.E.: Effect of nitrogen compounds on deactivation of hydrotreating catalyst by coke. *Catalysis today* 37: pp267, 1997

Duayne W., Takaaki I., Isoao M., Present State of the Art and Future Challenges in the Hydrodesulphurisation of Polyaromatic Sulphur Compounds, *Advances in catalysis*, Vol. 42, 2001

Fafet, A., Magne-Drisch, J. Quantitative Analysis of Middle Distillates by GC/MS Coupling: Application to Hydrotreatment Process Mechanism. *Rev. Inst. Fr. Pétrol*, 50, pp391 – 404, 1995

Flory, P.J., Molecular size distribution in linear condensation polymers, *J. Am. Chem. Soc.*, 58, pp1877, 1936

Fogler, F. S., Elements of Chemical Reaction Engineering, 2nd ed., Prentice Hall, NJ, 1992

Froment, G., Bischoff, K., Chemical reactor analysis and design. 2nd edition: John Wiley & Sons, Singapore, 1990

Froment, G.F., Modelling of Catalytic Reforming Unit; Chem.Eng.Sci., 42, pp1073 – 1087, 1987

Froment, G. F., Modeling in the development of hydrotreatment processes. CATALYSIS TODAY, 98, pp43-54, 2004

Froment, G. F., Depauw, G. A., Vanrysselberghe, V., Kinetic modelling and reactor simulation in hydrodesulfurization of oil fractions, In Symposium on Catalytic Reaction Engineering for Environmentally Benign Processes, at the 207th National Meeting of the American-Chemical-Society, pp2975-2988. San Diego, Ca: Amer Chemical Soc, 1994

Froment, G. F., Castaneda-Lopez, L. C., Marin-Rosas, C., Kinetic modelling of the hydrotreatment of light cycle oil and heavy gas oil using the structural contributions approach. In International Symposium on Advances in Hydroprocessing of Oils Fractions, pp446-454. Morelia, MEXICO: Elsevier Science Bv, 2007

García, C.L., Hudebine, D., Schweitzer, J.M., Verstraete, J.J., Ferré, D. In-depth modeling of gas oil hydrotreating: From feedstock reconstruction to reactor stability analysis. Catalysis Today 2010, 150, pp279-299

Gary, J., Handwerk, G.: Petroleum refining technology and economics. 4th edition: Marcel Dekker, Inc., New York., 2001

Gates, B. C., Katzer, J. R., Schuit, G. C., A.: Chemistry of catalytic processes. McGraw-Hill, New York, 1979

George, J. A., Abdullah M. A, Catalytic Naphtha Reforming, Marcel Dekkar, Inc, New York, 2004

Ghosh, K. J., S. B., Development of a Detailed Gasoline Composition – Based Octane Model, *Industrial & Engineering Chemistry Research*, 45, pp337 – 345, 2006

Ghosh, P., S. Jaffe (2006) Detailed composition-based model for predicting the cetane number of diesel fuels. *Industrial & Engineering Chemistry Research*, 45, pp346-351

Girgis, M. J., Gates, B.C.: Reactivities, reaction networks, and kinetics in high pressure catalytic hydroprocessing. *Industrial & engineering chemistry research* 30: 2021, 1991

Goto, S., Smith, J. M., Tickle-bed Reactor Performance: I. Holdup and Mass Transfer Effects, *AIChE J.*, 21, 706, 1975

Gray, R.D. Jr., Heidman, J.L., Springer, R.D., Tsonopoulos, C., Exxon Research and Engineering Co., Characterisation and property prediction for heavy petroleum and synthetic liquids, pp355 - 376 in *Fluid Phase Equilibrium*, (53) 1989.

Grossmann, I. E., Biegler, L. T., Optimizing chemical processes, *Chem. Tech.*, December, pp27-35, 1995

Gupta, S., Planning and scheduling of refinery operations, PhD Thesis, 2008

Habib, E. T., Effect of Catalyst, Feedstock and Operating Conditions on the Composition and Octane Number of FCC Gasoline. Presentation before the ACS Symposium Division of Petroleum Chemistry, Miami, FL, Sep pp10-15, 1989.

Hallale, N., Moore, I., Vauk, D.: Hydrogen: Liability or asset? *Chemical engineering progress* 98: pp66-75, 2002

Hariu, O. H.; Sage, R. C. Crude Split Figured by Computer, *Hydrocarbon proc.*, 48(1), pp143 – 148, 1969

Hartmann, J.C.M., Distinguish between scheduling and planning models, *Hydrocarbon Processing*, pp93 – 100, July 1998

Haskell, B., Beavon, D. K., Front End Volatility of Gasoline Blends, Ind. Eng. Chem., Vol. 34, No. 2, pp167 – 170, 1942

Healey, W. C. Jr., Maasen, C. W., Peterson, R. T., A new approach to blending octanes, Proc. 24th Meeting API Refining Division, Vol. 39, New York, 1959

Heinrich G., Duee D., Modern Petroleum Technology, John Wiley & Sons Ltd., England, 2001

Henningsen, J.; Bundgaard, N. M. Chem. Eng., 15, pp1073 – 1087, 1970

Hillewaert, L.P, Dierickx, J.L., Forment, G.F., Computer generation of reaction schemes and rate equations for thermal cracking, pp17-24 in AIChE J. (34) 1988

Houalla, M., Broderick, D.H., Sapre, A.V., Nag, N.K., de Beer, V.H.J., Gates, B.C., Kwart, H., Hydrodesulphurisation of methyl-substituted dibenzothiophenes catalysed by sulphided CoMo/Gamma-Al₂O₃, the reaction network. AIChE Journal 24: pp1015, 1978

Hu, S. Y.; Zhu, X. X., Molecular Modelling and Optimization for Catalytic Reforming, Chem. Eng. Commun, 191, pp500–512, 2004

Hudebine, D., Vera, C., Wahl, F., Verstraete, J. J., Molecular representation of hydrocarbon mixtures from overall petroleum analysis, In AIChE 2002 Spring Meeting, pp 27a

Hudebin, D., Verstraete, J. J. (2004), Molecular reconstruction of LCO gasoils from overall petroleum analyses, Chemical Engineering Science, 59, pp4755 – 4763

Hudebine, D., Reconstruction molecular composition of petroleum, PhD Thesis, Ecole Normale Supérieure De Lyon, 2003

[Http://eur-lex.europa.eu/JOIndex.do](http://eur-lex.europa.eu/JOIndex.do) - Official Journal of the European Communities

International Energy Agency, World Energy Outlook, 2009

International Energy Agency, Oil Market Report, 2009

Jacob, S. M., Gross, B., Voltz, S. E., Weekman, V. W., A Lumping and Reaction
Linnhoff, B. and Hindmarsh, E.: The Pinch Design Method for Heat-Exchanger
Networks. Chemical Engineering Science 38: pp745-763, 1983

Jabr, N.; Alatiqi, I. M.; Fahim, M. A., An Improved Characterization Method for
Petroleum Fractions, Can. J. Chem. Eng., 70, pp765 – 773, 1992

James, The Times Science Review, Summer , 1966

Jenkins J. H., Stephens T.W., Kinetics of catalytic reforming, Hydrocarbon Proc.,
1 (59), pp163-167, 1980

Johansen, N.G., Etter, L.S., Miller, R.L., Quantitative analysis of hydrocarbons in
gasolines by capillary gas-liquid Chromatography II: Isothermal and temperature-
programmed analysis, pp177-190 in Journal of Chromatography, (346) 1985.

Joback, K. G., Reid, R.C.: Estimation of pure-component properties from group-
contributions. Chemical Engineering Communications 57: pp233 - 243, 1987

Katz, D. L.; Brown, G. G. Vapour pressure and vaporisation of petroleum
fractions, Ind. Eng. Chem., 25, pp1373 – 1384, 1933

Katzer, J., M. Ramage, A. Sapre, Petroleum Refining: Poised for Profound
Changes, Chem. Eng. Process., pp41–51, 2000

Kirkpatrick, S., Gellat, C.D., Vecchi, M.P.: Optimisation by simulated annealing.
Science 220 (4598): pp671 - 680, 1983

Klein, M. T., Hou, G., Bertolacini, R. J., Broadbelt, L. J., Kumar, A.: Molecular
modelling in heavy hydrocarbon conversions, 2006

Kmak, W.S., A Kinetic Simulation Model of the Power Forming Process; AIChE
Meeting, Houston, TX, 1972

- Korre, S. C., Klein, M. T., Quann, R. J.: Effect of Temperature on Quantitative Structure-Reactivity Correlations for Hydrocracking Polynuclear Aromatics. Abstracts of Papers of the American Chemical Society 210: 120-Fuel, 1995
- Korre, S. C., Klein, M. T., Quann, R. J.: Polynuclear Aromatic hydrocarbons hydrogenation. 1. Experimental reaction pathways and kinetics. Industrial & engineering chemistry research 34: pp101-117, 1995
- Korre, S. C., Neurock, M., Klein, M. T., Quann, R. J.: Hydrogenation of polynuclear aromatic hydrocarbons. 2. quantitative structure/reactivity correlations. Chemical Engineering Science 49: pp4191, 1994
- Korsten, H., Hoffmann, U., Three-phase reactor model for hydrotreating in pilot trickle-bed reactors. AIChE Journal, 42, pp1350-1360, 1996
- Krane, H. G.; Groh, A. B.; Shulman, B. D.; Sinfeit, J. H. Proceedings of the 5th world Petroleum Congress, pp39 – 51, 1959
- Landau, M. V., Herskowitz, M., Givoni, D., Laichter, S., Yitzhaki, D., Medium Severity Hydrotreating and Hydrocracking of Israeli Shale Oil, Fuel, Vol.77, No. 14, pp1589, 1998
- Lappas, Production of reformulated gasoline in the FCC unit. Effect of feedstock type on gasoline composition, Catalysis Today, 50, pp73-85, 1999
- Lee, B. I., Kesler, M.G.: A generalised thermodynamic correlation based on three-parameter corresponding states. AIChE Journal 21: pp510, 1975
- Libanati, C., Monte Carlo simulation of complex reactive macromolecular systems, Ph.D. dissertation, University of Delaware, Newark, 992
- Liguras, D. K., Allen, D. T., Structural models for catalytic cracking. 1. Model compound reactions. Industrial & Engineering Chemistry Research, 28, pp665, 1989a

Linguras, D. K., Allen, D. T., Structural models for catalytic cracking. 2. Reactions of simulated oil mixtures. *Industrial & Engineering Chemistry Research*, 28, pp674, 1989b

Linnhoff, B., Hindmarsh, E., The Pinch Design Method for Heat-Exchanger Networks. *Chemical Engineering Science* 38: pp745-763, 1983

Liu, F., Hallale, N.: Refinery hydrogen management for clean fuels production. *Advances in environmental research* 6: pp81-98, 2001

Liu, F.: Hydrogen integration in oil refineries. Department of process integration, UMIST, Manchester, 2002

Liu, F., Zhang, N.: Strategy of purifier selection and integration in hydrogen networks. *Chemical engineering research and design* 82: pp1315-1330, 2004

Lugo, H.J., Correlations between Octane Numbers and Catalytic Cracking Naphtha Composition, *Industrial & Engineering Chemistry Research*, 38 (5), pp 2171–2176, 1999

Lukszo, Z., Salverda, M., Bosman, P., A decision support tool for Process Optimisation of Sulphur Free Diesel Production, 16th European Symposium on Computer Aided Process Engineering and 9th International Symposium on Process Systems Engineering, 2006

Marin, G.B.; Froment, G.F., The Development and Use of Rate Equations for Catalytic Refinery Processes; *EFCE Publ. Ser.*, Vol 2. , No.27, C 117, 1983

Marafi, A., Al-Hendi, A., Al-Mutawa, A., Stanislaus, A., Studies on hydrotreating of diesel streams from different Kuwait crudes for ultralow sulfur diesel production. *Energy & Fuels*, 21, pp3401-3405, 2007

Martin, A. J. P., Synge R. L. M., A new form of chromatogram employing two liquid phases, *Biochem. J.*, 35, pp1358, 1941

Matisová, E.; Krupčik, J; Quantitative analysis of hydrocarbons in gasolines by capillary gas-liquid chromatography, *Journal of Chromatography*, 346, pp177-190, 1985

Mederos, F., J. Ancheyta, Mathematical modelling and simulation of hydrotreating reactors: Cocurrent versus counter current operations. *Applied Catalysis A – General*, 332, pp8-21., 2007

Meusinger, R., Gasoline analysis by ¹H nuclear magnetic resonance spectroscopy, pp1235-1243 in *Fuel*, Vol. 75, No.10, 1996

Meyers, R. A., *Handbook of petroleum refining processes*, 3rd edition, McGraw-Hill, 2004

Morris, W. E., The interaction approach to gasoline blending, NPRA 73rd Annual Meeting, Paper no. AM-75-30, Mar., 1975.

Muller, A., New method produces accurate octane blending values, *Oil and Gas Journal*, March 23, pp80-90, 1992

Neurock, M.; Nigam, A.; Libanati, C.; Klein, M. T. Monte Carlo Simulation of Complex Reaction Systems: Molecular Structure and Reactivity in Modelling Heavy Oils. *Chem. Eng. Sci.*, 45, pp2083 – 2088, 1990

Neurock, M.; Nigam, A.; Trauth, D.; Klein, M. T. Molecular Representation of Complex Hydrocarbon Feedstocks through Efficient Characterisation and Stochastic Algorithms. *Chem. Eng. Sci.*, 49, pp4153 – 4177, 1994

Nylén, U., Delgado, J., Jaras, S., Boutonnet, M., Characterization of alkylated aromatic sulphur compounds in light cycle oil from hydrotreated vacuum gas oil using GC-SCD. *Fuel Processing Technology*, 86, pp223-234, 2004

Oka, M., Chang, H.C., Gavales, G.R., Computer-assisted molecular structure construction for coal-derived compounds, pp3-8, *Fuel*, (56) 1977.

Padmavathi G., Chaudhuri, K.K., Modelling and simulation of commercial catalytic naphtha reformers, *Can. J. Chem. Eng.*, 75 (10), pp930, 1997

- Pederson, K.S., Blilie, A.L., Meisingset, K.K., PVT calculations of petroleum reservoir fluids using measured and estimated compositional data for the plus fraction, *Industrial & Engineering Chemistry Research*, 31, pp1378 – 1384, 1992
- Peng, B.: *Molecular modelling of refinery processes*. UMIST, Manchester, 1999
- Petrakis, L., Allen, D., Gavalas, G.R., Gates, B.C., Functional group analysis of synthetic fuels, Page 1557 in *Analytical Chemistry*, (55) 1983
- Pille, R. C., Froment, G. F. Kinetic study of the hydrogen sulphide effect in the conversion of thiophene on supported Co-Mo catalysts, *Journal of Molecular Catalysis*, 94, pp369-387, 1994
- Pinto, J. M.; Joly, M., Moro, L. F. L., Planning and scheduling models for refinery operations, *Computers and Chemical Engineering*, 24, pp2259-2276, 2000
- Prausnitz, J. M., Poling, B. E., O'Connell, J. P.: *The properties of gases and liquids*. 5th edition: McGraw-Hill: New York, 2001
- Quann, R.J., Jaffe, S.B., Structural-oriented lumping: describing the chemistry of complex mixtures, *Industrial & Engineering Chemistry Research*, (31) 1992: pp2483-2497
- Quann, R. J., Jaffe, S. B., Building Useful Models of Complex Reaction Systems in Petroleum Refining, *Chem. Eng. Sci.*, 51(10), pp1615, 1996
- Rahimpour M.R., Esmailian S., Bagheri-Ghaleghazi N., A kinetic and activation model for industrial catalytic naphtha reforming, *Iranian J. Sc. & Tech. Transition B*, 27 (B2), pp280, 2003
- Read, R.C., *The Enumeration of Acyclic Chemical Compounds*. Chemical Applications of Graph Theory, A.T. Academic Press, Inc., 1976.
- Reid, C. R., Prausnitz, J. M., Poling, B. E., *The properties of Gases & Liquids*, McGraw-Hill, New York, 1987
- Riazi, M. R.: *Characterisation and properties of petroleum fractions*. ASTM International, Philadelphia, PA, 2005

- Riazi, M. R. A Distribution Model for C7+ Fractions Characterization of Petroleum Fluids, *Industrial and Engineering Chemistry Research*, Vol.36, pp4299 – 4307, 1997
- Rice, R. G., Do, D. D., *Applied Mathematics and Modelling for Chemical Engineers*, John Wiley & Sons, 1995
- Robert A. M., *Handbook of Petroleum Refining Processes*, Third Edition, McGraw-Hill Handbooks, 2003
- Rodriguez, M. A., Ancheyta, J., Modelling of hydrodesulfurization (HDS), hydrodenitrogenation (HDN), and the hydrogenation of aromatics (HDA) in a vacuum gas oil hydrotreater. *Energy & Fuels*, 18, pp789-794, 2004
- Ronmanow-Garcia, S., Cleaner fuels-it's just not that simple, Editorial column in *Hydrocarbon Processing*. Vol. 79, No.9, September 2000
- Rusin, M. H., Chung, H. S., Marshall, J. F., A transformation method for calculating the research and motor octane numbers of gasoline blends, *Industrial Engineering Chemistry Fundamentals*, 20, 1981
- Scott, E. J. Y. Knock Characteristics of Hydrocarbon Mixtures. *Proc. API DiV. Refin.* 1958, 38, 90
- Shah, Y. T., *Gas-Liquid-Solid Reactor Design*, McGraw-Hill, New York, 1979
- Shibata, S.K., Sandler, S.I., Behrens, R.A., Phase equilibrium calculations for continuous and semi-continuous mixtures, *Chem. Eng. Sci.*, 42, pp1977-1988, 1987
- Simon, C. C., *Managing the molecule II*, Foster Wheeler technical papers, 2001
- Simon, C. C., *Managing the molecule-refining in the next millennium*, Foster Wheeler Energy Ltd. 2007
- Singh, B. B.: Impact of gas phase impurities on refinery hydrogen network management. *Process integration research consortium*, Manchester, 2000

- Smith, R.B., Kinetic analysis of naphtha reforming with platinum catalyst. Chem. Eng. Progr., 55(6): pp76-80, 1959
- Sotelo-Boyas, R., Froment, G.F., Fundamental Kinetic Modelling of Catalytic Reforming, Industrial & Engineering Chemistry Research, 2009, 48 (3), pp1107–1119
- Stanislaus, A., Cooper, B.H., Aromatic hydrogenation catalysis: a review, Catalysis Review Science and Engineering 36, pp75–123, 1994
- Stewart, W.E., Predict octanes for gasoline blends, Petroleum Refiner, 38, pp135–139, 1959
- Stull, D. R., Westrum, E. F., Sinke, G. C., The Chemical Thermodynamics of Organic Compounds, Wiley, New York, 1969.
- Sun, J.: Molecular modelling and integration analysis of hydroprocessors. PhD thesis, University of Manchester, 2004
- Swain, E. J., US refining crude slates continue towards heavier feeds, high sulphur contents. Oil & Gas J. 96(40): pp43-47, 1998
- Tamm P. W., Harnsberger H. P. and Bridge A. G., Ind. Eng. Chem. Proc. Des. Dev., 20, pp262, 1981.
- Taskar, U., Riggs, J.B., Modelling and optimization of a semiregenerative catalytic naphtha reformer, AIChE J. **43**, pp740–753, 1997
- Teng, S. T., Williams, A. D., Urdal, K.: Detailed hydrocarbon analysis of gasoline by GC-MS (SI-PIONA). Journal of high resolution chromatography 17, 1994
- Towler, G. P., Mann, R., Serriere, A.J., Gabaude, C.M.D., Refinery hydrogen management: Cost analysis of chemically integrated facilities. Industrial and engineering chemistry research 35: pp2378-2388, 1996
- Turpin L.E., Modelling Commercial Reformers, Marcel Dekker, New York, 1995.

Twu, C. H.; Coon, J. E., Estimate octane numbers using an enhanced method, *Hydrocarbon Process. Int. Ed.*, 76, 65, 1997

Van Geem K.M., Hudebine D., Reyniers M.F., Wahl F., Verstraete J.J., Marin G.B., Molecular reconstruction of naphtha steam cracking feedstocks based on commercial indices, *Computers and Chemical Engineering*, 31(9), pp1020-1034, 2007

Van Leeuwen, J. A.; Jonker, R. J.; Gill, R., Octane number prediction based on gas chromatographic analysis with nonlinear regression techniques. *Neth. Chem. Intell. Lab. Syst.*, 25, 325, 1994

Van Parijs, I. A., Hosten, L. H., Froment, G. F.: Kinetics of hydrodesulphurisation on a CoMo/Al₂O₃ catalyst. 2. Kinetics of the hydrogenolysis of benzothiophene. *Industrial & engineering chemistry product research & development* 25: pp437, 1986

Van Trimpont, P.A., Marin, G.B., Froment, G.F., Reforming of C₇ Hydrocarbons on a Sulfided Commercial Pt/Al₂O₃ Catalyst. *Industrial & Engineering Chemistry Research* 27, pp51–57, 1988

Vanparijs, I. A., Froment, G. F., Kinetic of Hydrodesulfurization on a CoMo/Gamma-Al₂O₃ Catalyst 1. Kinetics of the Hydrogenolysis of Thiophene. *Industrial & Engineering Chemistry Product Research and Development*, 25, pp431-436, 1986

Vanrysselberghe, V., Froment, G. F., Hydrodesulfurization of dibenzothiophene on a CoMo/Al₂O₃ catalyst: Reaction network and kinetics. *Industrial & Engineering Chemistry Research*, 35, pp3311-3318, 1996

Vanrysselberghe, V., Froment, G. F., Kinetic modelling of hydrodesulfurization of oil fractions: Light cycle oil. *Industrial & Engineering Chemistry Research*, 37, pp4231-4240, 1998

Vanrysselberghe, V., R. Le Gall, Froment, G. F., Hydrodesulfurization of 4-methyldibenzothiophene and 4,6-dimethyldibenzothiophene on a CoMo/Al₂O₃

catalyst: Reaction network and kinetics. *Industrial & Engineering Chemistry Research*, 37, pp1235-1242, 1998

Vazques-Esparragoza, J.J., Iglesias-Silva, G.A., Hlavinka, M.W., Bullin, J., How to estimate RVP of blends, *Hydrocarbon Processing*, August, pp135-138, 1992

Vrinat, M. L., The Kinetics of the Hydrodesulphurisation Process: A Review, *Appl. Catal.* 6, pp137, 1983.

Wahl, F., Hudebine, D., Verstratete, J. J., Reconstruction of the molecular composition of FCC Gasolines from overall petroleum analyses, *Oil and Gas Science and Technology – Review IFP*, 2002

Wammes, W. J. A., Mechielsen, S. J., Westerterp, K. R., The Transition between Trickle Flow and Pulse Flow in a Cocurrent Gas-Liquid Trickle-Bed Reactor at Elevated Pressures. *Chem. Eng. Sci.*, 45, pp3149, 1990

Warquier, J.-P. *Petroleum Refining*; Editions Technip: Paris, 1995; vol. 1

Watkins, T. N. *Petroleum Refinery Distillation*, 2nd ed., Gulf publishing company: Houston, 1979

Weekman, V. W., Lumps, Models and Kinetics in Practice, *Chem. Eng. Prog. Monogr. Ser.*75, 1979

Wei, W.; Bennett, C. A.; Tanaka, R.; Hou, G.; Klein, M. T. J.; Klein, M. T., Computer Aided Kinetic Modelling with KMT and KME. *Fuel Process. Technol.*, 89, pp350–363, 2008

Whitson, C.H., Characterizing hydrocarbon plus fractions, *Soc. Pet. Eng. J.*, 683, 1990

Zhang, J., Refinery optimisation and debottlenecking, Ph.D. thesis, UMIST 1999

Zhang, N. Optimisation is Key to High-performing Refineries, *Business Briefing: Oil & Gas Processing Review*, pp33 – 35, 2006

Zhang, N., Novel modelling and decomposition for overall refinery optimisation and debottlenecking, PhD thesis, UMIST, 2000

Zhang, Y.: Molecular modelling of petroleum processes. PhD thesis, UMIST, Manchester, 1999

Zhorov Y.M., Panchenkov G.M., Shapiro I.Y., Mathematical Model of platforming under stationary conditions with allowance for isomerization reactions, Khim. Technol. Topl. Mas., 15 (7), pp9, 1980

Appendix A Joback Group Contribution

Table A.1 Joback group contribution for boiling point and Gibbs energy

Property	tbk	Gfk
Units	K	cal/mol
Group k		
CH3(1)	23.58	-43.96
CH2(2)	22.88	8.42
CH(3)	21.74	58.36
C(4)	18.25	116.02
=CH2(1)	18.18	3.77
=CH(2)	24.96	48.53
=C(3)	24.14	92.36
=C=(2)	26.15	136.7
≡CH(1)	9.2	77.71
≡C(2)	27.38	109.82
CH2(ss)(2)	27.15	-3.68
CH(ss)(3)	21.78	40.99
C(ss)(4)	21.32	87.88
=CH(ds)(2)	26.73	11.3
=C(ds)(3)	31.01	54.05
NH2(1)	73.23	14.07
NH(2)	50.17	89.39
NH(ss)(2)	52.82	75.61
N(3)	11.74	163.16
=N-(2)	74.6	X
=N-(ds)(2)	57.55	79.93
=NH(1)	X	119.66
SH(1)	63.56	-22.99
S(2)	68.78	33.12
S(ss)(2)	52.1	27.76

Appendix B Parameters of Kinetic Model of Catalytic Reformer

Table B.1 Factors for pressure effect (Ancheyta, 1994)

Reaction k	α_k
isomerisation	0.370
dehydrocyclization	-0.700
hydrocracking	0.433
hydrodealquilation	0.500

Table B.2 Activation energies for each reforming reaction (Henningsen, 1970)

Reaction j	EA _j (kcal/mol)
paraffins	
$P_n \rightarrow N_n$	45
$P_n \rightarrow P_{n-I} + P_i$	55
naphthenes	
$N_n \rightarrow A_n$	30
$N_n \rightarrow N_{n-I} + P_i$	55
$N_n \rightarrow P_n$	45
aromatics	
$A_n \rightarrow A_{n-i} + P_i$	40
$A_n \rightarrow P_n$	45
$A_n \rightarrow N_n$	30

Table B.3 Kinetic constants of the model (Ancheyta, 2000)

Reaction step	<i>k</i>	reaction step	<i>k</i>	reaction step	<i>k</i>
P11->N11	0.0356	P8->P4	0.007	N8->N7 + P1	0.0007
P10->N10	0.0243	P7->P6 + P1	0.0027	N11->A11	0.6738
P9->N9	0.05	P7->P5 + P2	0.0018	N10->A10	0.3198
P8->N8	0.0266	P7->P4 + P3	0.0043	N9->A9	0.2205
P7->N7	0.0076	P6->P5 + P1	0.0018	N8->A8	0.215
P6->N6	0	P6->P4 + P2	0.0016	N7->A7	0.0788
P6->MCP	0.0042	P6->2P3	0.0025	N6->A6	0.1368
P11->P10+P1	0.0075	P5->P4 + P1	0.0018	A11->P11	0.0016
P11->P9 + P2	0.01	P5->P3 + P2	0.0022	A10->P10	0.0016
P11->P8 + P3	0.0135	N11->P11	0.005	A9->P9	0.0016
P11->P7 + P4	0.0135	N10->P10	0.0054	A8->P8	0.0011
P11->P6 + P5	0.0191	N9->P9	0.0054	A7->P7	0.0016
P10->P9 + P1	0.0015	N8->P8	0.0025	A11->A10 + P1	0.0006
P10->P8 + P2	0.0054	N7->P7	0.0019	A11->A9 + P2	0.0006
P10->P7 + P3	0.016	N6->P6	0.0204	A10->A9 + P1	0.0006
P10->P6 + P4	0.0095	MCP->P6	0.0008	A1->A8 + P2	0.0006
P10->2P5	0.0095	N11->N10+P1	0.0134	A10->A7 + P3	0
P9->P8 + P1	0.003	N11->N9 + P2	0.0134	A9->A8 + P1	0.0005
P9->P7 + P2	0.0039	N11->N8 + P3	0.008	A9->A7 + P2	0.0005
P9->P6 + P3	0.0068	N10->N9 + P1	0.0134	A8->A7 + P1	0.0001
P9->P5 + P4	0.0058	N10->N8 + P2	0.0134	A6->N6	0.0015
P8->P7 + P1	0.0019	N10->N7 + P3	0.008	MCP->N6	0.0238
P8->P6 + P2	0.0056	N9->N8 + P1	0.0127	N6->MCP	0.004
P8->P5 + P3	0.0034	N9->N7 + P2	0.0127		

Appendix C Parameters of Group Contribution Approach

Table C.1 Numerical values for the structural contributions for (s)DBT at 573K (Froment, 2004)

Hydrogenolysis	Hydrogenation
$K_{ST,\sigma}(4;0;0) = 0.310$	$K_{EL+ST,\tau}(m;0;0) = 1.04$
$K_{ST,\sigma}(4;6;0) = 0.238$	$K_{EL+ST,\tau}(m;n;0) = 1.11$
$k_{ST,\sigma}(4;0;0) = 0.588$	$k_{EL+ST,\tau}(m;0;0) = 6.05$
$k_{ST,\sigma}(4;6;0) = 0.050$	$k_{EL+ST,\tau}(m;n;0) = 6.07$
$k_{EL,\sigma}(m;n;p) = 1.000$	
$K_{EL,\sigma}(m;n;p) = 1.000$	

The structural contributions approach also could be applied for benzothiophene. A methyl substituent in position 2 and/or 7 decreases the hydrogenolysis rate with respect to that of benzothiophene. This is due to the steric hindrance of the methyl groups on the vertical adsorption through the sulphur atom and the surface reaction between the adsorbed species on the σ -sites. A methyl group in position 2 is closer to the sulphur atom than a methyl group in position 7; therefore its effect on the hydrogenolysis rate is more pronounced than that of a methyl group in position 7. Methyl substituents in positions 3, 4, 5, and/or 6 have almost no influence on the hydrogenolysis rate compared to that of benzothiophene. The substituted benzothiophenes the presence of methyl groups leads to a higher adsorption equilibrium constant on the τ sites, regardless of their position. Furthermore, in benzothiophenes with a methyl group in position 2, the C2-C3 bond, which is hydrogenated before hydrogenolysis occurs, has a lower bond order than that in benzothiophene.

Table C.2 Rate and adsorption parameters related to HDS of DBT (Froment, 2008)

Parameter	Units
$k_{DBT,\sigma} = 2.44336 \times 10^{10} \exp \left[\frac{-122.770 \times 10^3}{R_{gas} T} \right]$	kmol/kg _{cat} h
$K_{H,\sigma} = 3.36312 \times 10^{-11} \exp \left[\frac{113.232 \times 10^3}{R_{gas} T} \right]$	m ³ /kmol
$K_{DBT,\sigma} = 7.56868 \times 10^1$	m ³ /kmol
$k_{DBT,\tau} = 2.86757 \times 10^{16} \exp \left[\frac{-186.190 \times 10^3}{R_{gas} T} \right]$	kmol/kg _{cat} h
$K_{H,\tau} = 1.40255 \times 10^{-15} \exp \left[\frac{142.693 \times 10^3}{R_{gas} T} \right]$	m ³ /kmol
$K_{DBT,\tau} = 2.50395 \times 10^{-7} \exp \left[\frac{76.840 \times 10^3}{R_{gas} T} \right]$	m ³ /kmol
$K_{H2S,\sigma} = 1.47118 \times 10^{-8} \exp \left[\frac{105670}{R_{gas} T} \right]$	m ³ /kmol

This is also true for benzothiophenes with a methyl group in position 3. Methyl groups in the positions 4, 5, 6 and/or 7 increase the hydrogenation rate compared to that of benzothiophene. Based on these information, the structural contributions were estimated as follows (Vanrysselberghe and Froment, 1998):

$$f_{2,\sigma} = k_{EL,\sigma}^{sBT}(m;0;0;0)K_{EL,\sigma}^{sBT}(m;0;0;0)k_{ST,\sigma}^{sBT}(2;0;0;0)K_{ST,\sigma}^{sBT}(2;0;0;0) = 3.84047 \times 10^{-2} \exp \left[\frac{2745}{R_{gas} T} \right]$$

$$f_{3,\sigma} = f_{4,\sigma} = f_{5,\sigma} = f_{6,\sigma} = k_{EL,\sigma}^{sBT}(m;0;0;0)K_{EL,\sigma}^{sBT}(m;0;0;0) = 4.81232 \times 10^1 \exp \left[-\frac{17896}{R_{gas} T} \right]$$

$$f_{7,\sigma} = k_{EL,\sigma}^{sBT}(m;0;0;0)K_{EL,\sigma}^{sBT}(m;0;0;0)k_{ST,\sigma}^{sBT}(7;0;0;0)K_{ST,\sigma}^{sBT}(7;0;0;0) = 3.20070 \times 10^{-3} \exp \left[\frac{17073}{R_{gas} T} \right]$$

$$f_{2,\tau} = k_{EL,\tau}^{sBT}(m;0;0;0)K_{EL,\tau}^{sBT}(m;0;0;0)k_{ST,\tau}^{sBT}(2;0;0;0)K_{ST,\tau}^{sBT}(2;0;0;0) = 8.37053 \times 10^1 \exp \left[-\frac{26327}{R_{gas} T} \right]$$

$$f_{3,\tau} = k_{EL,\tau}^{sBT}(m;0;0;0)K_{EL,\tau}^{sBT}(m;0;0;0)k_{ST,\tau}^{sBT}(3;0;0;0)K_{ST,\tau}^{sBT}(3;0;0;0) = 2.33432 \times 10^0 \exp\left[-\frac{9932}{R_{gas}T}\right]$$

$$f_{4,\tau} = f_{5,\tau} = f_{6,\tau} = f_{7,\tau} = k_{EL,\tau}^{sBT}(m;0;0;0)K_{EL,\tau}^{sBT}(m;0;0;0) = 1.24161 \times 10^1 \exp\left[-\frac{9903}{R_{gas}T}\right]$$

As for the adsorption equilibrium constants for P, N, A, AA and AN are assumed as zero, which is confirmed by Froment (Froment, 1998).

Appendix D Physical Properties Calculation

In terms of the calculation of heat capacity of pure real compounds, procedure 7D3.6 (1997) from American Petroleum Institute (API) technical data book is successfully applied. The equation to be used is

$$\left(\frac{\tilde{C}_p^0 - \tilde{C}_p}{R} \right) = \left(\frac{\tilde{C}_p^0 - \tilde{C}_p}{R} \right)^{(0)} + \frac{\omega}{\omega^{(h)}} \left[\left(\frac{\tilde{C}_p^0 - \tilde{C}_p}{R} \right)^{(h)} - \left(\frac{\tilde{C}_p^0 - \tilde{C}_p}{R} \right)^{(0)} \right] \quad (\text{D.1})$$

where:

$\left(\frac{\tilde{C}_p^0 - \tilde{C}_p}{R} \right)$ = the dimensionless effect of pressure on isobaric heat capacity;

$\left(\frac{\tilde{C}_p^0 - \tilde{C}_p}{R} \right)^{(0)}$ = effect of pressure on the isobaric heat capacity for the simple fluid, to

be calculated from Equation D.2

$\left(\frac{\tilde{C}_p^0 - \tilde{C}_p}{R} \right)^{(h)}$ = effect of pressure on the isobaric heat capacity for the heavy reference

fluid, to be calculated from Equation D.2.

ω = acentric factor of the compound for which the pressure effect on isobaric heat capacity is sought

$\omega^{(h)}$ = acentric factor of the heavy reference fluid = 0.3978

The dimensionless effect of pressure on the isobaric heat capacity of the simple and heavy fluid is to be calculated from the following equations:

$$\left(\frac{\tilde{C}_p^0 - \tilde{C}_p}{R}\right)^{(i)} = 1 + \frac{T_r \left(\frac{\partial p_r}{\partial T_r}\right)_{V_r}^2}{\left(\frac{\partial p_r}{\partial V_r}\right)_{T_r}} + \left(\frac{\Delta \tilde{C}_V}{R}\right)^{(i)} \quad (\text{D.2})$$

Where

$$\left(\frac{\partial p_r}{\partial T_r}\right)_{V_r} = \frac{1}{V_r} \left\{ 1 + \frac{b_1 + b_3/T_r^2 + 2b_4/T_r^3}{V_r} + \frac{c_1 - 2c_3/T_r^3}{V_r^2} + \frac{d_1}{V_r^5} - \frac{2c_4}{T_r^3 V_r^2} \left[\left(\beta + \frac{\gamma}{V_r^2} \right) \exp\left(-\frac{\gamma}{V_r^2}\right) \right] \right\}$$

$$\left(\frac{\partial p_r}{\partial V_r}\right)_{T_r} = -\frac{T_r}{V_r^2} \left\{ 1 + \frac{2B}{V_r} + \frac{3C}{V_r^2} + \frac{6D}{V_r^5} + \frac{c_4}{T_r^3 V_r^2} \left(3\beta + \left\{ 5 - 2 \left(\beta + \frac{\gamma}{V_r^2} \right) \right\} \frac{\gamma}{V_r^2} \right) \exp\left(-\frac{\gamma}{V_r^2}\right) \right\}$$

$$\left(\frac{\Delta \tilde{C}_V}{R}\right)^{(i)} = \left(\frac{\tilde{C}_V^0 - \tilde{C}_V}{R}\right)^{(i)} \text{ which can be calculated by the following equations.}$$

$$\left(\frac{\tilde{C}_V^0 - \tilde{C}_V}{R}\right) = \left(\frac{\tilde{C}_V^0 - \tilde{C}_V}{R}\right)^{(0)} + \frac{\omega}{\omega^{(h)}} \left[\left(\frac{\tilde{C}_V^0 - \tilde{C}_V}{R}\right)^{(h)} - \left(\frac{\tilde{C}_V^0 - \tilde{C}_V}{R}\right)^{(0)} \right] \quad (\text{D.3})$$

The effect of pressure on the isochoric heat capacity for the simple and heavy fluid can be calculated by Equation D.4.

$$\left(\frac{\tilde{C}_V^0 - \tilde{C}_V}{R}\right)^{(i)} = -\frac{2(b_3 + 3b_4/T_r)}{T_r^2 V_r} + \frac{3c_3}{T_r^3 V_r^2} + 6 \frac{c_4}{2T_r^3 \gamma} \left\{ \beta + 1 - \left(\beta + 1 + \frac{\gamma}{V_r^2} \right) \exp\left(-\frac{\gamma}{V_r^2}\right) \right\} \quad (\text{D.4})$$

In those equations, $T_r = T/T_c$ is the reduced temperature, $V_r = p_c V / RT_c$ is obtained by solving Equation D.5.

$$\frac{p_r V_r}{T_r} = 1 + \frac{B}{V_r} + \frac{C}{V_r^2} + \frac{D}{V_r^5} + \frac{c_4}{T_r^3 V_r^2} \left(\beta + \frac{\gamma}{V_r^2} \right) \exp\left(-\frac{\gamma}{V_r^2}\right) \quad (\text{D.5})$$

Where

$$p_r = p/p_c = \text{the reduced pressure, } B = b_1 - b_2/T_r - b_3/T_r^2 - b_4/T_r^3, \\ C = c_1 - c_2/T_r + c_3/T_r^3, D = d_1 + d_2/T_r.$$

Two sets of constants are given below, one for the simple fluid, and the other for heavy reference fluid.

Table D.1 Constants for the simple and heavy reference fluid

Constant	Simple fluid	Heavy reference fluid
b_1	0.1181193	0.2026579
b_2	0.265728	0.331511
b_3	0.154790	0.027655
b_4	0.030323	0.203488
C_1	0.0236744	0.0313385
c_2	0.0186984	0.0503618
C_3	0.0	0.016901
C_4	0.042724	0.041577
$d_1 \times 10^4$	0.155488	0.48736
$d_2 \times 10^4$	0.623689	0.0740336
β	0.65392	1.266
γ	0.060167	0.03754

Equation D.5 is solved iteratively for Vr . The problem is that without a proper bound and initial guess on Vr , the iterative procedure always fails to find the solution. In order to get a proper bound, a Lee-kesler table (Lee and Kesler, 1975) is successfully applied combining a bisection method to find the solution.

Chung (1988) developed an empirically correlated function of density and temperature for viscosity of dense fluids as Equation D.6.

$$\mu = \mu_x + \mu_p \quad (D.6)$$

Where

$$\mu_x = \mu_0 \left[\frac{1}{G_2} + A_6 Y \right]$$

$$\mu_p = \left[36.344 \times 10^{-6} \frac{(MT_C)^{1/2}}{V_C^{2/3}} \right] A_7 Y^2 G_2 \exp \left(A_8 + \frac{A_9}{T^*} + \frac{A_{10}}{T^{*2}} \right)$$

$$\mu_0 = 4.0785 \times 10^{-5} \frac{(MT)^{1/2}}{V_C^{2/3} \Omega^*} F_C$$

$$F_C = 1 - 0.2756\omega$$

$$\Omega^* = \frac{A}{T^{*B}} + \frac{C}{\exp(DT^*)} + \frac{E}{\exp(FT^*)} + GT^{*B} \sin(ST^{*W} - H)$$

$$A = 1.16145, B = 0.14874, C = 0.52487, D = 0.77320, E = 2.16178, F = 2.43787, G = -6.435 \times 10^{-4}$$

$$H = 7.27371, S = 18.0323, W = -0.76830$$

$$T^* = \frac{1.2593T}{T_C}$$

$$Y = \frac{\rho V_C}{6}$$

$$G_1 = \frac{1.0 - 0.5Y}{(1 - Y)^3}$$

$$G_2 = \frac{\{A_1[1 - \exp(-A_4Y)]/Y + A_2G_1 \exp(A_3Y) + A_3G_1\}}{A_1A_4 + A_2 + A_3}$$

$$A_i = a_0(i) + a_1(i)\omega$$

Table D.2 Constants used for the generalised viscosity correlation

i	$a_0(i)$	$a_1(i)$
1	6.32402	50.41190
2	0.12102×10^{-2}	-0.0011536
3	5.28346	254.20900
4	6.62263	38.09570
5	19.74540	7.63034
6	-1.89992	-12.53670
7	24.27450	3.44945
8	0.79716	1.11764
9	-0.23816	0.067695
10	0.068629	0.34793

The same approach was employed by Chung (1988) to develop the thermal conductivities of pure fluids and mixtures. The equation is an empirically correlated function as Equation D.7.

$$k = k_{\kappa} + k_p \quad (\text{D.7})$$

Where

$$k_{\kappa} = k_0 \left[\frac{1}{H_2} + B_6 Y \right]$$

$$k_0 = 7.452 \frac{\mu_0}{M} \Psi$$

$$\Psi = 1 + \alpha \frac{0.215 + 0.28288\alpha - 1.0161\beta + 0.26665Z}{0.6366 + \beta Z + 1.061\alpha\beta}$$

$$\alpha = \frac{C_v^0}{R} - \frac{3}{2}$$

$$\beta = 0.7862 - 0.7109\omega + 1.3168\omega^2$$

$$Z = 2.0 + 10.5T_r^2$$

$$C_v = C_p - R$$

$$k_p = 3.039 \times 10^{-4} \frac{(T_c/M)^{1/2}}{V_c^{2/3}} B_7 Y^2 H_2 T_r^{1/2}$$

$$H_2 = \frac{B_1 [1 - \exp(-B_4 Y)] / Y + B_2 G_1 \exp(B_5 Y) + B_3 G_1}{B_1 B_4 + B_2 + B_3}$$

$$B_i = b_0(i) + b_1(i)\omega$$

b_0, b_i are given in Table D.3.

Table D.3 Constants used for the generalised correlation for thermal conductivity

i	$b_0(i)$	$b_1(i)$
1	2.41657	0.74824
2	-0.50924	-1.50936
3	6.61069	5.62073
4	14.54250	-8.91387
5	0.79274	0.82019
6	-5.86340	12.80050
7	81.17100	114.15800

It is necessary to know the molecular diffusivity D_i^L in the liquid which would be used to calculate the mass transfer coefficients. Assuming infinite dilution, the diffusivity can be estimated by a Tyn-Calus correlation (Reid et al., 1987) as equation D.8.

$$D_i^L = 8.93 \times 10^{-8} \frac{v_L^{0.267} T}{v_i^{0.433} \mu_L} \quad (\text{D.8})$$

Gas-liquid mass transfer coefficient is the function of the liquid superficial mass flow velocity, G_L . For its determination, the correlation developed by Goto and Smith (1975) is used as Equation D.9.

$$\frac{K_L a_L}{D_i^L} = 7 \left(\frac{G_L}{\mu_L} \right)^{0.4} \left(\frac{\mu_L}{\rho_L D_i^L} \right)^{1/2} \quad (\text{D.9})$$

The liquid-solid mass transfer in the low interaction regime can be estimated by the van Krevelen-Krekels equation (1948) as Equation D.10.

$$\frac{k_s}{D_i^L a_s} = 1.8 \left(\frac{G_L}{a_s \mu_L} \right)^{1/2} \left(\frac{\mu_L}{\rho_L D_i^L} \right)^{1/3} \quad (\text{D.10})$$

Where a_s is the specific surface area of the packing.

$$a_s = \frac{6}{d_p} (1 - \varepsilon) \quad (\text{D.11})$$

where d_p is the equivalent particle diameter, and ε is the void fraction of the catalyst bed.

By postulating that “the ratio of the momentum lost by skin friction between two sections a differential distance apart to the total momentum of the fluid will be the same as the ratio of the heat actually supplied by the surface to that which would have been supplied if the whole of the fluid had been carried up to the surface”, Chilton and Colburn (1934) developed an equation to correlate the mass and heat transfer coefficients as Equation D.12.

$$J_D = \frac{K_L}{u} \left(\frac{\mu}{\rho D_e} \right)^{2/3} = J_H = \frac{h_L}{C_p \rho u} \left(\frac{C_p \mu}{k} \right) \quad (\text{D.12})$$

Appendix E Boundary Value Problem

As for boundary value problem, an approximate method – orthogonal collocation method is applied to solve the ordinary differential equations. Orthogonal collocation method is one of methods of weighted residuals (Rice, 1995). The method of weighted residuals has been used in solving a variety of boundary value problems, ranging from fluid flow to heat and mass transfer problems. It is popular because of the interactive nature of the first step, that is, the user provides a first guess at the solution and this is then forced to satisfy the governing equations along with the conditions imposed at the boundaries. The left-over terms, called residuals, arise because the chosen form of solution does not exactly satisfy either the equation or the boundary conditions. How these residual terms are minimized provides the basis for parameter or function selection. Of course, the optimum solution depends on the intelligent selection of a proposed solution.

$$\text{Min} \int_V R(x)w_k(x)dx \quad (\text{E.1})$$

The residual R is in general nonzero over the whole domain of interest, so that it will be dependent on x , in the usual case. V is the domain of interest, and w_k is some selected set of independent functions, which are called the test functions. Various methods of weighted residuals differ selecting the test functions. The collocation method use the Dirac delta function (Equation E.2) at N interior points (called collocation points) within the domain of interest.

$$w_k = \delta(x - x_k) \quad (\text{E.2})$$

where δ is the trial function, x_k is the k th collocation point.

The full potential of the collocation method can only be realised by judicious selection of the collocation points. Moreover, the choice of functions is critical.

orthogonal functions, such as Jacobi polynomials, are particularly attractive, since they are compact and contain only a few terms. If these N interior collocation points are chosen as roots of an orthogonal Jacobi polynomial of N th degree, the method is called the orthogonal collocation method.

The Jacobi polynomial of degree N has the power series representation

$$J_N^{(\alpha,\beta)}(x) = \sum_{i=0}^N (-1)^{N-i} \gamma_{N,i} x^i \quad (\text{E.3})$$

Here, $\gamma_{N,i}$ are constant coefficients, and α and β are parameters characterising the polynomials. $J_N^{(\alpha,\beta)}$ is the polynomial orthogonal with respect to the weighting function $x^\beta(1-x)^\alpha$.

The explicit solution for γ is as follows:

$$\gamma_{N,i} = \frac{N!}{i!(N-i)!} \frac{\Gamma(N+i+\alpha+\beta+1)\Gamma(\beta+1)}{\Gamma(N+\alpha+\beta+1)\Gamma(i+\beta+1)} \quad (\text{E.4})$$

To obtain the roots of Jacobi polynomial, which are collocation points, Newton-Raphson method is applied to solve the equations iteratively.

After obtaining the collocation points, an interpolation polynomial as Equation E.5 is used to calculate the corresponding y value at x point by assuming an unknown data set.

$$y_N(x) = \sum_{i=1}^{N+1} y_i l_i(x) \quad (\text{E.5})$$

Where y_N is the N degree polynomial, y_i is the value at point x_i , and $l_i(x)$ is called the Lagrange interpolation polynomial as Equation E.6.

$$l_i(x) = \prod_{\substack{j=1 \\ j \neq i}}^{N+1} \frac{x - x_j}{x_i - x_j} \quad (\text{E.6})$$

Then the first and second derivatives of the interpolation polynomial at the interpolation points are as Equations E.7 and E.8.

$$\frac{dy_N(x_i)}{dx} = \sum_{j=1}^{N+1} \frac{dl_j(x_i)}{dx} y_i \quad (\text{E.7})$$

$$\frac{d^2 y_N(x_i)}{dx^2} = \sum_{j=1}^{N+1} \frac{d^2 l_j(x_i)}{dx^2} y_i \quad (\text{E.8})$$

The function vector is defined as values of y at $N + 1$ collocation points as

$$y = [y_1, y_2, y_3, \dots, y_N, y_{N+1}]^T \quad (\text{E.9})$$

The first and second derivate vectors can be written in terms of the function vector y using matrix notation

$$y' = A \cdot y \quad (\text{E.10})$$

$$y'' = B \cdot y \quad (\text{E.11})$$

where

$$A = \left\{ a_{ij} = \frac{dl_j(x_i)}{dx}; i, j = 1, 2, \dots, N, N+1 \right\} \quad (\text{E.12})$$

$$B = \left\{ b_{ij} = \frac{d^2 l_j(x_i)}{dx^2}; i, j = 1, 2, \dots, N, N+1 \right\} \quad (\text{E.13})$$

By applying the orthogonal collocation method, Equation 5.31 is converted into a set of equations in terms of collocation points as Equation E.14.

$$F_i(y) = 4u_i \left[\sum_{j=1}^N b_{ij} y_j + b_{i,N+1} \right] + 6 \left[\sum_{j=1}^N a_{ij} y_j + a_{i,N+1} \right] - \phi^2 G(y_i) = 0 \quad (\text{E.14})$$

where:

$$u_i = \left(\frac{x_i}{R} \right)^2$$

$$y_i = \frac{C(x_i)}{C_s}$$

$$\phi^2 = \frac{\rho_s R^2}{D_e C_S} \sum_{k=1}^{N_r} S[k, m] r_k(C_S)$$

The Newton-Raphson method is applied to solve these equations iteratively to obtain the concentration profile in a catalyst particle.

Quadrature defines the process of expressing the continuous integral as an approximate sum of terms as Equation E.15.

$$\int W(x) f(x) dx \approx \sum_{k=1}^N w_k f(x_k) \quad (\text{E.15})$$

Effectiveness factor defined as Equation 5.34 is calculated by the Gauss-Jacobi quadrature technique (1995) as Equation E.16.

$$\eta = \frac{3}{2r(C^0)} \int_0^1 r(C_i) \sqrt{u} du = \frac{3}{2r(C^0)} \sum_{k=1}^{N+1} w_k r(C_k) \quad (\text{E.16})$$

where:

$$w_k = \int_0^1 u^{1/2} (1-u)^0 l_k(u) du$$

$$r(C) = \sum_{k=1}^N r(C_k) l_k(u)$$

w_k can be obtained using the properties of the Lagrangian interpolation polynomials.

Appendix F RFCC Model

This RFCC model is developed based on the FCC model published by HPI Consultants, Inc. The RFCC model takes into account the influence of an additional feed property – Conradson Carbon Residue, apart from the other properties that have already been considered in HPI correlations. The new model is then regressed using unpublished industrial data.

Data requirement

Conversion level, LV%	C
Feed specific gravity, 60°F/60°F	SG _f
Feed API gravity	API _f
Feed volumetric average boiling point, °F	VABP _f
Feed aniline point, °F	AP _f
Feed sulphur content, wt%	S _f
Feed characterisation factor	K _f
Feed Conradson carbon residue content, wt%	CCR _f

RFCC model

Feed quality parameter

$$FQP = 70 - 0.065VABP_f - 0.9S_f + 0.6AP_f - 0.26AP_f / SG_f - 0.15CCR_f$$

Yield of C3 to 400°F product, LV%

$$C3_400 = (-25.6 + 1.88C - 0.0076C^2)(0.0667 + 1.82FQP/100 - 0.762(FQP/100)^2)$$

Ratio of C5/400°F to C3/400°F

$$RGASO = 0.713 + 0.628FQP/100 - 0.738(FQP/100)^2 - 0.015CCR_f$$

Gasoline yield, LV%

$$GASOV = RGASO * C3_400$$

LPG yield, LV%

$$LPG = C3_400 - GASOV$$

Ratio of C4 LPG to C3 LPG

$$RC4_C3 = 1.879 + 0.272FQP/100 - 0.611(FQP/100)^2$$

C3 LPG yield, LV%

$$C3 = LPG(RC4_C3 + 1)$$

C4 LPG yield, LV%

$$C4 = LPG - C3$$

Ratio of propylene to total C3 LPG

$$RC_3^- _C3 = 0.001425FQP + 0.5864$$

Propylene yield, LV%

$$C_3^- = RC_3^- _C3 * C3$$

Propane yield, LV%

$$nC3 = C3 - C_3^-$$

Ratio of butylenes in C4

$$RC_4^- _C4 = 0.001775FQP + 0.3573$$

Butylene yield, LV%

$$C_4^- = C_4 * RC_4^- - C_4$$

Normal butane yield, LV%

$$nC_4 = 0.125 * C_4$$

Isobutane yield, LV%

$$iC_4 = C_4 - C_4^- - nC_4$$

Coke and fuel gas yield, wt%

$$\ln(Coke_FG) = 2.462 * C / FQP - 0.2158$$

Ratio of coke yield to the yield of coke plus fuel gas

$$RCoke = -0.000978 * C + 0.766 + 0.441 FQP / 100 - 0.556 (FQP / 100)^2$$

Coke yield, wt%

$$Coke = Coke_FG * RCoke$$

Fuel gas yield, wt%

$$FG = Coke_FG - Coke$$

Ratio of H₂S yield to feed sulphur

$$RH_2S = -0.005075 FQP + 0.76$$

H₂S yield, wt%

$$H_2S = RH_2S * S_f$$

API gravity of gasoline

$$API_g = 66.84 - 15.5 * C / 100 + 9.33 (C / 100)^2 - 31.2 (FQP / 100) + 35.6 (FQP / 100)^2$$

Specific gravity of gasoline

$$SG_g = 141.5 / (131.5 + API_g)$$

Gasoline yield, wt%

$$GASOW = SG_g * GASOV / SG_f$$

Total cycle oil yield, LV%

$$TCOV = 100 - C$$

Ratio of heavy cycle oil to total cycle oil

$$RHCO = 0.931 - 0.053K_f + 0.003(K_f - 10)^2 S_f$$

Heavy cycle oil yield, LV%

$$HCOV = TCOV * RHCO$$

Light cycle oil yield, LV%

$$LCOV = TCOV - HCOV$$

Weight factor for total cycle oil

$$WF = (-1.4 + 6.5 * C / 100 - 3.25(C / 100)^2)(0.804 + 1.66 * FQP / 100 - 2.22(FQP / 100)^2)$$

Weight yield of total cycle oil

$$TCOW = TCOV + WF$$

Gravity factor for light cycle oil

$$\ln(LCOGF) = -0.000965 * C * FQP - 10.6919 + 0.1185 * C + 0.111FQP$$

Light cycle oil API gravity

$$API_{lco} = API_f - LCOGF$$

Light cycle oil specific gravity

$$SG_{lco} = 141.5 / (131.5 + API_{lco})$$

Light cycle oil yield, wt%

$$LCOW = SG_{lco} * LCOV / SG_f$$

Heavy cycle oil yield, wt%

$$HCOW = TCOW - LCOW$$

Heavy cycle oil specific gravity

$$SG_{hco} = SG_f * HCOW / HCOV$$

Sulphur in gasoline, wt%

$$S_g = 5.5S_f / GASOW$$

Sulphur in light cycle oil, wt%

$$S_{lco} = 21S_f / LCOW$$

Sulphur in heavy cycle oil, wt%

$$S_{hco} = 21S_f / HCOW$$

Sulphur in coke, wt%

$$S_{coke} = (100S_f - 94.12H_2S - S_g * GASOW - S_{lco} * LCOW - S_{hco} * HCOW) / Coke$$

Research octane number of gasoline

$$RON = 0.00139C * FQP - 0.0384C - 0.187FQP + 101.3$$

Motor octane number of gasoline

$$MON = 0.778RON + 9.5$$

Reid vapour pressure of gasoline, psia

$$RVP = -23.8 + 2.5K_f + 0.3S_f$$

Aniline point of light cycle oil, °F

$$AP_{lco} = 4.34API_{lco}$$

Aniline point of heavy cycle oil, °F

$$AP_{hco} = 4.65API_{hco} + 86$$